TECHNISCHE UNIVERSITÄT DARMSTADT

CRISPR/Cas9-mediated genome engineering of the *SMARCB1* gene locus

Fachbereich Biologie
der Technischen Universität Darmstadt

Zur Erlangung des Grades
Doctor rerum naturalium
(Dr. rer. nat.)

Dissertation
von Marion Brigitte Lechler

Erstgutachterin: Prof. Dr. Ulrike A. Nuber
Zweitgutachterin: Prof. Dr. M. Cristina Cardoso

Darmstadt 2020

Lechler, Marion Brigitte: CRISPR/Cas9-mediated genome engineering of the *SMARCB1* gene locus, Stem Cell and Developmental Biology
Darmstadt, Technische Universität Darmstadt,
Jahr der Veröffentlichung der Dissertation auf TUprints: 2021
URN: urn:nbn:de:tuda-tuprints-118851
Tag der mündlichen Prüfung: 10. September 2020

I. Table of contents

I. ..... Table of contents I

II..... Abbreviations IV

III. .. Abstract / Zusammenfassung VII

1..... Introduction 1

1.1. The tumour suppressor gene *SMARCB1* 1

1.2. BRG1-associated factor (BAF) complexes 2

1.3. Diseases associated with mutations affecting the *SMARCB1* gene 7

1.4. CRISPR/Cas9-mediated genome engineering 14

1.5. Aim of this thesis 17

2..... Materials and methods 22

2.1. Molecular biology methods 22

2.1.1. Polymerase chain reaction (PCR) amplification of DNA 22

2.1.2. Purification of DNA samples 23

2.1.3. Restriction endonuclease digestion 24

2.1.4. Agarose gel electrophoresis 25

2.1.5. Blunting of cohesive DNA ends 27

2.1.6. Dephosphorylation of DNA ends 27

2.1.7. Ligation of DNA fragments 28

2.1.8. Generation of chemically-competent *Escherichia coli* 29

2.1.9. Transformation of *Escherichia coli* DH5α and Stbl3 31

2.1.10. Colony PCR 32

2.1.11. Plasmid DNA preparations 33

2.1.12. Sanger sequencing of DNA samples 36

2.1.13. TA-cloning 36

2.1.14. Overlap extension method 38

2.1.15. Cloning of guide RNA sequences into multiplex CRISPR/Cas9(n) plasmids 39

2.1.16. Gateway cloning 41

2.1.17. RNA isolation 42

2.1.18. cDNA synthesis 43

2.1.19. Quantitative reverse transcription PCR (RT-qPCR) 44

2.2. Biochemical methods 46

2.2.1. Protein sample preparation and protein concentration measurement 46

2.2.2. Sodium dodecyl sulphate polyacrylamide gel electrophoresis 47

2.2.3. Immunoblotting 50

2.3. Cell culture methods 53

2.3.1. Cultivation and transfection of the human embryonic kidney cell line HEK293T 53

2.3.2. Cultivation and transfection of human induced pluripotent stem cells (hiPSC) 54

2.3.3. Cultivation and transfection of the human breast epithelial cell line MCF10A 55

2.3.4. Cultivation of mouse neural stem and progenitor cells as neurospheres (NSPs) 56

2.3.5. Flow Cytometry analysis and sort (FACS) 57

2.3.6. Electroporation of human cell lines 58

2.3.7. Generation and concentration of lentiviral particles 61

2.3.8. Transduction of mammalian cell lines 62

3..... Results 63
3.1. Design and generation of constructs for CRISPR/Cas9-mediated genome engineering of the *SMARCB1* locus in human cells 63
3.1.1. Design and generation of constructs for CRISPR/Cas9-mediated genome engineering of human cell lines with AT/RT-associated *SMARCB1* mutations 65
3.1.2. Design and generation of constructs for CRISPR/Cas9-mediated genome engineering of human cell lines with CSS-associated *SMARCB1* mutations 69
3.1.3. Design and generation of gRNA and Cas9 expression plasmids for CRISPR/Cas9-mediated genome engineering of the *SMARCB1* locus in human cells 70
3.2. Establishment and optimisation of CRISPR/Cas9-mediated genome engineering methods in HEK293T cells 74
3.2.1. Establishment and optimisation of the CRISPR/Cas9-mediated genome engineering of the *SMARCB1* locus in HEK293T cells using the generated AT/RT-associated constructs 74
3.2.2. Establishment and optimisation of the CRISPR/Cas9-mediated genome engineering of the *SMARCB1* locus in HEK293T cells using the generated CSS-associated constructs 79
3.3. Establishment and optimisation of methods for CRISPR/Cas9-mediated genome engineering in hiPSCs 80
3.4. Establishment and optimisation of methods for CRISPR/Cas9-mediated genome engineering in MCF10A cells 84
3.5. *Loss-of-function* mutations in *SMARCB1* de-regulate expression of *Hes* genes in murine neural stem and in HEK293T cells 86
3.5.1. *Loss-of-function* mutations in *SMARCB1* de-regulate expression of *Hes* genes in E14.5 mouse brain samples and in HEK293T cells 86
3.5.2. Cloning and lentiviral packaging of murine *Hes5*-IRES-mKate2 overexpression and IRES-mKate2 control plasmids for the transduction of murine neural stem cells 89
3.5.3. Establishment and optimisation of methods to overexpress *Hes5* in murine NSCs 90
4..... Discussion 93
4.1. Establishment and optimisation of methods and constructs for CRISPR/Cas9-mediated genome engineering of the *SMARCB1* gene locus in human cell lines 93
4.1.1. Transfer of large constructs into hiPSC#33 and re-evaluation of the HDR constructs 94
4.1.2. Transfer of large constructs into MCF10A cells 97
4.2. The designed multi-colour strategies for the CRISPR/Cas9-mediated genome engineering in comparison to other cellular modelling approaches at the *SMARCB1* locus 100
4.2.1. The designed three-colour reporter strategy in comparison to another cellular AT/RT model 100
4.2.2. The designed two-colour strategy in comparison to another cellular CSS model 102
4.3. *Loss-of-function* mutations in *SMARCB1* de-regulate expression of *Hes* genes 104
5..... Outlook 106
6..... Bibliography 107

7..... Appendix 117
7.1. Materials 117
7.1.1. List of oligonucleotides 117
7.1.2. List of restriction endonucleases 120
7.1.3. Guide RNA positioning within the genomic sequence of *SMARCB1* 121
7.1.4. Graphical overview of all constructs generated for the CRISPR/Cas9-mediated genome engineering of the human *SMARCB1* locus 122
7.1.5. Graphical overview of the cloning of the original lentiviral Hes5-IRES-mKate2 plasmid for overexpression of *Hes5* 128
7.1.6. Information of plasmids generated or used in this thesis 128
7.2. Publications 134
7.3. Scholarship 134
7.4. Contributions of others 134
7.5. Curriculum vitae 135
IV.... Acknowledgements IX
V. .... Assertion – Ehrenwörtliche Erklärung X

II. Abbreviations

1°	Primary, e.g. 1° antibody = primary antibody
2°	Secondary, e.g. 2° antibody = secondary antibody
° C	Degree Celsius
µL	Microliter
A260/A280	Ratio of the absorption at 260 and 280 nm, value for the purity of nucleic acids
AMP	Adenosine monophosphate
approx.	Approximately
AT/RT	Atypical-teratoid/rhabdoid tumour
ATP	Adenosine triphosphate
BAF	BRG1- or BRM-associated factor
bFGF	Basic fibroblast growth factor
bp	Base pair
BSA	Bovine serum albumin
BSD	Blasticidin S deaminase gene
Cas9n	Cas9 nickase
cDNA	Complementary DNA
CRISPR	Clustered regularly interspaced palindromic repeat
CSS	Coffin-Siris syndrome
c_T	Threshold cycle (RT-qPCR)
Δc_T	Difference of c_T values of the gene of interest and the housekeeping gene (RT-qPCR)
$\Delta\Delta$ c_T	Difference of delta c_T values of treatment and control samples
Da	Dalton, unified atomic mass unit
DH5α	Laboratory strain of *E. coli*
DMEM high glucose	Dulbecco's Modified Eagle's medium supplemented with 4500 mg/L glucose
DMEM/F12	Dulbecco's Modified Eagle's medium nutrient mixture F-12
DNA	Deoxyribonucleic acid
DNaseI	Deoxyribonuclease I
dNTP	Deoxyribonucleotide triphosphate
DPBS	Dulbecco's phosphate buffered saline
E	Embryonic day
E. coli	*Escherichia coli*
EGF	Epidermal growth factor
eGFP::ZeoR	Enhanced green fluorescent protein (eGFP) and zeocin resistance (ZeoR) fusion gene
FCS	Fetal calf serum
g	Gram
gDNA	Genomic DNA
gRNA	(single) guide RNA
GSG	Glycine-Serine-Glycine linker
$H_2O_{dest.}$	Deionised water
HDR	Homology directed repair
HEK293T	Human embryonic kidney 293 cells expressing mutant SV40 antigen T
Hes/HES	Mammalian homologues of Drosophila hairy and Enhancer of split
hiPSC(s)	Human induced pluripotent stem cell(s)
hiPSC#33	Human induced pluripotent stem cells clonal line #33

HL	Left homology arm, upstream/5' of the sequence to be inserted in a HDR construct
HR	Right homology arm, downstream/3' of the sequence to be inserted in a HDR construct
IDLV	Integrase-defective lentiviral particles
IDT	Integrated DNA Technologies
i.e.	id est, that is
inv	Sequence flanked by inverted loxP sites, inversion of the sequence between the inverted loxP sites upon *Cre* recombination
IRES	Internal ribosomal entry site
kb	Kilobase pair, 1,000 bp = 1 kb
LB	Luria's broth
loxP	Locus of X-over P1, 34 bp sequences, recombined by *Cre* recombinase based on directionality
LTR	Long terminal repeat
LV	Lentiviral particles
MCF10A	Human breast epithelial cell line
mg	Milligram
mL	Millilitre
M-MuLV	Moloney Murine Leukemia Virus
NEB	New England Biolabs
ng	Nanograms
NPC(s)	Neural progenitor cell(s)
NSC(s)	Neural stem cell(s)
NSP(s)	Neurosphere(s)
NSPM	Neurosphere medium
P2A	2A self-cleaving peptide of porcine *Teschovirus-1*
PAGE	Polyacrylamide gel electrophoresis
PAM	Protospacer adjacent motif
pBS	pBluescript
PEI	Polyethylenimine
PuroR	Puromycin resistance gene
PVDF	Polyvinylidene fluoride or polyvinylidene difluoride
RGC	Radial glial cell
RNA	Ribonucleic acid
RNaseA	Ribonuclease A
RNaseH	Ribonuclease H
rpm	Rounds per minute
RQ	Relative quantification (RT-qPCR)
RT	Reverse transcriptase
RT-qPCR	Reverse transcribed-quantitative PCR
SMARCB1	SWI/SNF-related matrix-associated actin-dependent regulator of chromatin subfamily B member 1
SOC	Super Optimal broth with Catabolite repression
Stbl3	Laboratory strain of *E. coli*
SVZ	Subventricular zone
T2A	2A self-cleaving peptide of *Thoseaasigna* virus
TAE	Tris-acetate EDTA

TfBI	Transformation buffer I
TfBII	Transformation buffer II
U	Unit
VSV-G	Coating glycoprotein of the Vesicular Stomatitis Virus
VTN	Vitronectin
VZ	Ventricular zone
xg	Relative centrifugal force or G-force

III. Abstract / Zusammenfassung

Truncating or nonsense mutations in the ubiquitously expressed tumour suppressor and BAF chromatin remodelling complex core subunit gene *SMARCB1* cause malignant rhabdoid tumours (MRTs) of the brain, the kidney, and the soft tissues. MRTs show a high clinical variance despite a simple cancer genome with *SMARCB1* being the only gene recurrently mutated in these malignancies. MRTs of the brain are called atypical teratoid/rhabdoid tumours (AT/RT) and present a rare, but highly aggressive brain tumour entity with poor prognosis that predominantly occurs in very young children. In this thesis, diverse constructs for the generation of three-colour reporter cell lines with *SMARCB1* mutations found in AT/RTs were established and methods required for the CRISPR/Cas9-mediated genome engineering using these constructs were optimised. Heterozygous missense mutations or small in-frame deletions clustering in the last two exons of the *SMARCB1* gene are frequently observed in another disease entity, Coffin-Siris syndrome (CSS). CSS is a congenital neurodevelopmental disorder characterised by cognitive impairment, microcephaly, coarse facial features, and hypoplasia of the fifth finger- and/or toenail as well of the distal phalanx of the fifth finger and/or toe. CRISPR/Cas9 constructs for the generation of hiPSC and MCF10A cell lines with heterozygous *c.1091_1093del AGA SMARCB1* mutation were generated to investigate the cellular consequences of this mutation. Comparison of cellular AT/RT and CSS models would contribute to a better understanding of how different types of *SMARCB1* mutations can lead to two very different diseases and how particular mutations affect the gene expression of *SMARCB1* itself.

The recently published mouse model recapitulating *SMARCB1*-associated features of CSS, which is based on a partial *loss-of-function* of *Smarcb1*, revealed a diminished pool of neural progenitor cells (NPC) in the developing brain of these mice. To test the hypothesis if overexpression of *Hes5* can rescue the impairment of mouse neural stem cell (NSC) maintenance, a lentiviral system for the overexpression of *Cre* recombinase and of *Hes5* in *Smarcb1*$^{+/inv}$ *NesCre*$^{-/-}$ NSCs and NPCs was optimised.

SMARCB1 ist ein ubiquitär exprimiertes Tumorsuppressorgen und kodiert eine Kernkomponente der chromatinremodellierenden BAF Komplexe. Inaktivierende Mutationen des *SMARCB1*-Gens sind die einzige wiederkehrende genetische Veränderung in malignen rhabdoiden Tumoren (MRT) des zentralen Nervensystems, der Niere und weicher Gewebe. MRTs des Gehirns werden atypische teratoide/rhabdoide Tumore (AT/RTs) genannt und betreffen vorwiegend sehr junge Kinder. In dieser Arbeit wurden verschiedene Konstrukte erstellt um mit Hilfe der CRISPR/Cas9-Technologie Zelllinien mit drei Fluoreszenzreportern und Inaktivierung des *SMARCB1*-Gen zu erstellen. Methoden, die für diese CRISPR/Cas9-vermittelten Veränderungen im Genom benötigt werden, wurden etabliert und optimiert. Der Austausch oder Verlust einzelner Aminosäuren in der C-terminalen Region des SMARCB1-Proteins ist mit der Manifestation des Coffin-Siris Syndroms (CSS) assoziiert. Das CSS ist eine angeborene Entwicklungsstörung, die durch Verzögerungen in der geistigen Entwicklung, Mikrozephalie, und Hypoplasie des Nagels des kleinen Fingers und/oder Zehs sowie des letzten Gliedes des kleinen Fingers und/oder Zehs charakterisiert ist. Die am häufigsten auftretende Mutation des *SMARCB1*-Gens bei CSS ist die heterozygote Deletion des Lysin-codierenden Tripletts an Position 364 (*c.1091_1093del AGA*). In dieser Arbeit wurden CRISPR/Cas9-Konstrukte für das Einbringen dieser Mutation in hiPSC und MCF10A-Zellen entwickelt. Mit Hilfe dieser Zellmodelle wird es möglich sein, die durch die Mutation des *SMARCB1*-Gens veränderten zellulären Prozesse und deren Auswirkung besser zu untersuchen. Der Vergleich von Zellmodellen für AT/RTs und für das CSS kann dazu beitragen, besser zu verstehen wie unterschiedliche Mutationen desselben Gens zu verschiedenen Erkrankungen führen können und welchen Einfluss diese Mutationen auf die Genexpression von *SMARCB1* haben.

Bei dem kürzlich veröffentlichten Mausmodell, das *SMARCB1*-assoziierte Charakteristika von CSS rekapituliert und auf einem partiellen Funktionsverlust von *Smarcb1* beruht, wurde eine reduzierte Zahl an neuralen Vorläuferzellen (NPCs) während der Gehirnentwicklung festgestellt. Um zu überprüfen, ob die Überexpression von *Hes5* die durch Mutation des *Smarcb1*-Gens verursachte Reduktion neuraler Stammzellen (NSCs) ausgleichen kann, wurde ein lentivirales System zur Überexpression der *Cre* Rekombinase und des *Hes5*-Gens in *Smarcb1*$^{+/inv}$ *NesCre*$^{-/-}$ NSCs und NPCs optimiert.

1. Introduction

1.1. The tumour suppressor gene *SMARCB1*

SWI/SNF-related, matrix-associated, actin-dependent regulator of chromatin, subfamily B, member 1 - *SMARCB1* (also known as *BAF47*, *INI1*, *SNF5*) is a bona fide tumour suppressor gene located on the long arm of chromosome 22 (22q11.23), and truncating mutations of the *SMARCB1* gene are the main recurrent event causing malignant rhabdoid tumours in various organs (Wang, Cote et al. 1996, Versteege, Sevenet et al. 1998, Biegel, Zhou et al. 1999, Jackson, Sievert et al. 2009). The gene spans approx. 50 kb on Chr.22q11.23 and contains nine exons coding for two isoforms (a 385 amino acids, b 376 amino acids) of a ubiquitously expressed nuclear protein of approx. 44 kDa which is highly conserved from humans to *Caenorhabditi elegans* and *Drosophila melanogaster* (Versteege, Sevenet et al. 1998). The C-terminal SNF5 domain is even conserved to *Saccharomyces cerevisiae* (Muchardt, Sardet et al. 1995, Wang, Xue et al. 1996). This conservation led to the identification of the SMARCB1 protein as a human homolog to yeast Snf5 binding to HIV-1 integrase (Kalpana, Marmon et al. 1994, Muchardt, Sardet et al. 1995, Wang, Cote et al. 1996, Wang, Xue et al. 1996, Versteege, Sevenet et al. 1998). SMARCB1 is a core component of the highly conserved mammalian SWI/SNF or BAF chromatin remodeling complexes (Phelan, Sif et al. 1999). *SMARCB1* was shown to be essential for early development in mice and neural differentiation of human embryonic stem cells (Klochendler-Yeivin, Fiette et al. 2000, Langer, Ward et al. 2019). The SMARCB1 protein contains a N-terminal winged-helix domain, which was originally identified as a putative DNA binding domain, and a C-terminal domain (CTD), the SNF5 domain, which contains two imperfect tandem repeat domains (RPT1 and RPT2), a coiled-coil domain and an arginine and lysine-rich, positively charged region, a hot-spot for mutations associated with Coffin-Siris syndrome (CSS) (Kalpana, Marmon et al. 1994, Muchardt, Sardet et al. 1995, Morozov, Yung et al. 1998, Tsurusaki, Okamoto et al. 2012, Allen, Freund et al. 2015, He, Zhang et al. 2019). CSS-associated mutations mainly affect the arginine and lysine residues in this positively charged cluster resulting in a reduction of the positive charge of this region, either by amino acid exchanges or a shift in the secondary structure resulting in the burial of the positively charged amino acids. This reduction of the positive charge in the C-terminal region of SMARCB1 weakens the binding of the SMARCB1 protein to the acidic patch of the nucleosome (Valencia, Collings et al. 2019, He, Wu et al. 2020). Figure 1 summarises and graphically depicts the structural characteristics of the *SMARCB1* gene and protein.

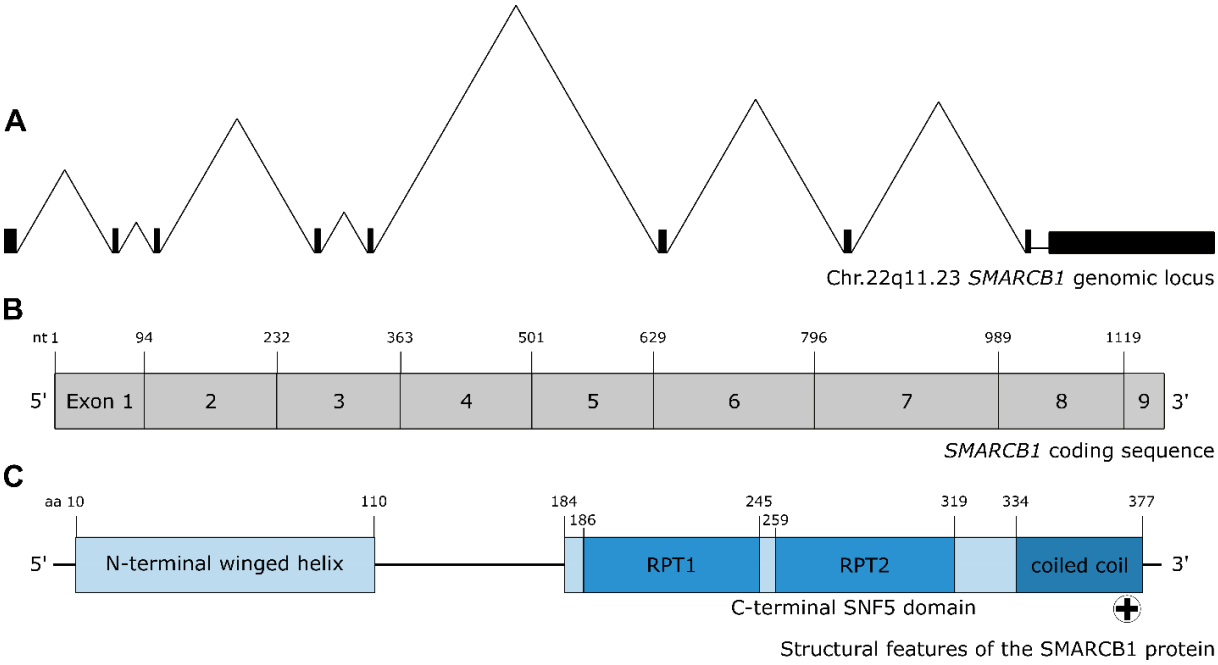

Figure 1: Graphical summary of the structural characteristics of the human *SMARCB1* gene and protein. **(A)** The human *SMARCB1* gene locates to the long arm of chromosome 22 (Chr.22q11.23) and stretches over 50 kb (exons black boxes, introns black lines). **(B)** The nine exons of the coding sequence translate to 385 amino acids in isoform a. Isoform b is generated by alternative splicing and lacks nine amino acids at the 3' end of exon 2 (376 amino acids). Nucleotide positions of each exon's first base are indicated above the coding sequence. **(C)** The amino acid sequence forms an approx. 44 kDa protein with specifically structured N- and C-terminus. N-terminally, human SMARCB1 protein folds into a winged helix and is C-terminally characterised by two imperfect repeat domains (RPT1 and RPT2) as well as a coiled coil domain which contains a lysine and arginine-rich, positively charged cluster (⊕). Amino acid positions of each structural component are indicated above the SMARCB1 protein depiction.

1.2. BRG1-associated factor (BAF) complexes

BRG1-associated factor (BAF) complexes are 2.2 MDa ATP-dependent chromatin remodeling complexes composed of up to 15 subunits (Wang, Cote et al. 1996, Wang, Xue et al. 1996, Kadoch, Hargreaves et al. 2013). BAF complex core subunits show high homology to the nucleosome remodeling Swi/Snf complexes originally identified in genetic screens in yeast (Wilson and Roberts 2011). In these screens several genes were identified, which result in similar phenotypes upon *knock-out*. One affected phenotype was the sucrose metabolism and genes causing a sucrose non-fermenting phenotype upon *knock-out* were named *Snf* genes (Neigeborn and Carlson 1984). The second group of knocked out genes were required for the activation of *HO* for mating type switching in yeast and, thus were termed *Swi* genes (Stern, Jensen et al. 1984). Compared to the mammalian BAF complexes, the Swi/Snf complexes are small and their transcription regulatory competences are limited to transcriptional activation. The latter is comprehensible considering the remarkably less complex regulatory structure of the yeast genome compared to the extent of regulatory elements present in the highly repressed mammalian genome. Therefore, the functions of BAF complexes in mammalian cells are more diverse than in yeast including transcriptional activation and repression of genes in an orchestrated manner (Alfert, Moreno et al. 2019). The subunits of the BAF complexes contain DNA- and/or histone-binding domains such as zinc fingers, AT-hooks, chromo- and bromodomains.

Therefore, the complexes can recognise binding sites based on DNA sequence, architectural characteristics, and pre-existing histone modifications (Alfert, Moreno et al. 2019). The BAF complexes couple chromatin state, histone modification, transcription factor binding, and ATP-dependent chromatin remodeling, mechanisms involved in the regulation of transcription. In general, mammalian BAF complexes are composed of more subunits than their yeast counterpart to fulfil these diverse functions. Additionally, most of the subunits present in mammalian BAF complexes are encoded by gene families, which further increase the observed and assumed diversity of BAF complexes found in mammalian cells (Wu, Lessard et al. 2009). So far, three distinct basic BAF complexes have been identified in mammalian cells: the canonical BAF complex (cBAF), the polybromo-associated BAF complex (PBAF), which is supposed to be highly related to the yeast RSC nucleosome remodeling complex, and most recently the non-canonical BAF complex (ncBAF) (Cairns, Lorch et al. 1996, Wang, Cote et al. 1996, Xue, Canman et al. 2000, Alpsoy and Dykhuizen 2018, Wang, Wang et al. 2019). These complexes differ in their subunit composition. cBAF and PBAF share the highly conserved core complex subunits SMARCB1 (BAF47), BAF155 (*SMARCC1*), and BAF170 (*SMARCC2*) in combination with one of the two mutually exclusive ATPase subunits BRM (BAF190B, *SMARCA2*, homolog of *D. melanogaster* Brahma) or BRG1 (BRM protein-like 1, BAF190, *SMARCA4*) (Figure 2B, C) (Phelan, Sif et al. 1999). Both complexes also differ in some subunits: PBAF-complexes specifically include BAF200 (*ARID2*), BAF180 (polybromo-BRM1, *PBRM1*), BAF45a (*PHF10*), and BRD7 subunits (Wang, Cote et al. 1996, Middeljans, Wan et al. 2012, Alfert, Moreno et al. 2019). The ncBAF differs more profoundly from cBAF and PBAF. It contains some distinctive subunits such as GLSTR1, BRD4 and BRD9, but lacks many of the core BAF subunits as well as some of the PBAF-specific subunits, namely SMARCB1, BAF57, BAF250, BAF180, BRD7 (Figure 2A) (Alpsoy and Dykhuizen 2018, Alfert, Moreno et al. 2019, Wang, Wang et al. 2019). These three basic BAF complexes already exemplify how the combinatorial assembly ensures complex variety and specificity and by this might allow regulation of mammalian gene expression. It was assumed that expression of unique subunits, leading to BAF complexes of diverse composition, represents a major contribution to the regulatory process of gene expression by these complexes via the binding to and coordination with tissue-specific transcription factors (Alfert, Moreno et al. 2019).

Indeed, complexes specific to tissues or biological functions have been identified e.g. in the context of neural development and function, heart development, muscle development, and maintenance of embryonic stem cell pluripotency (Alfert, Moreno et al. 2019). How orchestrated exchange of paralog BAF complex subunits changes the cellular properties was intensively studied in neural development, and can be used as an example for the epigenetic control of chromatin accessibility and gene expression by BAF complexes. In mouse embryonic stem cells (mESCs), the esBAF complex was identified to be required for maintenance of pluripotency, proliferation, and self-renewal in the context of a genome characterised by a high number of bivalent domains (Figure 2D). Exertion of these cell type-specific functions is dependent on the esBAF specific subunits Brg1, BAF250a, and especially a BAF155 homodimer in mice (Ho, Ronan et al. 2009). In hESCs, a BAF170::BAF155 heterodimer was shown to

be required to maintain pluripotency (Zhang, Li et al. 2014). In this latter example also a human to mouse species difference in the BAF complexes adds to the general tissue-specific diversity of BAF complexes. For the neural development in mice, the commitment of mESCs to neural progenitor cells (NPCs) coincides with the initiation of the transcription of Brm and BAF170 (Ho, Ronan et al. 2009, Narayanan and Tuoc 2014). In combination with the neural progenitor BAF complex (npBAF) specific subunits BAF45a/d (*PHF10/DPF3*), BAF53a (*ACTL6A*), and SS18 the self-renewal and proliferation of NPCs is maintained (Figure 2E) (Lessard, Wu et al. 2007, Alfert, Moreno et al. 2019). Since the NPC population shows heterogeneous molecular characteristics, e.g. differences in gene expression of early and late progenitors or NPCs with lower or upper neuronal fate, which are regulated by the sequential activation or repression of transcription factors, the combinatorial assembly of BAF complexes is also heterogeneous (Narayanan and Tuoc 2014). The npBAF depicted in Figure 2E thus is only one of several BAF complex combinations found in NPCs. Mitotic exit of NPCs and thus development to post-mitotic neurons is accompanied with the exchange of npBAF-specific subunits for their paralogs: BAF45b/c, BAF53b, and CREST to generate the nBAF complex (Figure 2F) (Staahl, Tang et al. 2013). The compositional switch in the BAF complex causes a switch in the proliferative capacity of the cells further highlighting the role of BAF complex-mediated regulation of chromatin and gene expression in neural development (Staahl, Tang et al. 2013).

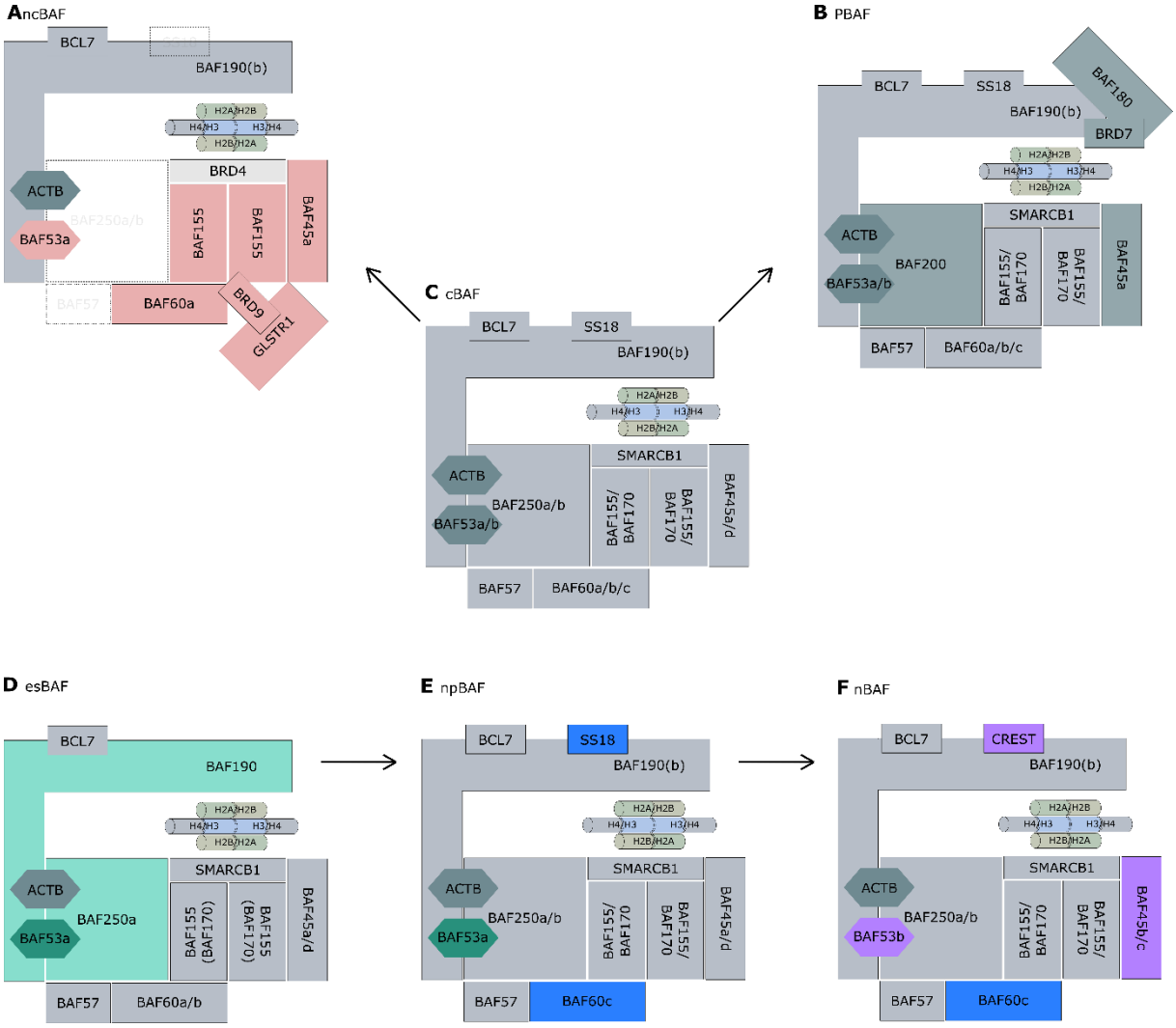

Figure 2: Combinatorial BAF complex composition facilitates tissue-specific regulation of chromatin and gene expression. **(C)** The canonical BAF complex (cBAF) is depicted in the centre. It is highly related to yeast Swi/Snf nucleosome remodeling complexes and is considered the basic state of the BAF complex. Alterations in subunit composition in the other BAF complexes are highlighted in different colours. Aside from the cBAF complex, there are two other, distinct, basic BAF complexes. **(A)** The non-canonical BAF complex (ncBAF) was recently discovered. Its subunit composition differs remarkably from the previously known cBAF and polybromo-associated BAF (PBAF) complexes and lacks several of the cBAF and PBAF core subunits. ncBAF complexes contain several new, and ncBAF defining subunits as GLSTR1, BRD4, and BRD9 (light grey colour indicates likely incorporated subunits or predicted position of a defining subunit, spaces indicate yet unidentified subunit equivalents to the cBAF complex). **(B)** The polybromo-associated BAF complex (PBAF) was identified early in BAF complex research, and is thought to be related to the yeast RSC complex. The PBAF complex contains several defining subunits as BAF180 (*PBRM1*), BRD7, BAF200, and BAF45a. Its assembly is also cell type-specific and thus facilitates specific biologic functions (not covered in detail here). **(D-F)** The mammalian neural development is a well-studied example of how specification of BAF complexes is achieved by distinct combinatorial assembly and by this drives the development of a specific cellular lineage. Here, the cBAF complex composition of ESCs developing into neuronal cell types is depicted. Upon neural cell fate commitment, the esBAF changes to the npBAF complex by incorporation of the SS18 subunit, the paralog exchange of BAF60a/b to BAF60c, and for murine development only, the incorporation of BAF170 to form BAF155::BAF170 heterodimers. Further commitment to neuronal cell types and mitotic exit in post-mitotic neurons is associated with paralog exchanges of BAF53b, BAF45b/c, and CREST to generate nBAF complexes from the npBAF. The heterogeneous NPC population was also found to express a variety of subtype-specific BAF complexes. The depicted BAF complex assembly in neural development is only one example of how BAF complexes facilitate cell type-specific development by gene expression control. (Ho, Ronan et al. 2009, Wu, Lessard et al. 2009, Zhang, Li et al. 2014, Kadoch and Crabtree 2015, Michel, D'Avino et al. 2018, Alfert, Moreno et al. 2019, He, Wu et al. 2020, Johann 2020)

After describing how the different subunits of BAF complexes are associated with cell type-specific gene expression, the mechanism of BAF complex-mediated ATP-dependent chromatin remodeling is addressed in the following section. In yeast, the nucleosomes are mobilised and moved across DNA to activate gene expression (Imbalzano, Kwon et al. 1994, Kwon, Imbalzano et al. 1994). This activity was found to be reconstituted *in vitro* by combination of the BAF core complex consisting of one ATPase subunit, SMARCB1, BAF170, and BAF155 (Phelan, Sif et al. 1999). Since BAF complexes contain up to 11 more subunits, this mechanism cannot be entirely sufficient to explain all actions exerted by mammalian BAF complexes. For BAF complex-mediated chromatin remodeling, two different mechanisms were suggested: nucleosome sliding or nucleosome ejection/insertion (Wilson and Roberts 2011). ATP-dependent nucleosome sliding is hypothesised to include DNA looping by formation of new contacts to histones and sliding of the nucleosome along the DNA via the translocase activity of ATPases (Wilson and Roberts 2011, Alfert, Moreno et al. 2019). Recently, the crystal structure of the nucleosome-bound human BAF complex was resolved (Figure 2) (He, Wu et al. 2020). The nucleosome is sandwiched between the catalytic ATPase subunit and the C-terminal domain of SMARCB1 (Han, Reyes et al. 2020, He, Wu et al. 2020). This clasping structure fits well with the proposed model of nucleosome sliding and ejection designed by Clapier, Iwasa et al. (2017). In this model, the ATPase subunit couples itself to the nucleosome octamer, and the ATPase-translocase domain consisting of two RecA-like lobes translocates the DNA one to two basepairs per ATP-hydrolysis along the surface of the nucleosome. Thereby, DNA tension on both sides of the translocase domain is generated which is resolved by sequential nucleosome-DNA contact disruption and nucleosome sliding. Ejection of nucleosomes is predicted to take place upon collision of the BAF complex-bound nucleosome with an adjacent histone octamer resulting in the DNA being peeled off the adjacent octamer. In this scenario, coupling activity to the nucleosome and ATPase activity are rather low. However, BAF complexes can also exhibit high coupling and ATPase activity leading to efficient and forceful DNA translocation, and eventually resulting in simultaneous rupture of several histone-DNA contacts. This rupture destabilises the histone octamer and causes nucleosome ejection. In both scenarios, BAF complex targeted regions of the genome potentially get depleted in nucleosomes, and thus get accessible for transcription factors or the transcriptional machinery resulting in activation of gene expression (Clapier, Iwasa et al. 2017, He, Wu et al. 2020).

Aside from regulating the accessibility of chromatin, i.e. nucleosome occupation, BAF complexes also play a role in the regional regulation of histone methylation. The BAF versus PRC2 (polycomb repressive complex 2) opposition is a well-studied example. The PRC2 subunits EZH1 and EZH2 are the only mammalian enzymes known to deposit the repressive chromatin mark of trimethylation of lysine residue 27 in histone H3 (H3K27me3) (Alfert, Moreno et al. 2019). mESCs show a decrease in the H3K27me3 chromatin mark at BAF complex-repressed genes and elevated levels of H3K27me3 marks at BAF complex-activated genes upon loss of Brg1 or its ATPase domain, while the expression of PRC2 and the genome wide H3K27me3 levels remain unaltered. The phenotype caused by loss of *Brg1* gene expression can be rescued by *knock-down* of another PRC2 subunit (Ho, Miller et al. 2011).

Furthermore, recruitment of BAF complexes to the *Oct4* gene locus removes PRC2 complexes and H3K27me3 histone marks and *vice versa*. Thus, the opposition between BAF and PRC2 complexes plays an important role in the balance of methylation of histone H3 and, again, chromatin accessibility (Wu, Lessard et al. 2009, Helming, Wang et al. 2014, Alfert, Moreno et al. 2019).

Considering the importance of cell type- and developmental stage-specific BAF complexes in neural development the association of mutations in BAF subunit genes with neurodevelopmental disorders is plausible (Alfert, Moreno et al. 2019). Additionally, the tissue-specificity of BAF complex assembly links the BAF complexes to cancer. Dependent on the affected BAF complex subunit, a variety tissues are affected by a distinct subset of cancers (Alfert, Moreno et al. 2019). In total, 20% of human cancers harbour mutations in BAF complex subunit genes (Kadoch and Crabtree 2015).

1.3. Diseases associated with mutations affecting the *SMARCB1* gene

As described above, a key role of BAF complexes is to regulate the balance between stem cell states and more mature cell states during development (Masliah-Planchon, Bieche et al. 2015). Among the BAF complex-regulated genes, many are associated with cancer. BAF complexes, for example, are involved in downregulating the expression of the cyclin-dependent kinase inhibitor $p16^{INK4A}$, in repressing RB target genes including the E2F factor, promote *c-MYC* oncogene-mediated transactivation, and in inducing aberrant activation of Sonic Hedgehog (SHH) signalling by interaction with GLI1 (Cheng, Davies et al. 1999, Versteege, Medjkane et al. 2002, Isakoff, Sansam et al. 2005, Jagani, Mora-Blanco et al. 2010). Additionally, BAF complexes contribute to invasion and metastasis by control of genes involved in cellular adhesion and motility (Caramel, Quignon et al. 2008). The fact that chromatin remodelling by BAF complexes plays a role in many different cellular processes is also related to their cooperation with various transcription factors (Masliah-Planchon, Bieche et al. 2015).

Involvement of BAF complexes in tumorigenesis was first observed in malignant rhabdoid tumours (MRTs). MRTs are aggressive tumours with an exceptional low mutational burden mainly affecting very young children. They were initially histologically defined by the presence of rhabdoid cells and of cells of all three germ layers (Figure 3A) (Burger, Yu et al. 1998, McKenna, Sansam et al. 2008). Rhabdoid cells possess a prominent nucleolus, uncondensed chromatin, and characteristic cytoplasmic eosinophilic inclusions consisting of whorls of intermediate filaments (Masliah-Planchon, Bieche et al. 2015). MRTs can be found in various organs, e.g. the kidney, soft tissue, liver, or the brain, but are considered one tumour entity due to the common histological features as well as loss of expression of *SMARCB1* (Masliah-Planchon, Bieche et al. 2015). Aside from MRTs, somatic loss of *SMARCB1* expression can give rise to a broader spectrum of tumours, e.g. choroid plexus carcinoma, meningioma, ependymoma, malignant glioma, epithelioid malignant peripheral nerve sheath tumours, epithelioid sarcomas, sinonasal carcinomas, paediatric hepatoblastomas, or cribriform neuroepithelial tumours (CRINET) (Strother 2005, Masliah-Planchon, Bieche et al. 2015).

This thesis focuses on MRTs of the central nervous system, so-called atypical-teratoid/rhabdoid tumours (AT/RTs). AT/RTs are highly aggressive brain tumours occurring predominantly in very young children with 75% of the patients being younger than three years of age at diagnosis (Strother 2005). They represent only 1 to 2% of paediatric brain tumours, but 10% of tumours of the central nervous system (CNS) in infants (Biegel 2006). Despite aggressive therapy approaches and advancement in treatment options, the diagnosis of an AT/RT is still fatal for most affected children (Schrey, Carceller Lechon et al. 2016). Most AT/RT patients exhibit somatic mutations of both *SMARCB1* alleles resulting in complete loss of its protein and 25 to 30% of affected children are carriers of germline mutations of the *SMARCB1* gene (Bourdeaut, Lequin et al. 2011, Eaton, Tooke et al. 2011). Most of the germline mutations are *de novo* mutations linked to gonadal or early post-zygotic mosaicism, but there are rare cases of the rhabdoid tumour predisposition syndrome 1 (RTPS1) in which families are affected by MRTs and schwannomas due to inherited germline mutations of the *SMARCB1* gene (Ammerlaan, Ararou et al. 2008, Masliah-Planchon, Bieche et al. 2015, Sredni and Tomita 2015). Upon the development of mouse models for AT/RTs, constitutional loss of *Smarcb1* was shown to be early embryonic lethal in mice. *Smarcb1*$^{+/-}$ mice compensate for the loss of one allele by upregulation of the transcription from the remaining wildtype allele of *Smarcb1*, but are susceptible to develop MRTs in soft-tissues or in the head upon loss of the wildtype allele of *Smarcb1* (Klochendler-Yeivin, Fiette et al. 2000, Roberts, Galusha et al. 2000, Guidi, Sands et al. 2001, Guidi, Veal et al. 2004). Conditional *knock-out* of the *Smarcb1* gene in *Smarcb1*$^{flox/-}$ mice by *Cre* recombination in early embryonic development circumvents the embryonic lethality and results in highly penetrant and unprecedented rapid tumour formation within 11 weeks (Roberts, Leroux et al. 2002). Timely controlled biallelic inactivation of the *Smarcb1* gene by *Cre* recombination upon tamoxifen treatment revealed that loss of *Smarcb1* expression at an early developmental stage in which stem cells start to differentiate into specified progenitors (embryonic day 6 to 10) causes intracranial tumours with rhabdoid tumour-like characteristics (Han, Richer et al. 2016). These findings in mice support the notion of *SMARCB1* being a tumour suppressor gene, and correspond to the rarity of RTPS1, the young age of tumorigenesis observed in patients suffering from AT/RTs, and hint to the clinical heterogeneity observed in AT/RT cohorts. This heterogeneity is unexpected considering the very simple tumour genome observed in AT/RTs with inactivation of *SMARCB1* being the only recurrent event in these tumours aside from very rare cases with mutations in the ATPase subunit BAF190/BRG1 (Fruhwald, Hasselblatt et al. 2006, Hasselblatt, Nagel et al. 2014). Definition and characterization of the biological heterogeneity of AT/RTs may help to understand how tumour biology shapes the response and treatment outcome of these tumours, and thus to improve the currently poor prognosis for AT/RT patients (Ho, Johann et al. 2020). Two groups independently analysed AT/RT cohorts and each identified three distinct subgroups of AT/RT based on clinicopathological findings, DNA methylation, and gene expression studies (Torchia, Picard et al. 2015, Han, Richer et al. 2016, Johann, Erkek et al. 2016, Torchia, Golbourn et al. 2016). In order to define a standard subgrouping scheme similar to schemes which have been proven beneficial for the

treatment of other childhood brain cancers such as medulloblastoma, a meta-analysis of a large cohort of individual AT/RT cases was conducted (Ho, Johann et al. 2020). Based on DNA methylation, gene expression profiling, and gene set enrichment analyses three distinct subgroups of AT/RT were defined: AT/RT-SHH, AT/RT-TYR, AT/RT-MYC (Figure 3B) (Ho, Johann et al. 2020).

AT/RT-SHH subgroup tumours are characterised by overexpression of SHH and NOTCH pathway members (*GLI2*, *PTCHD1*, *BOC*, or *ASCL1*, *HES1*, *DTX1*). Overexpression of the SHH marker genes appears to be activated directly or indirectly by loss of *SMARCB1* gene expression. The lack of this effect in the other subgroups may hint to a different cellular origin of the tumours. This notion is supported by AT/RT-SHH tumours showing features of neuronal differentiation while AT/RT-TYR and –MYC subgroups show rather mesenchymal characteristics. AT/RT-SHH tumours mostly exhibit inactivation of the *SMARCB1* gene by heterozygous point mutations and are mainly found in patients of an intermediate age group (median age at diagnosis 20 months). DNA methylation analysis shows some level of heterozygosity within this subgroup and reveals two subtypes associated with either supratentorial or infratentorial tumour localisation. (Ho, Johann et al. 2020)

The AT/RT-TYR subgroup is mainly characterised by the overexpression of tyrosinase (*TYR*) and the upregulation of components of the melanosomal pathway. Additionally, the bone morphogenetic protein pathway (*BMP*) and developmentally related transcription factors as orthodenticle homeobox 2 (*OTX2*) are upregulated in AT/RT-TYR tumours. Gene set enrichment analyses show overexpression of genes of the melanosomal pathway, the tyrosine metabolism, and epithelial proliferation indicating a neuroectodermal origin of these tumours. In general, AT/RTs of the AT/RT-TYR subgroup affect a younger patient group (median age at diagnosis 12 months) with the highest proportion of patients younger than three years. Tumours of the AT/RT-TYR subgroup are mostly located infratentorially, and predominantly show whole or partial loss of one copy of chromosome 22 in combination with an inactivating e.g. point mutation in the *SMARCB1* sequence of the second allele. Compared to the other subgroups, and corresponding to the youngest age group affected, the tumours show a more open chromatin structure suggesting a more primitive epigenetic landscape. Also, CRINETs are reported to exhibit a DNA methylation pattern similar to AT/RT-TYR and express *TYR*. This raises the possibility that CRINETs and AT/RT-TYR may be two histological variants of a tumour with a common cell of origin. (Ho, Johann et al. 2020)

Elevated expression of the *MYC* oncogene as well as overexpression of several *HOX* cluster genes characterizes the AT/RT-MYC subgroup and distinguishes it from the AT/RT-TYR group. AT/RT- MYC tumours mainly arise upon a homozygous broad loss of the *SMARCB1* gene covering several hundred kilobase pairs. Similar to the AT/RT-TYR subgroup, tumours of the AT/RT-MYC subgroup appear more mesenchymal, but are found in young and also the oldest patients in the cohort (median age at diagnosis 27 months). Most of the AT/RT-MYC tumours were located supratentorially, and all spinal tumours were clustered into the AT/RT-MYC subgroup. Also, the rare adult cases of AT/RT were assigned to resemble entities of the AT/RT-MYC subgroup. Similarities between AT/RT-MYC tumours and extracranial MRTs for example occurring in the

kidney were highlighted by recent reports indicating a common cell of origin different from the other two identified subgroups of AT/RTs. (Ho, Johann et al. 2020)

Recently, Fruhwald, Hasselblatt et al. (2019) identified an age at diagnosis of <1 year and a non-AT/RT-TYR gene expression signature to be independent negative predictors of the overall survival of patients.

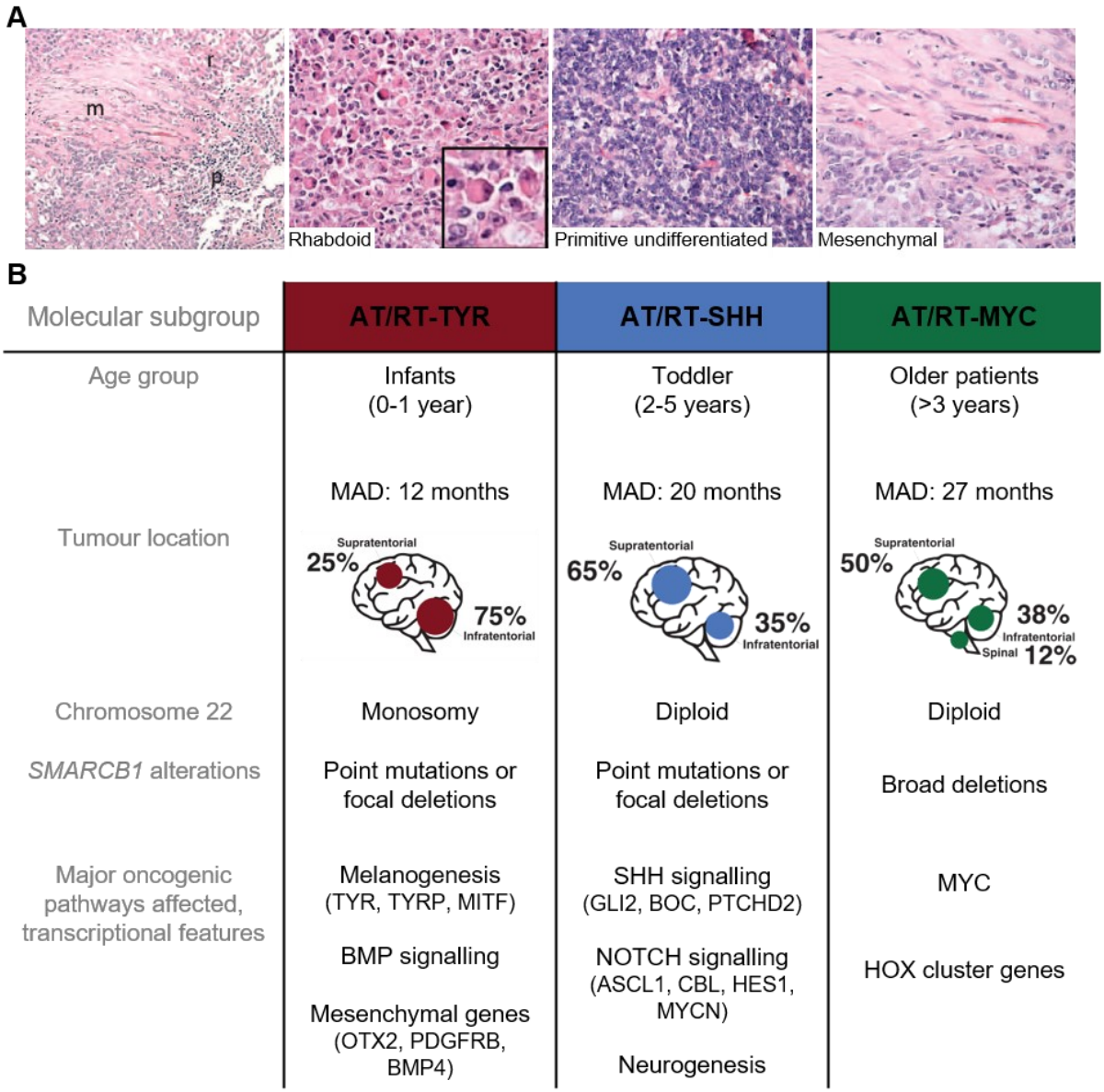

Figure 3: Summary of the main clinical characteristics of AT/RTs. **(A)** AT/RTs exhibit a heterogeneous histology with regions containing the characteristic rhabdoid, round cells with acentric nuclei and cytoplasmic eosinophilic inclusions consisting of whorls of intermediate filaments. Areas of rhabdoid cells are present aside regions exhibiting a primitive undifferentiated phenotype as well as areas of mesenchymal cells. Adapted from Sredni and Tomita (2015). **(B)** Summary of the consensus AT/RT molecular subgroup-defining properties by Ho, Johann et al. (2020), figure 5. MAD = median age at diagnosis, TYR = tyrosinase, TYRP = tyrosinase-related protein, MITF = melano-oncogene, BMP = bone morphogenic protein, OTX2 = orthodenticle homeobox 2, PDGFRB = platelet derived growth factor receptor B, SHH = Sonic Hedgehog, GLI2, BOC, PTCHD2 = SHH pathway members, ASCL1, CBL, HES1, MYCN = NOTCH pathway members, HOX = homeobox genes.

In summary, each subgroup has specific clinical and molecular characteristics which should be considered in the development of targeted therapies. Insights into the inhibition of sensitive processes should help to tailor therapy plans for each subgroup to finally improve each patient's outcome (Ho, Johann et al. 2020). By subgrouping it also was highlighted that the kind and extent of mutation affecting the *SMARCB1* gene may play a role in the phenotypical outcome. In general, mutations of the *SMARCB1* gene associated with the development of AT/RTs are truncating, nonsense, or frameshift mutations resulting in inactivation of both alleles and complete loss of gene expression (Versteege, Sevenet et al. 1998, Biegel, Tan et al. 2002). Heterozygous missense mutations of the *SMARCB1* gene are reported in the context of the neurodevelopmental disorder Coffin-Siris syndrome (CSS) (Tsurusaki, Okamoto et al. 2012). These diverse outcomes indicate that a specific type of germline mutation of the *SMARCB1* gene can lead to distinct disease phenotypes.

CSS is a rare congenital anomaly syndrome characterised by growth deficiency, intellectual disability, microcephaly, coarse facial features, hypoplastic nail of the fifth finger and/or toe, feeding difficulties in infancy, and numerous organ abnormalities, i.e. affecting the cardiovascular system, the gastrointestinal and genitourinary tract caused by mutations in BAF complex subunits (Figure 4B) (Coffin and Siris 1970, Tsurusaki, Okamoto et al. 2014, Alfert, Moreno et al. 2019). Mutations in *ARID1A* (BAF250a), *ARID1B* (BAF250b), *DPF2* (BAF45d), *SMARCA4* (BAF190), *SMARCE1* (BAF57), and in *SMARCB1* have been identified in patients with CSS (Tsurusaki, Okamoto et al. 2014). Mutational analysis of large patient cohorts identified the majority of patients exhibiting pathogenic variants in the *ARID1B* gene (Tsurusaki, Okamoto et al. 2012, Tsurusaki, Okamoto et al. 2014, Sekiguchi, Tsurusaki et al. 2019). However, missense mutations and small in-frame deletions in the *SMARCB1* gene were also observed frequently. Seven of the nine reported pathogenic variants in the *SMARCB1* gene associated with CSS cluster in exons 8 and 9, especially in the positively charged amino acid patch in the C-terminal coiled coil region of the highly conserved SNF5 domain (amino acids 363 to 377, Figure 4A). The *c.1091_1093del AGA* in-frame deletion of lysine residue 364 in exon 8 of the *SMARCB1* gene is the most recurring one of the pathogenic variants observed in CSS patients with mutations in the *SMARCB1* gene (Table 1) (Tsurusaki, Okamoto et al. 2012, Santen, Aten et al. 2013, Wieczorek, Bogershausen et al. 2013, Sekiguchi, Tsurusaki et al. 2019).

Table 1: Overview of the pathogenic variants of the *SMARCB1* gene identified in patients diagnosed with CSS

GENETIC VARIANT	ALTERATION	AFFECTED INDIVIDUALS
c.314G>A missense, exon 3	p.Arg105Gln	1 (Santen, Aten et al. 2013)
c.806A>G missense, exon 7	p.His269Arg	1 (Sekiguchi, Tsurusaki et al. 2019)
c.1052dup frameshift, exon 8	p.Leu352Thrfs*9	1 (Sekiguchi, Tsurusaki et al. 2019)
c.1087A>G missense, exon 8	p.Lys363Glu	1 (Sekiguchi, Tsurusaki et al. 2019)
c.1089G>T missense, exon 8	p.Lys363Asn	1 (Santen, Aten et al. 2013)
c.1091_1093del AGA deletion, exon 8	p.Lys364del	12 (Tsurusaki, Okamoto et al. 2012, Santen, Aten et al. 2013, Tsurusaki, Okamoto et al. 2014, Filatova, Rey et al. 2019, Sekiguchi, Tsurusaki et al. 2019)
c.1096C>T missense, exon 8	p.Arg366Cys	1 (Wieczorek, Bogershausen et al. 2013)
c.1096C>G missense, exon 8	p.Arg366Gly	1 (Sekiguchi, Tsurusaki et al. 2019)
c.1121G>A missense, exon 8	p.Arg374Gln	4 (Wieczorek, Bogershausen et al. 2013, Filatova, Rey et al. 2019, Sekiguchi, Tsurusaki et al. 2019)
c.1130G>A missense, exon 9	p.Arg377His	1 (Tsurusaki, Okamoto et al. 2012)

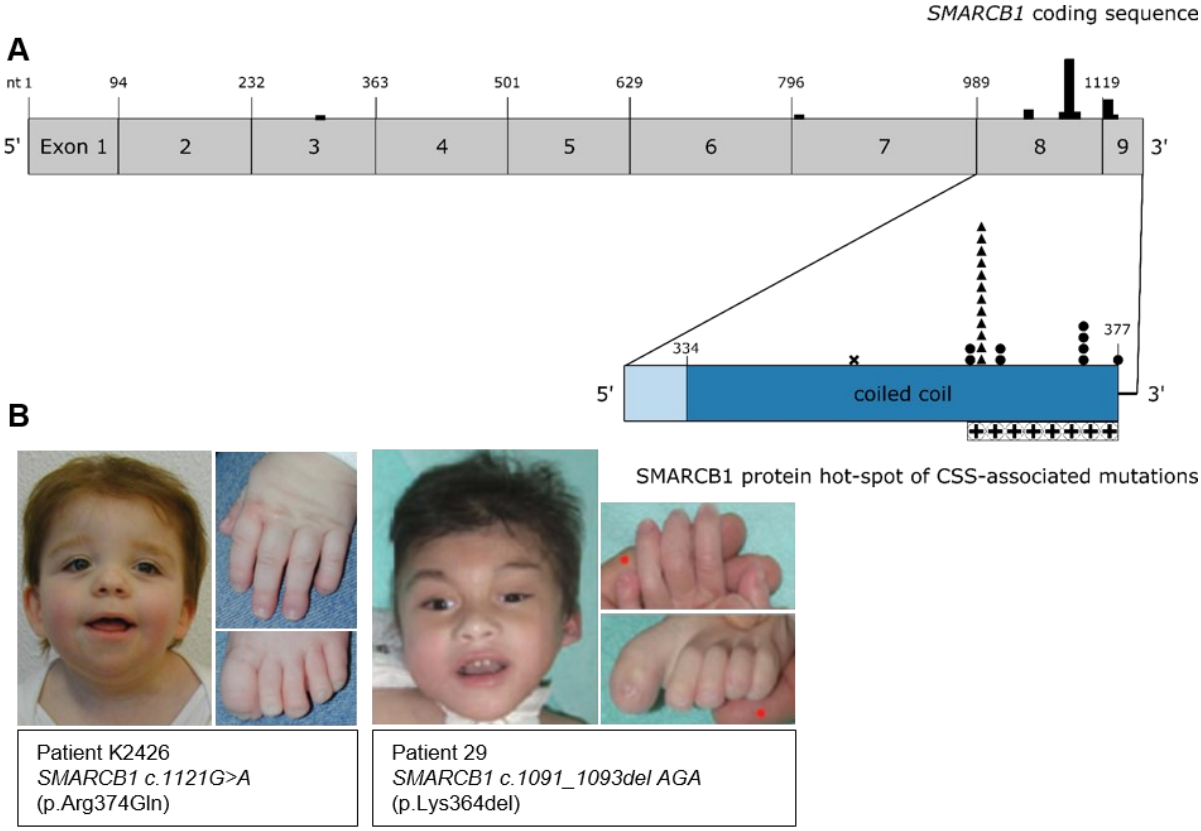

Figure 4: Anatomical and genetic characteristics of patients affected by CSS-associated mutations in the *SMARCB1* gene. **(A)** Graphical overview of the distribution of mutations in the *SMARCB1* gene identified in patients diagnosed with CSS on the gDNA and protein level. The black bars in the coding sequence of *SMARCB1* represent the position and frequency of the identified mutation which are specified in Table 1. Magnification of the mutational hot-spot of exon 8 and 9 of the *SMARCB1* gene displays the position, frequency, and type of the observed mutations on the protein level. The majority of the identified mutations cluster in the region of the positively charged amino acid patch between amino acid 363 and 377 in the coiled coil region of the highly conserved C-terminal SNF5 domain of SMARCB1. Twelve cases of CSS-patients affected by the *c.1091_1093del AGA* mutation in exon 8 (p.Lys364del) were identified in large patient cohorts. It is the most frequently recurring variant of *SMARCB1* found in CSS-patients. A black cross indicates a frameshift mutation, black circles stand for missense mutations, and black triangles represent small in-frame deletions. **(B)** Representative images of children diagnosed with CSS. Both patients carry mutations in the *SMARCB1* gene. Patient K2426 (Wieczorek, Bogershausen et al. 2013) is affected by the *SMARCB1 c.1121G>A* (p.Arg374Gln) missense mutation in exon 8, while patient 29 (Tsurusaki, Okamoto et al. 2014) carries the recurring in-frame deletion *c.1091_1093del AGA* (p.Lys364del) in exon 8 of the *SMARCB1* gene. Both children show the CSS-characteristic facial features (wide mouth with thick, everted upper and lower lips, a broad nasal bridge and nasal tip, thick eyebrows and long eyelashes) and hyperplastic finger and toenails as well as hypoplasia of the fifth distal phalanx.

Recently, the first mouse model recapitulating features of *SMARCB1*-associated CSS-like neurodevelopmental disorders was published by the Stem Cell and Developmental Biology group of the Technical University of Darmstadt (Filatova, Rey et al. 2019). The heterozygous nervous system-specific partial *loss-of-function* mutation of the *Smarcb1* gene by inversion of exon 1 resulted in a 30% decrease of *Smarcb1* transcript level, microcephaly, and several anatomical defects of the brain, i.e. agenesis of the corpus callosum, and choroid plexus hyperplasia (Filatova, Rey et al. 2019). The anatomical aberrations observed in these mutant mice were similar to the brain defects seen in magnetic resonance images of CSS-patients with mutations in different BAF complex components (Wieczorek, Bogershausen et al. 2013, Filatova, Rey et al. 2019). Comparison of this mouse model with

AT/RT mouse models further highlights the differential impact of the type of a germline mutation affecting the *SMARCB1* gene on brain and tumour development. A congenital complete loss of one allele of *Smarcb1* predisposes to the development of tumours, which occur upon spontaneous loss of the second allele, while partial loss of Smarcb1 protein function by inversion of exon 1 of the *Smarcb1* gene causes severe developmental defects in the brain of affected mice (Guidi, Sands et al. 2001, Filatova, Rey et al. 2019).

1.4. CRISPR/Cas9-mediated genome engineering

The CRISPR/Cas9 genome engineering tool is based on the clustered regularly interspaced palindromic repeat (CRISPR)/CRISPR-associated (Cas) type II archaeal and bacterial adaptive defence system to protect these organisms from the invasion of foreign plasmid or viral DNA (Horvath and Barrangou 2010, Jinek, Chylinski et al. 2012, Wiedenheft, Sternberg et al. 2012). The microbial immune response depends on *Cas* gene operons and CRISPR arrays, genome-targeting sequences (protospacers) interspersed with identical repeats. It consists of two phases. In phase one, the immunization or adaptive phase, organisms with one or more CRISPR loci respond to the challenge of invading nucleic acids by integrating a short fragment of the foreign sequence (protospacer) into the CRISPR array on its chromosome. After surviving this first infection, the organism has stored some genetic information on its attacker, which will be used to defend itself against a second infection in phase two of the bacterial immune response. In the subsequent immunity or expression and interference phase (phase two), transcription and processing of the CRISPR locus elements takes place. CRISPR RNAs (crRNAs) that guide Cas9 endonucleases to nucleic acid sequences complementary to the saved protospacer sequences are generated. In this process, the transactivating-crRNA (tracrRNA) hybridises to the repeat regions of the pre-crRNA transcribed from the repeat-protospacer array. In the presence of Cas9 this pre-crRNA:tracrRNA hybrid is cleaved by endogenous RNase III, and the 5' end of the spacer is removed resulting in a mature crRNA associated with tracrRNA and Cas9 protein. This ribonucleic protein complex then targets and cleaves complementary protospacer sequences in the invading plasmid or viral nucleic acid. Cas9-mediated site-specific cleavage requires complementary base-pairing between the mature crRNA and the target protospacer DNA in combination with a short, protospacer adjacent motif (PAM) on the target DNA to differentiate between self and non-self DNA targets (Figure 5A). Cas9-mediated cleavage of DNA is facilitated by the HNH- and RuvC1-homologous domains of the protein (Figure 5). (Horvath and Barrangou 2010, Jinek, Chylinski et al. 2012, Wiedenheft, Sternberg et al. 2012, Mali, Esvelt et al. 2013)

Utilization of this targeted DNA cleavage for genome editing in mammalian, i.e. human, cells was achieved by programming the CRISPR/Cas9 system of *Streptoccocus pyogenes* to target the Cas9 endonuclease to a specific genomic locus by a chimeric crRNA:tracrRNA hybrid (Jinek, Chylinski et al. 2012). This guide RNA (gRNA) is expressed from a human U6 RNA polymerase III promoter and combined with a human-codon-optimised Cas9 protein with a nuclear localisation signal (NLS) in a mammalian expression system (Figure 5B, C) (Cong, Ran et al. 2013, Mali, Yang et al. 2013). The

gRNA consists of the 20 nucleotides targeting protospacer sequence led by a guanine base, fused to a gRNA scaffold. In total, this gRNA-gRNA scaffold construct resembles the mature crRNA:tracrRNA hybrid necessary for Cas9 targeting and cleavage. With this programmable system, theoretically any genomic sequence in the form of 5' GN_{19-20} 3' directly followed by the 5' NGG 3' PAM sequence of *S. pyogenes* can be targeted (where N is any nucleotide), making the CRISPR/Cas9 system a versatile tool for targeted genome engineering in human cells (Mali, Yang et al. 2013, Ran, Hsu et al. 2013).

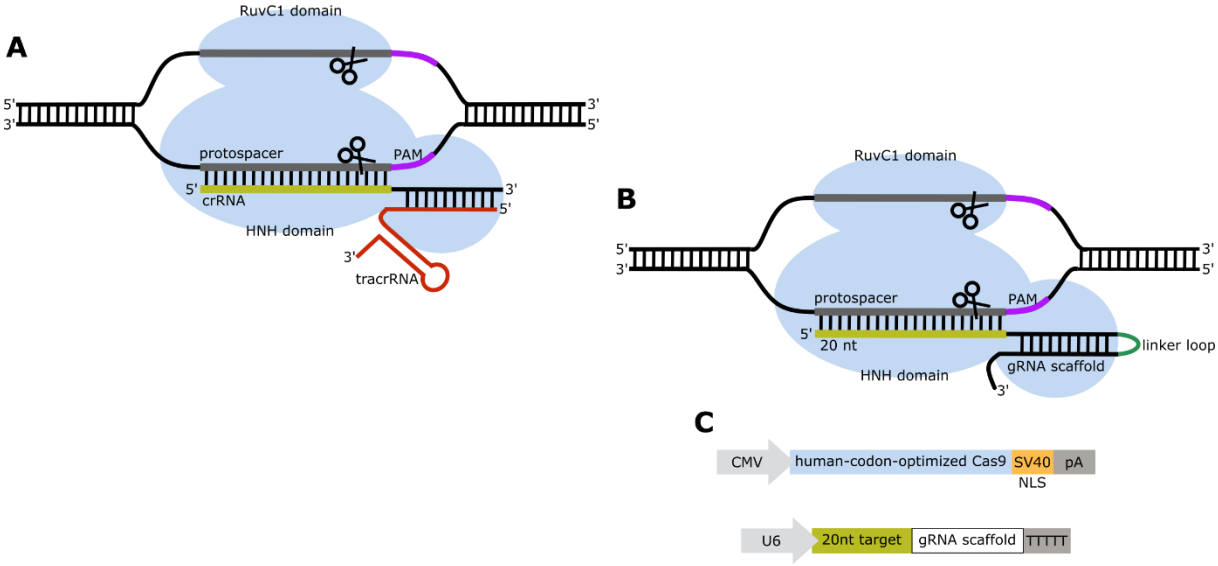

Figure 5: Graphical overview of the active CRISPR/Cas9 ribonucleic protein complex in microbial immune response and programmed for genome editing. **(A)** Depiction of the mature crRNA base-paired with the tracrRNA in the active Cas9 complex after detection of the complementary protospacer sequence in invaded foreign DNA. Scissors indicate the cleavage site of the endonuclease domains 3 bp upstream of the PAM. **(B)** Recombinant chimeric gRNA complexed by Cas9 programmed for targeted genome engineering bound to the 20 nt target sequence in the genome. The 20 nt complementary targeting crRNA is fused to a gRNA scaffold replacing the base paired region of the crRNA:tracrRNA hybrid connected by a linker loop. **(C)** Graphical summary of the mammalian expression system necessary for programmed CRISPR/Cas9-mediated genome engineering in human cells. The human-codon-optimised Cas9 with SV40 nuclear localisation signal (NLS) and polyA tail is expressed by a constitutively active cytomegalovirus (CMV) promoter. The gRNA expression cassette is expressed by the human U6 RNA polymerase III promoter and contains the variable 20 nt target sequence directly upstream of the gRNA scaffold. Adapted from Jinek, Chylinski et al. (2012) and Mali, Yang et al. (2013).

Mechanistically, CRISPR/Cas9-mediated genome editing starts with the binding of a gRNA to the primary binding channel of Cas9, activating it to the gRNA-directed target DNA search mode. As soon as it has found the target protospacer DNA, the Cas9/gRNA complex binds to the protospacer DNA. In cooperation with the PAM interacting domain of Cas9, the gRNA starts interrogating the double-stranded DNA by base pairing starting from the PAM proximal position. The primary binding channel of Cas9 gradually changes its conformation to bind the gRNA/target DNA heteroduplex, while the non-target DNA strand is bound by the minor binding channel of Cas9. As the base-pairing process continues to the PAM distal end of the complementary 20 nt target sequence, the HNH endonuclease domain of Cas9 turns by 180° until it is perfectly positioned near the third nucleotide position of the target DNA strand proximal to the PAM. Meanwhile the RuvC1 domain of Cas9 is changed from the buried to the exposed state, and is positioned at the HNH-respective location on the non-target DNA strand. Upon correct positioning, the nuclease activity of HNH and RuvC1 domains

breaks both strands simultaneously resulting in a blunt ended DNA double strand break (DSB) three base pairs upstream of the PAM sequence (Figure 5B) (Zhang, Adikaram et al. 2016).

The generated DSB activates the cellular DNA damage response and recruits the DNA repair machinery (Ran, Hsu et al. 2013). Repair of the DSB promotes gene editing by either of one DNA repair pathways. Most DSBs are repaired by the predominant, error prone non-homologous end joining (NHEJ) pathway. During NHEJ, the DSB ends are processed by nucleases, and are subsequently re-joined by ligase IV (Cahill, Connor et al. 2006, Ran, Hsu et al. 2013). DSB repair via NHEJ can result in small insertions or deletions (indel), which can cause the *knock-out* of the targeted gene if the indel leads to a frameshift or a pre-mature stop codon in the coding region of the gene (Cong, Ran et al. 2013, Ran, Hsu et al. 2013). In the presence of a sister chromatid or an exogenous repair template (plasmid or single-stranded oligonucleotide) in late S/G2-phase of the cell cycle, DSBs can also be repaired by the homology directed repair (HDR) pathway (Cahill, Connor et al. 2006). During HDR, the processed DSB ends are coated by Rad51 and form double Holliday junctions with a homologous repair template to complement the lost genetic information by copying the presumably correct sequence (Cahill, Connor et al. 2006, Ran, Hsu et al. 2013). Exploiting this mechanism, the cell can be tricked into integrating new sequences, e.g. reporter genes, flanked by sequences homologous to the genetic information up- and downstream of the Cas9-mediated DSB resulting in a precisely edited *knock-in* (Ran, Hsu et al. 2013).

Different studies identified specificity issues when editing a genome by CRISPR/Cas9 due to mismatch tolerance in the gRNA sequence (Cong, Ran et al. 2013, Fu, Foden et al. 2013). Even though off-target editing events are rare, DSB generation and indel insertion at off-target sites present a major obstacle for the use of CRISPR/Cas9 for the generation of specific, single mutation disease models or cell therapy applications (Fu, Foden et al. 2013, He, Tan et al. 2016). Point mutations of catalytic residues of the Cas9 HNH or RuvC1 endonuclease domain can selectively inactivate one domain leading to a DNA single-strand nick upon targeting by a gRNA (Jinek, Chylinski et al. 2012). These nicks are predominantly repaired by the high-fidelity base excision repair pathway (Ran, Hsu et al. 2013). Combination of two offset gRNAs with a Cas9 nickase containing a p.Asp10Ala (D10A) mutation in its RuvC1 endonuclease domain (Cas9n) generates readily repaired single-strand nicks at all off-target sides of each gRNA, but a DSB only at the on-target site where both gRNAs bind in close proximity (Figure 6) (Ran, Hsu et al. 2013). This DSB then triggers the cellular DNA damage response and is repaired either by NHEJ or HDR as described above (Ran, Hsu et al. 2013).

Figure 6: Visualization of the DSB generation by a pair of Cas9n/gRNA complexes. D10A mutation of the catalytic aspartic acid residue of the RuvC1 domain (grey) of Cas9 diminishes the endonuclease activity of this domain. Thereby, only the complementary DNA strand can be cleaved by the HNH domain of Cas9 resulting in a DNA single-strand nick. Combination of two offset gRNAs with Cas9n results in a DSB with cohesive ends by simultaneous nicking both DNA strands. gRNA offset is defined as the distance between the PAM-distal (5') ends of the 20 nt targeting sequence of a given gRNA pair. Adapted from Ran, Hsu et al. (2013).

Taking these studies into consideration, both, a conventional and a double nicking approach were applied for the CRISPR/Cas9-mediated genome editing of hiPSCs and MCF10A cells in this thesis. The selection of the gRNA sequences and the design of the HDR construct were based on the recommendations made by Ran, Hsu et al. (2013). The HDR construct was optimised to prevent re-cutting of edited loci (Hendriks, Warren et al. 2016). CRISPR/Cas9-mediated cleavage of DNA was shown to be dependent on the presence of the 5' NGG 3' PAM sequence (Jinek, Chylinski et al. 2012, Zheng, Hou et al. 2017). Silent mutations in the -3 position of the PAM at the 3' end of the PAM are not tolerated and ablate CRISPR/Cas9-mediated DNA cleavage. A silent mutation at this position was introduced in the homologous sequences of the HDR constructs to prevent re-cutting after insertion (Zheng, Hou et al. 2017). If the introduction of a silent mutation of the -3 position of the PAM was not possible, position -2 was mutated guanine to either thymine or cytosine. Both mutations were shown to remarkably reduce Cas9 cleavage activity (Zheng, Hou et al. 2017). In some cases, silent mutation of the PAM was not possible since base exchange of either guanine residue of the PAM site would have resulted in an amino acid exchange. In these cases, the profound compromising effects of mismatches in the core sequence of the gRNA (positions +4 to +6/+7, counting 3' to 5' starting at the PAM proximal position) were exploited (Zheng, Hou et al. 2017). A single mismatch in these bases was shown to prevent base-pairing between the gRNA and target DNA, and thus provides three to four additional positions for the insertion of a silent mutation to prevent re-cutting after genome editing (Zheng, Hou et al. 2017).

1.5. Aim of this thesis

This thesis had three aims: the establishment and optimisation of methods for the introduction of AT/RT and CSS-associated *SMARCB1* mutations into human cells by CRISPR/Cas9-mediated genome engineering, and the establishment and optimisation of the transduction of mouse neurospheres (NSPs) to analyse the effect of overexpression of *Hes5* on *Smarcb1*-mutated neurosphere-forming cells (NSPs contain neural stem (NSCs) and progenitor cells (NPCs)).

For the generation of the hiPSC- and MCF10A *SMARCB1* mutant cell lines, a strategy for CRISPR/Cas9-mediated insertion of promoterless selectable fluorescence reporter cassettes and loxP sites co-expressed with mutant *SMARCB1* gene variants was established. The MCF10A cell line was

chosen to be CRISPR/Cas9-mediated genome engineered at the *SMARCB1* locus since MCF10A cells are diploid for chromosome 22 while showing higher DNA transfer efficiencies compared to hiPSCs and could have represented an adequate intermediate model until the establishment of the hiPSC models (Marella, Malyavantham et al. 2009). For the hiPSC line with AT/RT-associated *SMARCB1* mutations, a CRISPR/Cas9(n)-mediated genome engineering strategy to generate cells which co-express the *SMARCB1* gene with three different fluorescence reporters was established and optimised. The insertion of loxP sites up- and downstream of the engineered locus allows a removal of the complete genomic sequence of *SMARCB1* and the flanking reporter genes by *Cre* recombination. This design allows the inactivation of the *SMARCB1* gene at any developmental stage upon introduction of *Cre*, e.g. by lentiviral transduction. This inactivation could be homo- or heterozygous, dependent on the presence of loxP sites on both or only one allele of *SMARCB1* (Figure 7).

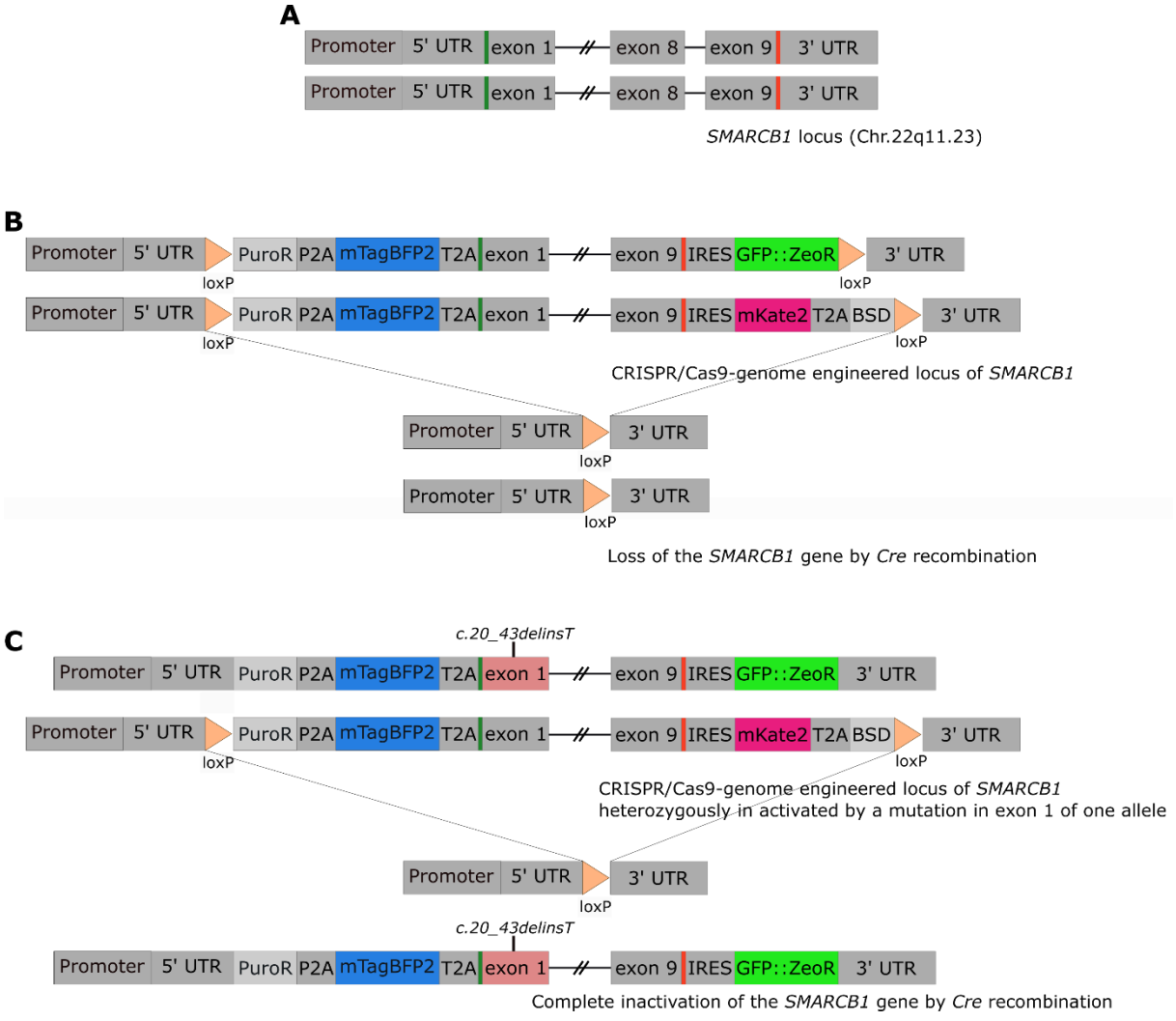

Figure 7: Graphical overview of the envisaged CRISPR/Cas9- genome engineered human *SMARCB1* locus in the three-colour reporter system. **(A)** The wildtype *SMARCB1* locus. **(B)** The *SMARCB1* locus in the AT/RT cell model for homozygous deletion of the whole sequence of *SMARCB1* and the result of *Cre* recombination. **(C)** Mutation of exon 1 (depicted as an example) or exon 9 in one HDR construct used for insertion of the reporter cassettes would introduce the nonsense mutations identified in AT/RT patients.

In addition to the complete deletion of the *SMARCB1* gene, other types of AT/RT-associated mutations were included in the *SMARCB1* mutated human cell lines. Therefore, HDR constructs were generated to facilitate inactivation of *SMARCB1* by the combination of the heterozygous loss of the complete *SMARCB1* coding sequence with the heterozygous inactivation of *SMARCB1* by AT/RT-associated nonsense point mutations in one cell (Figure 7C). Since the insertion of the point mutations would also be linked to the insertion of a reporter cassette, the mutations had to be located in the first or last exon of the *SMARCB1* gene. Literature research identified several cases of AT/RT with the *c.1148delC* mutation in exon 9 of the *SMARCB1* gene (Biegel, Tan et al. 2002, Kordes, Gesk et al. 2010). Additionally, two mutations in exon 1 of the *SMARCB1* gene were reported in the germline of AT/RT patients (*c.20_43delins T*, *c.93G>C*) (Eaton, Tooke et al. 2011). With this array of human cell lines with AT/RT-associated *SMARCB1* mutations, the genetic background and possibly the different tumour subtypes observed in AT/RT patients could be modelled.

To generate a human cell model for the CSS-associated mutation of the *SMARCB1* gene, the frequently observed deletion of lysine residue 364 in exon 8 of the *SMARCB1* gene (*c.1091_1093del AGA*) was selected (Table 1). This mutation was included in the HDR construct for the insertion of a reporter downstream of the native stop codon of the *SMARCB1* gene and would be combined with insertion of another reporter on the second, wildtype allele of *SMARCB1* (Figure 8). These genetic alterations were designed to be introduced in hiPSC and MCF10A cells. The hiPSC lines with CSS-associated *SMARCB1* mutations should be used to better understand the cellular consequences of the *c.1091_1093del AGA* mutation during embryonic organ, i.e. brain, development, which are observed in CSS patients and in the mouse model recapitulating *SMARCB1*-associated CSS.

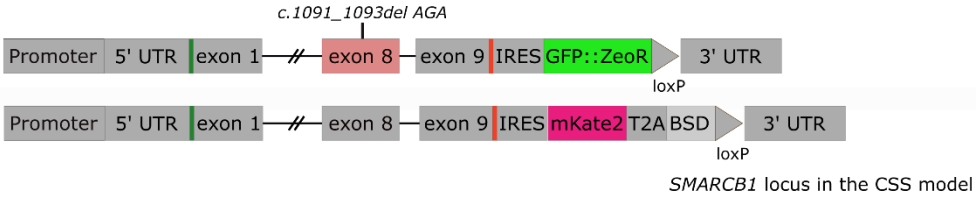

Figure 8: Graphical depiction of the human *SMARCB1* locus after genome engineering to introduce the CSS-associated mutation. The *c.1091_1093del AGA* mutation in exon 8 was introduced into the HDR construct designed for insertion of the eGFP::ZeoR reporter cassette.

Both, the hiPSC- and MCF10A cell lines with CSS-associated *SMARCB1* mutations could in principle be used to analyse the effect of the mutation on the expression of *SMARCB1* from each of its alleles by e.g. RT-qPCR analysis of the transcription of the co-expressed reporter genes (Figure 9). hiPSC and MCF10A cells expressing the *SMARCB1* gene with point mutations associated either with AT/RT or CSS could help to identify the cellular mechanisms underlying tumour formation and CSS upon specific congenital alteration of the *SMARCB1* sequence.

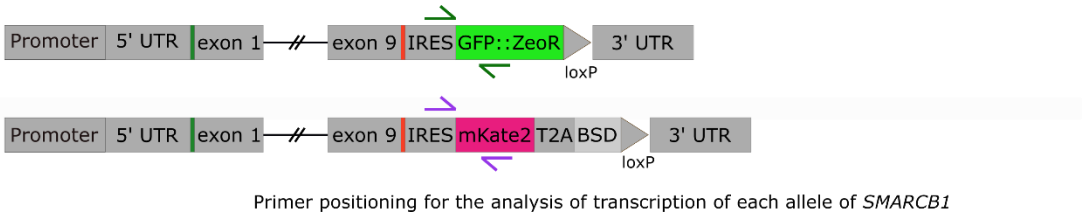

Figure 9: Primer positioning for the allele-specific RT-qPCR analysis of the expression of each allele of the *SMARCB1* gene in the engineered locus. The introduction of AT/RT or CSS-specific point mutations allows to analyse the effect of either mutation on the expression of the mutated and wildtype allele.

AT/RT-associated inactivation of the *SMARCB1* gene by *Cre* recombinase in MCF10A cells, similar to hiPSCs, could also help to understand how cells cope with loss of *SMARCB1*. Comparison of gene expression changes observed in MCF10A cells to the changes observed in hiPSCs upon loss of *SMARCB1* gene expression could hint to coping mechanisms activated independent of the developmental state of the cell, which could present potential targets for tumour treatment.

Another aim of this thesis was the establishment of methods to overexpress *Hes5* in neurosphere-forming cells. Murine NSCs/NPCs isolated from *Smarcb1*$^{+/inv}$ *NesCre*$^{+/-}$ mice, the first mouse model recapitulating *SMARCB1*-associated CSS recently published by the Stem Cell and Developmental Biology group of the Technical University of Darmstadt, showed diminished sphere forming abilities. Neurospheres (NSPs) are three-dimensional floating spheroid cell clusters that arise from NSP-forming cells, which can be both NSCs or NPCs, isolated from the mammalian CNS (Jensen and Parmar 2006, Singec, Knoth et al. 2006, Pastrana, Silva-Vargas et al. 2011). Upon *in vitro* cultivation, the heterogeneity of NSPs increases and aside from proliferative, NSP-forming NSCs and NPCs, also post-mitotic neurons and glia cells can be found within one sphere (Jensen and Parmar 2006). Nonetheless, NSP culture can be applied as a functional assay and is a useful tool to analyse proliferation, self-renewal capacity, and multipotency of the NSP-forming NSCs and NPCs over serial clonal passages (Jensen and Parmar 2006). Therefore, a loss of sphere forming ability as observed in cells isolated from mutant brains in Filatova, Rey et al. (2019) indicates a lack of cells presenting NSC or NPC characteristics in the NSP culture system e.g. due to impairment of NSC maintenance or loss of self-renewal in NSCs and NPCs. Additionally, RNA *in situ* hybridisation analyses revealed reduced expression of *Hes5* in the radial glia cell (RGC) population of the glial wedge in *Smarcb1*$^{+/inv}$ *NesCre*$^{+/-}$ brain sections of E15.5 mice (Filatova, Rey et al. 2019). These findings led to the hypothesis that overexpression of *Hes5* in *Smarcb1*$^{+/inv}$ *NesCre*$^{+/-}$ NSCs could potentially rescue their sphere forming abilities. Therefore, the transduction of NSP-forming cells isolated from *Smarcb1*$^{+/inv}$ *NesCre*$^{-/-}$ mice (E15.5), which possess sphere forming abilities, was established and optimised to generate a system in which *Cre* recombinase and *Hes5* could be overexpressed to test the hypothesis. Expression of *Cre* recombinase inverts the floxed exon 1 of the *Smarcb1* gene in the infected cells. The inversion is reversible and continues forth and back as long as *Cre* is expressed (Filatova, Rey et al. 2019). Thereby, some of the NSP-forming cells would exhibit a genotype analogous to the mice in the CSS-model and

would be expected to lose their sphere forming abilities. Simultaneous overexpression of *Hes5* might rescue the partial *loss-of-function* of *Smarcb1* occurring upon heterozygous inversion of exon 1 (Figure 10).

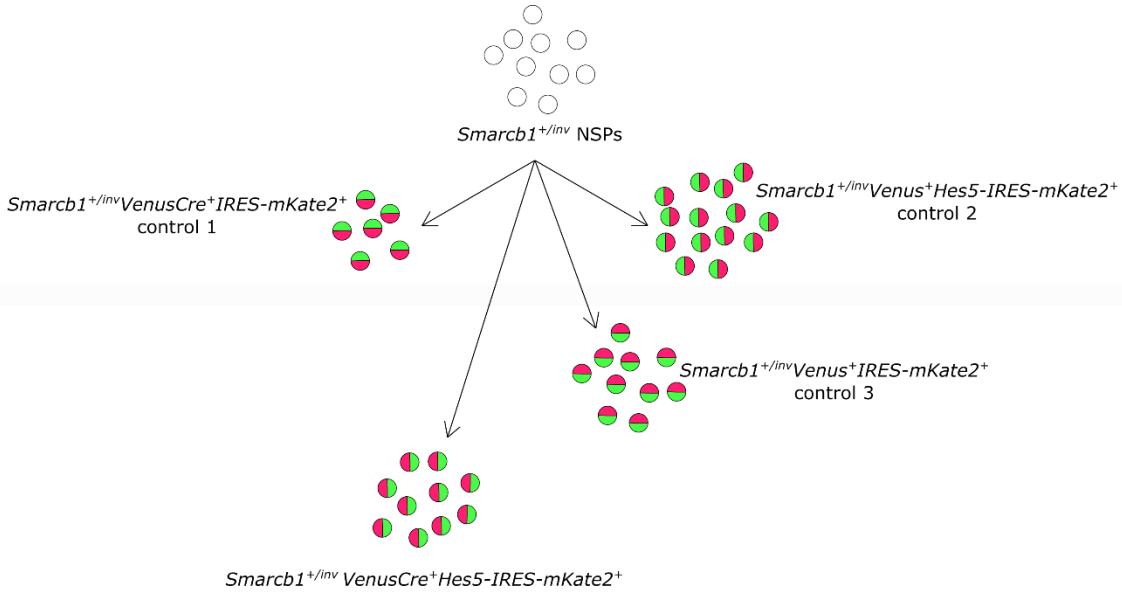

Figure 10: Experimental design to test the hypothesis if overexpression of *Hes5* can rescue the impaired sphere forming ability of murine NSP-forming cells upon continuous inversion of exon 1 of the *Smarcb1* gene. *Smarcb1*$^{+/inv}$ NSPs should be transduced with lentiviral particles transferring a Venus*Cre* and a *Hes5*-IRES-mKate2 expression system (*Smarcb1*$^{+/inv}$ *VenusCre*$^{+}$ *Hes5-IRES-mKate2*$^{+}$ NSPs, red halves on the left). Upon expression of Venus*Cre*, the transduced NSP-forming cells would inverse the loxP-flanked exon 1 of the *Smarcb1* gene. *Smarcb1*$^{+/inv}$ *VenusCre*$^{+}$ *IRES-mKate2*$^{+}$ NSP-forming cells (red halves on the bottom, control 1) are hypothesised to lose their sphere forming ability, similar to the *Smarcb1*$^{+/inv}$ *NesCre*$^{+/-}$ NSCs/NPCs (Filatova, Rey et al. 2019). Overexpression of *Hes5* in NSP-forming cells is hypothesised to enhance the sphere forming ability of transduced NSPs, resulting in an increase of sphere number, due to its role in the maintenance of NSCs (*Smarcb1*$^{+/inv}$ *Venus*$^{+}$ *Hes5-IRES-mKate2*$^{+}$ NSPs, red halves on the right, control 2) (Kageyama, Ohtsuka et al. 2008). Simultaneous presence of both expression systems is hypothesised to rescue the impairment in sphere formation caused by the inversion of exon 1 of the *Smarcb1* gene, thereby increasing the number of spheres observed compared to NSP-forming cells expressing only Venus*Cre* (*Smarcb1*$^{+/inv}$ *VenusCre*$^{+}$ *Hes5-IRES-mKate2*$^{+}$ NSPs, red halves on the left). As control for the impact of the effect of the transduction and subsequent overexpression of the fluorescence genes, expression systems only encoding eGFP or mKate2, without *Cre* recombinase or *Hes5* coding sequence respectively, are used (*Smarcb1*$^{+/inv}$ *Venus*$^{+}$ *IRES-mKate2*$^{+}$ NSPs, red halves on the top, control 3).

2. Materials and methods

2.1. Molecular biology methods

2.1.1. Polymerase chain reaction (PCR) amplification of DNA

Polymerase chain reaction (PCR) is a basic molecular biology method used to amplify specific sequences of DNA from different kinds of DNA templates, e.g. genomic, plasmid or bacterial DNA. In a thermal cycling reaction DNA polymerase adds free nucleotides to primers, initial building blocks of DNA. Primers are short oligonucleotides (typically ≥18 bp) complementary to the 3' ends of the sense and antisense strands of the DNA sequence which is amplified and thus have to be custom-made for each sequence. A list of all oligonucleotides ordered at Sigma Aldrich and used in this work can be found in the appendix (section 7.1.1).

In the first step, the PCR reaction is heated to 98° C to initially separate the template's DNA strands (denaturation). After this, the thermal cycling starts. Every cycle is composed of a denaturation step (98°C, 10 to 30 seconds), followed by reduction of the temperature allowing primer annealing to the template strands (10 to 30 seconds; each primer's melting temperature has to be identified using the IDT OligoAnalyzer, https://eu.idtdna.com/calc/analyzer). The reaction is completed by an extension step at 72° C during which the DNA polymerase condenses the 5'-phosphate groups of the free deoxyribonucleotide triphosphates (dNTPs) to the 3'-hydroxyl group of the nascent DNA strand. In a standard reaction, this thermal cycle is repeated 25 to 35 times before a final extension step (72° C, 2 to 10 minutes) completes the amplification process.

For cloning purposes, Phusion or Q5 High-Fidelity DNA polymerases (NEB, M0530 or M0491) were used. These DNA polymerases are characterised by fast amplification and extremely low amplification error rates. PCR reactions using Phusion or Q5 High-Fidelity DNA polymerases were set up on ice following the pipetting scheme of Table 2.

Table 2: Set up of PCR reactions using Phusion of Q5 High-Fidelity DNA polymerases.

REACTION COMPONENT	FINAL CONCENTRATION	VOLUME
5x Q5 Reaction Buffer OR 5x Phusion HF Buffer	1x	10 µL
5x Q5 GC Enhancer (optional)	1x	10 µL
10 mM dNTPs (N0446S, NEB)	200 µM	1 µL
10 µM Forward Primer	0.5 µM	2.5 µL
10 µM Reverse Primer	0.5 µM	2.5 µL
Q5 High-Fidelity DNA polymerase	0.02 U[1]/µL	0.5 µL
Template DNA	10-100 ng	x µL
Nuclease free water		Add to 50 µL

[1] 1 Unit of enzyme is defined as the amount of enzyme that will incorporate 10 nmol of dNTP into acid insoluble material in 30 minutes at 74° C (https://international.neb.com/products/m0491-q5-high-fidelity-dna-polymerase#Product%20Information_Properties%20&%20Usage, November 30, 2019)

The PCR mixture was placed in a thermal cycler (peqSTAR 2x Universal Gradient, 732-2889DE, VWR) running the following programme (Table 3).

Table 3: Thermal cycling programme for PCR reactions setup with Phusion or Q5 High-Fidelity DNA polymerases.

PCR STEP	TEMPERATURE	TIME
Initial Denaturation	98° C	30 seconds
25-35 Cycles: Denaturation	98° C	10 seconds
Annealing	[2]50-72° C	10 seconds
Extension	72° C	15-20 seconds/kb
Final Extension	72° C	2 minutes
Hold	15° C	∞

PCR amplified DNA sequences were analysed by agarose gel electrophoresis (section 2.1.4) and, if necessary, purified for further processing.

2.1.2. Purification of DNA samples

Purification of DNA samples after processing e.g. after PCR or restriction endonuclease digestion is necessary to remove salts and enzymes from the mixture yielding pure DNA (A260/A280 > 1.8) which can be further used for various downstream applications.

Purification of DNA samples using the Clean & Concentrator-5 Kit (D4004, Zymo Research)

The Zymo Clean & Concentrator-5 Kit was used to purify processed DNA samples containing only one specific DNA sequence. For example, after PCR amplification of a specific sequence or restriction endonuclease digestion, yielding only one fragment of DNA as after digestion of a PCR product or plasmid linearization. The DNA samples were processed as described in the manufacturer's handbook[3]. In brief: In a 1.5 mL microcentrifuge tube, five volumes of DNA Binding Buffer were added to each volume of DNA sample and mixed briefly by vortexing or pipetting (e.g. 50 µL DNA sample + 250 µL of DNA Binding Buffer). The mixture was transferred to an uncapped Zymo-Spin Column in a collection tube and centrifuged for 30 seconds at maximum speed (21,700 xg). The flow-through was discarded. 200 µL of DNA Wash Buffer (diluted with 100% ethanol) was added to the column and centrifuged for 30 seconds at maximum speed. This wash step was repeated once. The column was transferred to a sterile 1.5 mL microcentrifuge tube, 15 µL of pre-warmed (55° C) nuclease-free water were added directly to the column matrix, and incubated at room temperature for five minutes. Finally, the DNA was eluted by centrifugation at maximum speed for 60 seconds. DNA concentration and purity were determined using the NanoDrop2000c (software version 1.6, Thermo Scientific) and 1 µL of the purified DNA sample.

[2] Primer melting temperature as calculated by IDR OligoAnalyzer https://eu.idtdna.com/calc/analyzer

[3] https://files.zymoresearch.com/protocols/_D4003T_D4003_D4004_D4013_D4014_DNA_Clean_Concentrator_-5_ver_1_2_1_LKN-SW__1.pdf, November 24, 2019

Purification of DNA samples using the GeneJET Gel extraction kit (K0692, Thermo Scientific)
DNA samples containing fragments of different size are separated by agarose gel electrophoresis in 1x TAE buffer (section 2.1.4). Purification of the separated and excised DNA bands is achieved with the GeneJET Gel extraction kit. The excised agarose gel slices are processed as described in the manufacturers protocol[4]. In brief: Binding buffer was added 1:1 to the gel slice (volume:weight, e.g. 100 µL Binding buffer to each 100 mg of agarose gel) and incubated at 55° C for 10 minutes while rapidly shaking. It was ensured that the gel was completely dissolved before proceeding to the next step. The solubilised gel solution was transferred to a GeneJET purification column and centrifuged at maximum speed (21,700 xg) for 60 seconds. The flow-through was discarded. This step was repeated until all solution was passed through the column. 700 µL of Wash Buffer (diluted with 100% ethanol) was added to the column, and centrifuged at maximum speed for 60 seconds. The wash step was repeated once. The empty column was centrifuged at maximum speed for two minutes to dry the column matrix completely. Following this, the column was transferred to a sterile 1.5 mL microcentrifuge tube, 25 µL of pre-warmed (55° C) nuclease-free water were added directly to the column matrix and incubated at room temperature for five minutes. Finally, the DNA was eluted by centrifuging at maximum speed for 60 seconds. DNA concentration and purity were determined using the NanoDrop2000c (software version 1.6, Thermo Scientific) and 1 µL of the purified DNA sample.

2.1.3. Restriction endonuclease digestion

Restriction endonucleases are enzymes which recognise specific sequences of typically six to eight bases and cleave the DNA within or close to these recognition sites. Cloning of DNA fragments can be achieved by using restriction endonuclease recognition sites present in both the plasmid and insert sequences. If specific cloning cannot be achieved by the given recognition sites and their corresponding restriction endonucleases, suitable recognition sequences need to be added to the 5' end of PCR primers[5]. Efficient cleavage close to the ends of the PCR amplified sequences has to be enabled by adding sufficient bases 5' of the recognition sequence. The number of added bases required for efficient cleavage of the used New England Biolabs (Masliah-Planchon, Bieche et al.) restriction endonucleases, can be found online (https://www.neb.com/tools-and-resources/usage-guidelines/cleavage-close-to-the-end-of-dna-fragments).
The NEB restriction endonucleases available in the laboratory are listed in the appendix (section 7.1.2). Restriction endonuclease digestion reactions were set up on ice following the scheme of Table 4:

[4] https://assets.thermofisher.com/TFS-Assets/LSG/manuals/MAN0012661_GeneJET_Gel_Extraction_UG.pdf, November 24, 2019
[5] https://www.neb.com/applications/cloning-and-synthetic-biology/dna-preparation/restriction-enzyme-digestion#tabselect3, October 27, 2019

Table 4: Reaction setup of restriction endonuclease digestions of DNA.

REACTION COMPONENT	VOLUME, µL
DNA (up to 10 µg)	x µL
Restriction endonuclease 1, 1 U[6]/µg of DNA (Masliah-Planchon, Bieche et al.)	0.2-1.5 µL
Restriction endonuclease 1, 1 U/µg of DNA (Masliah-Planchon, Bieche et al.)	0.2-1.5 µL
10x Reaction buffer e.g. CutSmart (Masliah-Planchon, Bieche et al.)	5 µL
Nuclease free water	Add to 50 µL

The restriction endonuclease reactions were incubated at the appropriate reaction temperature, mostly 37° C, for 30 minutes to three hours. If applicable, the enzymes were inactivated at the required inactivation temperature (section 7.1.2). Subsequently, the DNA sample was purified as described in section 2.1.2 to remove the enzymes.

2.1.4. Agarose gel electrophoresis

Agarose gel electrophoresis is an effective and simple way to separate DNA fragments of different sizes. Agarose is a mixture of L- and D-galactose subunits which form non-covalently interacting bundles. The density of these bundles and thus, the pore size of the agarose gel depends on the agarose concentration. The higher the concentration of agarose in the mixture, the smaller the pores in the resulting gel. For separation of smaller DNA fragments, a higher concentration of agarose and for larger fragments a lower concentration of agarose is used (Table 5). The agarose gel electrophoresis is run in an electrophoresis chamber filled with 1x TAE (Tris-acetate-EDTA, Table 6) buffer. Application of an electric current facilitates separation of the DNA sample. Based on the negative charge of the phosphate backbone of the DNA, the DNA fragments migrate through the agarose gel towards the positively charged anode. The distance migrated in the electric field is inversely proportional to the log of the fragments' molecular weight due to DNA's uniform mass to charge ratio. All samples were supplemented with 1x loading dye (Table 7), applied to the pre-cast wells of the agarose gel, and separated at 90 to 120 V for 30 to 60 minutes. For each gel, a DNA standard (N3231 for 100 bp to 1,517 bp, N3232 500 bp to 10,000 bp, NEB, Figure 11) was added to determine each DNA band's fragment size. The separated DNA fragments were visualised using UV light. Therefore, a staining agent that binds to the minor groove of helical nucleic acids and emits a green fluorescent light when excited by UV light (Roti-GelStain, 3865, Carl Roth, 1 µL/20 mL of TAE buffer)[7] was supplemented in the agarose gel.

[6] 1 U = 1 unit of restriction enzyme completely digests 1 µg of substrate DNA in a 50 µL reaction in 60 minutes, https://international.neb.com/protocols/2012/12/07/optimizing-restriction-endonuclease-reactions, October 27, 2019

[7] https://www.carlroth.com/downloads/ba/en/3/BA_3865_EN.pdf, December 10, 2019

Table 5: Concentration of agarose recommended for different sizes of DNA fragments.

AGAROSE CONCENTRATION	SIZE OF DNA FRAGMENTS
1%	>1,000 bp
2%	<1,000 bp

Table 6: Formula of 50x Tris-acetate-EDTA (TAE) buffer for agarose gel electrophoresis.

REAGENT	AMOUNT
Tris base (4855.1, Carl Roth)	121 g
0.5 M EDTA pH 8.0 (E6758, Sigma Aldrich)	50 mL
Acetic acid (100063, Merck)	28.55 mL

Add $H_2O_{dest.}$ to 500 mL.

For agarose gel electrophoresis, a 1X TAE buffer was used.

Table 7: Composition of 6x loading dye for supplementation of DNA samples for agarose gel electrophoresis.

REAGENT	FINAL CONCENTRATION	AMOUNT
Ficoll-400 (CN90.1, Carl Roth)	15%	7.5 g
1 M Tris-HCl pH 8.0	20 mM	1.0 mL
0.5 M EDTA	60 mM	6.0 mL
SDS (1.12533.0250, Merck)	0.48%	0.24 g
Xylene Cyanol (1.10590.0005, Merck)	0.03%	0.015 g
Orange G (15925, Merck)	0.12%	0.06 g

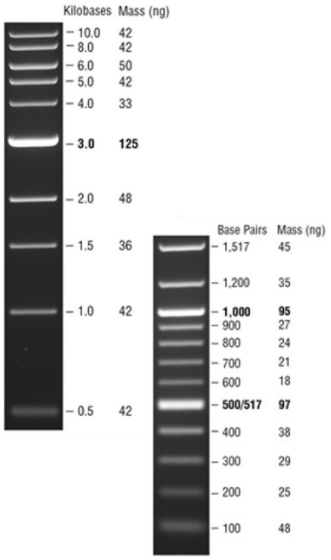

Figure 11: DNA standards for agarose gel electrophoresis, ref. https://international.neb.com/products/n3232-1-kb-dna-ladder#Product%20Information;https://international.neb.com/products/n3231-100-bp-dna-ladder#Product%20Information, January 06, 2020

2.1.5. Blunting of cohesive DNA ends

In some cases, molecular cloning via complementary cohesive 5' and 3' DNA overhangs is not possible. Thus, the blunting of cohesive DNA ends is adopted in cases in which no restriction endonuclease site that generates blunt DNA ends can be used. The cohesive DNA overhangs resulting from restriction endonuclease digestion are removed by T4 DNA polymerase (M0203, NEB). T4 DNA polymerase exhibits 5' to 3' polymerase and 3' to 5' exonuclease activity. By these activities, the enzyme fills in 5' recessed ends and resects 3' overhanging bases.[8] DNA end blunting reactions were set up on ice as follows (Table 8).

Table 8: Reaction setup of DNA end blunting reactions.

REACTION COMPONENT	VOLUME
DNA with cohesive end(s) (1 µg)	x µL
100 µM dNTPs (N0446S, NEB)	0.25 µL
10x NEBuffer 2.1 (B7202, NEB)	2.5 µL
T4 DNA polymerase, 1 U/µg of DNA (M0203, NEB)	0.25 µL
Nuclease free water	Add to 12.5 µL

The reaction mix was incubated at 12° C for 15 minutes and immediately purified as described in section 2.1.2 to avoid extensively recessed ends due to 3' to 5' exonuclease activity of the T4 DNA polymerase.

2.1.6. Dephosphorylation of DNA ends

Cleavage of DNA by restriction endonucleases generates 3'-hydroxyl on one and 5'-phosphate residues on both sides of the cut. During ligation, both groups are essential to form the phosphodiester bond of the DNA backbone linking adjacent plasmid and insert DNA fragments covalently. The phosphodiester bond may also be formed between the two adjacent ends of linearised plasmid DNA leading to self-ligation of the plasmid and a high number of transformants carrying self-ligated plasmid. Dephosphorylation of the digested plasmid was performed using Antarctic phosphatase (M0289, NEB) which efficiently hydrolyses the ester bond between the terminal 5'-nucleoside of the DNA fragment and its phosphate group, prevents self-ligation of linearised plasmid DNA, and thus enhances cloning efficiency.[9] Dephosphorylation reactions were set up on ice as described in Table 9.

[8] https://international.neb.com/products/m0203-t4-dna-polymerase#Product%20Information, January 06, 2020

[9] https://www.neb.com/products/m0289-antarctic-phosphatase#Product%20Information, October 27, 2019

Table 9: Reaction setup of the dephosphorylation of plasmid-backbone DNA.

REACTION COMPONENT	VOLUME
Linearised plasmid-backbone DNA (1 µg)	x µL
Antarctic phosphatase, 5 U[10]/reaction (M0289, NEB)	1 µL
10x Antarctic phosphatase reaction buffer (Masliah-Planchon, Bieche et al.)	2 µL
Nuclease free water	Add to 20 µL

The reaction mix was incubated at 37° C for 30 minutes. Subsequently, the thermo-labile phosphatase was irreversibly inactivated at 80° C for two minutes and the dephosphorylated DNA was used in ligation reactions without any further purification step. The concentration of plasmid DNA for subsequent ligation reactions is calculated by dividing the amount of DNA in nanograms by the total reaction volume of the dephosphorylation reaction (20 µL). It is recommended to test the efficiency of the dephosphorylation reaction by setting up a ligation reaction of the dephosphorylated backbone only followed by transformation of chemically competent *E. coli*.

2.1.7. Ligation of DNA fragments

Ligation of two adjacent and compatible DNA fragments is the final step in the cloning process of recombinant plasmids. During ligation, a covalent bond between the ends of two DNA fragments is formed in a three-step process. First, T4 DNA ligase self-adenylates a lysine residue in its active centre by reaction with free adenosine triphosphate (ATP). This phospho-adenyl group is then transferred to the 5' end of the DNA, and in a third step, forms the covalent phosphodiester bond with the 3'-hydroxyl acceptor group on the adjacent DNA end while releasing adenosine monophosphate (AMP).[11] When ligating blunt DNA ends, the addition of polyethylene glycol (PEG) is recommended. The macromolecule PEG acts as a crowding agent which increases the effective concentration of T4 DNA ligase and DNA substrates, and by this increases ligation efficiency.

For ligation reactions, T4 DNA ligase of Thermo Fisher (5 U/µL[12], EL0014) was used. Ratios of 1:3, 1:5, and 1:10 of plasmid to insert DNA were applied. The amount of DNA necessary for each ligation ratio was calculated using the NEBioCalculator based on 50 ng of plasmid DNA (https://nebiocalculator.neb.com/#!/ligation). The reactions for cohesive end ligation were set up on ice as follows (Table 10).

[10] 1 U = 1 unit is defined as the amount of enzyme that will dephosphorylate 1 µg of pUC19 vector DNA cut with a restriction endonuclease generating 5' recessed ends in 30 minutes at 37° C; https://international.neb.com/products/m0289-antarctic-phosphatase#Product%20Information_Properties%20&%20Usage; October 27, 2019

[11] https://international.neb.com/tools-and-resources/video-library?term=ligase, January 06, 2020

[12] One Weiss unit is equivalent to approximately 200 cohesive end ligation units (CEU). 1 Weiss Unit = 200 CEU. One CEU is defined as the amount of enzyme required to give 50% ligation of HindIII fragments of lambda DNA in 30 minutes at 16°C. https://assets.thermofisher.com/TFS-Assets/LSG/manuals/MAN0011987_T4_DNA_Ligase_5_Weiss_1000_Weiss_U_UG.pdf, January 06, 2020

Table 10: Ligation reaction setup for joining of cohesive ends using T4 DNA ligase of Thermo Fisher.

REACTION COMPONENT	VOLUME
Prepared plasmid-backbone DNA	50 ng
Prepared insert DNA	Amount as calculated
T4 DNA ligase (EL0014, Thermo Fisher, 5 U/µL)	1 µL
10x T4 DNA ligase buffer (Thermo Fisher)	1 µL
Nuclease free water	Add to 10 µL

The ligation reaction was incubated at 16° C for 15 hours or at 22° C for two hours and inactivated at 65° C for 10 minutes before transforming chemically-competent *E. coli*. A ligation of only plasmid backbone DNA was always included as a control to determine the rate of self-ligation of the plasmid. When ligating blunt ends, 5 µL of T4 DNA ligase per 20 µL reaction was used, the mixture was supplemented with 2 µL of 50% PEG-4000, and the inactivation step of T4 DNA ligase had to be skipped.

2.1.8. Generation of chemically-competent *Escherichia coli*

Amplification of ligation products is performed in bacteria. Treatment of bacteria with Calcium (Cas^{2+}) ions in combination with cold temperatures and a heat pulse can confer the bacteria the competence to take up DNA. Calcium chloride ($CaCl_2$) treatment of the cells allows exogenous DNA to attach to the bacterial cell membrane. A subsequent heating pulse renders the bacteria transiently permeable by opening pores in the cell membrane. Treatment of the cells with a mixture of $CaCl_2$, magnesium (Mg^{2+}), manganese (Mn^{2+}), and rubidium (Rb^{+}) or potassium (K^{+}) ions can further stimulate the transfer efficiency (Hanahan 1983).

There are different laboratory strains of *Escherichia coli* (*E. coli*) which are optimised for cloning purposes and commonly used. The strain *E. coli* DH5α is a non-pathogenic laboratory strain of *E. coli*. Its genome contains two defining mutations which allow for optimal plasmid stability and DNA yield upon purification. A mutation in *recA1* disables the cell's recombinase and inactivates homologous recombination, mutation of *endA* inactivates the intracellular endonuclease and prevents plasmid degradation. By the *lacZM15* mutation, this strain is also compatible with blue/white screening.[13] *E. coli* Stbl3 is another non-pathogenic laboratory strain which allows for the cloning and propagation of unstable DNA, e.g. DNA for packaging in lentiviral particles with flanking long terminal repeats (LTRs).[14]

The chemically-competent bacteria used here were originally obtained from Thermo Fisher (DH5α 18265017, Life Technologies; Stbl3 10193952, Fisher Scientific). From these commercial aliquots,

[13] https://www.thermofisher.com/de/de/home/life-science/cloning/competent-cells-for-transformation/competent-cells-strains/dh5a-competent-cells.html, January 06, 2020

[14] https://www.thermofisher.com/order/catalog/product/C737303?SID=srch-srp-C737303#/C737303?SID=srch-srp-C737303, January 06, 2020

fresh stocks of chemically-competent *E. coli* were prepared using the rubidium chloride (RbCl) method adapted from Green and Rogers (2013).

Generation of chemically-competent *E. coli* DH5α or Stbl3 – RbCl method:

On day one, a 5 mL Luria Broth (LB (Lennox), X.964.2, Carl Roth) pre-culture of the desired *E. coli* strain was inoculated from its glycerol stock using a sterile inoculation loop and incubated at 37° C and 220 rpm overnight.

On day two, two times 100 mL of pre-warmed LB were inoculated with 2 mL of pre-culture each and incubated at 37°C, 220 rpm until the culture reached an optic density of 0.4 to 0.5 at 550 nm (approx. 2.5 hours of incubation). The cells were then abruptly cooled down in ice water for 10 minutes. 100 mL of culture were harvested in 50 mL aliquots in pre-cooled tubes by centrifuging the cell suspension at 4° C and 5,000 xg for 15 minutes. Each bacterial pellet was carefully re-suspended in 30 mL of pre-cooled (4° C) TfBI buffer (Table 11). The suspension was incubated on ice for 15 minutes to 1.5 hours and harvested again by centrifuging the tubes at 4° C and 5,000 xg for 15 minutes. The supernatant was discarded, and each pellet carefully re-suspended in 4 mL of ice-cold TfBII buffer (Table 12). Finally, 50 µL of the chemically-competent bacteria were aliquoted to -80° C pre-cooled 1.5 mL microcentrifuge tubes and flash frozen in liquid nitrogen. The aliquots were stored at -80° C for further use.

Table 11: Transformation buffer I (TfBI) for the generation of chemically-competent *E. coli* using the RbCl method.

COMPONENT	CONCENTRATION	MASS
RbCl (83980, Fluka)	100 mM	1.21 g
$MnCl_2$*4H_2O (5927.0100, Merck)	50 mM	0.989 g
$CaCl_2$*2H_2O (1.02383.0250, Merck)	100 mM	0.147 g
KAc (1.04820.1000, Merck-Millipore)	30 mM	0.29 g
100% glycerol (7530.4, Carl Roth)	15%	18.9 g

All components were dissolved in $H_2O_{dest.}$ in a graduated measuring cylinder. While stirring, the buffer's pH was adjusted to 5.8 (S20 SevenEasy pH, 51302803, Mettler Toledo) by adding 0.2 M acetic acid. After removing the magnetic stir bar, the volume was filled up to 100 mL with H_2O_{dest}. The buffer was sterile filtered into a sterile glass bottle and stored at 4° C.

Table 12: Transformation buffer II (TfBII) for the generation of chemically-competent *E. coli* using the RbCl method.

COMPONENT	CONCENTRATION	MASS
MOPS (6979.2, Carl Roth)	10 mM	0.105 g
RbCl (83980, Fluka)	10 mM	0.06 g
$CaCl_2$ (C-2661, Sigma Aldrich)	75 mM	0.55 g
100% glycerol (7530.4, Carl Roth)	15%	9.45 g

All components were dissolved in $H_2O_{dest.}$ in a graduated measuring cylinder. While stirring, the buffer's pH was adjusted to 7.0 (S20 SevenEasy pH, 51302803, Mettler Toledo) by adding 0.2 M NaOH. The magnetic stir bar was removed, and the volume filled up to 50 mL with $H_2O_{dest.}$ After sterile filtering the buffer into a sterile glass bottle, it was cooled to 4° C and used immediately.

2.1.9. Transformation of *Escherichia coli* DH5α and Stbl3

Transformation of chemically-competent bacteria describes the transfer of exogenous DNA, e.g. plasmid DNA, into competent bacteria in the presence of calcium ions (Ca^{2+}) in combination with cold temperatures and a heat pulse.

For the transfer of ligation product into *E. coli* laboratory strains DH5α or Stbl3, one aliquot of chemically-competent bacteria per ligation reaction was thawed on ice. Per aliquot, 5 µL of ligation reaction were added and mixed well by flipping the tube. This bacteria-DNA suspension was incubated on ice for 30 minutes. During this incubation time 250 µL of SOC (Super Optimal broth with Catabolite repression, Table 13) medium, and two LB agar (X965.2, Carl Roth) plates with suitable antibiotic supplementation (200 µg/mL ampicillin K029.1, Carl Roth; 50 µg/mL kanamycin T832.1, Carl Roth) were pre-warmed to 37° C. After 30 minutes, the transformation reactions were heat-pulsed at 42° C for 30 to 45 seconds and immediately put back on ice for two minutes to open the cell membrane's pores, transfer the DNA, and allow the pores to close again. 250 µL of SOC medium was added to each reaction, and the bacteria were incubated at 37° C for one hour while shaking. Finally, 60 µL and 200 µL of the final transformation reaction were plated on LB agar plates and incubated at 37° C for a maximum of 18 hours (overnight). Resulting colonies were analysed by colony PCR (section 2.1.10).

Table 13: Preparation of SOC medium.

COMPONENT	CONCENTRATION	AMOUNT PER L
Tryptone (8952.2, Carl Roth)	2%	20 g
Yeast extract (9213.0500, Chemsolute)	0.5%	5 g
NaCl (3957.2, Carl Roth)	10 mM	2 mL of a 5 M stock
KCl (6781.1, Carl Roth)	2.5 mM	2.5 mL of a 1 M stock
$MgCl_2*6H_2O$ (2189.1, Carl Roth)	10 mM	10 mL of a 1 M stock
$MgSO_4*7H_2O$ (5886.1000, Merck)	10 mM	10 mL of a 1 M stock

All components were dissolved in $H_2O_{dest.}$, and the medium's pH was adjusted to 7.0 (S20 SevenEasy pH, 51302803, Mettler Toledo) by adding NaOH. The medium was sterilised by autoclaving (121° C, 20 minutes). Sterile filtered glucose ((D+) Glucose monohydrate 1.08342.1000, Merck) was added to the sterile medium to a final concentration of 20 mM (add 7.2 mL of a 50% stock per litre of medium).

2.1.10. Colony PCR

Colony PCR is a standard polymerase chain reaction with bacterial colony material as template and is used to identify bacterial colonies which replicate the cloned recombinant plasmid (positive colony). Identification of positive colonies works best when the PCR's primers are selected in a way that excludes false positives. One primer complementary to the plasmid-backbone sequence close to the plasmid-insert junction and the other one complementary to the insert-sequence close to the same junction are desirable. Ideally, the fragment amplified with these primers does not exceed 1,000 bp. The colony PCR is an analytical tool only and does not require the reading accuracy of PCR amplifications for cloning purposes. Therefore, a non-commercial *Taq* polymerase and a cost-effective commercial PCR buffer can be used. The colony PCR was set up as described in Table 14.

Table 14: Colony PCR setup using a non-commercial *Taq* polymerase.

REACTION COMPONENT	FINAL CONCENTRATION	VOLUME
10x PCR buffer (10390885, Fisher Scientific)	1x	2.5 µL
10 mM dNTPs (N0446S, NEB)	200 µM	0.5 µL
10 µM Forward Primer	0.2 µM	0.5 µL
10 µM Reverse Primer	0.2 µM	0.5 µL
Non-commercial *Taq* polymerase		0.3 µL
Nuclease free water		20.7 µL

Some bacterial colony material was picked from the transformation plate with a sterile 10 µL pipette tip, a replica plate (LB agar plate with suitable antibiotic supplementation, incubation at 37° C overnight) was inoculated, and the remaining colony material from the tip was re-suspended in the PCR mixture. A positive control with 1 µL of ligation product was included. The PCR mixtures were placed in a thermal cycler (peqSTAR 2x Universal Gradient, 732-2889DE, VWR) running the following programme (Table 15).

Table 15: PCR programme for colony PCR using a self-made *Taq* polymerase.

PCR STEP	TEMPERATURE	TIME
Initial Denaturation	95° C	5 minutes
30 Cycles: Denaturation	95° C	30 seconds
Annealing	[15]50-72° C	30 seconds
Extension	72° C	60 seconds/kb
Final Extension	72° C	2 minutes

The PCR products were analysed by Agarose gel electrophoresis (section 2.1.4). Colonies which yielded a PCR product of the expected size were picked from the replica plate to inoculate 5 mL overnight cultures (LB medium supplemented with antibiotics, incubated at 37° C and 220 rpm for a

[15] Primer melting temperature as calculated by IDR OligoAnalyzer https://eu.idtdna.com/calc/analyzer

maximum of 16 hours). The next day, these cultures were used to purify plasmid DNA and analyse the replicated plasmid DNA sequence in detail (section 2.1.11).

2.1.11. Plasmid DNA preparations

Recombinant plasmids are replicated in bacteria. For further analysis and use of the plasmid, the plasmid DNA has to be purified from the cells. The most common method for the extraction of plasmid DNA from bacteria is alkaline lysis. In a first step, the cells are re-suspended in a buffer containing EDTA to complex divalent cations, thus inactivating DNases. Secondly, lysis buffer containing sodium hydroxide (NaOH) and sodium dodecyl sulphate (SDS) is added to the cell suspension. SDS solubilizes the cell membrane and denatures most of the cells' proteins. NaOH helps to break down the bacterial cell wall and disrupts the hydrogen bonds between the two complementary DNA strands. The lysis buffer thus opens the cells and denatures double-stranded DNA to single-stranded DNA. In a third step, the lysis reaction is neutralised by decreasing the alkalinity of the mixture. This allows the re-establishment of hydrogen bonds between complementary DNA strands to form double-stranded DNA. Since hybridisation of small DNA fragments is much more efficient compared to longer DNA fragments, the small plasmid DNA rings are hybridising while the bacterial genomic DNA remains single-stranded. The double-stranded plasmid DNA is soluble in aqueous solutions while cellular proteins, single-stranded genomic DNA, and SDS are precipitated. Finally, the plasmid DNA can be purified from the solution, e.g. using a silica-based membrane. Depending on the DNA quality required and the purpose of the purified plasmid DNA, different plasmid DNA purification kits were used.

E.Z.N.A. Plasmid DNA Mini Kit (D6943-02, VWR):

For purification of DNA for the final restriction endonuclease analysis and sequencing of newly cloned recombinant plasmids, the E.Z.N.A. Plasmid DNA Mini Kit of Omega Bio-Tek (D6943-02, VWR) was used according to the manufacturer's handbook.[16] In brief: colonies which were tested positive in colony PCR (section 2.1.10) were used to inoculate 5 mL overnight cultures of LB medium with antibiotic supplementation (200 µg/mL ampicillin K029.1, Carl Roth; 50 µg/mL kanamycin T832.1, Carl Roth) and incubated at 37° C, 220 rpm for a maximum of 16 hours. Turbid cultures were used to prepare glycerol stocks of the bacteria for future propagation of the recombinant plasmid by combining 400 µL of a sterile 1:1 solution of LB medium and glycerol (7530.4, Carl Roth) and 600 µL of the overnight culture. The remaining bacterial suspension was harvested in two combining steps of 2 mL at 10,621 xg at 4° C for one minute in 2 mL microcentrifuge tubes. The resulting bacterial pellet was re-suspended in 250 µL of Suspension I supplemented with RNaseA by vortexing. Lysis was initiated by adding 250 µL of Solution II to the cell suspension. The tube was inverted three times to thoroughly mix the suspension and incubated at room temperature for three minutes to completely lyse the sample. Afterwards, 350 µL of Solution III was added and mixed immediately by inverting the tube to stop the lysis reaction. At this point a white, flocculent precipitate formed which contained all cellular

[16] E.Z.N.A. Plasmid DNA mini Kit – manual available at https://www.omegabiotek.com/product/e-z-n-a-plasmid-mini-kit-i-q-spin/

components except for the plasmid DNA. The precipitate was pelleted by centrifugation at maximum speed for 10 minutes and 850 µL of the cleared supernatant were transferred to a HiBind DNA mini column in a collection tube. Centrifugation at maximum speed for one minute passed the supernatant through the membrane, allowing the DNA to bind to it. The flow-through was discarded. A first wash step with 500 µL of HBC buffer diluted with 100% isopropanol was performed (maximum speed for one minute), followed by two washing steps with 700 µL of Washing buffer diluted with 100% ethanol each (maximum speed for 30 seconds). Every flow-through was discarded. Afterwards, the empty column was spun at maximum speed for two minutes to completely dry the matrix. Following this, the dried column was transferred to a sterile 1.5 mL microcentrifuge tube, 50 µL of pre-warmed (55° C) nuclease-free water were added directly to the membrane, and the column was incubated at room temperature for five minutes. Finally, the bound DNA was eluted by centrifuging the column at maximum speed for one minute. DNA concentration and purity were determined using the NanoDrop2000c (software version 1.6, Thermo Scientific) and 1 µL of the purified DNA sample.
500 ng of the obtained plasmid DNA were subjected to a restriction endonuclease digestion (section 2.1.3) which gave a first indication of the plasmid's identity by a characteristic pattern of bands in agarose gel electrophoresis.

E.Z.N.A. Plasmid DNA Midi Kit (D6904-03, VWR):

Transfection of HEK293T cells for the production of lentiviral particles requires larger amounts of plasmid DNA. For this purpose, the E.Z.N.A. Plasmid DNA Midi Kit of Omega Bio-Tek (D6904-03, VWR) was used according to the manufacturer's instructions.[17] In brief: 50 mL of LB medium with antibiotic supplementation (200 µg/mL ampicillin, or 50 µg/mL kanamycin) were inoculated from a bacterial glycerol stock using a sterile inoculation loop or with 100 µL of a previous overnight culture. The culture was incubated at 37° C, 220 rpm for a maximum of 16 hours and subsequently harvested in a 50 mL conical tube by centrifugation at 6,000 xg and 4° C for 15 minutes. Afterwards, the pellet was re-suspended in 2.25 mL of Solution I with RNaseA by vortexing. When the pellet was re-suspended completely, 2.25 mL of Solution II were added and the tube was slowly inverted for two minutes to completely lyse the sample. By addition of 3.2 mL of Solution III the lysis reaction was stopped and a white flocculent precipitate formed. The precipitate was pelleted at 10,000 xg for 20 minutes. The cleared supernatant was transferred to a HiBind DNA midi column in a tube in 3.5 mL steps and centrifuged at 4,000 xg for three minutes in a swinging bucket rotor. The flow-through was discarded. This step was repeated until all supernatant was passed through the column. Next, 3 mL of HBC buffer diluted with 100% isopropanol were added and the column centrifuged at 4,000 xg for three minutes. The flow-through was discarded. Remaining salts were washed from the membrane with two washing steps using 3.5 mL of Wash buffer diluted with 100% ethanol each. The flow-through was discarded, and the empty column centrifuged at 4,000 xg for five minutes to completely dry the membrane. The dried column was transferred to a sterile 15 mL conical tube, 500 µL of pre-

[17] E.Z.N.A. Plasmid DNA Midi Kit – manual available at https://www.omegabiotek.com/product/e-z-n-a-plasmid-midi-kit/

warmed (55° C) nuclease-free water were added to the matrix and incubated at room temperature for five minutes. Finally, the bound DNA was eluted by centrifugation at 4,000 xg for five minutes. To increase the DNA-yield, the eluate was used for a second elution step. The sample was transferred to a sterile 1.5 mL microcentrifuge tube, and DNA concentration as well as purity were determined using the NanoDrop2000c (software version 1.6, Thermo Scientific) and 1 µL of the purified DNA sample. 500 ng of the obtained plasmid DNA were subjected to a restriction endonuclease digestion (section 2.1.3) which verified the plasmid's identity by a characteristic pattern of bands in agarose gel electrophoresis.

Plasmid DNA purification using the HiSpeed Midi Kit (12643, QIAGEN):

Plasmid DNA used for transfection of hiPSCs has to be of high purity and quality. These requirements are only met using plasmid DNA purification kits of QIAGEN. The HiSpeed Midi Kit was used as described in the manual.[18] In brief: 50 mL of LB medium with antibiotic supplementation (200 µg/mL ampicillin, or 50 µg/mL kanamycin) were inoculated from a bacterial glycerol stock using a sterile inoculation loop or 100 µL of a previous overnight culture. The culture was incubated at 37° C, 220 rpm for a maximum of 16 hours and subsequently harvested in a 50 mL conical tube at 6,000 xg and 4° C for 15 minutes. After harvesting, the pellet is re-suspended in 6 mL of Buffer P1 supplemented with RNaseA and LyseBlue reagent by vortexing. Lysis was initiated by the addition of 6 mL of Buffer P2 followed by mixing through inversion and incubating the lysis reaction at room temperature for five minutes. Complete mixing of the solution was indicated by a uniform blue colouring of the mixture. During this incubation time, a QIAGEN filter cartridge was prepared by screwing a cap to the outlet nozzle. Addition of 6 mL of pre-cooled Buffer P3 and mixing by inversion stopped the lysis reaction, decoloured the solution, and formed a white flocculent precipitate. The lysate was poured into the prepared filter cartridge's barrel immediately and was incubated undisturbed at room temperature for five minutes. During this incubation time, a HiSpeed Midi tip was equilibrated by adding 4 mL of Buffer QBT to the membrane and allowing the column to empty by gravity flow. The cap was removed from the outlet nozzle of the filter cartridge, and the plunger was inserted to filter the lysate onto the HiSpeed Midi tip. The filtered lysate was allowed to enter the resin by gravity flow. After a gravity flow washing step using 20 mL of Buffer QC, the bound DNA was eluted into a sterile 15 mL tube using 5 mL of Buffer QF. Next, the eluted DNA was precipitated by the addition of 3.5 mL (0.7 volumes) of 100% isopropanol and incubation at room temperature for 10 minutes. A QIAGEN precipitator module was attached to the barrel of a 20 mL syringe, and the precipitated eluate/isopropanol mixture was poured into the barrel. By applying constant pressure, the eluate was filtered through the module. Two washing steps using 2 mL of 70% ethanol each were performed using the same 20 mL syringe. The precipitator module was dried by pressing air through the module using the 20 mL syringe and tapping the outlet nozzle with absorbent paper. After drying the membrane

[18] Plasmid DNA HiSpeed Midi Kit (QIAGEN) – manual available at https://www.qiagen.com/ca/resources/resourcedetail?id=5a63b6b2-7fd7-4fbf-b3cd-e50d8270fea1&lang=en

completely, a new 5 mL syringe-barrel was attached to the precipitator module, 500 µL of pre-warmed (55° C) nuclease-free water were applied, and incubated at room temperature for five minutes before inserting the plunger and eluting the DNA into a sterile 1.5 mL microcentrifuge tube. To increase the DNA-yield, the eluate was used for a second elution step. DNA concentration and purity were determined using the NanoDrop2000c (software version 1.6, Thermo Scientific) and 1 µL of the purified DNA sample.

500 ng of the obtained plasmid DNA were subjected to a restriction endonuclease digestion (section 2.1.3) which verified the plasmid's identity by a characteristic pattern of bands in agarose gel electrophoresis.

2.1.12. Sanger sequencing of DNA samples

Sequencing is used as a final verification of the successful cloning of the recombinant plasmid of interest. Plasmid DNA which showed the expected pattern of bands in agarose gel electrophoresis upon digestion with restriction endonuclease(s) was sent for sequencing to Microsynth Seqlab. Sequencing reactions were composed of 800 to 1200 ng of DNA in a total volume of 12 µL and three microliters of a 10 µM sequence specific primer which ideally binds 50 bp upstream of the site to be sequenced. The tube was labelled with a registered Barcode EasyRun label and deposited in the Seqlab box outside building B2/03 before 5:30 pm. Within 24 hours, the results were ready to be downloaded at https://srvweb.microsynth.ch/home/seqlab.

2.1.13. TA-cloning

TA-cloning is a fast and simple cloning technology based on the ligation of complementary A- and T-overhangs at plasmid and insert DNA ends. Blue-white selection of the transformants allows for direct visual identification of recombined colonies. The components needed for TA-cloning are pBluescript (plasmid #80) or any other backbone plasmid with a LacZ gene for blue-white screening, suitable blunt restriction endonuclease recognition site, and a *Taq* polymerase which adds single-base overhangs to the 3' end of DNA due to its transferase activity. First, pBluescript was linearised via the EcoRV restriction endonuclease recognition site within the LacZ gene, and the digested DNA was purified using the Clean&Concentrator-5 kit (section 2.1.2). The desired insert was PCR amplified using a proof-reading DNA polymerase as described in section 2.1.1. Using the *Taq* polymerase JumpStart Taq (D9307, Sigma) and dATP or dTTP, 3' A- or T-overhangs were added to the insert's or plasmid's blunt DNA ends, respectively (Figure 12 and Table 16).

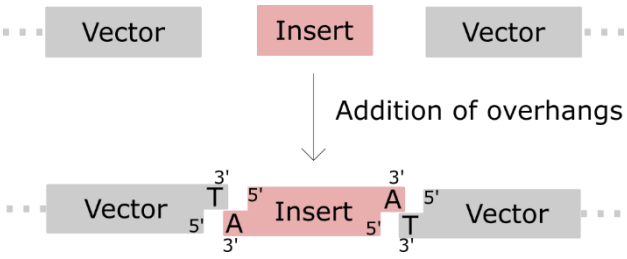

Figure 12: TA-Cloning. Schematic overview of the addition of 3' A- or T-overhangs to insert or plasmid DNA, respectively.

Table 16: Setup of the addition of 3' A-/T- overhangs to blunt DNA ends for TA-cloning.

REACTION COMPONENT	FINAL CONCENTRATION	VOLUME
Blunt ended DNA (insert/plasmid)	600 ng to 1 µg	2.5 µL
dATP/dTTP (R0441/R0171, Life Technologies)	2 mM	0.5 µL
10x JumpTaq Buffer	1x	0.5 µL
JumpStart Taq (D9307, Sigma)	2.5 U	0.5 µL
Nuclease free water		Add to 50 µL

The reaction mix was incubated at 68° C for 20 minutes, and the processed DNA fragments were purified using the Clean&Concentrator-5 Kit (Zymo, section 2.1.2). Subsequently, plasmid and insert were ligated as described in section 2.1.7 and transformed into chemically-competent *E. coli* (section 2.1.9). To initiate the blue-white selection, 40 µL of Isopropyl β-D-thiogalactopyranoside (IPTG, 20 mg/mL in water, 05684, Biomol) and 40 µL of 5-Bromo-4-chloro-3-indolyl β-D-galactopyranoside (X-Gal, 25 mg/mL in DMSO, BIO-37035, Bioline) were added to the transformation mix prior to plating. Transformants with an intact LacZ gene, without the insert, metabolize the chromogenic β-galactosidase substrate X-Gal producing galactose and 5-bromo-4-chloro-3-hydroxyindole. The latter spontaneously dimerises and is oxygenised into 5,5'-dibromo-4,4'-dichloro-indigo, an insoluble intense blue compound responsible for the blue colour of the negative colonies. Transformants with a disturbed LacZ gene, due to integration of the insert, cannot metabolize X-Gal and remain white. After overnight incubation of the transformation plates, it was necessary to incubate the plates at 4° C for two to four hours until the blue colour of the negative transformants becomes observable. Two to four white colonies were then used to inoculate LB-cultures and incubated at 37° C overnight for plasmid DNA isolation and a detailed analysis of the obtained plasmid (section 2.1.11).

2.1.14. Overlap extension method

Introduction of small insertions, deletions or point mutations into sequences close to suitable restriction endonuclease recognition sites is possible by the mutation of the oligonucleotide primer's sequence used for PCR amplification of the sequence of interest. If mutations are to be introduced which are located more distant to a restriction endonuclease recognition site, the overlap extension method can be applied for site-directed mutagenesis (Heckman and Pease 2007).

The overlap extension method for mutation of DNA sequences requires four oligonucleotide primers and three separate PCRs. Since the final PCR product will be used for cloning, the use of a proof-reading DNA polymerase like Phusion DNA polymerase is recommended (section 2.1.1). In the first round of PCR, the mutation is introduced to the 5' or 3' terminus of two independent DNA fragments, respectively. A "sense" mutated primer is combined with an "anti-sense" flanking primer and vice versa (Figure 13, adapted from Heckman and Pease (2007)). The purified PCR products are then used in a 1:2 mass ratio based on fragment size (100 ng of total DNA mass) as a template in the second round of PCR. In this last reaction, the "sense" and "anti-sense" flanking primers are used to amplify the mutated fragment and to add suitable restriction endonuclease recognition sites to the 3' and 5' end of the PCR product. Subsequently, the mutated PCR product can be cloned into the desired backbone plasmid via restriction endonuclease cloning (sections 2.1.3 and 2.1.7).

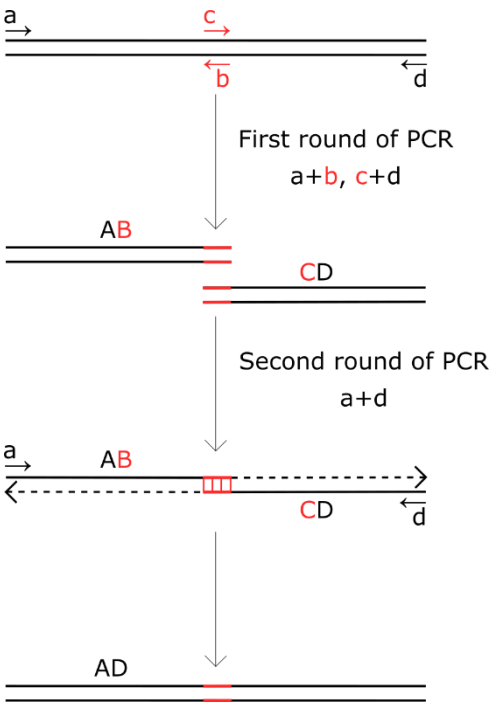

Figure 13: Schematic overview of the overlap extension method to introduce mutations into DNA sequences. Site directed mutagenesis is achieved by using the mutation-containing primers b and c and the flanking primers a and d to generate PCR products AB and CD. In a second round of PCR the PCR products AB and CD are combined in a 1:2 mass ratio and PCR product AD is amplified using the flanking primers a and d. (Heckman and Pease 2007)

The mutated primers have to be designed to be fully complementary containing the desired mutation in the sequence's centre. Due to the extensive overlap of the primers, also a chimeric gene product by artificial splicing can be generated. In this case, the "mutated" primers do not carry a mutation of the sequence but are half upstream and half downstream sequence of the chimeric gene product (10 bp each) generating a 20 bp overlap for the second round of PCR.

2.1.15. Cloning of guide RNA sequences into multiplex CRISPR/Cas9(n) plasmids

Target-specific sequences were cloned into the multiplex all-in-one plasmid system described by Sakuma, Nishikawa et al. (2014) (CRISPR/Cas9 Assembly System Kit #1000000055, Addgene, Figure 14).

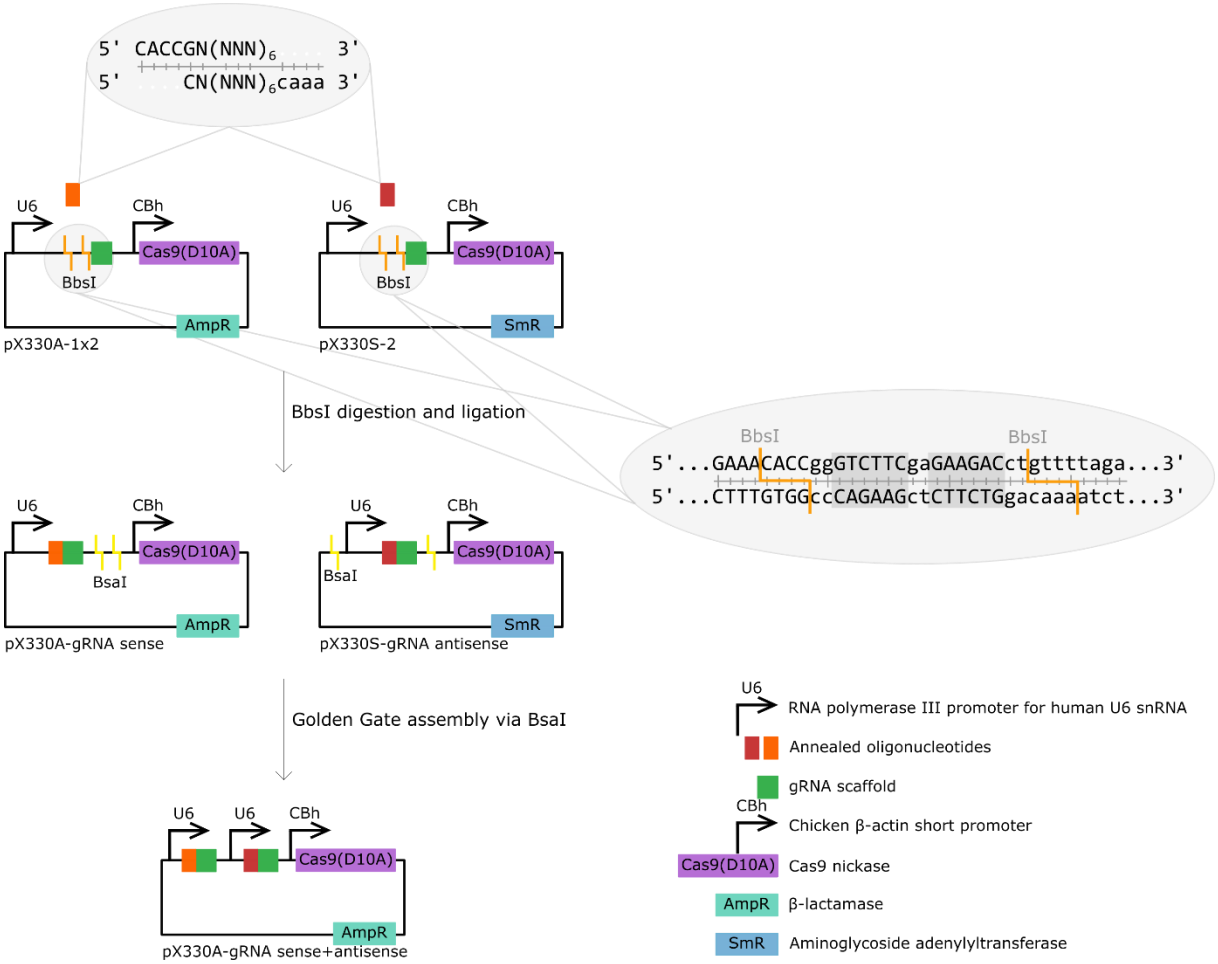

Figure 14: Schematic overview of the cloning of all-in-one multiplex CRISPR/Cas9n plasmids as described in Sakuma, Nishikawa et al. (2014). Annealed and phosphorylated sequences targeting the gene of interest are cloned into pX330A-1x2 or pX330S via BbsI. Subsequently, Golden Gate assembly using BsaI combines the sense and antisense gRNA expression cassettes in the pX330A backbone. AmpR, β-lactamase confers resistance to ampicillin. SmR, aminoglycoside adenylyltransferase confers resistance to spectinomycin. Adapted from Sakuma, Nishikawa et al. (2014).

Suitable sequences for targeting using the Cas9 nickase were identified using the CRISPR designing tool of MIT (http://tools.genome-engineering.org). For each targeting sequence, two oligonucleotides (forward and reverse) were ordered. To meet the requirements of the CRISPR/Cas9 Assembly kit overhangs complementary to the pX330 plasmids were added 5' to the oligonucleotides (5' CACCG to the forward, and 5' AAAC to the reverse oligonucleotide). The oligonucleotides were annealed and phosphorylated, as stated in Table 17.

Table 17: Reaction setup for the annealing and phosphorylation of oligonucleotides.

REACTION COMPONENT	VOLUME, 10 µL REACTION
Forward oligonucleotide, 100 µM	1 µL
Reverse oligonucleotide, 100 µM	1 µL
10x T4 DNA Ligase Buffer (B0202S, NEB)	1 µL
Nuclease free water	6.5 µL
T4 Polynucleotide Kinase (M0201S, NEB)	0.5 µL

The reaction mix was incubated at 37° C for 30 minutes, followed by 95° C for five minutes. Starting from 95° C, the reaction was cooled down to 25° C at a reduction rate of 5° C per minute. The annealed and phosphorylated oligonucleotides were diluted 1:250 in nuclease-free water and cloned into the pX330 plasmids.

As a first step in the cloning of the multiplex all-in-one plasmid system, a digestion and ligation reaction of the annealed targeting oligonucleotides and the pX330 plasmids using BbsI were prepared (Table 18, Figure 14). In general, the sequence targeting the sense strand of the gene of interest was cloned into pX330A-1x2 (plasmid #120, #217, #219, or #220) and the sequence targeting the antisense strand of the gene of interest was cloned into pX330S-2 (plasmid #145).

Table 18: Digestion and ligation reaction setup for the cloning of targeting sequences into pX330 plasmids.

REACTION COMPONENT	VOLUME
pX330A-1x2/pX330S-2	100 ng
Annealed and phosphorylated oligonucleotide, 1:250	2 µL
10x Tango Buffer (BY5, Thermo Fisher)	2 µL
dTTP, 10 mM (R0171, Life Technologies	1 µL
dATP, 10 mM (R0441, Life Technologies)	1 µL
BbsI-HF (R3539S, NEB, 20,000 U/mL)	0.5 µL
T4 DNA ligase (EL0014, Thermo Fisher, 5 U/µL)	0.5 µL
Nuclease free water	Add to 20 µL

The reaction mix was placed in a thermal cycler (peqSTAR 2x Universal Gradient, 732-2889DE, VWR) programmed with six cycles of incubation at 37° C for five minutes, followed by incubation at 23° C for five minutes. After transforming chemically-competent *E. coli* and plating them on LB-plates appropriately supplemented with antibiotics (pX330A-1x2 200 µg/mL ampicillin, pX330S-2 100 µg/mL spectinomycin PHR1441, VWR, section 2.1.9), two colonies per plasmid were picked, propagated, and plasmid DNA was analysed by BbsI digestion (section 2.1.11). Clones which inserted the targeting oligonucleotide will not be cut by BbsI as the restriction endonuclease's recognition site will be lost.

In a second step, the gRNA expression cassettes of pX330A-gRNA sense and pX330S-gRNA antisense were combined in the pX330A backbone using Golden Gate assembly via BsaI (Table 19, Figure 14).

Table 19: Golden Gate assembly of CRISPR/Cas9n multiplex plasmids.

REACTION COMPONENT	VOLUME
pX330A-gRNA sense	100 ng
pX330S-gRNA antisense	150 ng
10x Tango Buffer (BY5, Thermo Fisher)	2 µL
dTTP, 10 mM (R0171, Life Technologies	1 µL
dATP, 10 mM (R0441, Life Technologies)	1 µL
BsaI-HF (R3733S, NEB, 20,000 U/mL)	0.5 µL
T4 DNA ligase (EL0014, Thermo Fisher, 5 U/µL)	0.5 µL
Nuclease free water	Add to 20 µL

The reaction mixture was placed in a thermal cycler (peqSTAR 2x Universal Gradient, 732-2889DE, VWR) programmed with six cycles of incubation at 37° C for five minutes, followed by incubation at 23° C for five minutes each. *E. coli* DH5α were transformed with 5 µL of the Golden Gate reaction and supplemented with IPTG and X-Gal for blue/white screening (section 2.1.9). Up to ten white colonies were analysed by colony PCR using the oligonucleotides #666 and #667 (section 2.1.10). The forward primer #666 was binding the U6 promoter. Thus, two fragments of 1,000 bp and 500 bp were expected upon assembly of both gRNA expression cassettes in the pX330A backbone. Colonies showing both bands in colony PCR were propagated for plasmid DNA purification and analysed by BsaI digestion. Upon successful assembly, the BsaI restriction endonuclease recognition site will be lost, and positive clones will not be cut.

2.1.16. Gateway cloning

Gateway cloning was performed according to Katzen (2007). For this work, only the integrating LR reaction for the transfer of the gene(s) of interest from a donor plasmid (pENTR4, plasmid #174) to a lentiviral recipient plasmid (e.g. pLenti-UbC, plasmid #160) was required.
The LR reaction was set up on ice from the LR clonase II mix of Invitrogen (11791019, Thermo Fisher) according to the following scheme (Table 20).

Table 20: Reaction set up of the LR reaction in the Gateway Cloning process.

REACTION COMPONENT	VOLUME
Entry clone	150 ng
Recipient plasmid	150 ng
5x LR clonase enzyme mix	2 µL
TE buffer pH 8.0	Add to 10 µL

The reaction mix was incubated at 25°C for one hour. 1 µL of proteinase K was added, mixed, and incubated at 37° C for 10 minutes. Subsequently, *E. coli* Stbl3 were transformed with 5 µL of reaction mix and incubated at 30° C overnight to suppress any residual recombination activity (section 2.1.9).

2.1.17. RNA isolation

Cell samples for RNA isolation were obtained by detaching the cells from their culture flask's surface using the appropriate detaching agent and incubation time (section 2.3). Detached cells were harvested by centrifugation in a microcentrifuge tube at 200 xg for three minutes and washed in 500 µL of Dulbecco's Phosphate Buffered Saline (DPBS) twice to allow efficient lysis of the cells. The obtained pellet was either flash-frozen in liquid nitrogen for storage at -80° C or directly used for RNA isolation using the GenElute Total Mammalian RNA Miniprep Kit (RTN350, Sigma Aldrich).

GenElute Total Mammalian RNA Miniprep Kit

RNA was isolated from harvested, and DPBS washed cell pellets using the GenElute Total Mammalian RNA Miniprep Kit (RTN350, Sigma Aldrich) according to the manufacturer's instructions. In brief: 10 µL of β-mercaptoethanol (4227, Carl Roth) was added per 1 mL of lysis solution to achieve effective degradation of RNases present in the sample. 250 µL of lysis solution was used for samples containing less than $5x10^6$ cells, and 500 µL of Lysis solution was used for samples of $5x10^6$ to $1x10^7$ cells. The appropriate amount of lysis solution was added to the sample, and the cells were disrupted by vortexing vigorously for one minute. All samples containing more than $1x10^6$ cells had to be passed through a GenElute Filtration Column after lysis by centrifugation at maximum speed for two minutes. An equal volume of 70% ethanol was added to the flow-through and mixed well by pipetting. Up to 700 µL of this sample was transferred to a GenElute Binding Column and centrifuged at maximum speed for 15 seconds. The flow-through was discarded, and the binding step repeated until the complete sample was passed through the binding column. After a first wash step using 250 µL of Wash Solution I (centrifuged at maximum speed for 15 seconds), on-column DNaseI digestion was performed to remove all contaminating traces of DNA present in the sample. For DNaseI digestion, 10 µL of DNaseI stock was diluted in 70 µL of Buffer RDD (RNase free DNase Set, 79254, QIAGEN) by gently pipetting up and down. The complete 80 µL of DNase I reaction mix were applied to the binding column by directly pipetting it onto the membrane and incubated at room temperature for 15 minutes. Following, the binding column was washed to remove all remaining salts from the RNA sample. First, 250 µL Wash Solution I were added to the DNase I solution on the column and centrifuged at maximum speed for 15 seconds. The flow-through was discarded and the column placed in a new collection tube. Secondly, two subsequent wash steps using 500 µL of Wash Solution II and centrifugation for 15 seconds at maximum speed each were performed. The flow-through was discarded and the empty column centrifuged at maximum speed for one minute to completely dry the membrane. Finally, the column was placed in a new collection tube, 30 to 50 µL of nuclease-free water were applied to the column matrix, incubated at room temperature for five minutes, and the RNA was eluted by centrifuging the column at maximum speed for one minute. Eluted RNA was put on ice immediately. RNA concentration and purity were determined using the NanoDrop2000c (software version 1.6, Thermo Scientific), and RNA was stored at -80° C.

2.1.18. cDNA synthesis

Complementary DNA (cDNA) is used for different applications like the cloning of coding-sequences of interest in recombinant plasmids or as a template for the quantification of the gene of interest's transcript via PCR. cDNA is reversely transcribed from RNA and contains coding sequences of the gene locus. The enzymes catalysing the reverse transcription are reverse transcriptases (RTs), which use a random hexamer primer or a short primer complementary to the 3' end of RNA to prime the synthesis of first strand cDNA. The first strand cDNA can directly be used as a template in a PCR reaction during which it will be complemented to double-stranded cDNA and thus can be used for cloning of the gene of interest into recombinant plasmids.

In this thesis, the reverse transcriptase (RT) from the Moloney Murine Leukemia Virus (M-MuLV) was used. The enzyme is genetically optimised to be more thermostable than the wild-type form, lacks a 3' to 5' exonuclease activity and exhibits a reduced RNase H activity specific to RNA in RNA-DNA hybrids compared to other RTs. cDNA syntheses were set up on ice as follows (Table 21).

Table 21: Reaction setup cDNA synthesis - part I.

REACTION COMPONENT	VOLUME
Total RNA	1 µg
Random Hexamer Primer, 100 µM (SO142, Thermo Fisher)	1 µL
Nuclease free water	Add to 12.5 µL

The reaction was mixed, incubated at 65° C for five minutes in a thermal cycler (peqSTAR 2x Universal Gradient, 732-2889DE, VWR), and immediately put on ice. 7.5 µL of RT-reaction mix was added to each sample (Table 22), mixed and incubated in a thermal cycler at 25° C for 10 minutes, followed by incubation at 42° C for one hour. The enzyme was inactivated at 70° C for 10 minutes. 5 to 10 µL aliquots were prepared from the 20 µL reaction and stored at -20° C.

Table 22: Reaction setup cDNA synthesis - part II.

REACTION COMPONENT	VOLUME
5x RT reaction buffer	4 µL
10 mM dNTPs (N0446S, NEB)	2 µL
RiboLock RNase Inhibitor (40 U/µL, EO0382, Thermo Fisher)	0.5 µL
RevertAid RT (200 U/µL, EP0442, Thermo Fisher)	1 µL

2.1.19. Quantitative reverse transcription PCR (RT-qPCR)

Real-time or quantitative PCR (qPCR) is a method to measure the amplification of a DNA fragment as the reaction takes place. If RNA or complementary DNA (cDNA) is used as a template, the method is called quantitative reverse transcription PCR (RT-qPCR). Using RNA/cDNA as a template allows the indirect quantification of RNA and by this, the expression of a specific gene of interest.

The template's amplification is measured via the fluorescent dye SYBRGreen which weakly binds to single stranded nucleic acids like RNA or cDNA but emits a strong fluorescent signal as it binds to double-stranded DNA after PCR amplification. As soon as a signal intensity stronger than the background fluorescence is detectable, a quantification cycle or c_T (threshold) value is determined. The c_T value reflects the number of cycles necessary to reach a fixed signal threshold. With these values the target's relative abundance between two or more samples can be evaluated. c_T values thus allow to evaluate the effect of a treatment on gene expression of a gene of interest. Normalization to a gene, whose expression is not expected to vary within cell cycle or upon the treatment (housekeeping or reference gene), serves as a control for differences in RNA extraction, RNA quality, and efficiency of reverse transcription. Subtraction of the gene of interest's c_T from the housekeeping gene's c_T value gives the normalised expression value Δc_T. The difference of Δc_T values of different samples ($\Delta\Delta c_T$) expresses the direction and size of the change in gene expression between these samples. $\Delta\Delta c_T$ is the logarithm of the ratio of concentrations of cDNA or the log fold-change. Usually, the relative quantification RQ is blotted when analysing RT-qPCR data. RQ is the square of the negative $\Delta\Delta c_T$ and reflects the mean expression level of the gene of interest. The extending bars in these blots do not reflect error bars but represent the lowest and highest values of expression level of the gene of interest based on c_T values.

The StepOnePlus system of Applied Biosystems (4376600, Thermo Fisher) in combination with the PowerUp SYBRGreen Master Mix of Applied Biosystems (15320929, Fisher Scientific) and low profile 96-well microtitre plates (732-3221, Peqlab brand VWR) was used for RT-qPCR analysis. Primers used for RT-qPCR were validated against a relative standard curve prior to gene expression analyses. Amplification efficiency of 95 to 105% at the given primer annealing temperature was accepted for further experiments. RT-qPCR reactions were set up as described in Table 23.

Table 23: Setup of RT-qPCR reactions.

REACTION COMPONENT	VOLUME
PowerUp SYBRGreen Master Mix (15320929, Fisher Scientific)	12.5 µL
10 µM Forward Primer	0.5 µL
10 µM Reverse Primer	0.5 µL
Nuclease-free water	7.5 µL
Template cDNA	4 µL

Three technical replicates per sample and gene analysed were set up in a 96-well plate. All reaction components except for the cDNA were prepared as a master mix and stored on ice. The final reaction

was composed of the 4 µL template cDNA which were pipetted first into each well and 21 µL of the master mix which were added last. Each well was mixed by pipetting up and down three times. Finally, the microtitre plates were sealed with self-adhesive foil (BRND701367, VWR), and the contents were collected by centrifugation. The PCR was run in a StepOnePlus thermal cycler with the programme described in Table 24.

Table 24: RT-qPCR thermal cycler programme.

STAGE	TEMPERATURE	TIME
Holding stage	95° C	10 minutes
Cycling stage	95° C	15 seconds
40 Cycles	[19]55-60° C	1 minute
	95° C	15 seconds
Melt curve stage	95° C	15 seconds
	[20]55-60° C	1 minute
	T_m +0.3° C/0.1 min to 95° C	
	95° C	15 seconds

After the run, data was collected from the machine and analysed using StepOne Software (Version 2.3) and Microsoft Excel. The $\Delta\Delta c_T$ method was applied as described above and calculated RQ values were plotted as log fold-change of expression to the reference gene human TATA-box binding protein (*TBP*).

[19] Primer melting temperature as calculated by IDR OligoAnalyzer https://eu.idtdna.com/calc/analyzer

[20] Primer melting temperature as calculated by IDR OligoAnalyzer https://eu.idtdna.com/calc/analyzer

2.2. Biochemical methods

2.2.1. Protein sample preparation and protein concentration measurement

Samples for protein analyses by immunoblotting were harvested in Lämmli buffer (Table 25). An appropriate volume of Lämmli buffer (e.g. 150 to 200 µL per well of a 6-well plate) was added directly to the DPBS-washed, adherent cells which were detached using a cell scraper (3008, Costar, Corning). Alternatively, dissociated or sorted cells were washed in DPBS, and an appropriate volume of Lämmli buffer was added. The cells in Lämmli buffer were then heated to 95° C for five minutes, cooled down on ice, and subsequently sonicated (one minute, intervals of five seconds) to efficiently extract and denature the sample's proteins. The so prepared protein samples were stored at -20° C or directly used for protein concentration measurement.

Table 25: Composition of the protein extraction buffer after Lämmli (Lämmli buffer).

COMPONENT	FINAL CONCENTRATION	AMOUNT
1 M Tris-HCL, pH 7.5	10 mM	1 mL
SDS (112533, Merck)	2%	2 g
EGTA (108435, Merck)	2 mM	0.076 g
NaF (P756.1, Roth)	20 mM	0.084 g

All components were added to a graduated measuring cylinder, and dissolved in approx. 60 mL of MilliQ H_2O while stirring. As soon as all components were dissolved, the stirring bar was removed, and the volume was filled up to 100 mL with MilliQ H_2O.

Protein concentration measurement was performed using the DC protein assay of Bio-Rad (500-0116). This assay is based on the biuret reaction of the Lowry assay but optimised to show a faster and more stable colour reaction. The colorimetric assay relies on the reaction of proteins with an alkaline copper tartrate solution (reagent A) and a Folin reagent (reagent B). Colour development takes place in two steps: first, the proteins in the sample react with the copper in alkaline medium to form cuprous ions. Secondly, the Folin reagent interacts with these cuprous ions and side chains of tyrosine, tryptophan, and cysteine amino acid residues. Thus, the Folin reagent is reduced to several possible reduced species which emit the characteristic blue colour with a maximum absorbance at 750 nm.

For protein concentration measurements, the protein samples were thawed and centrifuged at 18,000 xg for three minutes. 25 µL of the sample in an appropriate dilution (1:5 in Lämmli buffer) was prepared in two technical replicates in spectrophotometer cuvettes (613101, semi-micro, Greiner bio- one). 25 µL of Lämmli buffer were prepared to serve for background measurement (Ostrom, de Blank et al.). To prepare the working reagent A', 20 µL of reagent S were added per 1 mL of reagent A. 125 µL of working reagent A' were then added to the protein dilution, and mixed with 1 mL of reagent B in the cuvette. The reaction was incubated in the dark for 15 minutes before measuring the absorbance at 750 nm in a spectrophotometer (Spectronic BioMate 3, 335904, Thermo). The measured absorbance values were compared to a protein concentration standard to determine the sample's concentration.

Based on these calculations, protein samples of equal protein concentration (10 to 15 µg) were prepared in 4x loading buffer to a final volume of max. 40 µL (Table 26) for the SDS PAGE. The calculated sample volume was supplemented with 4x protein loading buffer to a final concentration of 1x, and diluted with Lämmli buffer. The sample was mixed by vortexing. After incubating the prepared sample at 95° C for 10 minutes and cooling it down on ice, the sample was directly loaded onto the SDS-containing polyacrylamide gel or stored at -20° C.

Table 26: Composition of 4x protein sample buffer for SDS PAGE and immunoblotting.

COMPONENT	FINAL CONCENTRATION	AMOUNT
1 M Tris-HCL, pH 6.8	200 mM	1.6 mL
10% SDS (from 112533, Merck)	4%	4 mL
100% Glycerol (7530.4, Roth)	2 mM	2 mL
Bromphenol blue (11746, Merck)	0.02%	1.9 mg
MilliQ H_2O		1.9 mL

250 µL aliquots of the sample buffer were prepared and stored at -20° C. Prior to use, 1 µL of β- mercaptoethanol (4227.3, Roth) were added per 50 µL of sample buffer.

2.2.2. Sodium dodecyl sulphate polyacrylamide gel electrophoresis

Sodium dodecyl sulphate polyacrylamide gel electrophoresis (SDS PAGE) is a denaturing method to separate proteins according to their mass due to an overall negative charge imparted on the denatured proteins by the bound SDS detergent.

Polyacrylamide is a mixture of acrylamide and bisacrylamide which forms a cross-linked polymer network when the polymerizing agent ammonium persulfate (APS) is added. The polymerisation reaction is catalysed by tetramethylethylenediamine (TEMED) which promotes the production of free radicals by APS. For protein separation, two polyacrylamide gels with different characteristics are combined. The protein sample is concentrated in the stacking gel before entering the resolution gel. The stacking gel contains a lower concentration of polyacrylamide, therefore exhibits a larger pore size, has a lower pH, and a different ionic content compared to the resolution gel allowing the sample to move through it quickly and to be concentrated directly above the resolution gel. This concentration ensures optimal resolution of the proteins present in the sample.[21]

In this thesis, a discontinuous buffer system based on tris-glycine base of the Lämmli system was used to separate proteins in SDS PAGE prior to immunoblotting in the Mini Trans-Blot Electrophoretic Transfer cell (1703930, Bio-Rad). The SDS-containing polyacrylamide gels were always cast freshly prior to use. To cast the gel, two glass slides (1.5 mm) were cleaned with 70% EtOH and delicate task wipers, and fastened together with the casting clamp. The casting clamp was then fixed onto its holder to lay plane on the bottom. First, the resolution gel was prepared according to Table 27. For the

[21] https://www.thermofisher.com/de/en/home/life-science/protein-biology/protein-biology-learning-center/protein-biology-resource-library/pierce-protein-methods/overview-western-blotting.html, May 03, 2020

analysis of proteins larger than 50 kDa, 8% polyacrylamide gels, for the analysis of proteins smaller than 50 kDa, 12% polyacrylamide gels were cast. Upon addition of APS and TEMED, the gel components were mixed quickly and completely by inversion, and the mixture was directly poured in between the glass slides to approx. ¾ of the volume. The polymerizing gel was immediately overlaid by 100% isopropanol to prevent drying. During the 30 minutes' polymerisation, the stacking gel was prepared according to Table 28. Before adding APS and TEMED, the isopropanol layer on the resolution gel was removed completely by pouring it from the gel and absorbing the remaining fluid with strips of Whatman paper. Upon addition of APS and TEMED, the gel components were mixed quickly and completely by inversion and the mixture was directly poured in between the glass slides till an upper meniscus formed atop of the glass slides. A 10- lane comb (1.5 mm) was carefully pushed into the polymerizing stacking gel without any bubbles. After 30 minutes, the polymerised gel between the glass slides was carefully removed from the holder and two gels were fixed into the electrophoresis holder. After testing for leaks with running buffer (Table 31), the electrophoresis holder was placed in the electrophoresis chamber. The chamber was filled with the indicated amount of running buffer, the combs were removed, and each well of the gels was rinsed with running buffer to remove gel residues. Per gel, at least one well was loaded with 7 µL of pre-stained PageRuler (26616, Thermo Fisher), the remaining wells were loaded with the prepared protein samples (section 2.2.1). The samples were concentrated through the stacking gel right above the resolution gel by applying 80 V for 15 to 20 minutes. As soon as the samples formed a tight line above the resolution gel and the protein standard had started to move into the resolution gel, the voltage was increased to 130 V. Electrophoresis was run until the protein standard indicated an appropriate separation (approx. 60 minutes). For the analysis of SMARCB1 protein, the SDS PAGE was run until the 25 kDa band of the protein standard had moved to the lower edge of the gel to ensure separation of both isoforms of SMARCB1 while keeping the GAPDH reference on the gel.

Table 27: Composition of polyacrylamide gels for protein separation in a SDS PAGE (resolution gel). Volumes are sufficient for casting one gel in 1.5 mm slides. Polyacrylamide gels with 8% acrylamide were used to separate proteins larger than 50 kDa, 12% polyacrylamide gels were used to separate proteins smaller than 50 kDa. APS and TEMED were added last, and the gel was cast quickly upon addition of APS and TEMED.

COMPONENT	FINAL CONCENTRATION	AMOUNT
MilliQ H_2O		4.65 mL
Resolution gel buffer (Table 29)		2.6 mL
30% Acrylamide solution (3029.2, Roth)	**8%**	2.7 mL
10% APS (9592.2, Roth)	0.01%	100 µL
TEMED (2357.1 Roth)		5 µL

COMPONENT	FINAL CONCENTRATION	AMOUNT
MilliQ H_2O		3.5 mL
Resolution gel buffer (Table 29)		2.6 mL
30% Acrylamide solution (3029.2, Roth)	**12%**	4 mL
10% APS (9592.2, Roth)	0.01%	100 µL
TEMED (2357.1 Roth)		5 µL

Table 28: Composition of the polyacrylamide gels for sample concentration in a SDS PAGE (stacking gel). Volumes are sufficient for casting one gel in 1.5 mm slides. APS and TEMED were added last and the gel was cast quickly upon addition of APS and TEMED.

COMPONENT	FINAL CONCENTRATION	AMOUNT
MilliQ H_2O		3.05 mL
Stacking gel buffer (Table 30)		1.3 mL
30% Acrylamide solution (3029.2, Roth)	0.4%	0.65 mL
10% APS (9592.2, Roth)	0.005%	50 µL
TEMED (2357.1 Roth)		5 µL

Table 29: Composition of the resolution gel buffer required to prepare the resolution gel for SDS PAGE.

COMPONENT	FINAL CONCENTRATION	AMOUNT
Tris Base (4855.2 Roth)	1.5 M	18.17 g
20% SDS (from 112533, Merck)	0.4%	2 mL

Tris base was dissolved in 60 mL of MilliQ H_2O in a graduated measuring cylinder. The pH of the tris buffer was adjusted to pH 8.8 (S20 SevenEasy pH, 51302803, Mettler Toledo) by adding 5 M hydrochloric acid (HCl). SDS was added, and the volume filled up to 100 mL with MilliQ H_2O. The buffer was used immediately for preparation of the SDS-containing polyacrylamide resolution gel to ensure optimal resolution and sharp protein bands.

Table 30: Composition of the stacking gel buffer required to prepare the stacking gel for SDS PAGE.

COMPONENT	FINAL CONCENTRATION	AMOUNT
Tris Base (4855.2 Roth)	0.5 M	6.06 g
20% SDS (from 112533, Merck)	0.4%	2 mL

Tris base was dissolved in 50 mL of MilliQ H_2O in a graduated measuring cylinder. The pH of the tris buffer was adjusted to pH 6.8 (S20 SevenEasy pH, 51302803, Mettler Toledo) by adding 5 M hydrochloric acid (HCl). SDS was added, and the volume filled up to 100 mL with MilliQ H_2O. The buffer was used immediately for preparation of the SDS-containing polyacrylamide resolution gel to ensure optimal resolution and sharp protein bands.

Table 31: Composition of 10x running buffer for SDS PAGE.

COMPONENT	FINAL CONCENTRATION	AMOUNT
Tris Base (4855.2 Roth)	250 mM	60.6 g
Glycine (3790.2, Roth)	2 M	288 g
SDS (112533, Merck)	1%	20 g

Tris base, glycine, and SDS were dissolved in two litres of MilliQ H_2O and stored at room temperature. For SDS PAGE, the 10x running buffer was diluted 1:10 in MilliQ H_2O.

2.2.3. Immunoblotting

Immunoblotting, in general, describes the transfer of biologic samples from a gel to an adhesive membrane and subsequent qualitative or semi-quantitative detection of the sample on the membrane's surface by specific antibody-antigen interaction. For the purpose of this thesis, wet immunoblotting was used to identify target proteins in a sample after separation of the proteins using SDS PAGE.

For the transfer of the separated proteins from the polyacrylamide gel to a polyvinylidene difluoride (PVDF) membrane, the gel has to be in direct contact with the membrane's surface. Therefore, the polyacrylamide gel and the PDVF membrane were sandwiched between Whatman paper and foam pads soaked in transfer buffer in a transfer clamp in the following order: starting on the clear side of the transfer clamp, one foam pad, three pieces of transfer buffer-soaked Whatman paper (approx. 8.5x10.5 cm, 5421836, Opti-lab), the methanol-activated and hydrophilised PVDF membrane (3010040001, Sigma Aldrich), the SDS-containing polyacrylamide gel, three pieces of transfer buffer-soaked Whatman paper (approx. 8.5x10.5 cm), and one foam pad were stacked in transfer buffer (Table 33). Trapped air bubbles were removed by rolling a 15 mL tube over the stack, before tightly closing the clamp. The sandwich was inserted into the transfer holder with the black side of the sandwich facing the black side of the holder (black = negatively charged cathode). The transfer holder with the sandwich was then put in the electrophoresis chamber and placed on a stirring plate (preferably in a 4° C room). Transfer buffer was added up to the transfer mark on the electrophoresis chamber and an electric current of 300 V/250 mA was applied per sandwich inserted. The protein transfer was run for 1.5 hours. After the transfer, the membrane was washed twice in tris-buffered saline with Tween-20 (TBS-T, Table 34) for 10 minutes while shaking. To reduce the background due

to unspecific binding of the secondary antibody, the membrane surface was blocked with 5% milk in TBS-T (T145.2, Roth) for one hour at room temperature while shaking. Before probing the blocked membrane with the primary antibody to detect the gene of interest, it was cut to the area where the protein of interest was expected (for SMARCB1 and GAPDH protein the membrane was cut between the 70 and 55 kDa band and the 34 and 26 kDa band of the protein standard) to save on primary antibody. The cut membrane was placed in a small plastic dish and probed with the primary antibody in 5% milk in TBS-T (Table 32), and incubated overnight at 4° C while shaking. Afterwards, the membrane was washed three times in TBS-T for 10 minutes while shaking to remove any unbound antibody residues. For detection of the probed protein, a horse radish peroxidase (HRP)-coupled secondary antibody was diluted 1:2,000 in 5% milk in TBS-T, and incubated on the membrane for one hour at room temperature while shaking. Finally, the membrane was washed three times in TBS-T for 15 minutes while shaking and put into TBS for imaging. Imaging was performed using the Fusion FX device and Fusion Capt Advance software of Vilber at the laboratory of the Löbrich group in serial mode and the enhanced chemo-luminescence (ECL) reagent of Pierce (10455145, Thermo Fisher). The protein standard was detected in auto mode to verify the size of the detected protein.

Detection of GAPDH protein as a loading control required removal of the antibodies used to detect the gene of interest. Therefore, the membrane was incubated in glycine stripping buffer (Table 35) for one hour at room temperature, rinsed three times with TBS-T, and was re-blocked in 5% milk in TBS- T for 30 minutes to one hour at room temperature. Primary antibody probing against GAPDH was performed as described above with a shortened incubation time of one hour at room temperature.

Table 32: Summary of primary and complementary secondary antibodies used for immunoblotting.

1° ANTIBODY	DILUTION	2° ANTIBODY
α SMARCB1 (rabbit monoclonal, D8M1X, CST)	1:80,000	Goat α rabbit (HRP) 111-035-003, Dianova
α GAPDH (mouse monoclonal, Sc_47724, Santa Cruz)	1:2,000	Goat α mouse (HRP) 115-035-003, Dianova

Table 33: Composition of 10x immunoblotting transfer buffer.

COMPONENT	FINAL CONCENTRATION	AMOUNT
Tris Base (4855.2 Roth)	250 mM	30.3 g
Glycine (3790.2, Roth)	2 M	144 g

Both components were dissolved in 1 L of MilliQ H_2O to obtain a 10x concentrated transfer buffer stock. For protein transfer, the 10x stock was diluted in 1.4 L MilliQ H_2O and 0.4 L of methanol (4627.5, Roth). The 1x transfer buffer can be filtered after each transfer and used three to four times.

Table 34: Composition of 10x Tris buffered saline (TBS) to prepare 1x TBS and 1x TBS-T for immunoblotting.

COMPONENT	FINAL CONCENTRATION	AMOUNT
Tris Base (4855.2 Roth)	200 mM	24.2 g
NaCl (3957.2, Roth)	1.4 M	80 g

Both components were dissolved in 1 L of MilliQ H_2O for the 10x TBS stock. 100 mL of 10x TBS stock were diluted in 900 mL of MilliQ H_2O to obtain the 1x TBS buffer. To obtain the 1x TBS-T working buffer, 0.1% of Tween-20 (9127.2, Roth) were added to 1x TBS (1 mL of Tween-20 per 1 L of 1x TBS).

Table 35: Composition of the glycin stripping buffer.

COMPONENT	FINAL CONCENTRATION	AMOUNT
Glycine (3790.2, Roth)	200 mM	1.5 g
Tween-20 (9127.2, Roth)	0.05%	50 µL

The glycine was dissolved in a graduated measuring cylinder in approx. 70 mL of MilliQ H_2O, the pH was adjusted to 2.5 (S20 SevenEasy pH, 51302803, Mettler Toledo) with 1 M HCl, then Tween-20 was added. The volume was filled up to 100 mL. The buffer may be stored at room temperature for up to four weeks.

2.3. Cell culture methods

Mammalian cells have to be handled in designated laboratories under a laminar flow hood to ensure a sterile working environment. All cell lines were kept in an all copper carbon dioxide (CO_2) incubator at 37° C, 5% CO_2, and 85-95% humidity. Whenever an exact cell number had to be plated, 100 µL of cell suspension in 10 mL of CASYton (5651808, OLS) were counted using the CASY Model TT Cell Counter & Analyser (OLS) with the appropriate settings. All waste generated during the work with mammalian cells was collected and sterilised in an autoclave at 121° C for 20 minutes.

2.3.1. Cultivation and transfection of the human embryonic kidney cell line HEK293T

Human embryonic kidney 293 (HEK293) cells were first established in 1973 and are now a widely used immortalised cell line for scientific research. The derivative HEK293T cell line expressed a mutant version of the SV40 Antigen T and was used in this thesis (Stepanenko and Dmitrenko 2015).

HEK293T cells were grown in HEK293T growth medium composed of Dulbecco's Modified Eagle's Medium (DMEM) supplemented with 4,500 mg/L glucose (DMEM-high glucose, D5671, Sigma Aldrich), 10% fetal calf serum (FCS, F7524, Sigma Aldrich), 2 mM L-Glutamine (G7513, Sigma Aldrich), 100 Units Penicillin, and 100 µg Streptomycin (P/S, P0781, Sigma Aldrich).

When the cells grew to 70 to 90% confluency, HEK293T cells were passaged. After washing the T75 culture flask (83.3911.002, Sarstedt) with 10 mL of sterile Dulbecco's phosphate buffered saline (DPBS, D8537, Sigma Aldrich), 2 mL of Trypsin/EDTA solution (T3924, Sigma Aldrich) were rinsed over the cells and incubated at 37° C for three to five minutes. The detached cells were dissociated by pipetting up and down and were collected in at least 4 mL of HEK293T growth medium to inactivate the trypsin reaction. The cell suspension was centrifuged at 200 xg for three minutes, the supernatant was aspirated, and the cell pellet re-suspended in an appropriate volume, e.g. 5 mL, of growth medium. Depending on the number of cells required and the timing of the next experiment, HEK293T cells were re-seeded at a ratio of 1:5 to 1:100 in a T75 culture flask containing 10 mL of HEK293T growth medium.

Transfection of HEK293T cells was performed using polyethylenimine (PEI), a stable cationic polymer that complexes DNA into positively charged particles which can bind negatively charged cell membranes. These PEI-DNA complexes enter the cell via endocytosis where the DNA is released into the cytoplasm (Boussif, Lezoualc'h et al. 1995, Sonawane, Szoka et al. 2003). The protocol applied for transfection of HEK293T cells was adapted from Longo, Kavran et al. (2013). In brief: One day prior to transfection, HEK293T cells were seeded at $0.4x10^6$ cells per well of a 6-well cell culture plate (83.3920.500, Sarstedt) in 2 mL of HEK293T growth medium. Late in the afternoon of the day of transfection, the transfection mix was prepared. Two microcentrifuge tubes were needed per transfection. Tube I contained 100 µL of DMEM-high glucose and two to four micrograms of purified plasmid DNA (section 2.1.11). In tube II 100 µL of DMEM-high glucose were combined with PEI (1 µg/µL, 23966-1, Polyscience Inc.) at a ratio of 1:4 of DNA to PEI (e.g. 2 µg of DNA and 6 µg of PEI). Both tubes were mixed thoroughly by vortexing and incubated at room temperature for

five minutes. The contents of both tubes were combined in one, mixed thoroughly by vortexing, and incubated at room temperature for 10 minutes. During this incubation time, the cells to transfect were prepared for transfection. The cells' medium was changed to 1.8 mL of pre-warmed HEK293T growth medium with 12% of FCS to account for the medium's dilution upon addition of the transfection mix. The transfection mix was slowly pipetted up and down before adding it dropwise to the prepared HEK293T cells. The well's contents were mixed by cross-shaking the plate and the transfection was incubated at 37° C for a maximum of 16 hours. To stop the transfection, the medium was changed to HEK293T growth medium. Already 24 hours after addition of the transfection mix, expression of the transferred genes could be observed. If larger culture vessels than 6-wells were transfected, the experiment was scaled up linearly.

Table 36 summarizes the concentrations of selection agents used for the selection of HEK293T cells expressing the respective resistance genes.

Table 36: Selection agents and their concentrations used to select HEK293T cells expressing the respective resistance genes.

SELECTION AGENT	STOCK CONCENTRATION	FINAL CONCENTRATION
Blasticidin (ant-bl, invivogen)	10 mg/mL	10 µg/mL
Puromycin (P8833, Sigma Aldrich)	10 mg/mL	1 µg/mL
Zeocin (ant-zn, invivogen)	100 mg/mL	200 µg/mL

2.3.2. Cultivation and transfection of human induced pluripotent stem cells (hiPSC)

Human induced pluripotent stem cell clone #33 (hiPSC#33) was derived from normal fibroblasts from a healthy, male donor and re-programmed using Sendai viruses by Nils Offen. hiPSC#33 were cultivated in a feeder-free culture system on Vitronectin-coated culture vessels (VTN, A14700, Life Technologies) with StemMACS iPSBrew XF Medium and Supplement (130-104-368, Miltenyi Biotech).

Culture vessels were coated with VTN at 5 µg/mL in a 1:100 dilution of VTN in DPBS (D8537, Sigma Aldrich) and incubated at room temperature for one hour prior to detachment of the cells. As soon as the hiPSC#33 grew to dense colonies, non-enzymatic passaging was performed. The culture medium was aspirated, and the cells were washed with DPBS once. After washing, 2 mL of 0.5 mM EDTA in DPBS (15575020, Life Technologies) was added and incubated at room temperature for four minutes. The EDTA solution was aspirated and the cells detached as small clumps by rinsing the vessel with an appropriate volume of StemMACS iPSBrew XF Medium and Supplement. Depending on the subsequent experiment, cells were plated at a ratio of 1:2 to 1:8 onto the VTN-coated 60 millimetres dishes containing 3 mL of StemMACS iPSBrew XF Medium and Supplement.

Single-cell seeding of hiPSC#33 was performed for transfection or transduction experiments. One day prior to the experiment hiPSC#33 were detached using 2 mL of accutase (A6964, Sigma Aldrich) at 37° C for three minutes. Repeated pipetting of the cell suspension with a 1 mL tip as well as passing the cells through a 40 µm cell strainer (732-2757, VWR) ensured single cell dissociation. The single-

cell suspension was diluted in pre-warmed DMEM/F12 (51445C, Sigma Aldrich), the cells were counted and collected at 200 xg for three minutes. Pelleted cells were re-suspended in an appropriate volume of StemMACS iPSBrew XF Medium and Supplement enriched with 1x RevitaCell (A2644501, Life Technologies) and seeded to VTN-coated culture vessels containing StemMACS iPSBrew XF Medium and Supplement enriched with 1x RevitaCell.

Transfection of hiPSC#33 was performed using five microliters of Lipofectamine Stem Reagent (STEM00015, Life Technologies) and 1.25 µg of DNA per well of a 6-well culture plate according to the manufacturer's instructions.[22] In brief, 125 µL of DMEM/F12 and 1.25 µg of DNA in tube I are added to tube II containing 125 µL of DMEM/F12 and 5 µL of Lipofectamine Stem reagent. The transfection reaction is mixed well by pipetting and incubated at room temperature for 10 minutes. The mixture was added drop-wise to one 6-well containing $3x10^5$ hiPSC#33 which were seeded 24 hours prior to transfection and were incubated with fresh StemMACS iPSBrew XF Medium and Supplement enriched with 1x RevitaCell for at least one hour prior to transfection.

Table 37 summarizes the concentrations of selection agents used for the selection of hiPSC#33 cells expressing the respective resistance genes.

Table 37: Selection agents and their concentrations used to select hiPSC#33 cells expressing the respective resistance genes.

SELECTION AGENT	STOCK CONCENTRATION	FINAL CONCENTRATION
Blasticidin (ant-bl, invivogen)	10 mg/mL	3-5 µg/mL
Puromycin (P8833, Sigma Aldrich)	10 mg/mL	150 ng/mL
Zeocin (ant-zn, invivogen)	100 mg/mL	150 ng/mL

2.3.3. Cultivation and transfection of the human breast epithelial cell line MCF10A

The MCF10A cell line is a spontaneously immortalised line of mammalian breast epithelial cells which contains a normal chromosome set except for triploidy of chromosome 8 (47 chromosomes in total) (Marella, Malyavantham et al. 2009).

An aliquot of these cells was obtained from Alexander Löwer at Technical University of Darmstadt and cultured in MCF10A growth medium composed of DMEM/F12 (21041-025, Life Technologies), 5% horse serum (16050-122, Life Technologies), 20 ng/mL epidermal growth factor (EGF, AF-100-15, Preprotech), 0.5 µg/mL hydrocortisone (H0888, Sigma Aldrich), 100 ng/mL Cholera toxin (C8052, Sigma Aldrich), 10 µg/mL Insulin (I9278, Sigma Aldrich), 2 mM L-Glutamine (G7513, Sigma Aldrich), 100 Units Penicillin, and 100 µg Streptomycin (P/S, P0781, Sigma Aldrich).

Upon reaching 80 to 90% confluency, the cells were washed once with DPBS (D8537, Sigma Aldrich), detached using 2 mL of Trypsin/EDTA solution (T3924, Sigma Aldrich) per 10 cm dish (83.3902, Sarstedt) which was incubated on the cells at 37° C for 20 minutes. The detached cells were then

[22] Lipofectamine Stem Reagent user guide available at: https://assets.thermofisher.com/TFS-Assets/LSG/manuals/MAN0017080 LipofectamineStem_UG.pdf

dissociated to single cells using a 1 mL tip and pipetting the suspension up- and down 30 times. To stop the trypsin-reaction, the cell suspension was diluted in at least 4 mL of MCF10A resuspension medium (DMEM/F12, 20% horse serum, 100 Units Penicillin, and 100 µg Streptomycin). If an exact cell number was required, 100 µL of the diluted cell suspension were counted using CASY cell counter before collecting the cells by centrifugation at 200 xg for 3 min. The cell pellet was then re-suspended in an appropriate volume of MCF10A growth medium and seeded in the required density.

Transfection of MCF10A was either performed using linear polyethylenimine (PEI) as described for HEK293T cells in section 2.3.1 or using Lipofectamine 3000 reagent (L3000001, Thermo Fisher) according to the manufacturer's instructions[23]. In brief: 125 µL of DMEM/F12 were mixed with 7.5 µL of Lipofectamine 3000 reagent in a microcentrifuge tube (tube 1). In another microcentrifuge tube, 125 µL of DMEM/F12 were mixed with 5 µL of P3000 reagent, and 2.5 µg of plasmid DNA (tube 2). The contents of tube 2 were then added to tube 1 and mixed well. After an incubation at room temperature for five minutes, the transfection mix was added drop-wise to MCF10A cells in one well of a 6-well plate containing 1.8 mL of MCF10A growth medium. For either method PEI or Lipofectamine 3000, MCF10A cells were seeded at a density of $0.3x10^6$ cells per well of a 6-well plate in 2 mL of MCF10A growth medium.

Table 38 summarizes the concentrations of selection agents used for the selection of MCF10A cells expressing the respective resistance genes.

Table 38: Selection agents and their concentrations used to select MCF10A cells expressing the respective resistance genes.

SELECTION AGENT	STOCK CONCENTRATION	FINAL CONCENTRATION
Blasticidin (ant-bl, invivogen)	10 mg/mL	7.5 µg/mL
Puromycin (P8833, Sigma Aldrich)	10 mg/mL	0.75 µg/mL
Zeocin (ant-zn, invivogen)	100 mg/mL	400 µg/mL

2.3.4. Cultivation of mouse neural stem and progenitor cells as neurospheres (NSPs)

Mouse neural stem/progenitor cells (NSCs/NPCs) were isolated from embryonic mouse brains by Alina Filatova. NSCs/NPCs were cultured as free floating spheres (NSPs) in full NSP medium (NSPM) composed of DMEM/F12 (21041-025, Life Technologies), 1x B27 supplement (17504-044, Life Technologies), 30 mM HEPES Buffer (12509079, Fisher Scientific), 100 Units Penicillin, and 100 µg Streptomycin freshly supplemented with 20 ng/mL Epithelial Growth Factor (EGF, 236-EG-200, R&D) and 20 ng/mL basic Fibroblast Growth Factor (bFGF, 233-FB-025, R&D). The spheres were dissociated when they reached approximately 100 µm of diameter. This was done by collecting the NSPs by centrifugation at 200 xg for three minutes, aspiration of the supernatant, and careful resuspension of the NSPs in 1 mL of accutase solution. After an incubation at 37° C for 15 minutes, the spheres were dissociated to single cells by slowly pipetting up and down the suspension with a

[23] Lipofectamine 3000 user guide available at: https://tools.thermofisher.com/content/sfs/manuals/lipofectamine3000_protocol.pdf

1 mL tip for at least 20 times and passing it through a 40 µm cell strainer (732-2757, VWR). The suspension was diluted in at least 9 mL of DMEM/F12 and seeded at $0.1x10^6$ cells/mL for stock or at $0.5x10^6$ cells per millilitre in preparation for experiments in T25 cell culture flasks (83.3910.002, Sarstedt).

2.3.5. Flow Cytometry analysis and sort (FACS)

Flow cytometry can be used to analyse the expression of different, antibody-fluorescent labelled markers or transgenes in single cells. A single cell solution is run through the flow cytometer, focused by a sheath flow, and each single cell passes a laser which excites the expressed fluorescent proteins or fluorophores attached to staining antibodies. The emitted light is detected and recorded to analyse the rate of cells expressing the gene of interest. All cells passing the laser are analysed in real-time, which allows for sorting of the cells with the desired characteristics, e.g. the expression of a fluorescent transgene into multi-well plates or tubes.

FACS was used in this work to analyse and enrich HEK293T cells subjected to CRISPR/Cas9-mediated introduction of fluorescent reporter cassettes into the *SMARCB1* gene locus. For this purpose, HEK293T cells were transfected with Cas9(n) and gRNA plasmids targeting the desired genomic region and suitable HDR constructs in a 1:4 mass ratio using PEI (section 2.3.1). 60 hours after transfection, the cells were dissociated using trypsin/EDTA and collected in FACS tubes (55.526.006, Sarstedt, section 2.3.1). After inhibition of the trypsin reaction, the cells were washed once in 1 mL of cold DPBS (vortexing, followed by centrifugation at 200 xg, 3 minutes), and twice in cold FACS buffer (Table 39). After the last wash, the cells were re-suspended in the FACS buffer that remains in the FACS tubes after discarding the supernatant. The cell suspension was then analysed using an Aria III FACS device (BD-Biosciences). For the detection of fluorophores, control samples of HEK293T cells transfected with plasmids carrying the same fluorophores as the samples were used to set the cytometer settings and define the necessary gates. mTagBFP(2) expression was analysed in the Pacific Blue channel, eGFP expression in the FITC channel, mKate2 expression in the PE-Cy5 channel, and SytoxRed staining in the APC channel.

For cell sorting, the 100 nm nozzle was used. The cells were either sorted into FACS tubes or into multi-well plates containing cold HEK293T medium. Populations that were to be subjected to RT- qPCR expression analyses were sorted into 96-well plates containing 20 µL of lysis buffer (500 to 1000 cells/96-well, Table 40).

After the sort, multiple wells containing the same cell populations were pooled in a 1.5 mL microcentrifuge tube, and lysis was supported by carefully pipetting the suspension. After incubation on ice for more than 10 minutes, the lysate was centrifuged at 13,000 xg and 4° C for 10 minutes, transferred to a new microcentrifuge tube, and stored at -80° C. Per cDNA synthesis reaction, 12 µL of lysate were used as RNA input (section 2.1.18). The synthesised cDNA was then used for RT-qPCR analyses (section 2.1.19).

Table 39: FACS buffer composition.

COMPONENT	CONCENTRATION	VOLUME
HEPES (1 M, 12509079, Fisher Scientific)	25 mM	12.5 mL
EDTA (0.5 M, 15575020, Life Technologies)	2 mM	20 mL
Bovine Serum Albumin (BSA, A8022, Sigma Aldrich)	1%	5 g
P/S (P0781, Sigma Aldrich)	1%	5 mL
DPBS (D8537, Sigma Aldrich)		500 mL

All components were mixed and dissolved in MilliQ H_2O. After sterile filtering into a sterile bottle, the buffer was stored at 4° C.

Table 40: Lysis Buffer composition for the lysis of FAC-sorted cells.

COMPONENT	CONCENTRATION	VOLUME
NP-40 Alternative (4%, IGEPAL, US1492016-100ml, Merck)	0.4%	100 µL
RiboLock RNase Inhibitor (40 U/µL, EO0382, Thermo Fisher)	0.5 U/µL	12.5 µL
Nuclease-free water		887.5 µL

The NP-40 Alternative was added to the water, and shook for 30 minutes to one hour to completely dissolve it. The basic buffer was cooled down on ice before the RNase inhibitor was added.

All FACS experiments were performed in together with Alina Filatova or Nils Offen. The method of cell lysis upon sorting was established by Nils Offen.

2.3.6. Electroporation of human cell lines

Electroporation is a method of transfection which utilizes high voltage electric shocks to transiently open pores in mammalian cell membranes to allow DNA to be introduced into the cell (Potter and Heller 2011). Upon electroporation, DNA is directly introduced into the nucleus which is advantageous for CRISPR/Cas9-mediated genome engineering, and renders electroporation also applicable to non-dividing cells (Cao, Xie et al. 2010).

Another advanced method of electroporation is nucleofection. It combines the electric shocks to open pores in the cell's membrane with cell type-specific reagents to transfer DNA directly into the nucleus.[24] In both methods, the cells to be electroporated need to be prepared as a single cell solution in a method-specific buffer, and transferred to an electroporation cuvette before an electric current is applied.

[24] https://bioscience.lonza.com/lonza_bs/SE/en/nucleofector-technology, April, 22 2020

Preparation of the cells:

The cells to be electroporated were cultured until they reached 70 to 80% confluency. HiPSCs were pre-treated with 1x RevitaCell supplement (A2644501, Life Technologies) one to three hours prior to dissociation to inhibit dissociation-induced apoptosis. The cells were dissociated as described in sections 2.3.1, 2.3.2, and 2.3.4 to obtain single cell suspensions in a high volume of dilution medium. After determination of the cell number using the CASY cell counter, the cell pellet (200 xg, three minutes) was washed with 1 mL of cold DPBS (D8537, Sigma Aldrich) twice before re-suspending the cells in an appropriate volume of electroporation/nucleofection buffer.

Electroporation in self-made electroporation buffer in the Amaxa Nucleofector 2b device (AAB-1001, Lonza):

Per electroporation experiment 10^6 cells in 100 µL of the self-made electroporation buffer (Table 41) were transferred to a 1.5 mL microcentrifuge tube and mixed with DNA (up to 10 µg). This mixture was then transferred into an electroporation cuvette (Z706086, Sigma Aldrich). The Nucleofector 2b device was kindly provided by the research group of Markus Löbrich. Upon completion of the electroporation, 900 µL of pre-warmed growth medium (e.g. StemMACS iPSBrew XF Medium and Supplement (130-104-368, Miltenyi Biotech) supplemented with 1x RevitaCell for hiPSC#33) were added to the cell suspension in the cuvette, and the cells were carefully seeded to a culture vessel of appropriate size (e.g. 10^6 hiPSC#33 to one to two wells of a 6-well plate coated with VTN (A14700, Life Technologies)). 24 hours after electroporation the cells were analysed for reporter gene expression.

Table 41: Composition of the self-made electroporation buffer used with the Amaxa Nucleofector 2b device.

COMPONENT	CONCENTRATION	AMOUNT
KCl (P9541, Sigma Aldrich)	5 mM	0.037 g
MgCl2 (Hexahydrat) (H9272, Sigma Aldrich)	15 mM	0.310 g
1 M Na_2HPO_4/NaH_2PO_4, pH 7.2 *	120 mM	12 mL
Mannitol (M9546, Sigma Aldrich)	50 mM	0.910 g

All components were combined in a graduated measuring cylinder, and the volume filled up to 100 mL with MilliQ-water to dissolve all solid components. The buffer was stored at 4° C after sterile filtering.

* For 100 mL of 1 M Na_2HPO_4/NaH_2PO_4, pH 7.2 prepare 100 mL of 1 M Na_2HPO_4 (1.06580.1000, Merck) and NaH_2PO_4 (1.06346.1000, Merck) each. Mix 28 mL of 1 M NaH_2PO_4 and 72 mL of Na_2HPO_4.

Electroporation using the Neon transfection system (MPK5000, MPP100, Thermo Fisher):

The Neon transfection system of Thermo Fisher is an electroporation device in a tip-cuvette format. Therefore, pipetting steps to transfer the cell suspension into and from the cuvette are performed with the cuvette itself. In this work, the 10 µL tip system was used to electroporate hiPSC#33 (MPK1025, Thermo Fisher, kindly provided by the research group of M. Cristina Cardoso and Thermo Fisher). Prior to transfection, the VTN coated 6-well plates for seeding were prepared with 1 mL of StemMACS iPSBrew XF Medium and Supplement supplemented with 1x RevitaCell and 25 mM HEPES Buffer (12509079, Fisher Scientific) per well and put into the incubator to adjust to the cell's growth conditions. The prepared single cell dilution was then re-suspended in R buffer of the Neon kit to 10^7 cells per millilitre. 10 µL of the cell suspension were mixed with an appropriate amount of DNA and aspirated with the Neon Pipette and 10 µL tip. The Neon Pipette and tip were then placed in the Neon Device, and the experiment's parameters were set. See https://tools.thermofisher.com/content/sfs/manuals/neon_device_man.pdf for the parameters to test when establishing transfection of a cell line. Upon electroporation, the cell suspension was directly seeded to one well of the prepared plate and incubated for 24 hours before analysing the cells for expression of the fluorescence reporter.

Nucleofection using the Amaxa Nucleofector 4D System (AAF-1002X, AAF-1002B, Lonza) and the P3 Kit (V4XP-3024, Lonza):

Similar to the Neon procedure, the Amaxa Nucleofector 4D System (kindly provided by Julia Weigand of the Süß research group) was only used for the transfection of hiPSC#33 and the plates required for seeding of the cells were prepared in advance (VTN coated 24-well plates, 500 µL of StemMACS iPSBrew XF Medium and Supplement supplemented with 1x RevitaCell).

After DPBS wash, the cell pellet was re-suspended in P3 solution to $0.6x10^6$ cells per 100 µL. Per reaction, 100 µL of cell suspension were transferred to a microcentrifuge tube. DNA (molar mass) was added to be equal to 2 µg of pMAX-GFP (plasmid #376) and the mixture was pipetted into an Amaxa 4D Nucleocuvette. After nucleofection using the programme CB-150, 200 µL of pre-warmed StemMACS iPSBrew XF Medium and Supplement supplemented with 1x RevitaCell were added directly to the Nucleocuvette and the complete volume was transferred to one well of the prepared 24-well plate. 24 hours after nucleofection, the cells were analysed for the expression of the fluorescent reporter.

2.3.7. Generation and concentration of lentiviral particles

The transfer of plasmid DNA, especially of large plasmids, into cells can be very inefficient. Introduction of DNA into cells via viral transduction offers higher transfer efficiencies. Lentiviruses are a subgroup of retroviruses. Both virus groups contain single-stranded RNA as their genome but only lentiviral particles can infect dividing and non-dividing cell types. The generation of lentiviral particles requires three different components. The transfer plasmid carries the gene(s) to be transferred flanked by long terminal repeats (Cheng, Davies et al.) and is packed by a packaging system consisting of a packaging plasmid coding for the viral genes *Gag*, *Rev*, *Pol*, and *Tat*, and the envelope plasmid coding for the coating glycoprotein of the Vesicular Stomatitis Virus (VSV-G). All three plasmids have to be transfected into the packaging cell line HEK293T at once.

Depending on the cell type to be infected different packaging and VSV-G envelope plasmids were used. Generally, 0.4×10^6 HEK293T cells per 6 well or 4×10^6 HEK293T cells per T75 flask were seeded one day prior to transfection (section 2.3.1). Late in the afternoon, the cells were transfected using PEI: per 6-well 700 ng transfer plasmid are combined with 700 ng of packaging and envelop plasmid each. For T75 flasks, 7,000 ng transfer plasmid are combined with 7,000 ng of packaging and envelop plasmid each. The transfection was performed as described in section 2.3.1. From the start of the transfection on the experiment was classified as biological safety group S2 and the required safety standards were met. 16 hours post addition of the transfection mix the medium was changed to HEK293T growth medium or the growth medium of the cells which were to be transduced. The cells were incubated for another 48 hours at 37° C before the lentivirus-containing supernatant was harvested. Cellular debris was removed from the supernatant by centrifugation at 200 xg for three minutes. Sterile filtering of the supernatant through a 0.2 µm PVDF syringe filter (SLGV033RS, Merck Chemicals) is optional, but recommended. The cleared supernatant was directly used for transduction or was concentrated to obtain higher viral titers and/or change of the medium system.

One way of concentration of lentiviral particles is ultracentrifugation. For this purpose, 30 mL of cleared lentivirus-containing supernatant were transferred to UV-sterilised screw-cap polycarbonate tubes (355618, Beckman Coulter) and balanced to 0.01 g with the counterweight. The ultracentrifugation was run at 55,000 xg and 4° C for two hours in an LM-8 Ultracentrifuge (Beckman Coulter). Before removing the tubes from the rotor type 70Ti (337922, Beckman Coulter), the outward-facing side of the tube, where the virus pellet was expected, was marked. The supernatant was completely removed and the virus pellet re-suspended in 125 µL of sterile-filtered DMEM supplemented with 1% of Bovine Serum Albumin (BSA, A8022, Sigma Aldrich) at 4° C for 10 to 15 minutes. Careful pipetting dissolved the pellet. The virus solution was directly used for transduction or aliquots of 10 to 20 µL were stored at -80° C.

Concentration of lentiviral particles over a sucrose cushion at speeds below ultracentrifugation is gentler and reduces the risk of damaging the particles compared to ultracentrifugation. According to

Jiang, Hua et al. (2015), lentivirus containing supernatant was harvested 48 hours after the stop of PEI transfection, and laid over a 10% sucrose buffer (Table 42) at a 5:1 v/v ratio in a 50 mL conical tube. For concentrating the virus in the sucrose layer, the tube was centrifuged at 10,000 xg and 4° C for four hours. After centrifugation, the lentiviral particles were visible as a white pellet in the sucrose layer, and the supernatant was removed carefully. The empty tube was then placed upside down on paper for three minutes to dry. For reconstitution, 1/50 of the original supernatant volume in DPBS was added to the pellet, and the tube was kept at 4° C overnight. The next day, the loosened pellet was carefully re-suspended by pipetting and used for transduction.

Table 42: Composition of sucrose-containing buffer for concentration of lentiviral particles.

COMPONENT	CONCENTRATION	VOLUME
Sucrose	10%	10 g
Tris-HCl pH 7.4 (1 M,	50 mM	5 mL
NaCl	100 mM	0.584 g
EDTA (0.5 M, 15575020, Life Technologies)	0.5 mM	100 µL

All components were dissolved in Milli-Q water to 100 mL, sterile filtered, and stored at 4° C.

2.3.8. Transduction of mammalian cell lines

DNA transfer into difficult to transfect cells like NSP-forming cells was facilitated using lentiviral particles. The efficiency of viral infection was increased by supplementing the transduction mixes with the cationic polymer hexadimethrine bromide (polybrene, H9268, Sigma Aldrich). HEK293T cells were used as transduction controls. 500 µL to 1 mL of cleared virus-containing supernatant supplemented with 6 µg/mL polybrene was directly added to $0.4x10^6$ HEK293T cells per well of a 6- well plate seeded one day ahead of transduction. The cells were incubated with the transduction mix at 37° C for 24 hours.

For the transduction of NSPs, $0.5x10^6$ NSCs were seeded per millilitre of NSPM one day ahead. The next day NSPs were transduced with 1 mL of virus-containing supernatant made from NSPM and supplemented with 6 µg/mL polybrene, 20 ng/mL EGF and bFGF in one well of a 6-well plate. 24 hours after addition of the transduction mix, the NSPs were collected at 200 xg for three minutes and re-suspended in full NSPM.

Cell health and expression of the transgenes was monitored after the transduction.

3. Results

3.1. Design and generation of constructs for CRISPR/Cas9-mediated genome engineering of the *SMARCB1* locus in human cells

A fluorescence-based reporter approach was chosen for CRISPR/Cas9-mediated genome engineering of the *SMARCB1* locus in human cells. Guide RNA (gRNA)-Cas9 expression plasmids, which facilitate the co-expression of Cas9 and a fluorescence gene were used so that a direct fluorescent readout for transfection and expression of the Cas9 endonuclease was possible. The constructs applied as a template for homology-directed repair (HDR construct) encoded for a promoterless fluorescent reporter which was only expressed upon directed integration into the genome. In this way, upon genome engineering, the *SMARCB1* alleles should be co-expressed with three different fluorescence genes. Upstream of the native start codon of the *SMARCB1* gene, a loxP site and a mTagBFP2 reporter cassette were introduced, linked by a T2A sequence. Downstream of the stop codon of the *SMARCB1* gene, either an eGFP or a mKate2 reporter cassette and a loxP site was inserted, linked by an IRES sequence (Figure 7). CRISPR/Cas9-mediated introduction of all three HDR constructs results in a sophisticated three-colour reporter system. This system not only allows the rapid identification of recombined cells by the expression of the fluorescence reporter genes – which would be time and cost intensive if the insertion of a loxP site or point mutation alone had to be verified – but also indicates the deletion of each marked allele of *SMARCB1* by loss of the fluorescence signal upon *Cre* recombination. Additionally, the insertion of the fluorescence reporters facilitates the differentiation between the two *SMARCB1* alleles. Therefore, differences in the gene expression from either allele can be detected by RT-qPCR analysis of the fluorescence genes' transcripts even though the sequence differences, e.g. due to point mutations, are too subtle to be recognised by primers (Figure 9).

HDR constructs homologous either to the sequences flanking the start (exon 1 HDRs) or stop (exon 9 HDRs) codon of *SMARCB1* were generated. Therefore, genomic sequences of *SMARCB1* up- and downstream of the Cas9 cleavage site were cloned up- and downstream of the reporter sequences to be introduced. The homologous sequences selected to edit the genome at chromosome 22q11 were 1.5 to 1.7 kb long and were referred to as homology arms. The homology arm upstream of the reporter was termed "left" homology arm (HL), the genomic sequence downstream of the reporter was termed "right" homology arm (HR). All cloning steps were performed using a restriction endonuclease-based cloning approach. According to Zhang, Ge et al. (2014), Zheng, Hou et al. (2017), protospacer adjacent motif (PAM) sites and/or bases essential for gRNA-target pairing were mutated in the cloned homology arms to prevent Cas9-mediated cleavage of the HDR constructs and excision after integration. The sequence changes were chosen to be silent base exchanges and are labelled in the sequences (Figure 31 and Figure 32) The functionality of the CRISPR/Cas9 approach using the generated constructs was tested in HEK293T cells (section 3.2). Based on these test results, the

CRISPR/Cas9 strategy was adapted further to optimise the gene editing process or outcome. The characteristics of all constructs generated can be found in the appendix (section 7.1.6).

As mentioned before, mutations of the tumour suppressor gene *SMARCB1* may cause either the neurodevelopmental syndrome Coffin-Siris (CSS) or can lead to aggressive rhabdoid tumours dependent on the type of mutation and if *SMARCB1* is altered hetero- or homozygously. The developmental timing and the type of mutation appears to be of decisive importance for the phenotypic outcome (Han, Richer et al. 2016, Filatova, Rey et al. 2019). In most cases, CSS is caused by germline heterozygous non-truncating missense mutations or small in-frame deletions in exons 8 or 9 of the *SMARCB1* gene (Tsurusaki, Okamoto et al. 2012). Germline mutations causing the rhabdoid tumour predisposition syndrome (RTPS1) usually are heterozygous truncating *loss-of-function* mutations or large deletions that can occur in several exons of the *SMARCB1* gene (Sevenet, Sheridan et al. 1999, Sredni and Tomita 2015). Importantly, RTPS1 individuals carrying such heterozygous germline mutations do not show any neurodevelopmental phenotypes. For the rhabdoid tumour-associated germline mutations, a complete loss of gene expression is observed upon spontaneous mutation/deletion of the second allele of *SMARCB1*.

Germline mutations of the *SMARCB1* gene, either causing CSS or RTPS1 were selected to analyse the effect of each mutation on the expression of the gene on mRNA and protein level. Germline mutations of the *SMARCB1* gene reportedly predisposing to AT/RTs and located close to the start or stop codon of the gene were selected. Three mutations were identified from Eaton, Tooke et al. (2011). The AT/RT predisposing nonsense mutation *c.20_43delins T* which leads to several pre-mature termination codons in exon 1 of the *SMARCB1* gene and thus to a loss of the protein, and the predicted splice-site mutation *c.93G>C* at the border of exon and intron 1 of *SMARCB1* were cloned into the *SMARCB1* e1 HDR constructs. The heterozygous CSS-associated missense mutation of *SMARCB1* selected was *c.1091_1093del AGA*, one of the most common CSS-associated *SMARCB1* (Tsurusaki, Okamoto et al. 2012, Kosho, Okamoto et al. 2014). Additionally, the reported AT/RT-associated somatic *SMARCB1* mutation *c.1148delC* in exon 9 of the gene was included in the analysis as there were no AT/RT-associated germline mutations in exon 8 or 9 of the *SMARCB1* gene reported so far (Biegel, Tan et al. 2002, Kordes, Gesk et al. 2010).

Therefore, constructs to generate human cell lines with a reporter cassette upstream and downstream of the coding sequence of *SMARCB1* with and without AT/RT- or CSS-related mutations in the coding sequence of *SMARCB1* were established.

3.1.1. Design and generation of constructs for CRISPR/Cas9-mediated genome engineering of human cell lines with AT/RT-associated *SMARCB1* mutations

HDR constructs to insert a reporter cassette downstream of the stop codon of the *SMARCB1* gene were generated as described in the following. The initial plasmid (plasmid #83) was a pBluescript (pBS) backbone containing a T2A peptide, an in frame enhanced green fluorescent-zeocin resistance fusion gene (eGFP::ZeoR), and a loxP site, the T2A peptide was optimised for optimal self-cleavage upon translation (Chng, Wang et al. 2015). Oligonucleotides of the T2A peptide sequence, a 5' Glycine-Serine-Glycine (GSG) linker, and 5' Acc65I/ 3' AvrII-specific cohesive ends (oligonucleotides #743, #744) were cloned into plasmid #83. Insertion of the HR corresponding to the sequence upstream of the stop codon of the *SMARCB1* gene was achieved by PCR amplification (1.6 kb, oligonucleotides #317, #318) from hiPSC#33 genomic DNA (gDNA) while adding PspXI and EcoRI restriction endonuclease recognition sites. The HL was generated by PCR amplifying the sequence downstream of the stop codon of the *SMARCB1* gene from hiPSC#33 gDNA (1.7 kb, oligonucleotides #315, #316), followed by insertion into pBluescript (plasmid #80) via TA-Cloning. Subsequently, the HL was transferred to the target plasmid via the PsiI and BsrGI restriction endonuclease recognition sites which were added by the PCR primers. Figure 15 schematically depicts the cloning steps leading to the resulting plasmid *SMARCB1* e9 HDR T2A-eGFP::ZeoR (plasmid #226).

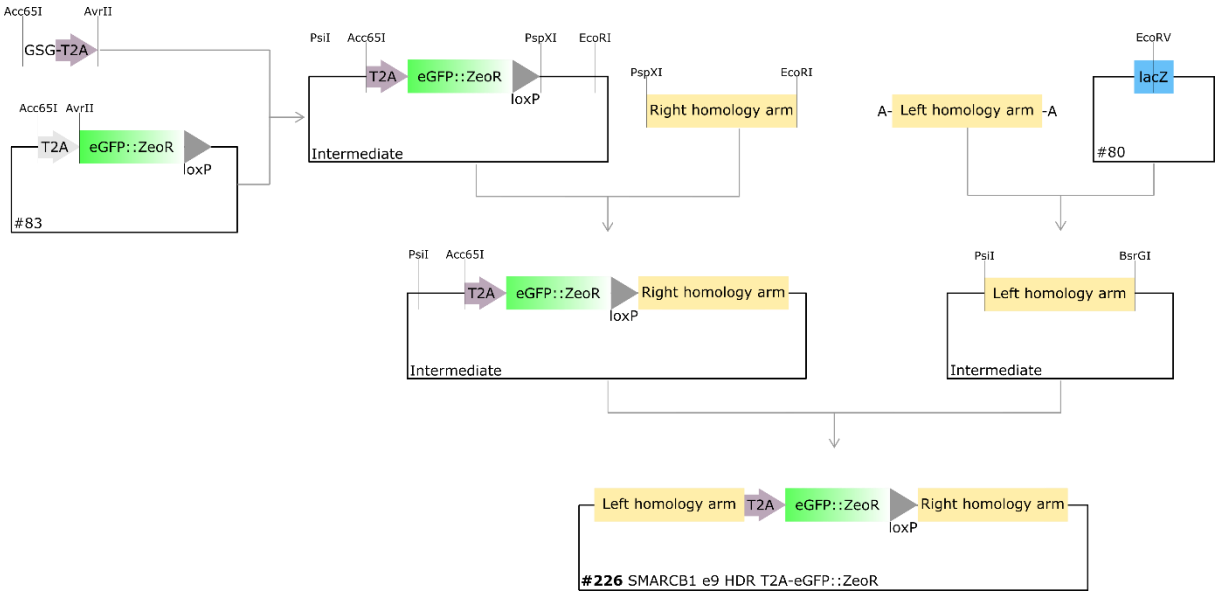

Figure 15: Schematic overview of the cloning steps leading to *SMARCB1* e9 HDR T2A-eGFP::ZeoR, plasmid #226. The left and right homology arms, corresponding to the sequences up- and downstream of the stop codon of *SMARCB1* were amplified from gDNA and cloned into the final plasmid using the restriction endonuclease recognition sites PsiI/BsrGI or PspXI/EcoRI, respectively. The left homology arm covers the sequence of the NCBI reference genome NG_009303.1 positions 50,538 to 52,218. The right homology arm covers the sequence of NCBI reference genome NG_009303.1 positions 52,219 to 53,787, directly adjacent.

After testing in HEK293T cells (section 3.2.1), the T2A peptide linking gene expression of *SMARCB1* and the eGFP::ZeoR reporter was exchanged for an internal ribosomal entry site (IRES). Multicistronic expression of genes linked by an IRES is facilitated by the additional binding of

ribosomes to IRES on the complete mRNA of the linked genes (Jang, Krausslich et al. 1988). Cloning of the exon 9 HDR construct with IRES was achieved via the pBS-IRES-eGFP::ZeoR-loxP intermediate. The IRES2 sequence (IRES, oligonucleotides #890, #891) and the eGFP::ZeoR-loxP sequence (oligonucleotides #892, #893) were PCR amplified from plasmid #128 and #83, respectively. Restriction endonuclease digestion of #80 and the PCR amplicons generated compatible cohesive ends which were ligated to combine the intermediate pBS-IRES-eGFP::ZeoR-loxP (plasmid #227). The homology arms of *SMARCB1* exon 9 HDR were PCR amplified from gDNA similarly to plasmid #226 (oligonucleotides HL #315, #887; HR #888, #889). The cloning steps for the generation of *SMARCB1* e9 HDR IRES-eGFP::ZeoR (plasmid #243) are summarised in Figure 16.

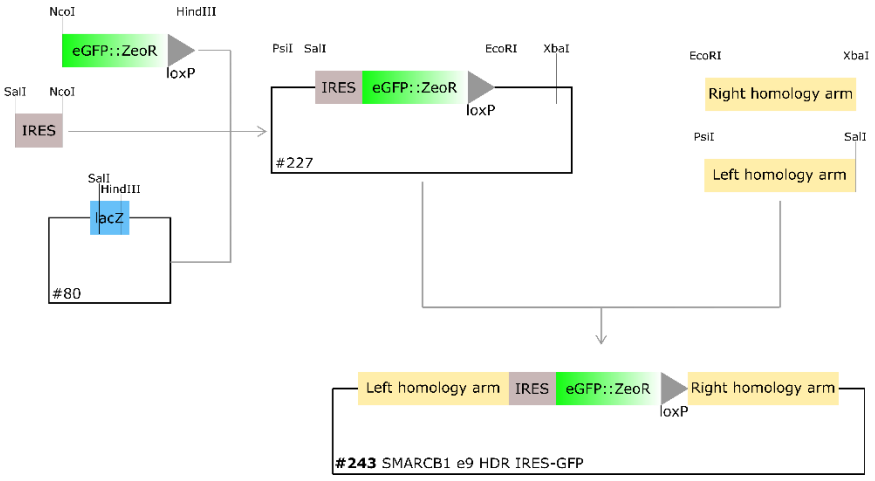

Figure 16: Schematic overview of the cloning steps required to generate *SMARCB1* e9 HDR IRES-eGFP::ZeoR, plasmid #243. The left and right homology arms, corresponding to the sequences up- or downstream of the stop codon of *SMARCB1* were PCR amplified from gDNA and cloned into the target plasmid via PsiI/SalI or EcoRI/XbaI, respectively

Based on plasmid #243, the selectable fluorescence reporter eGFP::ZeoR was exchanged for the far-red fluorophore mCardinal by SalI/EcoRI restriction endonuclease digestion of plasmid #272 and cloning of the IRES-mCardinal cassette (*SMARCB1* e9 HDR IRES-mCardinal, plasmid #277, Figure 33).

The *SMARCB1* exon 9 HDR construct was further optimised with the exchange of mCardinal for the smaller far-red fluorescence gene mKate2. mKate2 was PCR amplified (oligonucleotides #1137, #1107) from plasmid #311, and cloned into plasmid #243 via plasmid #227 (*SMARCB1* e9 HDR IRES-mKate, plasmid #318, Figure 33).

Optimisation of the identification and isolation of successfully genome-engineered cells was achieved by adding a T2A-linked blasticidin resistance cassette downstream of the mKate2 sequence in the HDR construct. The eGFP::ZeoR-loxP reporter cassette of plasmid #227 was exchanged for an IRES-mKate2-T2A sequence, resulting in intermediate plasmid #385. For this purpose, mKate2 was PCR amplified (oligonucleotides #1137, #1105) from plasmid #318 and the T2A sequence was annealed from oligonucleotides #982, #983. Subsequently, the blasticidin resistance gene (BSD) and a loxP site were PCR amplified (oligonucleotides #1440, #1441) from plasmid #355 and inserted into

plasmid #385. The IRES-mKate2-T2A-BSD-loxP reporter cassette was cloned into plasmid #318 (*SMARCB1* e9 HDR IRES-mKate2-T2A-BSD, plasmid #386, Figure 17).

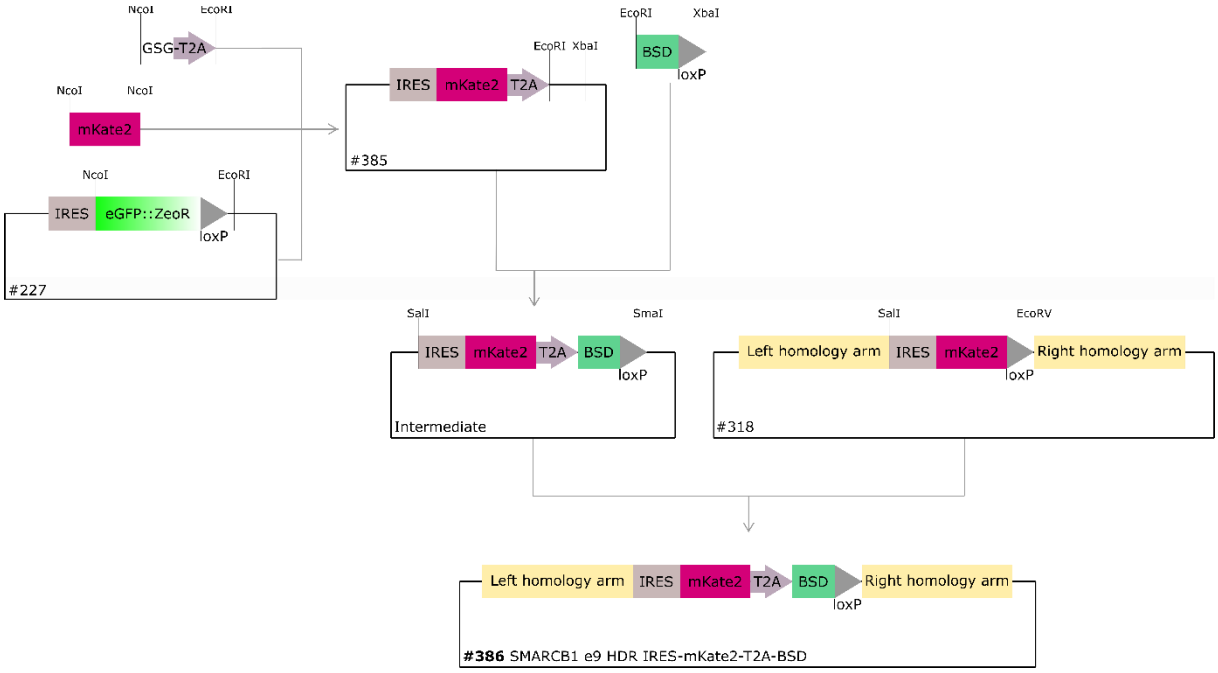

Figure 17: Schematic overview of the cloning steps required to obtain the plasmid *SMARCB1* e9 HDR IRES-mKate2-T2A-BSD. mKate2 with NcoI restriction endonuclease recognition sites at the 3' and 5' end of the sequence was amplified from plasmid #318. The T2A sequence was annealed from oligonucleotides #982, #983 and was flanked by NcoI and EcoRI restriction endonuclease recognition sites. The final selectable reporter cassette IRES-mKate2-T2A-BSD-loxP was cloned into plasmid #318 via SalI and compatible SmaI/EcoRV DNA ends, resulting in plasmid #386.

The cloning of the *SMARCB1* exon 1 HDR constructs was performed analogously to the exon 9 HDR constructs. The homology arms comprising the sequences up- and downstream of the native start codon of *SMARCB1* were cloned into a pBluescript backbone containing a loxP-eGFP::ZeoR-T2A cassette to facilitate co-expression of the reporter and the *SMARCB1* gene. To fit into the three-colour reporter strategy and to take differences in observed fluorescence intensity of different fluorophores into account, the encoded reporter upstream of the HR was exchanged to mTagBFP2. A depiction of the cloning steps to generate the *SMARCB1* e1 HDR constructs is provided in Figure 34. Regarding the decision for which of the three selected fluorescence genes to include in which HDR construct, the differences in signal brightness were considered (brightness according to https://www.fpbase.org/). E.g. eGFP is brighter than mKate2, which is also brighter than mTagBFP2. Tests in HEK293T cells showed that fluorescence genes linked downstream of the *SMARCB1* coding sequence via an IRES result in a weaker signal compared to the same fluorescence gene co-expressed upstream to the coding sequence of *SMARCB1* (data not shown, compare section 3.2.1 and 3.2.2). Similar to the exon 9 HDR constructs, a selectable marker was added to the exon 1 HDR constructs to allow enrichment of successfully engineered cells. A more complex cloning strategy with two intermediates was necessary to obtain the wildtype exon 1 HDR construct *SMARCB1* e1 HDR PuroR-P2A-mTagBFP2-T2A (plasmid #380) containing a Puromycin resistance cassette (PuroR, Figure 35).

HDR constructs to insert a AT/RT-associated point mutation into the coding sequence of *SMARCB1* and a reporter cassette upstream of the start codon/downstream of the stop codon of the *SMARCB1* gene were generated applying a similar strategy for genome engineering as described above (Figure 7C). In a literature-based research, three different (germline) mutations which were observed in more than one AT/RT case in exon 1 or exon 9 of the *SMARCB1* sequence were identified (Eaton, Tooke et al. 2011). Due to the use of a reporter for the selection of successfully engineered cells, the mutations to be introduced needed to be located at either the 3' or 5' end of the coding sequence of *SMARCB1*.

Based on the HDR construct *SMARCB1* e9 HDR IRES-eGFP::ZeoR (plasmid #243), the somatic single base deletion at position 1148 (*c.1148delC*) was introduced into exon 9 of the *SMARCB1* sequence in the left homology arm. Using an oligonucleotide primer containing the *c.1148delC* mutation, the mutated HL was PCR amplified (oligonucleotides #315, #1309) and cloned into the pBS-IRES-eGFP::ZeoR-loxP-HR intermediate via PsiI and SalI restriction endonuclease sites (Figure 18). The final product *SMARCB1 c.1148delC* e9 HDR IRES-eGFP::ZeoR, plasmid #363 was used for further experiments.

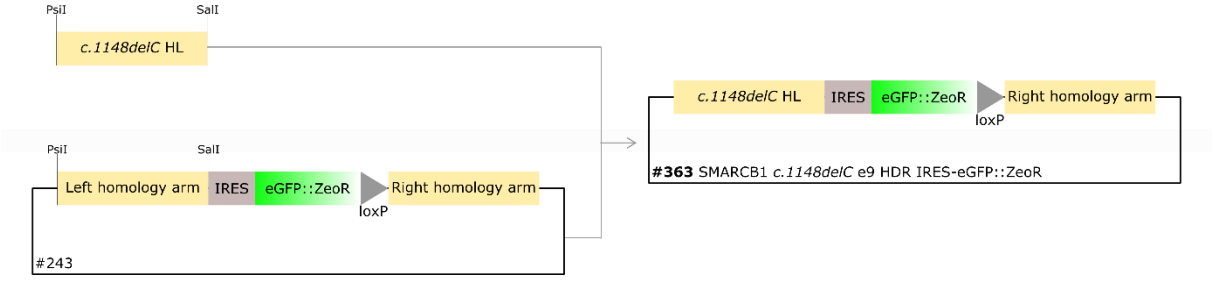

Figure 18: Schematic overview of the cloning of *SMARCB1 c.1148delC* e9 HDR IRES-eGFP::ZeoR, plasmid #363. The left homology arm containing the mutation *c.1148delC* was PCR amplified using plasmid #243 and subsequently cloned into plasmid #243 via PsiI and SalI restriction endonuclease cloning.

The second and third AT/RT-associated germline mutations of the *SMARCB1* gene were cloned into *SMARCB1* e1 HDR mTagBFP2-T2A, plasmid #346 (Figure 34) The replacement of 23 bp for a single T in exon 1 (*c.20_43delins T*) was achieved by PCR amplification of the mTagBFP2 sequence and the mutated part of the right homology arm using plasmid #346 and applying an oligonucleotide primer containing the mutation (oligonucleotides #1207, #1381). Finally, the amplicon was cloned into plasmid #346 via ClaI, PvuII and PciI restriction endonuclease sites, resulting in *SMARCB1 c.20_43delins T* HDR mTagBFP2-T2A, plasmid #379 (Figure 34).

The splice site mutations *c.93G>C* in intron 1 of the *SMARCB1* gene was introduced via the overlap extension method (section 2.1.14). Fragment A (mTagBFP2-*c.93G>C* HR) was PCR amplified (oligonucleotides #1207, #1314) and combined with fragment B (oligonucleotides #1315, #988) to amplify the final fragment C containing the *c.93G>C* mutation in the HR of the e1 HDR construct (oligonucleotides #1207, #988). Fragment C (mTagBFP2-*c.93G>C* HR) was then cloned into plasmid #346 via ClaI and PciI restriction endonuclease sites, resulting in *SMARCB1 c.93G>C* HDR mTagBFP2-T2A, plasmid #378 (Figure 34). Insertion of the PuroR selection cassette was achieved

by replacing the original mTagBFP2-T2A fluorescence reporter cassette in plasmids #378 and #379 for the complete PuroR-P2A-mTagBFP2-T2A reporter cassette of *SMARCB1* e1 HDR PuroR-P2A-mTagBFP2-T2A (plasmid #380) to obtain *SMARCB1 c.93G>C* HDR PuroR-P2A-mTagBFP2-T2A, plasmid #381 and *SMARCB1 c.20_43delins T* HDR PuroR-P2A-mTagBFP2-T2A, plasmid #382 (Figure 35).

3.1.2. Design and generation of constructs for CRISPR/Cas9-mediated genome engineering of human cell lines with CSS-associated *SMARCB1* mutations

Starting from plasmid #243, the *c.1091_1093del AGA* mutation of the *SMARCB1* gene was inserted into the HDR construct's left homology arm. For this purpose, the HL was divided into two parts. An upstream mutated part from the 3' end to the BssSαI restriction endonuclease recognition site in exon 8 of the *SMARCB1* gene and a downstream wildtype part from the BssSαI recognition site to the 5' end of the sequence of the HL (Figure 19). The mutation was introduced into the upstream portion of the HL by PCR using a mutated oligonucleotide for amplification (oligonucleotides #928, #929). Restriction endonuclease digestion of #243 using BssSαI and SalI yielded the second, wildtype portion of the HL. Both parts of the HL were ligated and cloned into pBluescript and from there transferred into plasmid #243 to generate the CSS HDR construct plasmid #253 (*SMARCB1* CSS e9 HDR IRES-eGFP::ZeoR, Figure 19).

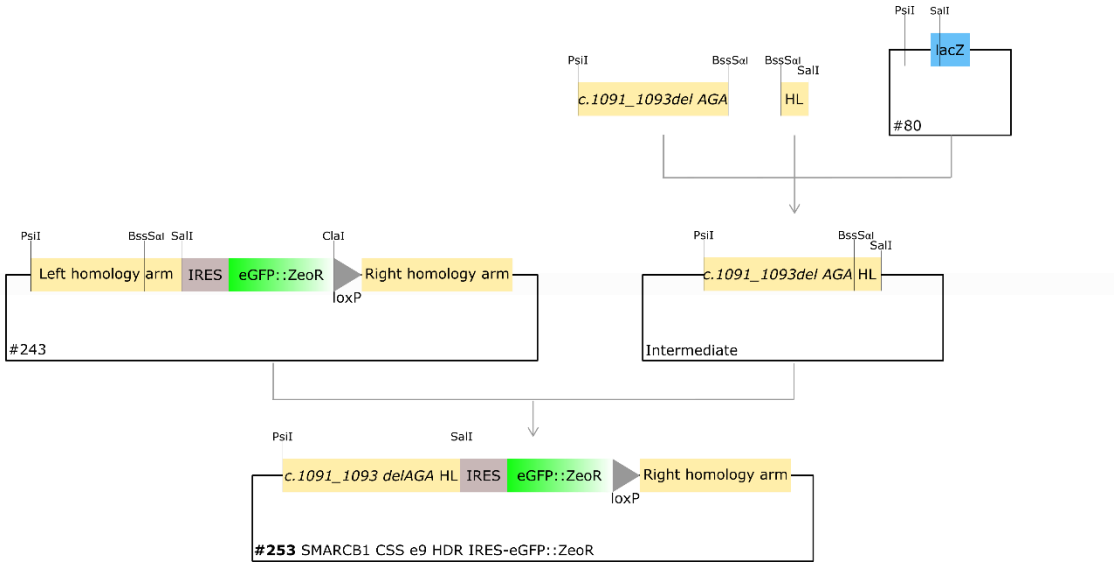

Figure 19: Schematic overview of the cloning steps to generate the *c.1091_1093del AGA* HDR construct to introduce a CSS-specific mutation into exon 8 of the *SMARCB1* gene. The mutation was introduced by using a mutated oligonucleotide primer for PCR amplification of the HL. The complete *c.1091_1093del AGA* HL sequence was sub-cloned into pBluescript plasmid #80 as an intermediate before inserting the complete HL sequence into the *SMARCB1* wildtype HDR construct plasmid #243 to generate *SMARCB1* CSS e9 HDR IRES-eGFP::ZeoR, plasmid #253.

Similar to the HDR construct for the insertion of a reporter gene downstream of the stop codon of *SMARCB1*, the plasmid was optimised to encode the IRES-mKate2-T2A-BSD reporter. For this purpose, the left homology arm carrying the *c.1091_1093del AGA* mutation was cloned into

plasmid #386 via PsiI and SalI resulting in the construct *SMARCB1* CSS e9 IRES-mKate2-T2A-BSD, plasmid #422.

3.1.3. Design and generation of gRNA and Cas9 expression plasmids for CRISPR/Cas9-mediated genome engineering of the *SMARCB1* locus in human cells

gRNA and Cas9 nickase (Cas9n) expression plasmids were obtained using the Multiplex CRISPR/Cas9 Assembly System Kit from Addgene (Kit #1000000055). An approach with Cas9n and two targeting gRNAs per cleavage site was chosen for genome editing of the genomic sequence of *SMARCB1*. Fluorescence reporter cassettes linked to Cas9n via a T2A sequence were inserted into the pX330A-1x2 plasmid (plasmid #131). Proceeding from plasmid #120 which encoded an eGFP::ZeoR reporter linked to Cas9n via T2A, the self-cleavage of the T2A peptide was optimised by insertion of a GSG-linker upstream of the T2A sequence and subsequently, mCardinal, dsRedExpress2, and mTagBFP sequences were cloned into Cas9n plasmids separately (Chng, Wang et al. 2015). In each case, the fluorescence gene was PCR-amplified with AvrII and ClaI restriction endonuclease recognition sites added 5' or 3' of the sequence, respectively (Figure 36). Table 43 gives and overview of the oligonucleotides used for amplification and the identification numbers of the resulting plasmids.

Table 43: Summary of fluorescence reporter genes inserted into the original pX330A-1x2 Cas9 plasmid.

PLASMID	FLUORESCENCE REPORTER	OLIGONUCLEOTIDES USED
#216	mCardinal	Restriction endonuclease cloning
#217	GSG-T2A-mCardinal	#745, #746
#219	mTagBFP	#668, #669 from plasmid #215
#220	dsRedExpress20	#787, #801 from plasmid #128

The gRNA sequences targeting the sequence flanking the stop codon of the *SMARCB1* gene were selected using the CRISPR designing tool of the MIT (http://tools.genome-engineering.org) according to Ran, Hsu et al. (2013). Cloning of sequences encoding the selected gRNA pairs into pX330A-1x2 Cas9n expression constructs was performed according to Sakuma, Nishikawa et al. (2014), section 2.1.15. Figure 31 in the appendix shows the exact position and cleavage sites of the selected gRNAs. Figure 20 depicts the cloning of the gRNA pairs D1, D2, and D3 targeting the genomic region flanking the Stop codon of the *SMARCB1* gene into multiplex Cas9n plasmids. Table 44 summarises the oligonucleotides (oligo) used to generate the gRNAs required for the targeting of the sequences flanking the stop codon of the *SMARCB1* gene.

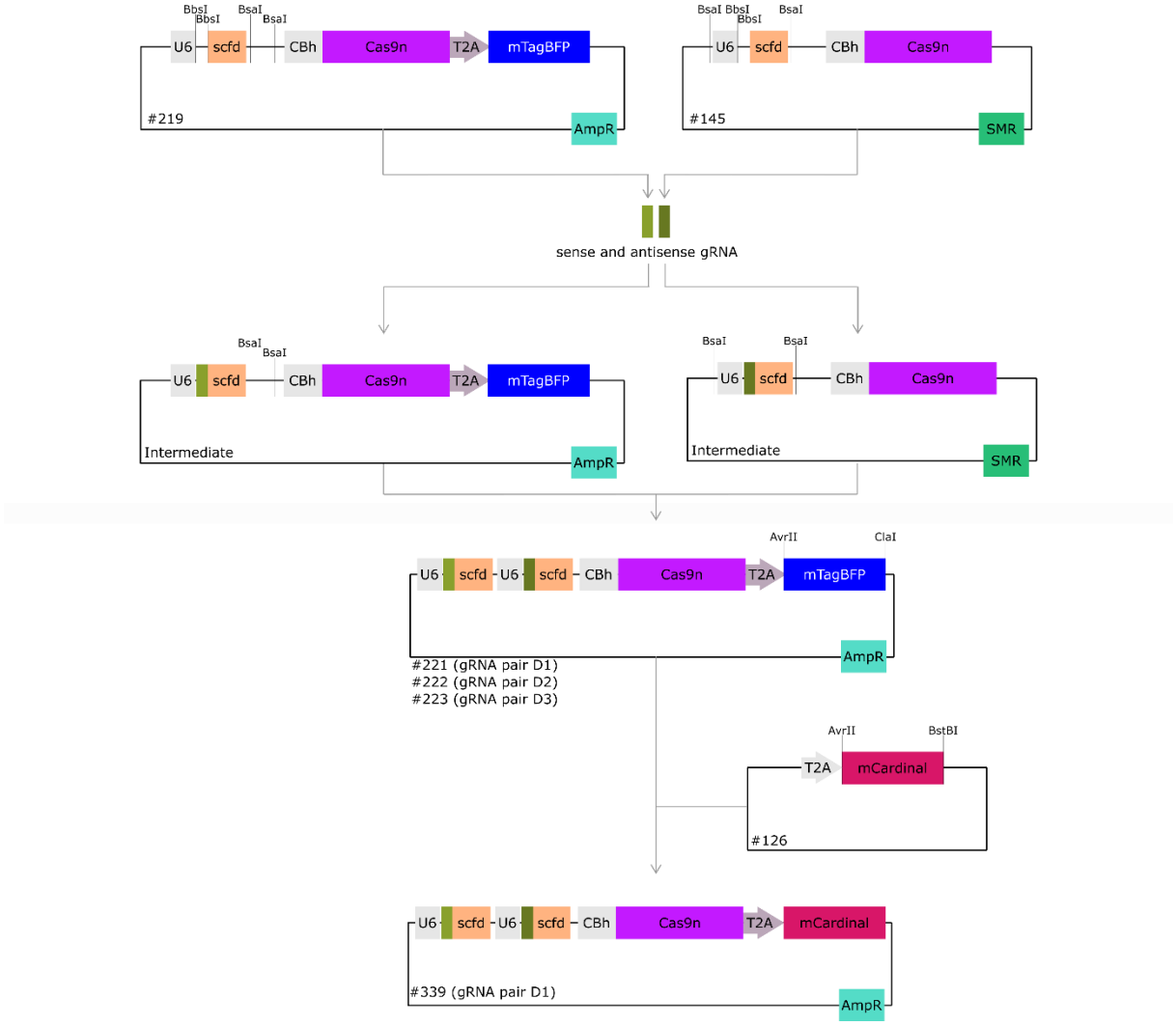

Figure 20: Schematic overview of the cloning of the sequences encoding gRNA pairs D1, D2, and D3 targeting the genomic region flanking the *SMARCB1* gene into multiplex Cas9n expression plasmids. As described in section 2.1.15, the 20 nt targeting sequence of the gRNAs were annealed from ordered oligonucleotides carrying overhangs at their 5' and 3' ends complementary to the overhangs generated by cleavage of the plasmid using BbsI. The annealed and phosphorylated oligonucleotides were first cloned into the original pX330 plasmids: The sense gRNAs into plasmid #219, the antisense gRNAs into plasmid #145. Combinatorial Golden Gate cloning via BsaI yielded Cas9n plasmids with both gRNA expression cassettes of one pair (plasmids #221-223). Later in the project, another fluorescence reporter was required. Thus, the mTagBFP sequence was exchanged for the mCardinal sequence from plasmid #126 via AvrII and ClaI/BstBI cloning (plasmid #339).

Table 44: Oligonucleotides annealed to generate the double-stranded sequences encoding for the gRNAs targeting the genomic sequence flanking the Stop codon of the tumour suppressor gene *SMARCB1*. The 5' overhangs required for the Golden Gate cloning into the Cas9 plasmids are highlighted in green.

gRNA NAME	gRNA SEQUENCE, *5'→3'*	OLIGO
D1 sense	CACCGACGGAGCATCTCAGAAGATT	#305
	AAACAATCTTCTGAGATGCTCCGTC	#306
D1/2 antisense	CACCGTTACCAGGCCGGGGCCGTGT	#307
	AAACACACGGCCCCGGCCTGGTAAC	#308
D2 sense	CACCGCCATCAGCACACGGCTCCCA	#309
	AAACTGGGAGCCGTGTGCTGATGGC	#310
D3 sense	CACCGTAACCAGCCCATCAGCACA	#311
	AAACTGTGCTGATGGGCTGGTTAC	#312
D3 antisense	CACCGGCAAGACGCCTCATCCGCC	#313
	AAACGGCGGATGAGGCGTCTTGCC	#314

Transfer of large plasmids as the Cas9n plasmids into hiPSCs and other difficult to transfect cell lines is challenging. To overcome this limitation, the Cas9n sequence was removed from plasmid #221 to obtain the gRNA-only plasmid #310 which was co-delivered with recombinant, purified Cas9(n) protein (Figure 37).

Further optimisation of the genome engineering of the *SMARCB1* gene in hiPSCs required the cloning of wildtype Cas9 (Cas9) plasmids. The Cas9 plasmids #03 and #07 were completed with the sequence of antisense gRNA D3 (plasmid #388 and #387, respectively; Figure 38). The highest scoring gRNA targeting the sequence flanking the *SMARCB1* stop codon selected in the original gRNA search. Additionally, the Cas9n sequence of plasmid #221 was exchanged for the wildtype Cas9 sequence via AgeI and EcoRV restriction endonuclease recognition sites, resulting in a construct with two gRNAs that target wildtype Cas9 molecules to exon 9 of the *SMARCB1* gene thus increasing cleavage efficiency of the targeted region (plasmid #408, Figure 38).

The gRNA sequences targeting the sequence flanking the start codon of the *SMARCB1* gene were also selected using the CRISPR designing tool of the MIT (http://tools.genome-engineering.org) according to Ran, Hsu et al. (2013). Cloning of sequences encoding the selected gRNA pairs into pX330A-1x2 Cas9n expression constructs was performed according to Sakuma, Nishikawa et al. (2014), section 2.1.15. The gRNA pair C3 was designed to target the region flanking the start codon of *SMARCB1*. Figure 31 and Figure 32 show the exact position and cleavage sites of the selected gRNA sequences targeting the genomic regions flanking the start and stop codon of the tumour suppressor gene *SMARCB1*. The sequences encoding gRNA pair C3 were cloned into the multiplex gRNA and Cas9n plasmids #220 (dsRedExpress reporter) and #218 (mTagBFP reporter) analogously to pairs D1-D3 (Figure 20). The resulting plasmids were named pX330A_D10A-dsRedExpress *SMARCB1* gRNA pair C3 and pX330A_D10A-mTagBFP *SMARCB1* gRNA pair C3 (#256).

Analogous to *SMARCB1* gRNA pair D1, the coding sequence of Cas9n was removed from plasmid #256 generating a gRNA pair C3 and mTagBFP reporter plasmid which was co-transfected with recombinant Cas9 protein (plasmid #309, compare to Figure 37). Table 45 summarises the characteristics of the oligonucleotides used to generate sense and antisense gRNA C3 sequences.

Table 45: Overview of the gRNA sequence pairs selected to target the region flanking the native start codon of the human *SMARCB1* gene.

gRNA NAME	**gRNA SEQUENCE, *5'→3'***	**OLIGO**
C3 sense	CACCGTGGCGCTGAGCAAGACCTTC	#302
	AAACGAAGGTCTTGCTCAGCGCCAC	#303
C3 antisense	CACCGATCATTGCGGCGGCAGAGGC	#300
	AAACGCCTCTGCCGCCGCAATGATC	#301

3.2. Establishment and optimisation of CRISPR/Cas9-mediated genome engineering methods in HEK293T cells

HEK293T cells were used as a system to test the functionality of all generated plasmids for the genome editing of the *SMARCB1* gene locus. HEK293T cells are easy to transfect and appeared to be rather readily genome engineered, probably due to their tetraploidy (Stepanenko and Dmitrenko 2015).

3.2.1. Establishment and optimisation of the CRISPR/Cas9-mediated genome engineering of the *SMARCB1* locus in HEK293T cells using the generated AT/RT-associated constructs

The first approach of CRISPR/Cas9-mediated engineering included a Cas9 nickase in combination with one of three pairs of gRNA sequences targeting the genomic region flanking the native stop codon of *SMARCB1* (gRNA pairs D1, D2, D3, section 7.1.3) and a HDR construct to insert a co-expressed eGFP-zeocin resistance (eGFP::ZeoR) cassette as well as a loxP site downstream of the stop codon of *SMARCB1* (compare to Figure 7B). Co-expression was facilitated by deletion of the native stop codon of *SMARCB1* and in-frame addition of a T2A sequence with flexible glycine-serine-glycine linker (plasmid #226, Figure 15). Flow cytometry analysis showed similar recombination efficiencies for all three of the gRNA pairs tested to insert the eGFP::ZeoR reporter cassette downstream of the native *SMARCB1* stop codon. The portion of eGFP positive cells within the Cas9n/gRNA expressing BFP-positive population was similar for either of the gRNA pairs used (Figure 21). For further experiments only the gRNA-Cas9 plasmid expressing the targeting sequence of gRNA pair D1 was used.

Engineered HEK293T cells were enriched by zeocin selection, and the engineered cell population was analysed for growth rate and for synthesis of the SMARCB1 protein. Due to the nature of the self-cleavage of 2A peptides, 22 amino acids are added to the protein expressed upstream of the linker peptide. As expected, this was observed by a shift of the SMARCB1/T2A protein band to 46.4 kDa in protein samples of engineered HEK293T cells (Figure 22C). In addition to the altered C-terminus of the SMARCB1 protein, HEK293T cells engineered to co-express eGFP::ZeoR downstream of the *SMARCB1* gene also showed a significantly reduced growth rate compared to HEK293T wildtype control cells (Figure 22A, B). Since only little is known about the folding of the SMARCB1 protein, the impact of the additional 22 amino acids added by T2A self-cleavage cannot be assessed, but may interfere with the binding of the nucleosome by the BAF complex (He, Wu et al. 2020). Due to the observed growth retardation, an alternative approach for the co-expression of the reporter cassette was designed, namely the co-expression of the *SMARCB1* gene and the fluorescence reporter linked by an IRES.

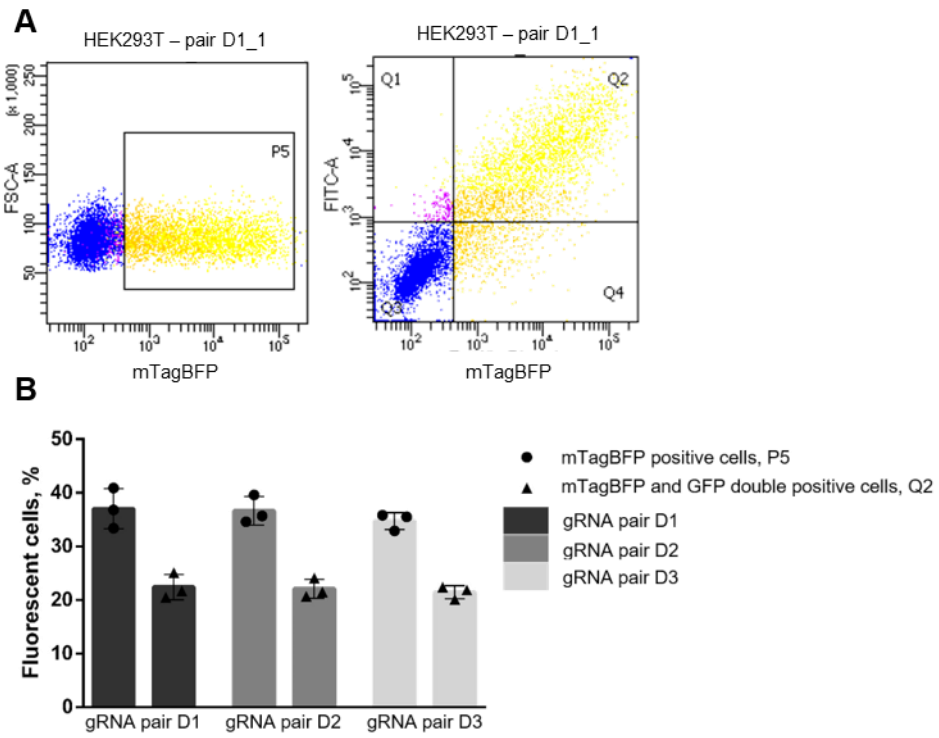

Figure 21: All three gRNA pairs targeting the region flanking the native stop codon of the *SMARCB1* gene show equivalent CRISPR/Cas9n-mediated genome engineering efficiencies in HEK293T cells. **(A)** Flow cytometry analysis showed 35% of mTagBFP positive cells, indicating a transfection efficiency of 35% for the gRNA and Cas9n plasmids #221, #222, #223. Each expressing one pair of gRNAs (pair D1, D2, and D3, respectively. Representative FACS plots are shown). **(B)** Analysis of three technical replicates per plasmid showed similar transfection efficiencies for all three plasmids. The percentage of eGFP positive cells within the mTagBFP population was similar for all three gRNA and Cas9n plasmids. This indicates a similar efficiency in facilitating CRISPR/Cas9n-mediated genome engineering since an eGFP signal was only expected upon targeted insertion of the eGFP::ZeoR reporter cassette from the co-transfected HDR plasmid #226. Sample size per condition was n = 3. Normal distribution of the results was verified by the Anderson-Darling test. Student's t-test did not reveal significant differences between transfection of genome engineering efficiencies facilitated by either of the three gRNA and Cas9n plasmids.

In this approach, HEK293T cells were genome-engineered using the nickase approach with the same three pairs of gRNAs but in combination with a different HDR construct facilitating co-expression of the *SMARCB1* gene and the eGFP::ZeoR reporter via an IRES sequence (plasmid #243, Figure 7B and Figure 16). Due to the direct binding of the ribosome to the IRES, no amino acids are added to the co-expressed genes. However, the protein coded downstream of the IRES is reported to be expressed at a lower rate (Trichas, Begbie et al. 2008). Flow cytometry analyses showed that genome engineering of the *SMARCB1* gene using the IRES strategy was similarly efficient compared to the T2A approach (Figure 22A). Western Blot analyses showed a protein band of SMARCB1 at the expected size of 44 kDa (data not shown, compare Figure 24). In growth analyses, HEK293T cells engineered to express the *SMARCB1*-IRES-eGFP::ZeoR transgene grew at even lower rates than HEK293T cells co-expressing the reporter via a T2A sequence (Figure 22B). However, the resulting protein was not altered, which was evaluated to be advantageous. The IRES co-expression approach was selected to be the method of choice for the genome editing of the *SMARCB1* gene.

Tests of different fluorophores in HEK293T cells showed that the expression of a fluorescence reporter alone was not sufficient to ensure enrichment of successfully engineered cells. Introduction of only a fluorescence reporter co-expressed with *SMARCB1* resulted in only temporary expression of the fluorescence reporter hampering the isolation of successfully engineered cells and diminishing the advantages of the multi-colour system (data not shown, section 3.1). Thus, the final chosen second fluorophore, mKate2, was linked to a blasticidin resistance cassette (plasmid #386, Figure 7B and Figure 17).

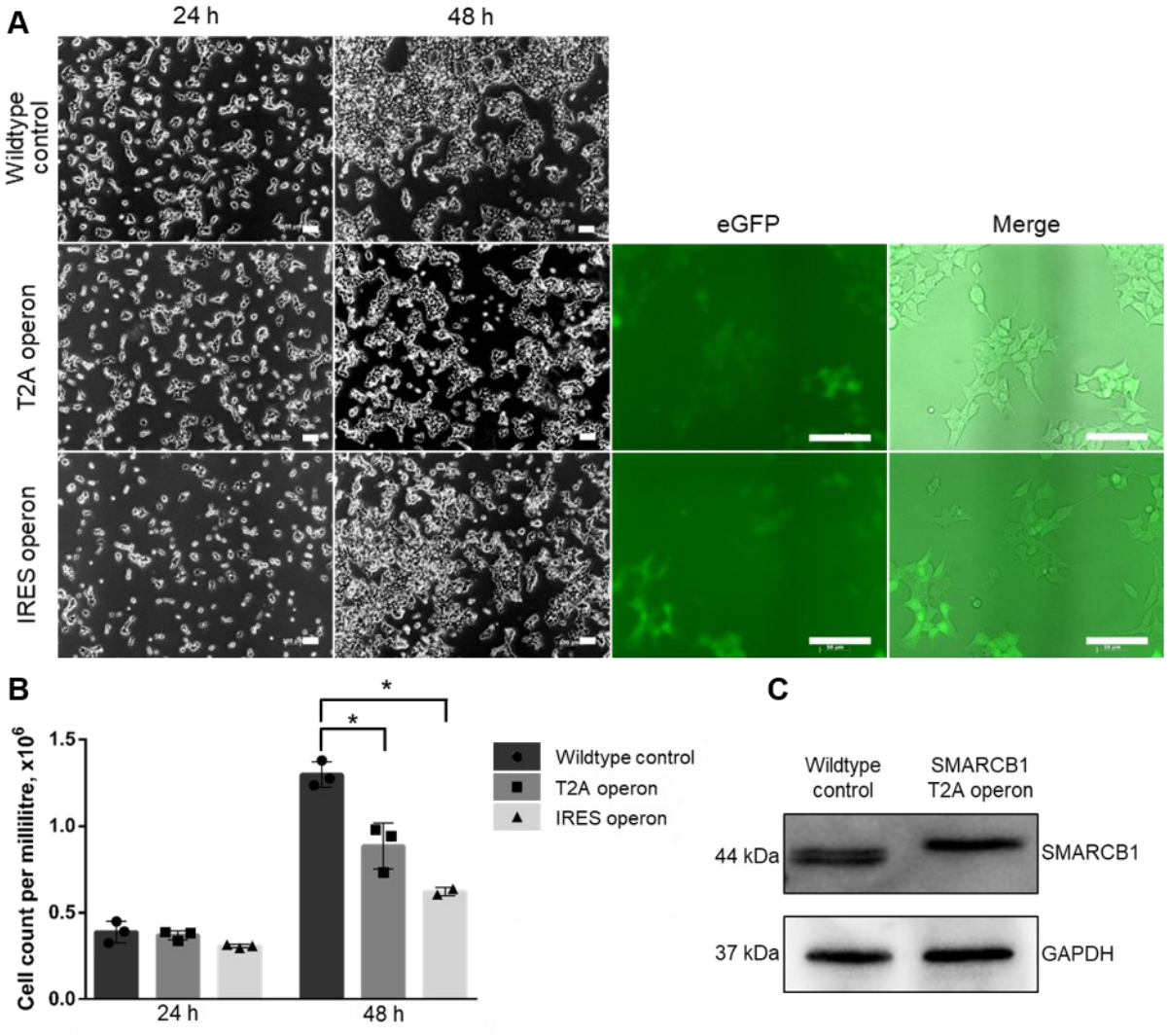

Figure 22: Analysis of the impact of the insertion of a T2A or IRES linked eGFP::ZeoR reporter downstream of the native stop codon of the *SMARCB1* gene. **(A)** Cell growth was monitored over 48 hours after seeding 0.2x10^6 HEK293T cells per well of a 6-well plate. Already 24 hours post seeding, the cell density in the wells with either the cells engineered to express *SMARCB1*-T2A-eGFP::ZeoR (T2A operon) and the cells engineered to express SMARCB1-IRES-eGFP::ZeoR (IRES operon) was lower compared to the wells with wildtype HEK293T cells (left panel). The eGFP expression in the engineered cells was detected by fluorescence microscopy 48 hours after seeding (right panel). **(B)** Every 24 hours, three wells per condition were detached using Trypsin/EDTA solution and counted using CASY cell counter. The cell count per millilitre was blotted for each condition. Already at 24 hours a slight decrease in cell count was observed for the IRES operon cells compared to T2A operon or wildtype HEK293T cells. At 48 hours, a significant decrease in cell count per millilitre was observed for both, the T2A and IRES operon cells which is more pronounced for IRES operon cells. **(C)** SMARCB1 protein analysis by Western blotting showed a size difference due to the addition of 22 amino acids to the C-terminus of SMARCB1 by self-cleavage of the T2A peptide. Per condition and time point, three wells were analysed. Scale bars in A represent 100 µm. Normal distribution of cell count data was verified by the Anderson-Darling test. Statistical analysis was performed using Student's t-test. * $p < 0.05$, ** $p < 0.001$.

The reporter co-expression via an IRES was considered to be the favoured approach and was thus further developed to allow the introduction of the CSS-associated mutation *c.1091_1093del AGA* in exon 8 of the *SMARCB1* gene as well as to express different fluorophores (Figure 8, section 3.1.2).

The CRISPR/Cas9 engineering of the regions flanking the start codon of *SMARCB1* was tested in HEK293T cells as described above. Here, a T2A sequence was used to link a fluorophore reporter with the *SMARCB1* gene to ensure approximately native expression rates of the *SMARCB1* gene (Figure 7B). 2A peptides are preferable to IRES sequences for this purpose, since the gene downstream of the IRES was shown to be expressed at lower rates (Szymczak and Vignali 2005). Additionally, the T2A sequence is much shorter (63 bp) than the IRES sequence (587 bp), resulting in an overall smaller HDR construct (Szymczak and Vignali 2005). The effect of the insertion of the reporter cassette upstream of the start codon of *SMARCB1* on the HEK293T cell growth was analysed. There was no negative impact on cell growth of HEK293T cells engineered to express the eGFP::ZeoR-T2A reporter cassette upstream of the native start codon of *SMARCB1* compared to wildtype control HEK293T cells observed. As expected, protein analysis of SMARCB1 showed only a slight increase in protein size due to the addition of three amino acids upstream of the first methionine of SMARCB1 resulting from T2A self-cleavage in the genome engineered sequence (Figure 23).
Again, different fluorophores were tested as co-expressed reporters and mTagBFP2 was chosen to fit into the three-colour reporter scheme. A Puromycin resistance gene was added upstream of the fluorescence gene, linked by P2A (plasmid #380, Figure 7B and Figure 35) to prevent homologous recombination and genetic instability due to repetitive sequences as in case of a second T2A sequence and to allow efficient enrichment of successfully engineered cells (Luke and Ryan 2018).

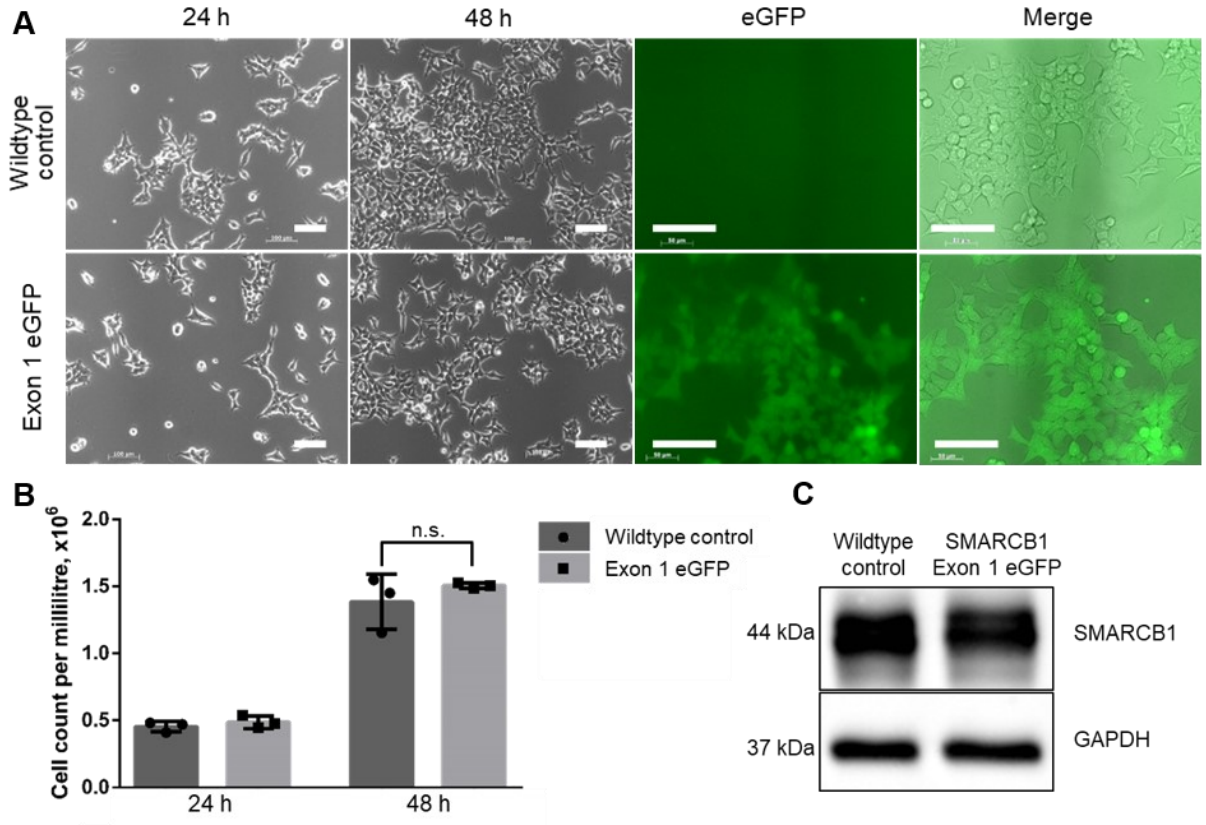

Figure 23: The addition of a T2A linked eGFP::ZeoR reporter upstream of the native start codon of the *SMARCB1* gene in genome engineered HEK293T cells did not reduce the growth rate of HEK293T cells. **(A)** Cell growth was analysed for 48 hours after seeding 0.1x10^6 HEK293T cells per well of a 6-well plate. For both time points analysed, no alteration in cell growth could be observed (left panel). The expression of eGFP was detected by fluorescence microscopy (right panel). **(B)** Every 24 hours, three wells per condition were detached and counted using CASY cell counter. The cell count per millilitre was blotted for both samples. There also was no difference observed between the eGFP::ZeoR-T2A-*SMARCB1* engineered compared to the wildtype cells in cell counting analysis. **(C)** SMARCB1 protein analysis by Western blotting showed the expected size of 44 kDa for SMARCB1 protein extracted from the wildtype control cells. For the eGFP::ZeoR-T2A-*SMARCB1* engineered cells, a slight increase in protein size probably due to the addition of three amino acids upstream of the first methionine residue of the SMARCB1 protein was observed. Per condition and time point, three wells were analysed, scale bars in A represent 100 µm. Normal distribution of cell count data was verified by the Anderson-Darling test. Statistical analysis was performed using Student's t-test. There was no significant difference observed.

HEK293T cells expressing a *c.1148delC* mutated allele of *SMARCB1* (plasmid #363, Figure 18) could be detected and enriched by the expressed eGFP::ZeoR reporter (data not shown). However, this was not the case for the cells engineered to express a *SMARCB1* allele with AT/RT-associated nonsense mutations in exon 1 (*c.20_43delins T*, *c.93G>C*, Figure 7C). The emerging pre-mature stop codons introduced by the mutations prevent the expression of *SMARCB1*, probably by rendering the mRNA for degradation. Since the reporter is translated from the same mRNA, its degradation would lead to a quick loss of expression of the fluorescence reporter, which therefore cannot be detected.

3.2.2. Establishment and optimisation of the CRISPR/Cas9-mediated genome engineering of the *SMARCB1* locus in HEK293T cells using the generated CSS-associated constructs

When engineering HEK293T cells to express the mutated form of *SMARCB1* associated with CSS, an enrichment of engineered cells by selection with zeocin was not possible. eGFP-positive HEK293T cells engineered to co-express the *c.1091_1093del AGA SMARCB1* and the eGFP::ZeoR reporter died upon zeocin selection, maybe due to low expression levels of the resistance gene, which were insufficient to confer resistance to zeocin (Figure 8 depicts the genotype). Therefore, HEK293T cells engineered to express this mutant form of the *SMARCB1* gene were enriched by flow cytometry and directly analysed for expression of the gene (Figure 24 and section 3.5.1). HEK293T were engineered using Cas9n plasmid #221 (mTagBFP reporter) and two HDR constructs inserting either an eGFP::ZeoR (plasmid #243or #253) or mKate2 (plasmid #318) reporter downstream of the native stop codon of the *SMARCB1* gene upon CRISPR/Cas9n-mediated homology directed repair. Two samples, WT/WT (serves as control, HDR plasmids #243, #318) and CSS/WT (plasmids #253, #318) were isolated by FACS for expression analyses on the mRNA and protein level. Due to the tetraploidy of HEK293T cells, no conclusive results on the impact of the CSS-associated mutation *c.1091_1093del AGA* in exon 8 of the *SMARCB1* gene on the transcription of eGFP and mKate-associated alleles of *SMARCB1* was obtained by RT-qPCR. SMARCB1 protein levels were reduced by 3.8% in CSS/WT HEK293T cells compared to WT/WT HEK293T cells (Figure 24).

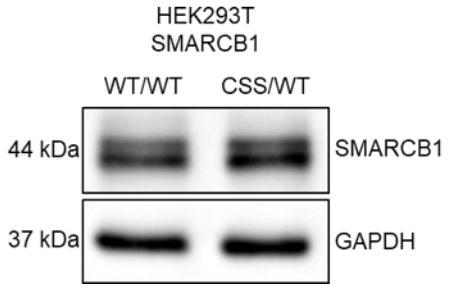

Figure 24: Analysis of SMARCB1 protein levels in HEK293T cells engineered to simultaneously produce two SMARCB1 proteins and one of two fluorescence reporters genomically linked by an IRES. For the WT/WT sample, HEK293T cells were transfected with Cas9n plasmid #221 and the two HDR constructs #243 (eGFP::ZeoR reporter) and #318 (mKate2 reporter). To obtain CSS/WT cells, HEK23T cells were transfected with plasmid #221 and the HDR constructs #253 (*c.1091_1093del AGA SMARCB1*, eGFP::ZeoR reporter) and #318 (mKate2 reporter). 48 hours after transfection, the cells were detached and analysed by flow cytometry. 3-4x10^5 eGFP and mKate2 double positive cells of the mTagBFP positive population (reporter on gRNA and Cas9n plasmid #221) were sorted into a tube, collected at 200xg for three minutes and lysed in 70 µL of Lämmli buffer. Image analysis of the not-saturated images revealed that the protein bands detected showed a 3.8% reduction in SMARCB1 protein in the CSS/WT compared to the WT/WT sample (image analysis performed with ImageJ, v1.52a).

3.3. Establishment and optimisation of methods for CRISPR/Cas9-mediated genome engineering in hiPSCs

Human induced pluripotent stem cell (hiPSC) lines differ in their growth rate, differentiation potential, and also ease of DNA transfer. In general, hiPSCs are difficult to transfect and especially the transfer of large plasmids – as necessary for CRISPR/Cas9-mediated genome engineering – is challenging. In the literature, electroporation of hiPSCs was reported to be highly effective in facilitating the transfer of large DNA fragments and thus CRISPR/Cas9-mediated genome engineering (Byrne, Mali et al. 2014, Smith, Ye et al. 2016, Carlson-Stevermer and Saha 2017). During this work, different devices (Amaxa Nucleofector 2b, and 4D, Neon transfection system) and protocols for electroporation and nucleofection were tested. None of which was successful in generating hiPSCs expressing the reporter fluorescence gene co-encoded on the large gRNA and Cas9(n) plasmids indicating successful transfer of the plasmid into the cells.

Thus, chemical transfection of the available hiPSC#33 line was evaluated. Transfection using Lipofectamine Stem reagent of Thermo Fisher was successful in efficiently transferring DNA of different sizes including gRNA and Cas9(n) plasmids of 9.8 kb. Naturally, the transfection efficiency declined with increasing plasmid size. For the large plasmids in this project, transfection efficiencies of approx. 10% could be achieved when transfecting hiPSC#33 seeded as single cells. Optimisation efforts like the application of the five-fold concentration of RevitaCell supplement for increasing the cells' surface (Yen, Yin et al. 2014), reverse transfection and adaption of DNA amount did not yield any improvement regarding transfection efficiency. Furthermore, it was observed that transfection of hiPSC#33 with gRNA and Cas9(n) plasmids targeting the *SMARCB1* gene was accompanied with lower transfection efficiencies (approx. 2% 48 hours post transfection, determined by FACS, data not shown) compared to transfection with gRNA and Cas9(n) plasmids targeting other genes like *OTX2* (*OTX2*-targeting plasmids kindly provided by Jana Frei). Additionally, more dead cells were observed in the *SMARCB1*-targeted condition 24 hours after transfection compared to transfections with gRNA and Cas9(n) plasmids targeting other genes like *OTX2* (data not shown, *OTX2*-targeting plasmids kindly provided by Jana Frei).

Transfection of cells with Cas9-gRNA ribonucleoprotein complexes (Cas9/gRNA RNPs) was reported to reduce the off-target cleavage of Cas9 by a shorter activity period and to bypasses the need to transfect the large Cas9 and gRNA plasmids (Liang, Potter et al. 2015, Yu, Liang et al. 2016). Transfer of the Cas9/gRNA or Cas9n/gRNA RNPs was performed using the protein transfection reagent Lipofectamine CRISPRMAX (CMAX00001, Thermo Fisher) or Lipofectamine Stem reagent. In both experimental approaches the HDR construct #243 for the insertion of an IRES-linked eGFP::ZeoR-loxP cassette downstream of the native stop codon of the *SMARCB1* gene was co-transfected. Neither did the transfected hiPSCs show any eGFP signal 24 to 48 hours after transfection nor could they be enriched by zeocin selection. Due to high costs and the lack of suitable controls, the transfection of Cas9(n)/gRNA RNPs was not followed up further.

Based on the experiments described above, two critical factors were identified which needed to be optimised for CRISPR/Cas9-mediated genome engineering in hiPSC#33: the low transfection efficiency of large plasmids and the high rate of cell death accompanied with Cas9(n) targeting the *SMARCB1* gene. The issue of the high rates of cell death was tackled by the overexpression of the dominant-negative form of p53 (p53DD).

Overexpression of the dominant-negative form of p53 (p53DD) to tackle the issue of Cas9 cleavage-induced cell death in hiPSCs

With the optimisation of the transfection of human induced pluripotent stem cells, the hiPSC#33 cell line used appeared to be very sensitive to Cas9(n)-induced cleavage of DNA. Especially when transfected with gRNA and Cas9(n) plasmids targeting the genomic region of the *SMARCB1* gene, the amount of floating dead cells was remarkably higher compared to cells transfected with gRNA and Cas9(n) plasmids targeting other genes like *OTX2* (data not shown, *OTX2*-targeting plasmids kindly provided by Jana Frei).

BAF complexes, in general, thus also the core component SMARCB1, are essential for the balance between cell proliferation and differentiation (Wilson and Roberts 2011). Loss of *Smarcb1* also was shown to be embryonic lethal in mice (Klochendler-Yeivin, Fiette et al. 2000). Moreover, Cas9-induced double strand breaks were shown to be toxic for hiPSCs, and the toxic response was shown to be *TP53*-dependent. Considering the regulating role of the BAF complexes and the embryonic lethality upon loss of *SMARCB1*, the high rate of cell death and the low genome editing efficiency in hPSCs may be associated with effects of the DSBs and with the *SMARCB1* gene locus itself on the cells. Overexpression of the dominant-negative form of the murine sequence of the tumour suppressor gene *Tp53* (p53DD) was shown to increase survival and genome editing efficiencies in hPSCs (Ihry, Worringer et al. 2018). Thus, a p53DD-encoding plasmid was co-delivered with the Cas9 plasmids. For this purpose, codons 1 to 13 and 302 to 390 of the murine coding region of *Tp53* were cloned into an episomal backbone (Bowman, Symonds et al. 1996, Hong, Takahashi et al. 2009, Ihry, Worringer et al. 2018). Similarly, the p53DD encoding sequence was amplified from murine cDNA from E14.5 *Smarcb1*$^{+/inv}$ individual E516 using the overlap extension method (section 2.1.14) and cloned into the transposable backbone of plasmid #01 yielding pMTE-p53DD (plasmid #415). The detailed cloning steps are summarised in Figure 25.

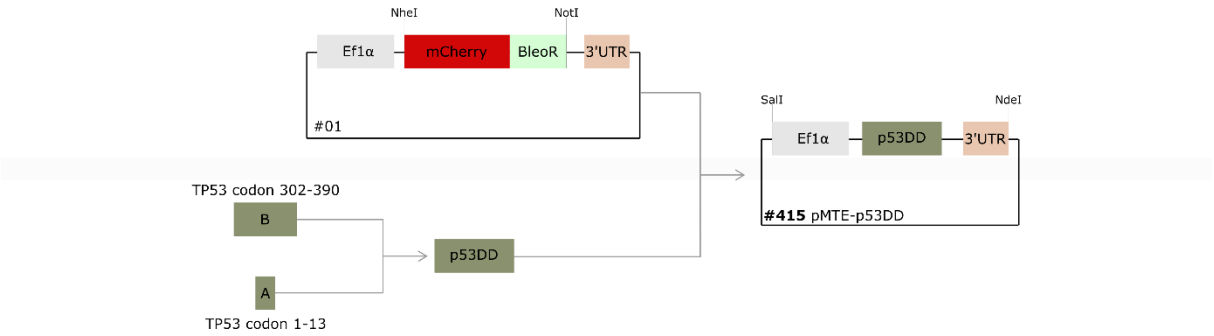

Figure 25: Schematic overview of the cloning steps to generate the transposable plasmid #415 and the lentiviral plasmid #416 for overexpression of *p53DD*. The *p53DD* sequence was PCR amplified from embryonal mouse cDNA of E14.5 *Smarcb1*$^{+/inv}$ individual E516 using the overlap extension method. For this purpose, fragment A comprising codons 1-13 of the mouse *Tp53* gene was amplified using primers #1479 and #1480. Fragment B comprising the codons 302-390 of the mouse *Tp53* gene was amplified using primers #1481 and #1482. Fragment A and B were combined in a third PCR, and the complete *p53DD* sequence was amplified using primers #1479 and #1482. The complete *p53DD* sequence was cloned into transposable plasmid #01 via NheI and NotI restriction endonuclease cloning resulting in plasmid #415. Ef1α = human elongation factor 1α (Ef1α) core promoter and truncated intron upstream of the start codon of human Ef1α; BleoR = Bleomycin resistance gene confers resistance to antibiotics of the bleomycin family, e.g. zeocin; 3'UTR = 3' untranslated region (Stojanova, Tu et al.) of the major beta-globin gene of *Xenopus laevis*.

The cloned transposable plasmid for overexpression of *p53DD* (plasmid #415, 5.3 kb) was applied to test the effect of expression of the dominant-negative form of p53 on the survival of hiPSC#33 upon transfection. Since the *p53DD* plasmid #415 does not contain a fluorescence reporter gene which allowed to directly assess the transfection efficiency, the gRNA and mTagBFP encoding plasmid #310 (5.4 kb, Figure 37) was used as a size-equivalent control. Furthermore, hiPSC#33 were also transfected with the *SMARCB1*-targeting gRNA and Cas9 plasmid #387 (eGFP reporter, 9.8 kb, Figure 38) alone or in combination with the p53DD plasmid. Figure 26 shows the flow cytometry analysis results of the effect of the expression of *p53DD* on the survival of hiPSC#33 upon transfection. As indicated by the amount of mTagBFP positive cells in gate P4 (Figure 26A, B), a transfection efficiency of 36.2% can be achieved for plasmids of around 5 kb size (2.5 µg of plasmid DNA). This percentage also remained stable when the cells were transfected with the same total amount of DNA but composed of even shares of two plasmids (e.g. #310 and #415, #380 and #415, 1.25 µg each, Figure 26C). Transfection of hiPSC#33 with the *SMARCB1*-targeting gRNA and Cas9 plasmid #387 showed very low transfection efficiencies of 0.9% 48 hours after transfection. Co-transfection of plasmid #387 and #415 did neither result in a remarkable increase of transfection efficiency (1.1%) nor in cell survival when assessed with the dead cell stain SytoxRed (Figure 26C, D).

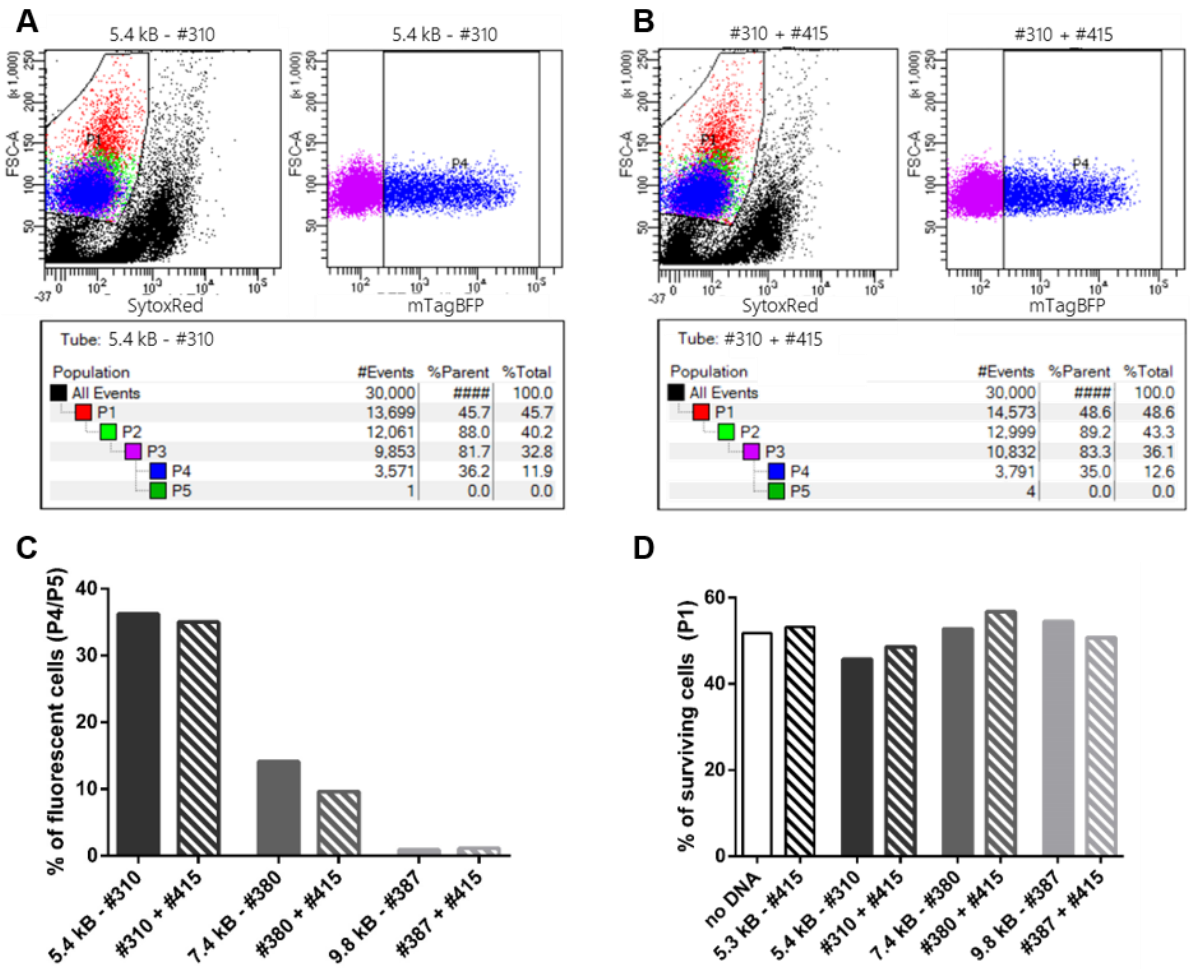

Figure 26: Flow cytometry analysis does not show a beneficial effect of the expression of *p53DD* on the survival of hiPSC#33 upon transfection with Cas9 plasmids. **(A)** Survival of hiPSC#33 was assessed by flow cytometry analysis and cell staining with the dead cell stain SytoxRed (left panel, gate P1). In general, the survival of hiPSC#33 was low for all conditions analysed in FACS (around 50%). Transfection efficiency was quantified as the percentage of fluorescent cells of the surviving cells in gate P1 (mTagBFP for plasmids #310 and #380, eGFP for plasmid #387, gate P4 or P5, respectively, right panel). **(B)** Upon co-transfection of the control plasmid #310 with the p53DD plasmid #415, the survival of the cells was only slightly increased while the transfection efficiency quantified as the number of fluorescent cells remained similar despite reducing the amount of plasmid DNA of #310 by 50% (compare gates P1 and P4). **(C)** Evaluation of all conditions analysed by flow cytometry showed a remarkable decrease in transfection efficiency with the increase of plasmid size from approx. 35% for 5.4 kb plasmids to 0.9% for the 9.8 kb *SMARCB1*-targeting gRNA and Cas9 plasmid #387 (solid bars). Co-transfection of the p53DD plasmid #415 while keeping the total amount of DNA transferred constant (1.25 µg each vs. 2.5 µg alone) only slightly decreased the number of fluorescent cells detected (striped bars). **(D)** Quantification of the survival showed a slight increase upon (co-) transfection of hiPSC#33 with the p53DD plasmid #415 for plasmids up to 7.4 kb in size but a slight decrease in survival of cells co-transfected with the *SMARCB1*-targeting gRNA and Cas9 plasmid #387. In A and B the FACS plots of the analysis of the transfection of hiPSC#33 with plasmid #310 and the effect of co-transfection of plasmid #415 are shown as representative images for the other conditions quantified in C and D.

3.4. Establishment and optimisation of methods for CRISPR/Cas9-mediated genome engineering in MCF10A cells

The constructs established in sections 3.1 and 3.2 were also to be used to edit the genome of MCF10A cells to analyse the gene expression of *SMARCB1* and the co-expressed reporter genes on the mRNA level via RT-qPCR. The MCF10A cell line was chosen since it is an established cell line, diploid for chromosome 22, and less difficult to transfect than hiPSC (Marella, Malyavantham et al. 2009). In MCF10A cells both alleles of *SMARCB1* were to be edited to co-express a fluorescent reporter. One allele in its wild-type form, while the other one either mutated with an AT/RT- or CSS-associated mutation. With this approach the hypothesis that heterozygous CSS-associated missense mutation of the *SMARCB1* gene causes either only a mild reduction of the gene expression level or a mildly malfunctioning protein which does not trigger the intracellular compensation by the second unaffected allele of *SMARCB1* should be tested. Likewise, it should be analysed if AT/RT-associated nonsense mutations of *SMARCB1* completely ablate the gene expression from the affected allele, causing an increase of transcription from the unaffected allele to compensate for the loss of gene product in case of RTPS1.

CRISPR/Cas9-mediated genome engineering in MCF10A cells requires an efficient transfer of the nuclease and gRNA plasmid, and a HDR construct for the introduction of a reporter insert. The most abundantly used method to deliver DNA into cells is transfection. The common transfection reagents PEI and Lipofectamine 3000 are widely used for the transfection of MCF10A cells and were tested to identify the method for the most efficient transfer of DNA.

In a conservative approach for transfection (seeding of cells 24 hours prior to transfection) with plasmids of different sizes, no remarkable difference in transfection efficiency of MCF10A cells between PEI and Lipofectamine 3000 reagent was observed. For small plasmids (plasmid #376, 5.4 kb) 20 to 40% of the transfected cells showed reporter gene expression. In contrast, the amount of reporter gene expressing cells decreased to a maximum of 10% for larger plasmids (e.g. plasmid #221, 9.8 kb, data not shown). The standard transfection approach was nonetheless tested for the generation of MCF10A *SMARCB1* reporter cell lines, but transfected cells could not be enriched for cells that integrated the reporter cassette by antibiotic selection. Therefore, different optimisation approaches were pursued. First, the co-transfection of Cas9n/gRNA constructs with linearised HDR constructs was tested. The linearization of the HDR constructs was reported to increase the ratio of homologous recombination and thus the introduction of the reporter gene insert (Stuchbury and Munch 2010, Song and Stieger 2017). Upon transfection of MCF10A cells with linearised HDR constructs, most of the cells died maybe due to higher toxicity of linear DNA fragments in the cells. As an alternative transfection method, a reverse transfection was performed. For this purpose, single cells in suspension were mixed with the transfection mix and incubated at room temperature for up to 30 minutes before plating. The reverse transfection was performed using either PEI or Lipofectamine 3000 reagent, but the MCF10A cells were not efficiently transfected with either of the reagents. All means of transfection to transfer DNA for CRISPR/Cas9-mediated genome editing mentioned above were tested with both,

Cas9 nickase and wildtype Cas9 nuclease plasmids. Seemingly, the chemical transfection is not the method of choice for the CRISPR/Cas9(n) engineering of MCF10A cells. Therefore, electroporation using the Amaxa Nucleofector 2b device in combination with a self-made electroporation buffer was tested (section 2.3.6). Based on the recommendations of Lonza for the optimisation of an electroporation setup, eleven different programmes were tested (A-020, T-020, T-030, X-001, X-005, L-029, D-023, S-005, T-013, W-001, U-017) for the transfer of a 9.5 kb plasmid (plasmid #273, mKate2 reporter). The different programmes had different effects on the MCF10A cells regarding the toxicity, but none resulted in a successful transfection of the cells, since they did not show fluorescence reporter expression 48 hours after the electroporation.

3.5. *Loss-of-function* mutations in *SMARCB1* de-regulate expression of *Hes* genes in murine neural stem and in HEK293T cells

A mouse model recapitulating neurodevelopmental features of the human CSS was established in the Stem Cell and Developmental Biology group at the Technical University of Darmstadt. In these mice (*Smarcb1*$^{+/inv}$ *NesCre*$^{+/-}$ mice, referred to as mutant), heterozygous inactivation of the *Smarcb1* gene occurs by inversion of the floxed region of *Smarcb1* exon 1 upon expression of the *Cre* recombinase under the control of the rat nestin promoter starting around embryonic day (E) 10.5 (Roberts, Leroux et al. 2002, Filatova, Rey et al. 2019). Targeted cells are mainly radial glial cells (RGCs). RGCs are neural stem cells which are only transiently present during neural development (Gotz and Barde 2005, Filatova, Rey et al. 2019). Aside from various structural deviations from the *Smarcb1*$^{+/inv}$ *NesCre*$^{-/-}$ control mice, *Smarcb1* mutant mice also exhibit a diminished RGC population. At E14.5 thinned layers of RGCs in the ventricular zone lining the lateral ventricles, as well as of intermediate progenitors in the subventricular zone, and of early-born cortical neurons were detected. Additionally, a decrease in neurosphere (NSP)-forming capacity of NSCs and NPCs in cultures from E15.5 mutant brain tissues was observed. Neurospheres (NSPs) are three-dimensional floating spheroid cell clusters that arise from NSP-forming cells, which can be both NSCs or NPCs, isolated from the mammalian CNS (Jensen and Parmar 2006, Singec, Knoth et al. 2006, Pastrana, Silva-Vargas et al. 2011). Upon *in vitro* cultivation, the heterogeneity of NSPs increases and aside from proliferative, NSP-forming NSCs and NPCs also post-mitotic neurons and glia cells can be found within one sphere (Jensen and Parmar 2006). Nonetheless, NSP culture can be applied as a functional assay and is a useful tool to analyse proliferation, self-renewal capacity, and multipotency of the NSP-forming NSCs and NPCs over serial clonal passages (Jensen and Parmar 2006). Different lines of reasoning were followed to determine the underlying cause for the reduced number of RGCs in *Smarcb1* mutant mouse brains (section 4.3).

3.5.1. *Loss-of-function* mutations in *SMARCB1* de-regulate expression of *Hes* genes in E14.5 mouse brain samples and in HEK293T cells

Engineered HEK293T cells generated in this project carrying the CSS-associated *SMARCB1* mutation *c.1091_1093del AGA* were analysed for changes in *HES1* and *HES5* gene expression. HEK293T cells were transfected with the plasmids encoding the CRISPR/Cas9 machinery for the editing of the region flanking the stop codon of the *SMARCB1* gene and with two HDR constructs for insertion of an eGFP and mKate2 reporter downstream of exon 9 of the *SMARCB1* gene. Equivalent to the mouse control samples, HEK293T control cells termed WT/WT were engineered using two HDR constructs without mutation in the *SMARCB1* gene and either an eGFP or a mKate2 reporter (plasmids #243 and #318). The engineered mutant HEK293T cell population termed CSS/WT was obtained by transfecting one HDR construct without mutation in the *SMARCB1* sequence (plasmid #318, mKate2 reporter) and a second HDR construct to introduce the CSS-associated mutation *c.1091_1093del AGA* in exon 8 of the *SMARCB1* gene (plasmid #253, eGFP reporter). 60 hours after transfection, the

HEK293T cells were subjected to flow cytometry analysis. The desired WT/WT or CSS/WT populations were identified by expression of the eGFP and mKate2 reporter genes. Therefore, eGFP and mKate2 double positive cells in the population of Cas9n/gRNA expressing cells (BFP positive) were sorted via FACS into lysis buffer for RT-qPCR analysis of *HES1* and *HES5* gene expression (Figure 27A). In HEK293T cells, *HES1* expression could not be detected, but the expression of *HES5* was significantly reduced by 50% (Figure 27B).

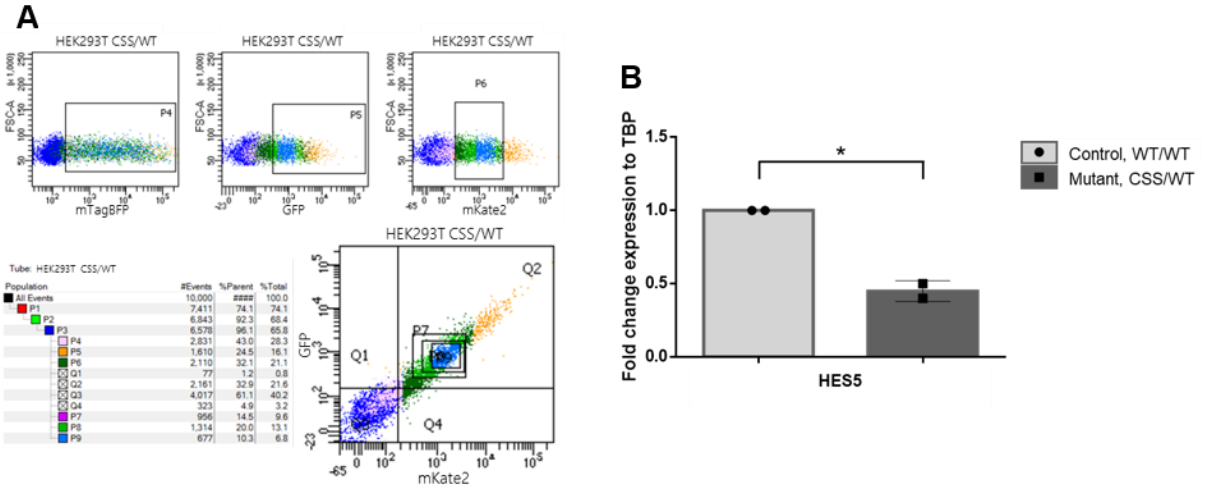

Figure 27: RT-qPCR expression analysis of sorted HEK293T cells which were CRISPR/Cas9-engineered to express one *c.1091_1093del AGA* mutated allele of the *SMARCB1* gene show a significant reduction in *HES5* transcript abundance compared to control cells. **(A)** HEK293T cells were transfected with Cas9n/gRNA plasmid #221 and the *SMARCB1* e9 wildtype HDR constructs #243 (eGFP::ZeoR) and #318 (mKate2) or *SMARCB1* e9 wildtype HDR construct #318 (mKate2) and the *SMARCB1* CSS e9 HDR construct #253 (eGFP::ZeoR). A sample blot of the FACS experiment is shown. **(B)** The sorted and lysed cells were directly used for cDNA synthesis. Depicted are the RQ means of two independent sorts of HEK293T WT/WT and CSS/WT cells. N = 2, statistical tests were performed on the original replicates of the sorts combined, normal distribution was not given for the control samples; thus, a Wilcoxon signed rank test was performed. * $p < 0.05$.

Based on the findings of reduced *HES5* expression in these HEK293T cells and in the developing glial wedge position at the medial walls of the lateral ventricles by RNA *in situ* hybridisation in E15.5 mutant brain sections in Filatova, Rey et al. (2019), RT-qPCR analyses of *Hes1* and *Hes5* expression in E14.5 mice brain samples were conducted (primers #1123 and #1124, amplicon 113 bp, and #1268 and #1269, amplicon 186 bp, respectively). The location of differential expression of *Hes5* in the developing brain is small and difficult to isolate. Moreover, the changes in expression of *Hes5* were only observed in the neural progenitor population lining the lateral ventricles. Thus, brain samples of different regions, i.e. forebrain and hemispheres, were analysed when applicable. Due to the affected population, RT-qPCR results were normalised to the *Nestin* gene (primers #1306 and #1307, amplicon 86 bp). *Nestin* (*Nes*) served as a reference gene in this context since it is described to be expressed in all RGCs at a similar level (Gotz and Barde 2005) and since the microcephaly phenotype of the mutant mice precluded the use of conventional reference genes such as the TATA box-binding protein (*Tbp*). In all samples analysed, regardless of brain region, the expression of *Hes1* was significantly increased by 20 to 40% in mutant compared to control RGCs at E14.5 (Figure 28). For the expression of *Hes5*

in *Nes* positive cells, the analyses were less distinct. In E14.5 forebrain samples a decrease in *Hes5* expression in these cells of up to 26% was observed, but this trend was only significant for one litter (Figure 28A, B). In E14.5 hemisphere samples, the expression of *Hes5* in *Nes* positive cells remained similar in control and mutant individuals (Figure 28A). Summarising, the data obtained for mutant E14.5 forebrain samples corresponded with the results of the RNA *in situ* hybridisation experiments shown in Filatova, Rey et al. (2019). The increase in *Hes1* expression in *Nes* positive cells during these stages of development was not observed in RNA *in situ* hybridisations of brain sections.

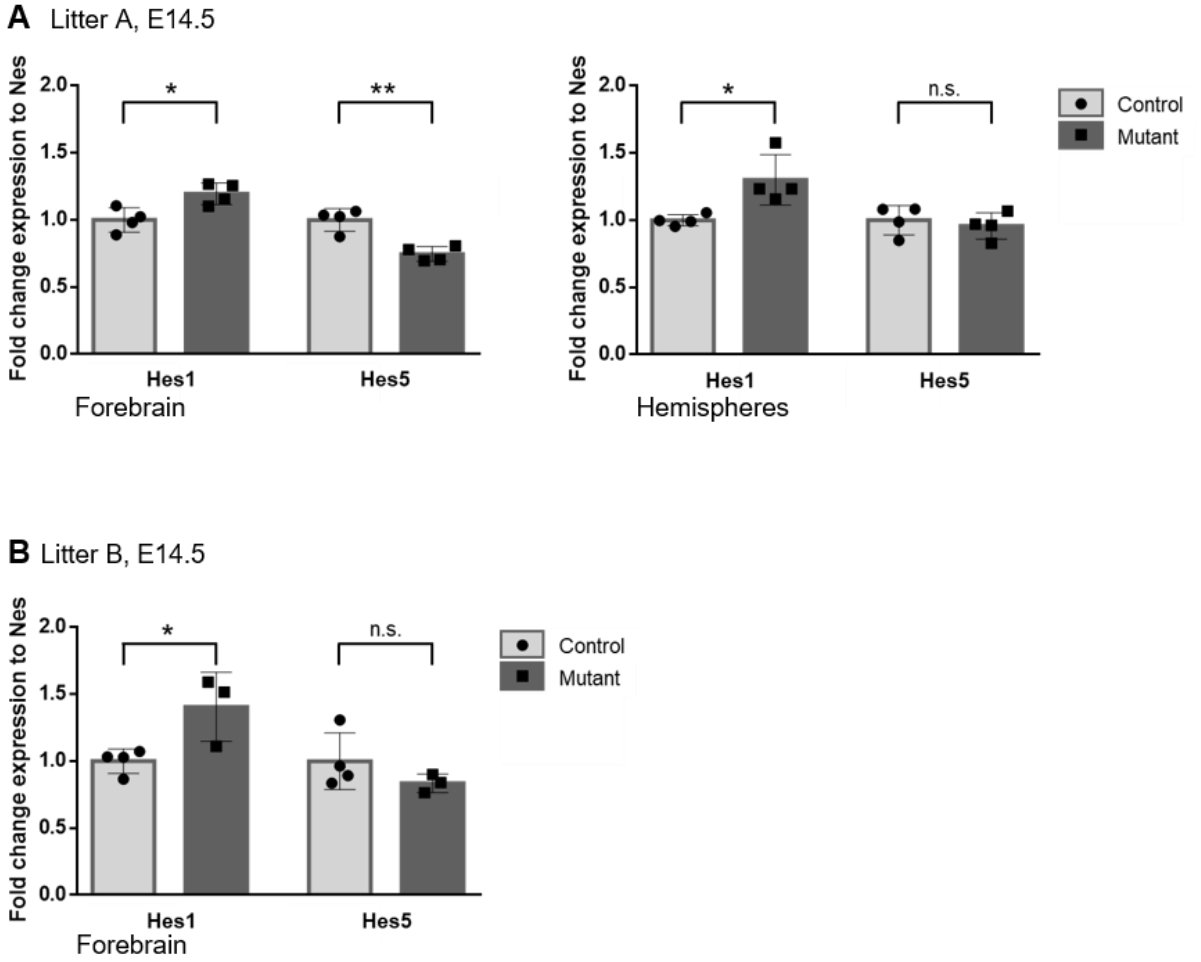

Figure 28: RT-qPCR analysis of *Hes1* and *Hes5* in control and mutant brain samples of E14.5 mice. **(A)** In forebrain samples of E14.5 mouse embryos of litter A, a significant reduction in the expression of *Hes5* normalised to *Nestin* (*Nes*) expression levels of mutant compared to control samples was observed alongside a significant increase of *Hes1* transcripts. The increase in *Hes1* transcript abundance was also true for the matching hemisphere samples. **(B)** For E14.5 litter B, only forebrain samples were available. Similar to (A) a significant increase in *Hes1* transcripts relative to *Nestin* expression levels of mutant compared to control samples was observed while expression of *Hes5* did not differ significantly between mutant and control samples. Control = *Smarcb1*$^{+/inv}$ *NesCre*$^{-/-}$, mutant = *Smarcb1*$^{+/inv}$ *NesCre*$^{+/-}$. N = 4 per group, except for mutant E14.5 litter B where n = 3. Normal distribution of the results was confirmed with the Anderson-Darling test. The results were analysed by a two-sided, unpaired Student's t-test. * $p < 0.05$, ** $p < 0.01$, *** $p > 0.0001$.

3.5.2. Cloning and lentiviral packaging of murine *Hes5*-IRES-mKate2 overexpression and IRES-mKate2 control plasmids for the transduction of murine neural stem cells

The murine *Hes5* overexpression construct was generated by linking the complete coding sequence of *Hes5* and the mKate2 fluorescent reporter via an IRES. A construct containing only IRES-mKate2 but no *Hes5* coding sequence served as a control for the effect of the integration of the lentiviral genome itself. Based on the first set of lentiviral plasmids (plasmids #372-375, Figure 39), the cassette for overexpression of *Hes5*-IRES-mKate2 and the IRES-mKate2 control cassette were introduced into the lentiviral backbone plasmid #258 via blunt end cloning (Figure 29). This new set of *Hes5*-IRES-mKate2 overexpression and IRES-mKate2 control plasmids was based on the same lentiviral backbone as the *Cre* recombinase plasmid #258 and its Venus control counterpart plasmid #340 which were selected to inverse the loxP-flanked exon 1 of the *Smarcb1* gene in E42 NSP-forming cells. The lentiviral plasmids were packed into lentiviral particles using packaging plasmid #438 (pCD- NL/BH) and VSV- G envelope plasmid #257 (pMD2.G) as described in section 2.3.7.

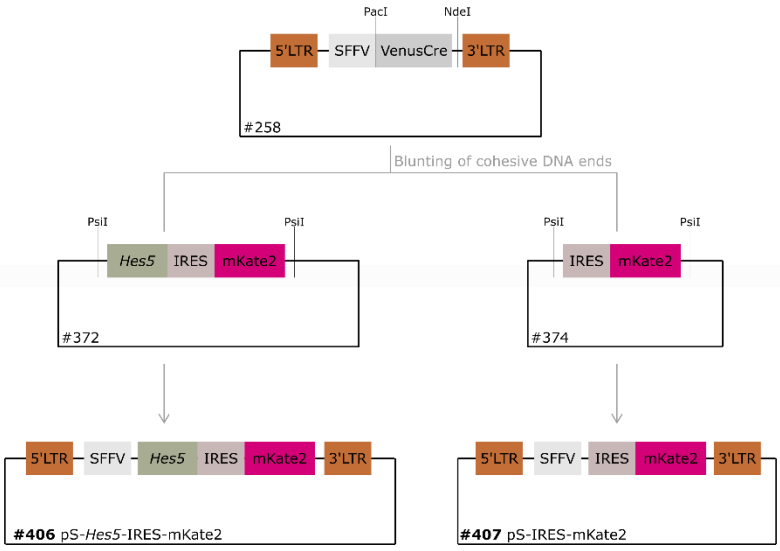

Figure 29: Schematic overview of the molecular cloning steps to generate the lentiviral plasmid for overexpression of murine *Hes5* co-expressed with a mKate2 reporter (plasmid #406) and a suitable mKate2 reporter control plasmid (plasmid #407) from plasmids #258, #372, and #374 via blunted DNA ends.

3.5.3. Establishment and optimisation of methods to overexpress *Hes5* in murine NSCs

In general, lentiviral particles are generated by transfecting HEK293T cells with a lentiviral packaging and envelope plasmid with the transfer plasmid coding for the gene(s) of interest to be packed into the viral particle. Consequently, after transfection of the HEK293T cells, the medium has to be changed to the growth medium of the cells which will be transduced with the produced viruses. For most cell types to be transduced and most transfer plasmids, this approach is suitable. For the transduction of E42 neurospheres (NSPs) of E15.5 *Smarcb1*$^{+/inv}$ *NesCre*$^{-/-}$ mice, this approach was not successful for all applied plasmids.

The aim was to transduce these spheres with a *Cre* recombinase carrying lentivirus to generate the *Smarcb1* mutation in the cells, namely a *Cre*-mediated inversion of exon1, and simultaneously transduce the cells with a virus carrying a *Hes5* overexpression cassette. Hence to test the hypothesis if overexpression of *Hes5* can rescue the loss of the sphere forming ability that occurs upon *Cre* recombination in *Smarcb1*$^{+/inv}$ *NesCre*$^{+/-}$ neural stem cells as seen in Filatova, Rey et al. (2019).

Transduction of E42 NSPs with Venus*Cre* expressing lentiviral particles and the matching control (transfer plasmids #258, and #340 respectively) was successful with the conventional transduction approach without concentration (section 2.3.7). Therefore, the lentiviral *Hes5*-IRES-mKate2 overexpression and IRES-mKate2 control transfer plasmids in a pLenti-UbC backbone were generated (plasmids #373, #375). Virus production in HEK293T cells and control transduction of HEK293T cells was efficient, but the viral particles generated repeatedly failed to generate mKate2-positive E42 NSP-forming cells. After different optimisation attempts regarding experimental timing, setup, and ratio of co-transfected helper plasmids, another set of *Hes5* overexpression and control transfer plasmids was cloned using the lentiviral backbone of the Venus*Cre* plasmid (plasmids #406, #407). While lentiviral particles with the *Hes5* overexpression cassette were infectious using the standard procedure, the matching mKate2 control viral particles failed to generate mKate2-positive E42 NSP-forming cells. Tests in HEK293T cells revealed that the transfer plasmid was intact and was successfully packed into infectious lentiviral particles. Upon further experiments, it became apparent, that these particles were only generated efficiently by HEK293T cells if they were cultured in HEK293T growth medium but not when the medium was changed to the NSP growth medium (NSPM) after the transfection. The necessity of HEK293T medium for the efficient production of lentiviral particles restricted the direct use of the virus containing supernatant for transduction of E42 NSPs.

Alternative strategies were devised to transduce NSPs without the need of concentration since the viral titer produced was sufficient. As a result, transduction of E42 NSPs in 1 mL of NSPM supplemented with EGF and bFGF to match the final volume of the transduction with 500 µL to 1 mL of virus containing supernatant from HEK293T medium was tested. 24 hours after transduction the cells showed mKate2 expression but all spheres had attached and could not be detached to form spheres again, indicating a differentiating influence of the residual components of the HEK293T growth medium on the NSP-forming cells. Henceforth, a method for medium exchange of the virus containing

supernatant prior to transduction of the NSPs was required. The best means to achieve a medium-independent system is centrifugation of the virus containing supernatant and re-constitution of the pelleted viral particles in an appropriate buffer or medium. Ultracentrifugation was chosen to pellet the viral particles. Re-constitution of the pellet in DMEM/F12 and 1% BSA followed by transduction of HEK293T and E42 NSPs compared to the non-concentrated HEK293T growth medium based virus containing supernatant revealed a decrease in infection rate for the ultracentrifuged *Hes5* overexpression particles compared to an equivalent volume of unconcentrated supernatant. E42 NSP-forming cells and HEK293T cells transduced with the matching control particles in concentrated virus preparations still did not show reporter expression. Transduction of HEK293T cells with unconcentrated virus-containing supernatant showed expression of the mKate2 reporter, as seen before at a much lower intensity compared to the *Hes5*-IRES-mKate2 transduced cells. Therefore, the concentration of lentiviral particles as described by Jiang, Hua et al. (2015) was applied. In this protocol, concentration of lentiviral particles is achieved by centrifugation at 10,000 xg over a 10% sucrose cushion. Thereby, reducing the centrifugal forces and damaging potential applied to the viral particles. In this final experimental setup, all four required lentiviral particles (from plasmids #258, #340, #406, #407) carrying the Venus*Cre* and *Hes5*-IRES-mKate2 expression systems as well as the respective controls were generated and concentrated (Figure 30). Transduction of E42 NSPs with combinations of the concentrated virus containing suspension resulted in spheres expressing Venus and mKate2 simultaneously (Figure 30B). Unfortunately, the transduced cells did not survive the first dissociation after transduction, and thus were not applicable for flow cytometry analysis and sort. Nonetheless, the transduction of E42 NSPs with the Venus*Cre* and *Hes5*-IRES-mKate2 expression systems was established in a growth medium-independent approach. This will allow to test the hypothesis if overexpression of *Hes5* can rescue the impaired sphere-forming ability of *Smarcb1*$^{+/inv}$ murine neural stem cells.

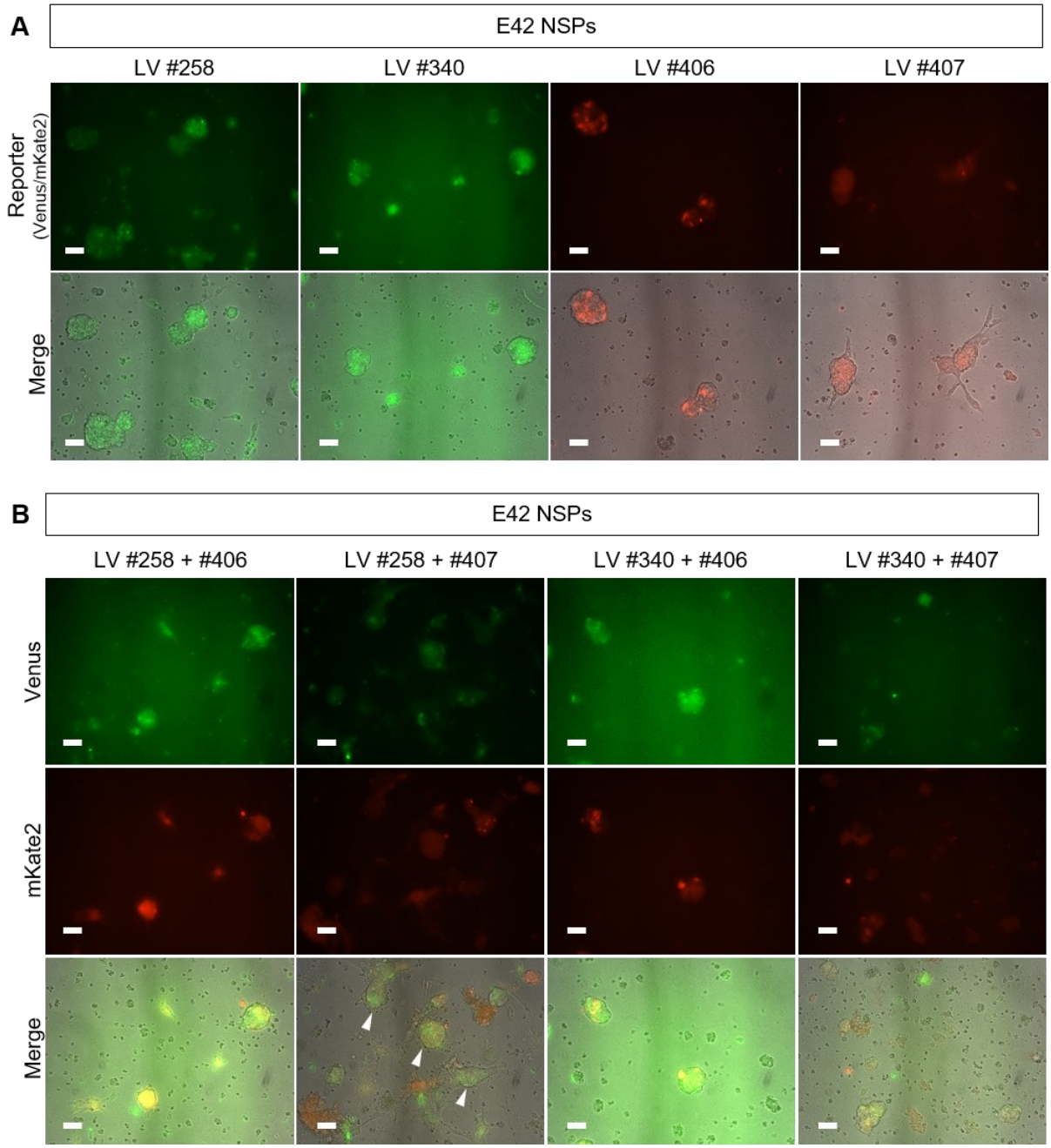

Figure 30: LV concentration over a 10% sucrose cushion facilitates transduction of E42 NSPs. **(A)** E42 NSPs were separately transduced with lentiviral particles generated from plasmids #258, #340, #406, #407. 48 hours after transduction, the NSP-forming cells showed reporter signals indicating successful transduction. Volumes of virus suspension used for transduction of E42 NSPs: #258 50 µL, #340 200 µL, #406 100 µL, #407 200 µL. **(B)** Transduction of E42 NSPs with combinations of the four LVs was successful in generating spheres expressing both reporter genes. For the combination #258 + #406, a lot of debris exhibiting mKate2 signals was present. Double positive spheres were thus marked by white arrow heads. Scale bars represent 50 µm.

4. Discussion

4.1. Establishment and optimisation of methods and constructs for CRISPR/Cas9-mediated genome engineering of the *SMARCB1* gene locus in human cell lines

In this thesis, a reporter system for the co-expression of two to three genes encoding fluorescent proteins and the human tumour suppressor gene *SMARCB1* was designed.

This reporter system, which is depicted in Figure 7, includes the introduction of a loxP-PuroR-P2A-mTagBFP2-T2A cassette upstream of the native start codon and either an IRES-eGFP::ZeoR-loxP or an IRES-mKate2-loxP reporter cassette downstream of the stop codon of the *SMARCB1* gene using the CRISPR/Cas9 technology. This system should allow a controlled homozygous or heterozygous deletion of the *SMARCB1* gene, as seen in AT/RTs, via *Cre* recombination. Heterozygous deletion of the gene in combination with point mutations of the *SMARCB1* gene found in AT/RT patients should facilitate the establishment of cell lines with different AT/RT-associated genotypes. The introduction of two HDR constructs with different fluorescence reporter cassettes, one with a *SMARCB1* wildtype sequence and one encoding for the CSS-associated mutation *c.1091_1093del AGA*, was used as a two-colour reporter system in human cell lines. These multi-colour reporter systems should allow not only the rapid identification of recombined cells by the expression of the fluorescence reporter genes which would be time and cost intensive if the insertion of a loxP site alone had to be verified, but also indicates the deletion of either marked allele of *SMARCB1* by loss of the fluorescence signal upon *Cre* recombination. Moreover, the insertion of the fluorescence reporters facilitates the discrimination between the two *SMARCB1* alleles. Therefore, differences in the gene expression of *SMARCB1* from either allele should be detectable by RT-qPCR analysis of the fluorescence genes' transcripts even though the sequence differences in the coding sequence of *SMARCB1* are too subtle to be recognised by primers. Extensive testing of each component was performed in HEK293T cells resulting in a preliminary cell system in which the *SMARCB1* gene was co-expressed with eGFP::ZeoR and mKate2-T2A-BSD reporter cassettes downstream of its native stop codon. In addition, HEK293T cells expressing the mKate2-T2A-BSD cassette linked to one allele of the *SMARCB1* gene in combination with the introduction of the CSS-associated mutation *c.1091_1093del AGA* and an eGFP::ZeoR reporter cassette were generated. With these two HEK293T cell systems, preliminary analyses of the effect of this mutation on the *SMARCB1* gene expression were conducted (sections 3.5 and 4.3).

4.1.1. Transfer of large constructs into hiPSC#33 and re-evaluation of the HDR constructs

Genome editing of the hiPSC cell line #33 proved to be very challenging. Despite extensive testing of diverse DNA transfer methods ranging from transfection of plasmid DNA, over transfection of pre-assembled Cas9/gRNA ribonucleoprotein complexes, to electroporation the CRISPR/Cas9-mediated gene editing to insert the approx. 1.7 kb IRES-reporter cassettes downstream of the native stop codon of the *SMARCB1* gene was not successful. Due to the large insert size and the comparably long homology arms selected[25], transfection efficiency not only of the 9.8 kb Cas9(n) and gRNA plasmid but also of the >7 kb HDR constructs was very low (Figure 26). Independent of the method or device the reported transfection efficiencies of up to 70% could not be achieved (Moore, Atze et al. 2010, Ran, Hsu et al. 2013, Byrne, Mali et al. 2014, Renaud, Boix et al. 2016).

A possible approach to overcome the poor DNA transfer efficiency could be use of integrase-defective lentiviral particles (IDLVs) as transduction is also reported to be highly effective in DNA transfer into hiPSCs (Lombardo, Genovese et al. 2007, Banasik and McCray 2010). IDLVs are generated with a packaging plasmid which carries an inactivating point-mutation in the viral integrase gene. Thus, these viral particles will not randomly integrate the transferred genes into the genome of the infected cell but targeted genome engineering can take place by expression of the CRIPSR/Cas9 machinery from the delivered nucleic acid. Nonetheless, extensive cell death as seen for transfection of hiPSC#33 most likely will also be an issue when transducing hiPSC#33 with IDLVs encoding for the CRISPR/Cas9-genome engineering machinery due to the long-lasting expression of the Cas9/gRNA ribonucleic complexes and thus, the high number of DSBs in the genome. The issue of extensive cell death was tackled in this thesis by the application of the Rho-associated kinase inhibitor mix RevitaCell of Thermo Fisher and the overexpression of the dominant negative form of p53 (p53DD) (Bowman, Symonds et al. 1996, Ohgushi, Matsumura et al. 2010, Ihry, Worringer et al. 2018). The latter approach was reported to inhibit the *TP53*-dependent toxic response to Cas9-induced DSBs in hiPSCs (Ihry, Worringer et al. 2018). Even though a transfection efficiency of the p53DD encoding plasmid of over 30% can be assumed based on the transfection of an equivalently sized reporter plasmid, no positive effect on cell survival was observed by flow cytometry analysis (Figure 26). Therefore, the applied system for CRISPR/Cas9-mediated genome engineering has to be further optimised.

Adjustments on the basis of the system should be considered to achieve the goal of a multi-colour reporter system which is co-expressed with the *SMARCB1* gene and will allow the controlled removal of one or two *SMARCB1* alleles by *Cre* recombination. First, re-evaluation and more extensive testing of the transfection of Cas9(n) RNPs could be implemented. The use of RNPs has different advantages. The half-life of these complexes and thus the Cas9-mediated cleavage activity is in the range of hours rather than weeks as for transfection of Cas9 and gRNA encoding plasmids and was reported to achieve indel insertion rates of 55 to 85% (Liang, Potter et al. 2015, Yu, Liang et al. 2016). This feature reduces the rate of off-target cleavage as well as the total load of double strand breaks in the genome of hPSCs

[25] https://www.addgene.org/crispr/zhang/faq/?gclid=Cj0KCQjwhtT1BRCiARIsAGlY51K0IZOZg2ywnBeaudJsDZdSeAN8Qm0jKveeUfm6YrLGoWNa5mM4-0EaAsi6EALw_wcB, May 15, 2020

(Liang, Potter et al. 2015). Both are considered to be beneficial in enhancing cell survival upon Cas9-cleavage of the genome. Additionally, the process of protein transfection using Lipofectamine Stem reagent was also observed to be less stressful for the cells compared to other methods like electroporation or transduction. One point regarding successful establishment and deployment of the transfection of Cas9/gRNA RNPs into hiPSCs is that there is no direct control of the functionality of this method in other cell lines. Transfer of Cas9/gRNA RNPs into readily transfected cell lines like HEK293T cells has to be performed with Lipofectamine CRISPRMAX which has been optimised for transfer of RNPs while transfer of the RNPs into hPSCs is most effective using Lipofectamine Stem reagent. The Lipofectamine Stem reagent was specifically developed for the transfection of hPSCs but is ineffective in transfecting DNA or protein into other cells lines (personal communication with Tim Wiese, Thermo Fisher and[26]). Also, a size equivalent and visibly observable control for the transfer efficiency of the RNPs is required. Cas9 is a large protein of approx. 160 kDa. This is a protein size which is not met by the fluorophores (e.g. protein size of eGFP: 26.9 kDa[27]). Additionally, the selected fluorescent control protein should be purchasable at low costs or should be synthesised and purified in-house with a comparable purity to the commercial Cas9 protein.

Second, the size of the HDR constructs necessary for the mediation of homologous repair and insertion of the reporter cassette and/or mutation of the genomic sequence could be re-considered. The recommendations of the Zhang laboratory on HDR construct design state that longer homologous sequences reduce the risk of unspecific integration at random sites in the genome, but also recommend homology arms of 800 bp at most (Ran, Hsu et al. 2013). These 800 bp homology arms were also reported to be sufficient for the insertions of DNA sequences of 1 kb.[28] In this project, homology arms of >1.6 kb were designed for the insertion of a >1.7 kb insert. This resulted in larger HDR constructs and reduced transfection efficiencies, thus lower chances for homology directed repair in Cas9-transfected cells due to the absence of a suitable repair template. The optimal length of the homology arms for efficient CRISPR/Cas9 genome editing differs and often is not disclosed in the publications on the generated hPSC reporter cell lines (Yu, Liu et al. 2015, Zhang, Termglinchan et al. 2019). Therefore, shorter homology arms should be considered for the generation of the *SMARCB1* reporter hiPSC line to overcome the discussed disadvantages of homology arms >1.6 kb. Re-evaluation of the design of the HDR constructs should also be considered, e.g. the IRES-GFP *knock-in* strategy as described by He, Tan et al. (2016) may be a convenient strategy to generate the *SMARCB1* reporter cell line. In this strategy, reporter insertion was achieved either by NHEJ-mediated *knock-in* alone or by a combination of NHEJ and HDR. In both cases *knock-in* frequencies were higher as for the conventional HDR approach. Following the experimental design of He, Tan et al. (2016), IRES-reporter cassette donor templates with gRNA target sites derived from prokaryotic sequences (sg-A)

[26] https://www.thermofisher.com/de/en/home/brands/product-brand/lipofectamine/lipofectamine-stem-transfection-reagent.html, May 16, 2020

[27] https://www.fpbase.org/protein/egfp/, May 16, 2020

[28] https://www.addgene.org/crispr/zhang/faq/?gclid=Cj0KCQjwhtT1BRCiARIsAGlY51K0IZOZg2ywnBeaudJsDZdSeAN8Qm0jKveeUfm6YrLGoWNa5mM4-0EaAsi6EALw_wcB, May 14, 2020

5' and 3' of the cassette have to be designed. This so-called double-cut donor template does not contain homologous sequences and reporter *knock-in* will be achieved by NHEJ alone. Co-transfection of the Cas9, a gRNA targeting the 3' UTR of the *SMARCB1* gene, and sg-A will lead to cleavage of the genome and the generation of an IRES-reporter fragment, which will be integrated into the genome at the Cas9 cleavage site via conventional NHEJ. Alternatively, a repair donor containing a 5' homology arm (left homology arm) containing the same gRNA target sequence as the genome and a standard 3' homology arm (right homology arm) should be designed to facilitate reporter *knock-in* via the combination of NHEJ due to Cas9 cleavage in the 5' homology arm and HDR by homologous sequences of the 3' homology arm. In both scenarios, *knock-in* frequencies are expected to be considerably higher compared to a classical HDR approach. This NHEJ-mediated *knock-in* strategy was reported to show low off-target integration even though the NHEJ-based repair may facilitate off-target reporter integration at higher rates compared to the homology-dependent HDR mechanism. Establishment of this method for the *knock-in* of reporter cassettes will also be beneficial for the generation of other hiPSC reporter lines, especially when the reporter cassette is to be integrated adjacent to silenced genes (He, Tan et al. 2016).

Zhang, Li et al. (2017) reported a similar *knock-in* method to He, Tan et al. (2016). They achieved high rates of precise editing in hiPSCs using a double cut donor with 600 bp homology arms flanking the up to 2 kb insert at two genomic loci. In this study, the double cut HDR donor showed a 2.5-fold increase in editing efficiency compared to a circular HDR donor with the same length of homology arms. The design of the double cut HDR donor in Zhang, Li et al. (2017) requires the addition of the gRNA target sequence including the PAM site that is used to target the genome 3' and 5' of the left and right homology arm, respectively. Thereby, the Cas9/gRNA complex targeting the genomic locus also cleaves the HL-insert-HR cassette from its plasmid backbone facilitating precise insertion possibly by the non-canonical HDR pathway of single strand annealing (SSA) (Zhang, Li et al. 2017).

Further enhancement of successful insertion of e.g. reporter cassettes can be achieved by applying the β3-adrenergic receptor agonist L755507 or brefeldin A which inhibits the intracellular protein transport from the endoplasmic reticulum to the Golgi apparatus. Both components have been reported to enhance the insertion of a GFP reporter gene via homologous directed repair in CRISPR/Cas9-mediated genome engineering approaches (Yu, Liu et al. 2015). Zhang, Li et al. (2017) report an increase of editing efficiency of 80% in hiPSCs when boosting the insert integration by adding the cell-cycle synchronising agent nocodazole in combination with CCND1 (cyclin D1). Both components increase the number of cells in S/G2/M phases when HDR is efficient while simultaneously decreasing the number of cells in G0/G1 phase when only NHEJ is responsible for DSB repair (Zhang, Li et al. 2017).

Combining both, the Cas9 delivery optimisation and the design optimisation of the HDR constructs should increase the cell survival, the number of cells transfected with both the CRISPR/Cas9 plasmid and the HDR construct, and therefore the chance of generating genome-engineered hiPSCs. Additionally, and independent of the HDR construct strategy, enhancement of repair pathways

supporting the integration of the insert by supplementation of small molecules or other agents should be implemented.

4.1.2. Transfer of large constructs into MCF10A cells

Aside from the designed AT/RT and CSS cell models based on hiPSC#33, the generated CRISPR/Cas9 plasmids were also to be used for the generation of genetically modified MCF10 cells with reporter genes co-expressed with the *SMARCB1* gene. This MCF10A cell system was pursued for two reasons: to allow the analysis of *SMARCB1* gene expression changes associated with different mutations of the *SMARCB1* gene which are found in the context of different diseases, and to determine if cellular mechanisms exist that control the expression of the *SMARCB1* gene as this could explain the different disease-associated cell fates upon different *SMARCB1* mutations in a near-diploid cell line (Marella, Malyavantham et al. 2009). To address these two issues, both alleles of the *SMARCB1* gene were to be engineered so that a co-expression with either eGFP and mKate2 fluorescence genes occurs. The co-expression of the reporters should enable the indirect assessment of the expression of the linked *SMARCB1* allele and thus allow to examine differences in expression level of each allele upon specific changes in the gene's genomic sequence. Upon mono-allelic inactivation of the *Smarcb1* gene in mice, the transcript levels of *Smarcb1* have been reported to remain at nearly equivalent levels compared to *Smarcb1* wildtype tissues due to a positive and negative regulation of the *Smarcb1* promoter by the amount of protein present (Guidi, Veal et al. 2004). Inversion of exon 1 of the *Smarcb1* gene leading to a CSS-associated phenotype in mice resulted in a reduction of *Smarcb1* mRNA levels by 30% compared to control animals. These results indicate a partial *loss-of-function* of the Smarcb1 protein upon inversion of exon 1 which does not sufficiently trigger the compensatory mechanisms to restore *Smarcb1* transcript levels equivalent to the control group (Filatova, Rey et al. 2019). In *Smarcb1*$^{+/inv}$ *NesCre*$^{+/-}$ mice the CSS-associated phenotype of brain abnormalities was assigned to the partial *loss-of-function* of the resulting protein. The analyses of different cell lines with the CSS-associated *SMARCB1*$^{+/1091\_1093del\,AGA}$ genotype by Valencia, Collings et al. (2019) confirmed that the de-regulation of various developmental processes and the resulting cell morphology cause a loss of interaction between the SMARCB1 protein with the acidic patch of the nucleosome. This results in an impairment of the chromatin remodelling activity of the BAF complexes (Valencia, Collings et al. 2019, He, Wu et al. 2020). Using MCF10A cells engineered according to the two-colour system designed in this thesis, a detailed analysis of the transcription rate of each allele of *SMARCB1* would be possible. By the introduction of different disease-associated *SMARCB1* mutations in conjunction with this two-colour reporter system, direct detection and assessment of the transcription driven from both alleles, the wildtype and affected *SMARCB1* allele, would be possible. Understanding the consequences of different *SMARCB1* mutations on the transcript levels of mutant alleles may contribute to better understand why some of the heterozygous mutations predispose to tumours, while others result in CSS (section 4.1).

The proposed selectable fluorescence reporter insertions downstream of the native stop codon of the *SMARCB1* gene, also in combination with the CSS-associated missense mutation *c.1091_1093del AGA* in exon 8 or the AT/RT-associated nonsense mutation *c.1148del C* in exon 9 of the gene, were successfully tested in HEK293T cells (Biegel 2006, Kordes, Gesk et al. 2010, Diets, Prescott et al. 2019). Genome engineering of the *SMARCB1* gene in MCF10A cells was more challenging compared to HEK293T cells and also than anticipated. The transfer of DNA proved to be similarly inefficient as for hiPSC#33. Despite several optimisation efforts regarding the transfection of the MCF10A cells, successfully engineered cells could not be obtained. The use of IDLVs to transfer the Cas9 and gRNA expression cassette as well as the HDR template as suggested for hiPSCs (section 4.1.1) should be considered.

Engineering of HEK293T and MCF10A cells to co-express a mTagBFP2 reporter gene directly upstream of the native start codon of the *SMARCB1* gene, also in combination with alteration of the genomic sequence exon 1 of the gene to contain mutations associated with RTPS1, was to be achieved (Eaton, Tooke et al. 2011). Insertion of the upstream PuroR-mTagBFP2 reporter cassette was more challenging compared to the insertion of the reporter cassette downstream of the native stop codon of the *SMARCB1* gene since the left homology arm necessary for homologous directed repair had to contain native *SMARCB1* promoter sequences. These sequences resulted in expression of the reporter genes directly from the HDR plasmid, even before directed insertion into the genome. Therefore, the addition of a selectable marker was strongly required. A prolonged puromycin selection period was applied to ensure the enrichment of cells which had incorporated the reporter cassette at its correct site and all transfected plasmid DNA was lost. This was applied at the expense of an increased possibility of random integration. However, random integration of the reporter at sites with low homology to the 3' and 5' homology arm sequences of the HDR construct is a very rare event. Due to the HDR design, random integration will most probably lead to an out of frame insertion of the 2A linked reporter cassette and thus a shift of the open reading frame preventing expression of functional fluorescent proteins. When keeping the wildtype sequence of exon 1 of the *SMARCB1* gene, this approach was successful. The single-cut HDR constructs as discussed above (section 4.1.1) may help solve the issue of pre-integration expression of the reporter and resistance genes. With this HDR construct, the upstream junction of genomic DNA and HDR construct would be achieved by NHEJ and does not require a 5' left homology arm, thus removing the native *SMARCB1* promoter sequences from the original HDR construct and diminishing expression of the reporter and resistance gene prior to integration (He, Tan et al. 2016).

Upon insertion of either the *c.20_43delins T* or the *c.93G>C* mutation into exon 1 of the *SMARCB1* gene which are both associated with the RTPS1 (Eaton, Tooke et al. 2011), the expression of *SMARCB1* and the inserted reporter gene from the mutated allele should be lost. In case of *c.20_43delins T*, expression of the fluorescence reporter would be lost due to a frameshift resulting in pre-mature stop codons. When mutating *c.93G>C*, the splice site at the start of intron 1 is affected causing loss of the mutant transcript either by alteration of splicing or enhanced decay of the mRNA

(Bacci, Sestini et al. 2010). Enrichment of successfully engineered cells would not be possible since there would be no directly visible indicator to discriminate wildtype from engineered cells. To solve this issue, cells engineered to homozygously express the wildtype form of *SMARCB1* linked to the reporter, thus expressing mTagBFP2 should be used as starting material to introduce the RTPS1-associated mutations *c.20_43delins T* and *c.93G>C* in exon 1 of the *SMARCB1* gene via single-stranded oligonucleotide HDR templates in a second round of CRISPR/Cas9-mediated genome engineering. The use of single-stranded oligonucleotides (ssODN) as repair templates has been reported to be highly efficient in the genome editing of small indels and small insertions of up to 100 bp in length, which is sufficient for the insertion of the RTPS1 associated mutations *c.20_43delins T* and *c.93G>C* into the *SMARCB1* gene (Renaud, Boix et al. 2016, Xu, Gao et al. 2018). Successfully engineered cells could be identified by weakening or loss of mTagBFP2 expression and therefore be enriched by FACS. Genotyping of the cells would verify if the mutation was introduced hetero- or homozygously. Alternatively, a first model co-expressing each *SMARCB1* allele with one fluorescence gene (e.g. mTagBFP2 and mKate2) could be used. With the resulting MCF10A cells expressing mTagBFP2 and *SMARCB1* in a wildtype or mutated genetic background, the differences in expression from each allele could be determined.

4.2. The designed multi-colour strategies for the CRISPR/Cas9-mediated genome engineering in comparison to other cellular modelling approaches at the *SMARCB1* locus

In principle, targeted CRISPR/Cas9-mediated indel mutation of the *SMARCB1* gene is possible as was shown by Terada, Jo et al. (2019) and Valencia, Collings et al. (2019). The genome engineering strategies applied in these publications are discussed and compared to the proposed multi-colour strategy in the following.

4.2.1. The designed three-colour reporter strategy in comparison to another cellular AT/RT model

Terada, Jo et al. (2019) generated hiPSC models with a complete loss of *SMARCB1* gene expression by disrupting the gene in exon 5 resulting in absence of the SMARCB1 protein. However, they disrupted the *SMARCB1* gene by random indels in exon 5 arising from NHEJ-mediated DSB repair upon Cas9 cleavage (Terada, Jo et al. 2019). Thus, the approach chosen by Terada, Jo et al. (2019) is considerably less complex compared to the designed three-colour reporter strategy with HDR constructs for the insertion of promoterless reporter cassettes of >1 kb size, since no HDR constructs were necessary for the introduction of random indels in exon 5 of the *SMARCB1* gene. The *SMARCB1 knock-out* hiPSC-model of Terada, Jo et al. (2019) revealed that tumours arising from hiPSC$^{SMARCB1-/-;TP53-/-}$, hiPSC$^{SMARCB1-/-}$, and *SMARCB1*-deficient neural progenitor-like cells with forced overexpression of reprogramming factors (OSKM-NPLC$^{SMARCB1-/-;TP53-/-}$) show the same histology and gene expression signature as aggressive rhabdoid tumours of the brain. This was not the case for tumours arising from NPLC$^{SMARCB1-/-;TP53-/-}$. Thus, the results and the identification of the ESC-like gene expression signature in the hiPSC$^{SMARCB1-/-;TP53-/-}$-derived tumours but not the NPLC$^{SMARCB1-/-;TP53-/-}$ tumours further defined the most likely cell type of origin responsible for the growth of AT/RTs in children to be a neural progenitor or neural stem cell with an ESC-like gene expression profile, e.g. induced by overexpression of *c-MYC* (Wong, Liu et al. 2008, Johann, Erkek et al. 2016, Poli, Fagnocchi et al. 2018, Terada, Jo et al. 2019, Vladoiu, El-Hamamy et al. 2019). Based on these results, a pluripotent cell, which is more immature than a neural progenitor cell, is hypothesised to be the cell of origin of AT/RTs. This differs from results of mouse models which indicated that neural progenitor cells which lost the Smarcb1 protein to represent the origin of AT/RT-like tumours (Bouffard, Sandberg et al. 2004, Deisch, Raisanen et al. 2011, Ng, Martinez et al. 2015, Han, Richer et al. 2016). Even though there is a hiPSC line with AT/RT-associated loss of *SMARCB1* available, the hiPSC model designed here is supplementary or even superior to it in many aspects. In the *in vitro* model generated by Terada, Jo et al. (2019), both alleles of the *SMARCB1* gene are disrupted in hiPSC, the earliest developmental stage *in vitro*. This allows analyses of the AT/RT development *in vitro*, but may not mimic the situation *in vivo* as neural stem cell pools are depleted in the developing brain by differentiation. The constitutional loss of both *SMARCB1* alleles and thus the complete loss of the SMARCB1 protein in hiPSC may also lead to different cellular consequences (i.e. gene expression

patterns and epigenetic alterations) than a sequential or simultaneous *loss of function* of the two *SMARCB1* alleles in NSCs/NPCs. In the hiPSC model designed in this thesis, the generation of homozygous and, most importantly, heterozygous deletion of the *SMARCB1* gene is facilitated. This allows the study of early stages of tumour development as well as of states of tumour predisposition. When evaluating the hypotheses based on the results obtained with *SMARCB1*$^{-/-}$ hiPSCs by Terada, Jo et al. (2019), which exhibit a seemingly normal differentiation behaviour, it has to be taken into consideration, that *SMARCB1* gene expression was reported to be indispensable for self-renewal and neuronal differentiation in hESCs (Langer, Ward et al. 2019), which appears to be different for the *SMARCB1*$^{-/-}$ hiPSCs.

Also, the genetic status seen in most patients suffering from an AT/RT differs from the homozygous disruption of the gene in exon 5 as established by Terada, Jo et al. (2019). Many AT/RT cases show large deletions at Chr.22q11 often comprising the complete coding sequence of the *SMARCB1* gene or single base deletions in exon 5 or 9 of the *SMARCB1* gene (Figure 3) (Versteege, Sevenet et al. 1998, Biegel, Zhou et al. 1999, Rousseau-Merck, Versteege et al. 1999, Biegel, Fogelgren et al. 2000, Biegel, Kalpana et al. 2002, Biegel 2006, Jackson, Sievert et al. 2009, Bourdeaut, Lequin et al. 2011, Fruhwald, Hasselblatt et al. 2019). Moreover, the established *SMARCB1*$^{-/-}$ hiPSC model does not reproduce the genetic situation observed in patients with heterozygous germline mutations in the *SMARCB1* gene. These patients are prone to develop rhabdoid tumours of the brain, kidney, or soft tissues due to a second hit affecting the intact allele of the *SMARCB1* gene thus causing complete loss of gene expression of *SMARCB1* (Sevenet, Sheridan et al. 1999, Sredni and Tomita 2015). In patients affected by the rhabdoid tumour predisposition syndrome 1 (RTPS1), therapeutic options for AT/RTs may exhibit negative effects also on all cells affected by the germline mutation of the *SMARCB1* gene, a situation which necessitates a careful consideration. For future therapy options it is also of utmost importance to model the tumours' different genetic background present in patients to possibly re-construct the three molecular subgroups of AT/RTs identified in patients which are associated with different prognoses and to rule out possible negative effects of the future treatment or drug. (Torchia, Picard et al. 2015, Johann, Erkek et al. 2016, Fruhwald, Hasselblatt et al. 2019, Ho, Johann et al. 2020) Most patients suffering from AT/RTs are young children or infants, who are highly susceptible for complications related with aggressive therapies as chemotherapy or radiation (Rorke, Packer et al. 1996, Burger, Yu et al. 1998, Biegel, Zhou et al. 1999, Hilden, Meerbaum et al. 2004). Using the diverse models designed here, tumours arising from cells with inactivation of the *SMARCB1* gene at very specific developmental stages or in a specific genetic background allow the analysis of cellular mechanisms to cope with the loss of this essential gene. Furthermore, the tumours could be evaluated for differences in their gene expression signature, aggressiveness, and susceptibility to different therapy options, thus being able to reflect the heterogeneity in tumour details seen in AT/RT patients (Birks, Donson et al. 2011, Torchia, Picard et al. 2015, Johann, Erkek et al. 2016, Vitte, Gao et al. 2017). Also, the testing of a therapy that effectively eliminates tumour cells with biallelic *SMARCB1 loss-of-function* which does not affect all other cells in the body of RTPS1 patients carrying

heterozygous germline *SMARCB1* mutations would be possible with the cellular systems proposed in this thesis. The designed cellular tumour models may also play an important role in identifying new potential therapeutic targets or establishing already hypothesised ones in AT/RT cells (Wang, Haswell et al. 2014, Terada, Jo et al. 2019). With these rhabdoid tumour models one might also be able to assess if the previously reported proteasome stress, overexpression of MEK/MELK, and EZH2 found in AT/RT cells may be exploited by inhibitors of these components or systems in combination with e.g. low dose radiation which may provide a promising but less collaterally damaging therapy option for the treatment of infants and young children suffering from AT/RTs with and without RTPS1 (Wilson, Wang et al. 2010, Hertwig, Meyer et al. 2012, Wei, Goldfarb et al. 2014, Moreno and Kerl 2016, Meel, Guillen Navarro et al. 2020).

4.2.2. The designed two-colour strategy in comparison to another cellular CSS model

A two-colour hiPSC model with *SMARCB1* gene mutations associated with CSS has the following advantages over the model published by Valencia, Collings et al. (2019): co-expression of two different fluorescence reporter genes with a wildtype and a mutant *SMARCB1* allele allows an immediate and simple assessment of gene expression from these two alleles. The functional effect of the deletion of lysine residue 364 resulting from the *c.1091_1093del AGA* missense mutation in exon 8 of *SMARCB1* was analysed in Valencia, Collings et al. (2019) by synthesis of the mutant protein in HEK293T cells and CRISPR/Cas9-mediated genome engineering of hiPSC to heterozygously delete bases 1091 to 1093 of the *SMARCB1* gene via single oligonucleotides as HDR templates. Frequent mutations of the *SMARCB1* gene associated with CSS are located in the highly conserved coiled-coil C-terminal domain (CTD) of the protein (Morozov, Yung et al. 1998, Diets, Prescott et al. 2019). The SMARCB1 CTD was shown to be an α-helical domain containing a dense region of basic, positively charged amino acids which binds to the nucleosomal acidic patch facilitating nucleosome remodelling and DNA accessibility (Valencia, Collings et al. 2019, Han, Reyes et al. 2020, He, Wu et al. 2020). Upon a CSS-associated single residue missense mutation as *c.1091_1093del AGA*, the α-helical organization is shifted and acidic residues within the CTD are repositioned to face the same direction as the basic cluster (Diets, Prescott et al. 2019). This shift decreases the charge potential of the positively charged cluster and diminishes its interaction with the nucleosomal acidic patch (Valencia, Collings et al. 2019). Analysis of hiPSC$^{SMARCB1+/1091_1093del\ AGA}$ revealed no difference of genome-wide BAF complex targeting and activating H3K27ac nucleosome marks to control hiPSC with wildtype SMARCB1 protein. 25% of the occupied sites presented decreased DNA accessibility, especially gene loci encoding for pluripotency factors with OCT, SOX, or NANOG motifs, underlining the importance of the BAF complex mediated chromatin remodeling for the maintenance of pluripotency (Singhal, Graumann et al. 2010, Langer, Ward et al. 2019). Upon Ngn2-induced neuronal differentiation of hiPSC$^{SMARCB1+/1091_1093del\ AGA}$, the reduced DNA accessibility at loci associated with CSS or other ID syndromes manifested and developmental processes of organ systems affected in CSS or ID (i.e. nervous system, cardiac muscle, kidney, mesenchyme, endocrine system, cell fate commitment) were

identified to be impaired (Valencia, Collings et al. 2019). Morphologically, neurons differentiated from hiPSC*SMARCB1+/1091_1093del AGA* showed diminished neurite outgrowth and neuron count as well as fewer neuronal projections recapitulating deficits observed in patient-derived cellular models of developmental delay (Valencia, Collings et al. 2019) and this possibly relates to phenotypic changes observed in the CSS mouse model described by Filatova, Rey et al. (2019).

The molecular mechanisms responsible for the phenotypic outcome of the inversion of exon 1 of the *Smarcb1* gene in the mouse model published by Filatova, Rey et al. (2019) are not fully understood yet. The inversion of exon 1 of the *Smarcb1* coding sequence likely leads to an absence of this transcript, as reduced transcript levels were observed when applying primers binding in exons further downstream of exon 1. The reduction in transcript abundance may have a similar effect on the generation of DNA accessibility at loci essential for nervous system development as the *c.1091_1093del AGA* missense mutation in the C-terminal α-helix of the *SMARCB1* gene accounting for the observed de-regulation of gene expression in the affected RGCs leading to the characteristic thin corpus callosum and hyperplastic choroid plexus as well as microcephaly in the CSS mouse model and CSS patients (Filatova, Rey et al. 2019).

Combining all the aspects and variants of the cell models designed in this thesis, a detailed representation of the genetic background observed in patients with RTPS1, CSS, and *de novo* loss of *SMARCB1* gene expression could be achieved. By this, a direct and informative comparison of the effect of each mutation on the expression of both *SMARCB1* alleles would be possible. The comparison of the anticipated hiPSC line carrying the CSS-associated *SMARCB1* mutation *c.1091_1093del AG*A with an additional hiPSC line carrying an inversion of exon 1 of the *SMARCB1* gene in long term differentiation studies will reveal the differences and similarities of affected developmental processes and could help to further understand the role of SMARCB1 protein in maintaining the structural and functional integrity of the BAF complex.

4.3. *Loss-of-function* mutations in *SMARCB1* de-regulate expression of *Hes* genes

The RT-qPCR analysis of *Hes* gene expression levels in mouse brain tissue and HEK293T samples was based on results obtained with the established CSS-mouse model (Filatova, Rey et al. 2019). A diminished radial glial cell (RGC) population in *Smarcb1*$^{+/inv}$ *NesCre*$^{+/-}$ mutant mice observed by Filatova, Rey et al. (2019) can have different causes. One may be the premature differentiation of RGCs, resulting in depletion of the neural progenitor (NPC) pool. Others could include cell death or decreased expansion of the NPCs. Many genes and pathways are involved in the regulation of the maintenance and expansion of the NPC pool and the gene expression of some possible pathways was explored in mouse brain samples (data not disclosed). Mutant mouse models of these genes show similarities to the established CSS-recapitulating mouse model, e.g. regarding the diminished neurosphere (NSP) forming ability of cells isolated from *Smarcb1*$^{+/inv}$ *NesCre*$^{+/-}$ mutant mice and the microcephaly observed in the CSS-recapitulating mouse model as well as in CSS patients (Coffin and Siris 1970, Filatova, Rey et al. 2019) but de-regulation of genes involved in these pathways could not be observed in RT-qPCR analyses of mouse brain tissue. A reduction of *Hes5* transcript levels was found in brain sections of mutant *Smarcb1*$^{+/inv}$ *NesCre*$^{+/-}$ mice in the area of the glial wedge RGC population lining the lateral ventricle compared to *Smarcb1*$^{+/inv}$ *NesCre*$^{-/-}$ control mice at E15.5 (Filatova, Rey et al. 2019). This reduction in *Hes5* gene expression explains certain midline alterations in these animals. Reduced *Hes5* mRNA levels were also seen in RT-qPCR analyses of one litter of E14.5 mouse forebrain samples, when normalizing the c_T values to the expression of the *Nestin* gene, which is expressed in RGCs. Reduced expression of *Hes5* in the RGCs in the glial wedge region lining at the ventricular surface might contribute to premature loss of RGC identity, and thus reduced cell numbers in the glial wedge guide post region as seen by a reduction in glial fibrillary acidic protein (GFAP)-positive cells in this area in *Smarcb1*$^{+/inv}$ *NesCre*$^{+/-}$ mutant brain sections (Filatova, Rey et al. 2019). The reduction in GFAP-positive cells in this guide post region impairs the correct guidance of corpus callosum axons resulting in no axons crossing the midline in *Smarcb1*$^{+/inv}$ *NesCre*$^{+/-}$ mutant brains (Shu and Richards 2001, Filatova, Rey et al. 2019). Due to the fact that the area of differential expression of *Hes5* is small and randomly distributed when sectioning the brain for RNA isolation, it might be explained why this trend was not detected for all samples analysed.

RT-qPCR analysis of *Hes1* gene expression revealed an increase of *Hes1* mRNA in mutant, compared to control mouse brain samples at E14.5. Conversely, overexpression of the *Hes1* gene in NSCs was reported to repress differentiation and maintain NSC identity, even promoting proliferation of NSCs (Kageyama, Ohtsuka et al. 2008). Persistent high expression of the *Hes1* gene was observed in non-neurogenic boundary cells at early developmental stages (Baek, Hatakeyama et al. 2006). Nonetheless, the increase of *Hes1* transcripts observed in *Nestin* expressing parts of brain tissue samples has to be evaluated carefully regarding its influence on neural development. RNA *in situ* hybridisations of E15.5 brain sections did not reveal an increase in *Hes1* mRNA levels in mutant compared to control brains. Moreover, *Nestin* is not only expressed in RGCs but also in the developing endothelial cells of brain vasculature (Mokry and Nemecek 1998, Mokry and Nemecek 1999, Suzuki, Namiki et al. 2010). Also,

Hes1 was reported to be a key transducer of *Notch* signalling in the developing vasculature of the brain (Kitagawa, Hojo et al. 2013).

Interestingly, HEK293T cells, genetically engineered to express at least one *c.1091_1093del AGA* mutated allele of *SMARCB1*, show a significant reduction in *HES5* mRNA transcripts compared to HEK293T cells expressing only wildtype alleles of *SMARCB1*. The CSS-associated alterations in SMARCB1 protein function seem to not trigger any compensatory mechanism to prevent the altered protein's effect on gene expression of *HES5*, even though one intact allele of the *Smarcb1* gene was reported to be sufficient to sustain Smarcb1 protein levels in mice (Guidi, Veal et al. 2004).

To further investigate the role and mechanism of the *Hes* gene de-regulation in mouse neural stem/progenitor cells (NSCs/NPCs) upon CSS-associated inversion of exon 1 of the *Smarcb1* gene, an *in vitro* model was to be established. NSCs and NPCs isolated from *Smarcb1*$^{+/inv}$ *NesCre*$^{+/-}$ mutant mice do not proliferate and cannot be cultured *in vitro* (Filatova, Rey et al. 2019). For this reason, transduction of NSP-forming cells established from *Smarcb1*$^{+/inv}$ *NesCre*$^{-/-}$ control mice with lentiviral particles transferring a constitutionally expressed *Cre* recombinase and a Venus reporter gene with and without a *Hes5* overexpression cassette was established to overcome the shortage of mutant NSCs and to test the hypothesis if overexpression of *Hes5* can rescue the growth arrest observed upon inversion of exon 1 of the *Smarcb1* gene in NSP-forming cells. Therefore, the transduction of NSPs with lentiviral particles which were concentrated over a 10% sucrose cushion was established (Jiang, Hua et al. 2015). Co-transduction of NSPs with Venus*Cre* and *Hes5* overexpression-facilitating lentiviral particles was successful in generating Venus and mKate2 double positive NSP-forming cells. However, these NSP-forming cells could not be maintained in culture for flow cytometry analysis. Based on these preliminary results, an optimised workflow with flow cytometry analysis 48 hours post transduction followed by sphere growth assay analyses is required to test if overexpression of the *Hes5* gene can rescue the sphere forming ability of *Smarcb1*$^{+/inv}$ mutant NSP-forming cells. This should facilitate comprehensive analyses of the functional effects of the CSS-associated partial loss of *Smarcb1* function in these cells.

5. Outlook

Mutations in the tumour suppressor gene *SMARCB1* are associated with different disease states and types. Biallelic loss of *SMARCB1* function due to truncating or nonsense mutations can cause malignant tumours of the brain with characteristic histology and a stem cell-like expression profile while heterozygous missense mutations or in-frame deletions of the *SMARCB1* gene are associated with developmental defects (Versteege, Sevenet et al. 1998, Biegel, Tan et al. 2002, Tsurusaki, Okamoto et al. 2012). In this thesis, diverse genome engineering constructs were designed, tested, and applied with the aim of establishing cellular disease models by introducing *SMARCB1* mutations present in human patients into human cell lines. With cellular disease models like these, the understanding of the biologic consequences of different mutations of the *SMARCB1* gene can be analysed. This may help to gain a better molecular understanding of the associated disease states and types, and could aid in the development of new treatment approaches.

Especially for patients affected by AT/RTs, sophisticated models recapitulating the molecular heterogeneity of these tumours may lead to the identification of specific and potential therapeutic targets which could ultimately result in advanced treatment strategies improving the survival rate of AT/RT patients while reducing the overall negative consequences of intensive cancer treatment in children (Butler and Haser 2006, Ho, Johann et al. 2020). *In vitro* cell models alone will not suffice to develop these therapeutic strategies, but the combination of the cell models with orthotopic xenograft transplantation could provide a platform to determine the effect of multimodal treatments on AT/RTs of the different subgroups.

The multi-colour cellular AT/RT model that should allow the controlled homo- and heterozygous inactivation of the *SMARCB1* gene as proposed in this thesis would also supplement the model established by Terada, Jo et al. (2019). Their model only recapitulates a simultaneous biallelic inactivation of the *SMARCB1* gene by indels in exon 5 while the genetic reality of RTPS1 patients with a predisposition for AT/RTs due to a congenital monoallelic inactivation of the *SMARCB1* gene present in the germline of these patients, cannot be recapitulated. Therefore, also the effect of potential AT/RT therapies on cells exhibiting a heterozygous loss of the *SMARCB1* gene cannot be analysed but may be of importance for treatment decisions. Therapeutic agents which also negatively impact cells with a monoallelic loss of *SMARCB1* may not be applicable for RTPS1 patients since most to all of their bodies' cells would react to the therapy resulting in a systemic detrimental effect of the treatment. This could be analysed pre-clinically with the heterozygous *SMARCB1 knock-out* model proposed here. Additionally, the proposed multi-colour approach of a cellular model for AT/RTs facilitates the sequential inactivation of the *SMARCB1* gene. Either by the combination of an inactivating point mutation of the *SMARCB1* gene with a second floxed allele or by controlled, sequential inactivation of both floxed alleles by *Cre* recombinase. For the latter approach, a sophisticated approach e.g. with a tamoxifen-inducible *Cre* recombinase or *Cre* recombinase under the control of promoters of developmentally differentially expressed genes has to be applied.

6. Bibliography

Alfert, A., N. Moreno and K. Kerl (2019). "The BAF complex in development and disease." Epigenetics Chromatin **12**(1): 19.

Allen, M. D., S. M. Freund, G. Zinzalla and M. Bycroft (2015). "The SWI/SNF Subunit INI1 Contains an N-Terminal Winged Helix DNA Binding Domain that Is a Target for Mutations in Schwannomatosis." Structure **23**(7): 1344-1349.

Alpsoy, A. and E. C. Dykhuizen (2018). "Glioma tumor suppressor candidate region gene 1 (GLTSCR1) and its paralog GLTSCR1-like form SWI/SNF chromatin remodeling subcomplexes." J Biol Chem **293**(11): 3892-3903.

Ammerlaan, A. C., A. Ararou, M. P. Houben, F. Baas, C. C. Tijssen, J. L. Teepen, P. Wesseling and T. J. Hulsebos (2008). "Long-term survival and transmission of INI1-mutation via nonpenetrant males in a family with rhabdoid tumour predisposition syndrome." Br J Cancer **98**(2): 474-479.

Bacci, C., R. Sestini, A. Provenzano, I. Paganini, I. Mancini, B. Porfirio, R. Vivarelli, M. Genuardi and L. Papi (2010). "Schwannomatosis associated with multiple meningiomas due to a familial SMARCB1 mutation." Neurogenetics **11**(1): 73-80.

Baek, J. H., J. Hatakeyama, S. Sakamoto, T. Ohtsuka and R. Kageyama (2006). "Persistent and high levels of Hes1 expression regulate boundary formation in the developing central nervous system." Development **133**(13): 2467-2476.

Banasik, M. B. and P. B. McCray, Jr. (2010). "Integrase-defective lentiviral vectors: progress and applications." Gene Ther **17**(2): 150-157.

Biegel, J. A. (2006). "Molecular genetics of atypical teratoid/rhabdoid tumor." Neurosurg Focus **20**(1): E11.

Biegel, J. A., B. Fogelgren, L. M. Wainwright, J. Y. Zhou, H. Bevan and L. B. Rorke (2000). "Germline INI1 mutation in a patient with a central nervous system atypical teratoid tumor and renal rhabdoid tumor." Genes Chromosomes Cancer **28**(1): 31-37.

Biegel, J. A., G. Kalpana, E. S. Knudsen, R. J. Packer, C. W. Roberts, C. J. Thiele, B. Weissman and M. Smith (2002). "The role of INI1 and the SWI/SNF complex in the development of rhabdoid tumors: meeting summary from the workshop on childhood atypical teratoid/rhabdoid tumors." Cancer Res **62**(1): 323-328.

Biegel, J. A., L. Tan, F. Zhang, L. Wainwright, P. Russo and L. B. Rorke (2002). "Alterations of the hSNF5/INI1 gene in central nervous system atypical teratoid/rhabdoid tumors and renal and extrarenal rhabdoid tumors." Clin Cancer Res **8**(11): 3461-3467.

Biegel, J. A., J. Y. Zhou, L. B. Rorke, C. Stenstrom, L. M. Wainwright and B. Fogelgren (1999). "Germ-line and acquired mutations of INI1 in atypical teratoid and rhabdoid tumors." Cancer Res **59**(1): 74-79.

Birks, D. K., A. M. Donson, P. R. Patel, C. Dunham, A. Muscat, E. M. Algar, D. M. Ashley, B. K. Kleinschmidt-Demasters, R. Vibhakar, M. H. Handler and N. K. Foreman (2011). "High expression of BMP pathway genes distinguishes a subset of atypical teratoid/rhabdoid tumors associated with shorter survival." Neuro Oncol **13**(12): 1296-1307.

Bouffard, J. P., G. D. Sandberg, J. A. Golden and L. B. Rorke (2004). "Double immunolabeling of central nervous system atypical teratoid/rhabdoid tumors." Mod Pathol **17**(6): 679-683.

Bourdeaut, F., D. Lequin, L. Brugieres, S. Reynaud, C. Dufour, F. Doz, N. Andre, J. L. Stephan, Y. Perel, O. Oberlin, D. Orbach, C. Bergeron, X. Rialland, P. Freneaux, D. Ranchere, D. Figarella-Branger, G. Audry, S. Puget, D. G. Evans, J. C. Pinas, V. Capra, V. Mosseri, I. Coupier, M. Gauthier-Villars, G. Pierron and O. Delattre (2011). "Frequent hSNF5/INI1 germline mutations in patients with rhabdoid tumor." Clin Cancer Res **17**(1): 31-38.

Boussif, O., F. Lezoualc'h, M. A. Zanta, M. D. Mergny, D. Scherman, B. Demeneix and J. P. Behr (1995). "A versatile vector for gene and oligonucleotide transfer into cells in culture and in vivo: polyethylenimine." Proc Natl Acad Sci U S A **92**(16): 7297-7301.

Bowman, T., H. Symonds, L. Gu, C. Yin, M. Oren and T. Van Dyke (1996). "Tissue-specific inactivation of p53 tumor suppression in the mouse." Genes Dev **10**(7): 826-835.

Burger, P. C., I. T. Yu, T. Tihan, H. S. Friedman, D. R. Strother, J. L. Kepner, P. K. Duffner, L. E. Kun and E. J. Perlman (1998). "Atypical teratoid/rhabdoid tumor of the central nervous system: a highly malignant tumor of infancy and childhood frequently mistaken for medulloblastoma: a Pediatric Oncology Group study." Am J Surg Pathol **22**(9): 1083-1092.

Butler, R. W. and J. K. Haser (2006). "Neurocognitive effects of treatment for childhood cancer." Ment Retard Dev Disabil Res Rev **12**(3): 184-191.

Byrne, S. M., P. Mali and G. M. Church (2014). "Genome editing in human stem cells." Methods Enzymol **546**: 119-138.

Cahill, D., B. Connor and J. P. Carney (2006). "Mechanisms of eukaryotic DNA double strand break repair." Front Biosci **11**: 1958-1976.

Cairns, B. R., Y. Lorch, Y. Li, M. Zhang, L. Lacomis, H. Erdjument-Bromage, P. Tempst, J. Du, B. Laurent and R. D. Kornberg (1996). "RSC, an essential, abundant chromatin-remodeling complex." Cell **87**(7): 1249-1260.

Cao, F., X. Xie, T. Gollan, L. Zhao, K. Narsinh, R. J. Lee and J. C. Wu (2010). "Comparison of gene-transfer efficiency in human embryonic stem cells." Mol Imaging Biol **12**(1): 15-24.

Caramel, J., F. Quignon and O. Delattre (2008). "RhoA-dependent regulation of cell migration by the tumor suppressor hSNF5/INI1." Cancer Res **68**(15): 6154-6161.

Carlson-Stevermer, J. and K. Saha (2017). "Genome Editing in Human Pluripotent Stem Cells." Methods Mol Biol **1590**: 165-174.

Cheng, S. W., K. P. Davies, E. Yung, R. J. Beltran, J. Yu and G. V. Kalpana (1999). "c-MYC interacts with INI1/hSNF5 and requires the SWI/SNF complex for transactivation function." Nat Genet **22**(1): 102-105.

Chng, J., T. Wang, R. Nian, A. Lau, K. M. Hoi, S. C. Ho, P. Gagnon, X. Bi and Y. Yang (2015). "Cleavage efficient 2A peptides for high level monoclonal antibody expression in CHO cells." MAbs **7**(2): 403-412.

Clapier, C. R., J. Iwasa, B. R. Cairns and C. L. Peterson (2017). "Mechanisms of action and regulation of ATP-dependent chromatin-remodelling complexes." Nat Rev Mol Cell Biol **18**(7): 407-422.

Coffin, G. S. and E. Siris (1970). "Mental retardation with absent fifth fingernail and terminal phalanx." Am J Dis Child **119**(5): 433-439.

Cong, L., F. A. Ran, D. Cox, S. Lin, R. Barretto, N. Habib, P. D. Hsu, X. Wu, W. Jiang, L. A. Marraffini and F. Zhang (2013). "Multiplex genome engineering using CRISPR/Cas systems." Science **339**(6121): 819-823.

Deisch, J., J. Raisanen and D. Rakheja (2011). "Immunohistochemical expression of embryonic stem cell markers in malignant rhabdoid tumors." Pediatr Dev Pathol **14**(5): 353-359.

Diets, I. J., T. Prescott, N. L. Champaigne, G. M. S. Mancini, B. Krossnes, R. Fric, K. Kocsis, M. C. J. Jongmans and T. Kleefstra (2019). "A recurrent de novo missense pathogenic variant in SMARCB1 causes severe intellectual disability and choroid plexus hyperplasia with resultant hydrocephalus." Genet Med **21**(3): 572-579.

Eaton, K. W., L. S. Tooke, L. M. Wainwright, A. R. Judkins and J. A. Biegel (2011). "Spectrum of SMARCB1/INI1 mutations in familial and sporadic rhabdoid tumors." Pediatr Blood Cancer **56**(1): 7-15.

Filatova, A., L. K. Rey, M. B. Lechler, J. Schaper, M. Hempel, R. Posmyk, K. Szczaluba, G. W. E. Santen, D. Wieczorek and U. A. Nuber (2019). "Mutations in SMARCB1 and in other Coffin-Siris syndrome genes lead to various brain midline defects." Nat Commun **10**(1): 2966.

Fruhwald, M. C., M. Hasselblatt, K. Nemes, S. Bens, M. Steinbugl, P. D. Johann, K. Kerl, P. Hauser, E. Quiroga, P. Solano-Paez, V. Biassoni, M. J. Gil-da-Costa, M. Perek-Polnik, M. van de Wetering, D. Sumerauer, J. Pears, N. Stabell, S. Holm, H. Hengartner, N. U. Gerber, M. Grotzer, J. Boos, M. Ebinger, S. Tippelt, W. Paulus, R. Furtwangler, P. Hernaiz-Driever, H. Reinhard, S. Rutkowski, P. G. Schlegel, I. Schmid, R. D. Kortmann, B. Timmermann, M. Warmuth-Metz, U. Kordes, J. Gerss, K. Nysom, R. Schneppenheim, R. Siebert, M. Kool and N. Graf (2019). "Age and DNA-methylation subgroup as potential independent risk factors for treatment stratification in children with Atypical Teratoid/Rhabdoid Tumors (ATRT)." Neuro Oncol.

Fruhwald, M. C., M. Hasselblatt, S. Wirth, G. Kohler, R. Schneppenheim, J. I. Subero, R. Siebert, U. Kordes, H. Jurgens and J. Vormoor (2006). "Non-linkage of familial rhabdoid tumors to SMARCB1 implies a second locus for the rhabdoid tumor predisposition syndrome." Pediatr Blood Cancer **47**(3): 273-278.

Fu, Y., J. A. Foden, C. Khayter, M. L. Maeder, D. Reyon, J. K. Joung and J. D. Sander (2013). "High-frequency off-target mutagenesis induced by CRISPR-Cas nucleases in human cells." Nat Biotechnol **31**(9): 822-826.

Gotz, M. and Y. A. Barde (2005). "Radial glial cells defined and major intermediates between embryonic stem cells and CNS neurons." Neuron **46**(3): 369-372.

Green, R. and E. J. Rogers (2013). "Transformation of chemically competent E. coli." Methods Enzymol **529**: 329-336.

Guidi, C. J., A. T. Sands, B. P. Zambrowicz, T. K. Turner, D. A. Demers, W. Webster, T. W. Smith, A. N. Imbalzano and S. N. Jones (2001). "Disruption of Ini1 leads to peri-implantation lethality and tumorigenesis in mice." Mol Cell Biol **21**(10): 3598-3603.

Guidi, C. J., T. M. Veal, S. N. Jones and A. N. Imbalzano (2004). "Transcriptional compensation for loss of an allele of the Ini1 tumor suppressor." J Biol Chem **279**(6): 4180-4185.

Han, Y., A. A. Reyes, S. Malik and Y. He (2020). "Cryo-EM structure of SWI/SNF complex bound to a nucleosome." Nature **579**(7799): 452-455.

Han, Z. Y., W. Richer, P. Freneaux, C. Chauvin, C. Lucchesi, D. Guillemot, C. Grison, D. Lequin, G. Pierron, J. Masliah-Planchon, A. Nicolas, D. Ranchere-Vince, P. Varlet, S. Puget, I. Janoueix-Lerosey, O. Ayrault, D. Surdez, O. Delattre and F. Bourdeaut (2016). "The occurrence of intracranial rhabdoid tumours in mice depends on temporal control of Smarcb1 inactivation." Nat Commun **7**: 10421.

Hanahan, D. (1983). "Studies on transformation of Escherichia coli with plasmids." J Mol Biol **166**(4): 557-580.

Hasselblatt, M., I. Nagel, F. Oyen, K. Bartelheim, R. B. Russell, U. Schuller, R. Junckerstorff, M. Rosenblum, A. H. Alassiri, S. Rossi, I. Schmid, N. G. Gottardo, H. Toledano, E. Viscardi, M. Balbin, L. Witkowski, Q. Lu, M. J. Betts, W. D. Foulkes, R. Siebert, M. C. Fruhwald and R. Schneppenheim (2014). "SMARCA4-mutated atypical teratoid/rhabdoid tumors are associated with inherited germline alterations and poor prognosis." Acta Neuropathol **128**(3): 453-456.

He, S., Z. Wu, Y. Tian, Z. Yu, J. Yu, X. Wang, J. Li, B. Liu and Y. Xu (2020). "Structure of nucleosome-bound human BAF complex." Science **367**(6480): 875-881.

He, W., L. Zhang, O. D. Villarreal, R. Fu, E. Bedford, J. Dou, A. Y. Patel, M. T. Bedford, X. Shi, T. Chen, B. Bartholomew and H. Xu (2019). "De novo identification of essential protein domains from CRISPR-Cas9 tiling-sgRNA knockout screens." Nat Commun **10**(1): 4541.

He, X., C. Tan, F. Wang, Y. Wang, R. Zhou, D. Cui, W. You, H. Zhao, J. Ren and B. Feng (2016). "Knock-in of large reporter genes in human cells via CRISPR/Cas9-induced homology-dependent and independent DNA repair." Nucleic Acids Res **44**(9): e85.

Heckman, K. L. and L. R. Pease (2007). "Gene splicing and mutagenesis by PCR-driven overlap extension." Nat Protoc **2**(4): 924-932.

Helming, K. C., X. Wang and C. W. M. Roberts (2014). "Vulnerabilities of mutant SWI/SNF complexes in cancer." Cancer Cell **26**(3): 309-317.

Hendriks, W. T., C. R. Warren and C. A. Cowan (2016). "Genome Editing in Human Pluripotent Stem Cells: Approaches, Pitfalls, and Solutions." Cell Stem Cell **18**(1): 53-65.

Hertwig, F., K. Meyer, S. Braun, S. Ek, R. Spang, C. V. Pfenninger, I. Artner, G. Prost, X. Chen, J. A. Biegel, A. R. Judkins, E. Englund and U. A. Nuber (2012). "Definition of genetic events directing the development of distinct types of brain tumors from postnatal neural stem/progenitor cells." Cancer Res **72**(13): 3381-3392.

Hilden, J. M., S. Meerbaum, P. Burger, J. Finlay, A. Janss, B. W. Scheithauer, A. W. Walter, L. B. Rorke and J. A. Biegel (2004). "Central nervous system atypical teratoid/rhabdoid tumor: results of therapy in children enrolled in a registry." J Clin Oncol **22**(14): 2877-2884.

Ho, B., P. D. Johann, Y. Grabovska, M. J. De Dieu Andrianteranagna, F. Yao, M. Fruhwald, M. Hasselblatt, F. Bourdeaut, D. Williamson, A. Huang and M. Kool (2020). "Molecular subgrouping of atypical teratoid/rhabdoid tumors-a reinvestigation and current consensus." Neuro Oncol **22**(5): 613-624.

Ho, L., E. L. Miller, J. L. Ronan, W. Q. Ho, R. Jothi and G. R. Crabtree (2011). "esBAF facilitates pluripotency by conditioning the genome for LIF/STAT3 signalling and by regulating polycomb function." Nat Cell Biol **13**(8): 903-913.

Ho, L., J. L. Ronan, J. Wu, B. T. Staahl, L. Chen, A. Kuo, J. Lessard, A. I. Nesvizhskii, J. Ranish and G. R. Crabtree (2009). "An embryonic stem cell chromatin remodeling complex, esBAF, is essential for embryonic stem cell self-renewal and pluripotency." Proc Natl Acad Sci U S A **106**(13): 5181-5186.

Hong, H., K. Takahashi, T. Ichisaka, T. Aoi, O. Kanagawa, M. Nakagawa, K. Okita and S. Yamanaka (2009). "Suppression of induced pluripotent stem cell generation by the p53-p21 pathway." Nature **460**(7259): 1132-1135.

Horvath, P. and R. Barrangou (2010). "CRISPR/Cas, the immune system of bacteria and archaea." Science **327**(5962): 167-170.

Ihry, R. J., K. A. Worringer, M. R. Salick, E. Frias, D. Ho, K. Theriault, S. Kommineni, J. Chen, M. Sondey, C. Ye, R. Randhawa, T. Kulkarni, Z. Yang, G. McAllister, C. Russ, J. Reece-Hoyes, W. Forrester, G. R. Hoffman, R. Dolmetsch and A. Kaykas (2018). "p53 inhibits CRISPR-Cas9 engineering in human pluripotent stem cells." Nat Med.

Imbalzano, A. N., H. Kwon, M. R. Green and R. E. Kingston (1994). "Facilitated binding of TATA-binding protein to nucleosomal DNA." Nature **370**(6489): 481-485.

Isakoff, M. S., C. G. Sansam, P. Tamayo, A. Subramanian, J. A. Evans, C. M. Fillmore, X. Wang, J. A. Biegel, S. L. Pomeroy, J. P. Mesirov and C. W. Roberts (2005). "Inactivation of the Snf5 tumor suppressor stimulates cell cycle progression and cooperates with p53 loss in oncogenic transformation." Proc Natl Acad Sci U S A **102**(49): 17745-17750.

Jackson, E. M., A. J. Sievert, X. Gai, H. Hakonarson, A. R. Judkins, L. Tooke, J. C. Perin, H. Xie, T. H. Shaikh and J. A. Biegel (2009). "Genomic analysis using high-density single nucleotide polymorphism-based oligonucleotide arrays and multiplex ligation-dependent probe amplification provides a comprehensive analysis of INI1/SMARCB1 in malignant rhabdoid tumors." Clin Cancer Res **15**(6): 1923-1930.

Jagani, Z., E. L. Mora-Blanco, C. G. Sansam, E. S. McKenna, B. Wilson, D. Chen, J. Klekota, P. Tamayo, P. T. Nguyen, M. Tolstorukov, P. J. Park, Y. J. Cho, K. Hsiao, S. Buonamici, S. L. Pomeroy, J. P. Mesirov, H. Ruffner, T. Bouwmeester, S. J. Luchansky, J. Murtie, J. F. Kelleher, M. Warmuth, W. R. Sellers, C. W. Roberts and M. Dorsch (2010). "Loss of the tumor suppressor Snf5 leads to aberrant activation of the Hedgehog-Gli pathway." Nat Med **16**(12): 1429-1433.

Jang, S. K., H. G. Krausslich, M. J. Nicklin, G. M. Duke, A. C. Palmenberg and E. Wimmer (1988). "A segment of the 5' nontranslated region of encephalomyocarditis virus RNA directs internal entry of ribosomes during in vitro translation." J Virol **62**(8): 2636-2643.

Jensen, J. B. and M. Parmar (2006). "Strengths and limitations of the neurosphere culture system." Mol Neurobiol **34**(3): 153-161.

Jiang, W., R. Hua, M. Wei, C. Li, Z. Qiu, X. Yang and C. Zhang (2015). "An optimized method for high-titer lentivirus preparations without ultracentrifugation." Sci Rep **5**: 13875.

Jinek, M., K. Chylinski, I. Fonfara, M. Hauer, J. A. Doudna and E. Charpentier (2012). "A programmable dual-RNA-guided DNA endonuclease in adaptive bacterial immunity." Science **337**(6096): 816-821.

Johann, P. D. (2020). "Invited Review: Dysregulation of chromatin remodellers in paediatric brain tumours - SMARCB1 and beyond." Neuropathol Appl Neurobiol **46**(1): 57-72.

Johann, P. D., S. Erkek, M. Zapatka, K. Kerl, I. Buchhalter, V. Hovestadt, D. T. Jones, D. Sturm, C. Hermann, M. Segura Wang, A. Korshunov, M. Rhyzova, S. Grobner, S. Brabetz, L. Chavez, S. Bens, S. Groschel, F. Kratochwil, A. Wittmann, L. Sieber, C. Georg, S. Wolf, K. Beck, F. Oyen, D. Capper, P. van Sluis, R. Volckmann, J. Koster, R. Versteeg, A. von Deimling, T. Milde, O. Witt, A. E. Kulozik, M. Ebinger, T. Shalaby, M. Grotzer, D. Sumerauer, J. Zamecnik, J. Mora, N. Jabado, M. D. Taylor, A. Huang, E. Aronica, A. Bertoni, B. Radlwimmer, T. Pietsch, U. Schuller, R. Schneppenheim, P. A. Northcott, J. O. Korbel, R. Siebert, M. C. Fruhwald, P. Lichter, R. Eils, A. Gajjar, M. Hasselblatt, S. M. Pfister and M. Kool (2016). "Atypical Teratoid/Rhabdoid Tumors Are Comprised of Three Epigenetic Subgroups with Distinct Enhancer Landscapes." Cancer Cell **29**(3): 379-393.

Kadoch, C. and G. R. Crabtree (2015). "Mammalian SWI/SNF chromatin remodeling complexes and cancer: Mechanistic insights gained from human genomics." Sci Adv **1**(5): e1500447.

Kadoch, C., D. C. Hargreaves, C. Hodges, L. Elias, L. Ho, J. Ranish and G. R. Crabtree (2013). "Proteomic and bioinformatic analysis of mammalian SWI/SNF complexes identifies extensive roles in human malignancy." Nat Genet **45**(6): 592-601.

Kageyama, R., T. Ohtsuka and T. Kobayashi (2008). "Roles of Hes genes in neural development." Dev Growth Differ **50 Suppl 1**: S97-103.

Kalpana, G. V., S. Marmon, W. Wang, G. R. Crabtree and S. P. Goff (1994). "Binding and stimulation of HIV-1 integrase by a human homolog of yeast transcription factor SNF5." Science **266**(5193): 2002-2006.

Katzen, F. (2007). "Gateway((R)) recombinational cloning: a biological operating system." Expert Opin Drug Discov **2**(4): 571-589.

Kitagawa, M., M. Hojo, I. Imayoshi, M. Goto, M. Ando, T. Ohtsuka, R. Kageyama and S. Miyamoto (2013). "Hes1 and Hes5 regulate vascular remodeling and arterial specification of endothelial cells in brain vascular development." Mech Dev **130**(9-10): 458-466.

Klochendler-Yeivin, A., L. Fiette, J. Barra, C. Muchardt, C. Babinet and M. Yaniv (2000). "The murine SNF5/INI1 chromatin remodeling factor is essential for embryonic development and tumor suppression." EMBO Rep **1**(6): 500-506.

Kordes, U., S. Gesk, M. C. Fruhwald, N. Graf, I. Leuschner, M. Hasselblatt, A. Jeibmann, F. Oyen, O. Peters, T. Pietsch, R. Siebert and R. Schneppenheim (2010). "Clinical and molecular features in patients with atypical teratoid rhabdoid tumor or malignant rhabdoid tumor." Genes Chromosomes Cancer **49**(2): 176-181.

Kosho, T., N. Okamoto and C. Coffin-Siris Syndrome International (2014). "Genotype-phenotype correlation of Coffin-Siris syndrome caused by mutations in SMARCB1, SMARCA4, SMARCE1, and ARID1A." Am J Med Genet C Semin Med Genet **166C**(3): 262-275.

Kwon, H., A. N. Imbalzano, P. A. Khavari, R. E. Kingston and M. R. Green (1994). "Nucleosome disruption and enhancement of activator binding by a human SW1/SNF complex." Nature **370**(6489): 477-481.

Langer, L. F., J. M. Ward and T. K. Archer (2019). "Tumor suppressor SMARCB1 suppresses super-enhancers to govern hESC lineage determination." Elife **8**.

Lee, P. Y., J. Costumbrado, C. Y. Hsu and Y. H. Kim (2012). "Agarose gel electrophoresis for the separation of DNA fragments." J Vis Exp(62).

Lessard, J., J. I. Wu, J. A. Ranish, M. Wan, M. M. Winslow, B. T. Staahl, H. Wu, R. Aebersold, I. A. Graef and G. R. Crabtree (2007). "An essential switch in subunit composition of a chromatin remodeling complex during neural development." Neuron **55**(2): 201-215.

Liang, X., J. Potter, S. Kumar, Y. Zou, R. Quintanilla, M. Sridharan, J. Carte, W. Chen, N. Roark, S. Ranganathan, N. Ravinder and J. D. Chesnut (2015). "Rapid and highly efficient mammalian cell engineering via Cas9 protein transfection." J Biotechnol **208**: 44-53.

Lombardo, A., P. Genovese, C. M. Beausejour, S. Colleoni, Y. L. Lee, K. A. Kim, D. Ando, F. D. Urnov, C. Galli, P. D. Gregory, M. C. Holmes and L. Naldini (2007). "Gene editing in human stem cells using zinc finger nucleases and integrase-defective lentiviral vector delivery." Nat Biotechnol **25**(11): 1298-1306.

Longo, P. A., J. M. Kavran, M. S. Kim and D. J. Leahy (2013). "Transient mammalian cell transfection with polyethylenimine (PEI)." Methods Enzymol **529**: 227-240.

Luke, G. A. and M. D. Ryan (2018). "Using the 2A Protein Coexpression System: Multicistronic 2A Vectors Expressing Gene(s) of Interest and Reporter Proteins." Methods Mol Biol **1755**: 31-48.

Mali, P., K. M. Esvelt and G. M. Church (2013). "Cas9 as a versatile tool for engineering biology." Nat Methods **10**(10): 957-963.

Mali, P., L. Yang, K. M. Esvelt, J. Aach, M. Guell, J. E. DiCarlo, J. E. Norville and G. M. Church (2013). "RNA-guided human genome engineering via Cas9." Science **339**(6121): 823-826.

Marella, N. V., K. S. Malyavantham, J. Wang, S. Matsui, P. Liang and R. Berezney (2009). "Cytogenetic and cDNA microarray expression analysis of MCF10 human breast cancer progression cell lines." Cancer Res **69**(14): 5946-5953.

Masliah-Planchon, J., I. Bieche, J. M. Guinebretiere, F. Bourdeaut and O. Delattre (2015). "SWI/SNF chromatin remodeling and human malignancies." Annu Rev Pathol **10**: 145-171.

McKenna, E. S., C. G. Sansam, Y. J. Cho, H. Greulich, J. A. Evans, C. S. Thom, L. A. Moreau, J. A. Biegel, S. L. Pomeroy and C. W. Roberts (2008). "Loss of the epigenetic tumor suppressor SNF5 leads to cancer without genomic instability." Mol Cell Biol **28**(20): 6223-6233.

Meel, M. H., M. Guillen Navarro, M. C. de Gooijer, D. S. Metselaar, P. Waranecki, M. Breur, T. Lagerweij, L. E. Wedekind, J. Koster, M. D. van de Wetering, N. Schouten-van Meeteren, E. Aronica, O. van Tellingen, M. Bugiani, T. N. Phoenix, G. J. L. Kaspers and E. Hulleman (2020). "MEK/MELK inhibition and blood-brain barrier deficiencies in atypical teratoid/rhabdoid tumors." Neuro Oncol **22**(1): 58-69.

Michel, B. C., A. R. D'Avino, S. H. Cassel, N. Mashtalir, Z. M. McKenzie, M. J. McBride, A. M. Valencia, Q. Zhou, M. Bocker, L. M. M. Soares, J. Pan, D. I. Remillard, C. A. Lareau, H. J. Zullow, N. Fortoul, N. S. Gray, J. E. Bradner, H. M. Chan and C. Kadoch (2018). "A non-canonical SWI/SNF complex is a synthetic lethal target in cancers driven by BAF complex perturbation." Nat Cell Biol **20**(12): 1410-1420.

Middeljans, E., X. Wan, P. W. Jansen, V. Sharma, H. G. Stunnenberg and C. Logie (2012). "SS18 together with animal-specific factors defines human BAF-type SWI/SNF complexes." PLoS One **7**(3): e33834.

Mokry, J. and S. Nemecek (1998). "Angiogenesis of extra- and intraembryonic blood vessels is associated with expression of nestin in endothelial cells." Folia Biol (Praha) **44**(5): 155-161.

Mokry, J. and S. Nemecek (1999). "Cerebral angiogenesis shows nestin expression in endothelial cells." Gen Physiol Biophys **18 Suppl 1**: 25-29.

Moore, J. C., K. Atze, P. L. Yeung, A. J. Toro-Ramos, C. Camarillo, K. Thompson, C. L. Ricupero, M. A. Brenneman, R. I. Cohen and R. P. Hart (2010). "Efficient, high-throughput transfection of human embryonic stem cells." Stem Cell Res Ther **1**(3): 23.

Moreno, N. and K. Kerl (2016). "Preclinical Evaluation of Combined Targeted Approaches in Malignant Rhabdoid Tumors." Anticancer Res **36**(8): 3883-3887.

Morozov, A., E. Yung and G. V. Kalpana (1998). "Structure-function analysis of integrase interactor 1/hSNF5L1 reveals differential properties of two repeat motifs present in the highly conserved region." Proc Natl Acad Sci U S A **95**(3): 1120-1125.

Muchardt, C., C. Sardet, B. Bourachot, C. Onufryk and M. Yaniv (1995). "A human protein with homology to Saccharomyces cerevisiae SNF5 interacts with the potential helicase hbrm." Nucleic Acids Res **23**(7): 1127-1132.

Narayanan, R. and T. C. Tuoc (2014). "Roles of chromatin remodeling BAF complex in neural differentiation and reprogramming." Cell Tissue Res **356**(3): 575-584.

Neigeborn, L. and M. Carlson (1984). "Genes affecting the regulation of SUC2 gene expression by glucose repression in Saccharomyces cerevisiae." Genetics **108**(4): 845-858.

Ng, J. M., D. Martinez, E. D. Marsh, Z. Zhang, E. Rappaport, M. Santi and T. Curran (2015). "Generation of a mouse model of atypical teratoid/rhabdoid tumor of the central nervous system through combined deletion of Snf5 and p53." Cancer Res **75**(21): 4629-4639.

Ohgushi, M., M. Matsumura, M. Eiraku, K. Murakami, T. Aramaki, A. Nishiyama, K. Muguruma, T. Nakano, H. Suga, M. Ueno, T. Ishizaki, H. Suemori, S. Narumiya, H. Niwa and Y. Sasai (2010). "Molecular pathway and cell state responsible for dissociation-induced apoptosis in human pluripotent stem cells." Cell Stem Cell **7**(2): 225-239.

Ostrom, Q. T., P. M. de Blank, C. Kruchko, C. M. Petersen, P. Liao, J. L. Finlay, D. S. Stearns, J. E. Wolff, Y. Wolinsky, J. J. Letterio and J. S. Barnholtz-Sloan (2015). "Alex's Lemonade Stand Foundation Infant and Childhood Primary Brain and Central Nervous System Tumors Diagnosed in the United States in 2007-2011." Neuro Oncol **16 Suppl 10**: x1-x36.

Park, J. H., E. J. Park, H. S. Lee, S. J. Kim, S. K. Hur, A. N. Imbalzano and J. Kwon (2006). "Mammalian SWI/SNF complexes facilitate DNA double-strand break repair by promoting gamma-H2AX induction." EMBO J **25**(17): 3986-3997.

Pastrana, E., V. Silva-Vargas and F. Doetsch (2011). "Eyes wide open: a critical review of sphere-formation as an assay for stem cells." Cell Stem Cell **8**(5): 486-498.

Phelan, M. L., S. Sif, G. J. Narlikar and R. E. Kingston (1999). "Reconstitution of a core chromatin remodeling complex from SWI/SNF subunits." Mol Cell **3**(2): 247-253.

Poli, V., L. Fagnocchi, A. Fasciani, A. Cherubini, S. Mazzoleni, S. Ferrillo, A. Miluzio, G. Gaudioso, V. Vaira, A. Turdo, M. Gaggianesi, A. Chinnici, E. Lipari, S. Bicciato, S. Bosari, M. Todaro and A. Zippo (2018). "Author Correction: MYC-driven epigenetic reprogramming favors the onset of tumorigenesis by inducing a stem cell-like state." Nat Commun **9**(1): 3921.

Potter, H. and R. Heller (2011). "Transfection by electroporation." Curr Protoc Cell Biol **Chapter 20**: Unit20 25.

Ran, F. A., P. D. Hsu, C. Y. Lin, J. S. Gootenberg, S. Konermann, A. E. Trevino, D. A. Scott, A. Inoue, S. Matoba, Y. Zhang and F. Zhang (2013). "Double nicking by RNA-guided CRISPR Cas9 for enhanced genome editing specificity." Cell **154**(6): 1380-1389.

Ran, F. A., P. D. Hsu, J. Wright, V. Agarwala, D. A. Scott and F. Zhang (2013). "Genome engineering using the CRISPR-Cas9 system." Nat Protoc **8**(11): 2281-2308.

Renaud, J. B., C. Boix, M. Charpentier, A. De Cian, J. Cochennec, E. Duvernois-Berthet, L. Perrouault, L. Tesson, J. Edouard, R. Thinard, Y. Cherifi, S. Menoret, S. Fontaniere, N. de Croze, A. Fraichard, F. Sohm, I. Anegon, J. P. Concordet and C. Giovannangeli (2016). "Improved Genome Editing Efficiency and Flexibility Using Modified Oligonucleotides with TALEN and CRISPR-Cas9 Nucleases." Cell Rep **14**(9): 2263-2272.

Roberts, C. W., S. A. Galusha, M. E. McMenamin, C. D. Fletcher and S. H. Orkin (2000). "Haploinsufficiency of Snf5 (integrase interactor 1) predisposes to malignant rhabdoid tumors in mice." Proc Natl Acad Sci U S A **97**(25): 13796-13800.

Roberts, C. W., M. M. Leroux, M. D. Fleming and S. H. Orkin (2002). "Highly penetrant, rapid tumorigenesis through conditional inversion of the tumor suppressor gene Snf5." Cancer Cell **2**(5): 415-425.

Rorke, L. B., R. J. Packer and J. A. Biegel (1996). "Central nervous system atypical teratoid/rhabdoid tumors of infancy and childhood: definition of an entity." J Neurosurg **85**(1): 56-65.

Rousseau-Merck, M. F., I. Versteege, I. Legrand, J. Couturier, A. Mairal, O. Delattre and A. Aurias (1999). "hSNF5/INI1 inactivation is mainly associated with homozygous deletions and mitotic recombinations in rhabdoid tumors." Cancer Res **59**(13): 3152-3156.

Sakuma, T., A. Nishikawa, S. Kume, K. Chayama and T. Yamamoto (2014). "Multiplex genome engineering in human cells using all-in-one CRISPR/Cas9 vector system." Sci Rep **4**: 5400.

Santen, G. W., E. Aten, A. T. Vulto-van Silfhout, C. Pottinger, B. W. van Bon, I. J. van Minderhout, R. Snowdowne, C. A. van der Lans, M. Boogaard, M. M. Linssen, L. Vijfhuizen, M. J. van der Wielen, M. J. Vollebregt, c. Coffin-Siris, M. H. Breuning, M. Kriek, A. van Haeringen, J. T. den Dunnen, A. Hoischen, J. Clayton-Smith, B. B. de Vries, R. C. Hennekam and M. J. van Belzen (2013). "Coffin-Siris syndrome and the BAF complex: genotype-phenotype study in 63 patients." Hum Mutat **34**(11): 1519-1528.

Schrey, D., F. Carceller Lechon, G. Malietzis, L. Moreno, C. Dufour, S. Chi, L. Lafay-Cousin, K. von Hoff, T. Athanasiou, L. V. Marshall and S. Zacharoulis (2016). "Multimodal therapy in children and adolescents with newly diagnosed atypical teratoid rhabdoid tumor: individual pooled data analysis and review of the literature." J Neurooncol **126**(1): 81-90.

Sekeres, M. J., L. Riggs, A. Decker, C. B. de Medeiros, A. Bacopulos, J. Skocic, K. Szulc-Lerch, E. Bouffet, B. Levine, C. L. Grady, D. J. Mabbott, S. A. Josselyn and P. W. Frankland (2018). "Impaired Recent, but Preserved Remote, Autobiographical Memory in Pediatric Brain Tumor Patients." J Neurosci **38**(38): 8251-8261.

Sekiguchi, F., Y. Tsurusaki, N. Okamoto, K. W. Teik, S. Mizuno, H. Suzumura, B. Isidor, W. P. Ong, M. Haniffa, S. M. White, M. Matsuo, K. Saito, S. Phadke, T. Kosho, P. Yap, M. Goyal, L. A. Clarke, R. Sachdev, G. McGillivray, R. J. Leventer, C. Patel, T. Yamagata, H. Osaka, Y. Hisaeda, H. Ohashi, K. Shimizu, K. Nagasaki, J. Hamada, S. Dateki, T. Sato, Y. Chinen, T. Awaya, T. Kato, K. Iwanaga, M. Kawai, T. Matsuoka, Y. Shimoji, T. Y. Tan, S. Kapoor, N. Gregersen, M. Rossi, M. Marie-Laure, L. McGregor, K. Oishi, L. Mehta, G. Gillies, P. J. Lockhart, K. Pope, A. Shukla, K. M. Girisha, G. M. H. Abdel-Salam, D. Mowat, D. Coman, O. H. Kim, M. P. Cordier, K. Gibson, J. Milunsky, J. Liebelt, H. Cox, S. El Chehadeh, A. Toutain, K. Saida, H. Aoi, G. Minase, N. Tsuchida, K. Iwama, Y. Uchiyama, T. Suzuki, K. Hamanaka, Y. Azuma, A. Fujita, E. Imagawa, E. Koshimizu, A. Takata, S. Mitsuhashi, S. Miyatake, T. Mizuguchi, N. Miyake and N. Matsumoto (2019). "Genetic abnormalities in a large cohort of Coffin-Siris syndrome patients." J Hum Genet **64**(12): 1173-1186.

Sevenet, N., E. Sheridan, D. Amram, P. Schneider, R. Handgretinger and O. Delattre (1999). "Constitutional mutations of the hSNF5/INI1 gene predispose to a variety of cancers." Am J Hum Genet **65**(5): 1342-1348.

Shu, T. and L. J. Richards (2001). "Cortical axon guidance by the glial wedge during the development of the corpus callosum." J Neurosci **21**(8): 2749-2758.

Singec, I., R. Knoth, R. P. Meyer, J. Maciaczyk, B. Volk, G. Nikkhah, M. Frotscher and E. Y. Snyder (2006). "Defining the actual sensitivity and specificity of the neurosphere assay in stem cell biology." Nat Methods **3**(10): 801-806.

Singhal, N., J. Graumann, G. Wu, M. J. Arauzo-Bravo, D. W. Han, B. Greber, L. Gentile, M. Mann and H. R. Scholer (2010). "Chromatin-Remodeling Components of the BAF Complex Facilitate Reprogramming." Cell **141**(6): 943-955.

Smith, C., Z. Ye and L. Cheng (2016). "Genome Editing in Human Pluripotent Stem Cells." Cold Spring Harb Protoc **2016**(4): pdb top086819.

Sonawane, N. D., F. C. Szoka, Jr. and A. S. Verkman (2003). "Chloride accumulation and swelling in endosomes enhances DNA transfer by polyamine-DNA polyplexes." J Biol Chem **278**(45): 44826-44831.

Song, F. and K. Stieger (2017). "Optimizing the DNA Donor Template for Homology-Directed Repair of Double-Strand Breaks." Mol Ther Nucleic Acids **7**: 53-60.

Sredni, S. T. and T. Tomita (2015). "Rhabdoid tumor predisposition syndrome." Pediatr Dev Pathol **18**(1): 49-58.

Staahl, B. T., J. Tang, W. Wu, A. Sun, A. D. Gitler, A. S. Yoo and G. R. Crabtree (2013). "Kinetic analysis of npBAF to nBAF switching reveals exchange of SS18 with CREST and integration with neural developmental pathways." J Neurosci **33**(25): 10348-10361.

Stepanenko, A. A. and V. V. Dmitrenko (2015). "HEK293 in cell biology and cancer research: phenotype, karyotype, tumorigenicity, and stress-induced genome-phenotype evolution." Gene **569**(2): 182-190.

Stern, M., R. Jensen and I. Herskowitz (1984). "Five SWI genes are required for expression of the HO gene in yeast." J Mol Biol **178**(4): 853-868.

Stojanova, A., W. B. Tu, R. Ponzielli, M. Kotlyar, P. K. Chan, P. C. Boutros, F. Khosravi, I. Jurisica, B. Raught and L. Z. Penn (2016). "MYC interaction with the tumor suppressive SWI/SNF complex member INI1 regulates transcription and cellular transformation." Cell Cycle **15**(13): 1693-1705.

Strother, D. (2005). "Atypical teratoid rhabdoid tumors of childhood: diagnosis, treatment and challenges." Expert Rev Anticancer Ther **5**(5): 907-915.

Stuchbury, G. and G. Munch (2010). "Optimizing the generation of stable neuronal cell lines via pre-transfection restriction enzyme digestion of plasmid DNA." Cytotechnology **62**(3): 189-194.

Suzuki, S., J. Namiki, S. Shibata, Y. Mastuzaki and H. Okano (2010). "The neural stem/progenitor cell marker nestin is expressed in proliferative endothelial cells, but not in mature vasculature." J Histochem Cytochem **58**(8): 721-730.

Szymczak, A. L. and D. A. Vignali (2005). "Development of 2A peptide-based strategies in the design of multicistronic vectors." Expert Opin Biol Ther **5**(5): 627-638.

Terada, Y., N. Jo, Y. Arakawa, M. Sakakura, Y. Yamada, T. Ukai, M. Kabata, K. Mitsunaga, Y. Mineharu, S. Ohta, M. Nakagawa, S. Miyamoto, T. Yamamoto and Y. Yamada (2019). "Human Pluripotent Stem Cell-Derived Tumor Model Uncovers the Embryonic Stem Cell Signature as a Key Driver in Atypical Teratoid/Rhabdoid Tumor." Cell Rep **26**(10): 2608-2621 e2606.

Torchia, J., B. Golbourn, S. Feng, K. C. Ho, P. Sin-Chan, A. Vasiljevic, J. D. Norman, P. Guilhamon, L. Garzia, N. R. Agamez, M. Lu, T. S. Chan, D. Picard, P. de Antonellis, D. A. Khuong-Quang, A. C. Planello, C. Zeller, D. Barsyte-Lovejoy, L. Lafay-Cousin, L. Letourneau, M. Bourgey, M. Yu, D. M. A. Gendoo, M. Dzamba, M. Barszczyk, T. Medina, A. N. Riemenschneider, A. S. Morrissy, Y. S. Ra, V. Ramaswamy, M. Remke, C. P. Dunham, S. Yip, H. K. Ng, J. Q. Lu, V. Mehta, S. Albrecht, J. Pimentel, J. A. Chan, G. R. Somers, C. C. Faria, L. Roque, M. Fouladi, L. M. Hoffman, A. S. Moore, Y. Wang, S. A. Choi, J. R. Hansford, D. Catchpoole, D. K. Birks, N. K. Foreman, D. Strother, A. Klekner, L. Bognar, M. Garami, P. Hauser, T. Hortobagyi, B. Wilson, J. Hukin, A. S. Carret, T. E. Van Meter, E. I. Hwang, A. Gajjar, S. H. Chiou, H. Nakamura, H. Toledano, I. Fried, D. Fults, T. Wataya, C. Fryer, D. D. Eisenstat, K. Scheinemann, A. J. Fleming, D. L. Johnston, J. Michaud, S. Zelcer, R. Hammond, S. Afzal, D. A. Ramsay, N. Sirachainan, S. Hongeng, N. Larbcharoensub, R. G. Grundy, R. R. Lulla, J. R. Fangusaro, H. Druker, U. Bartels, R. Grant, D. Malkin, C. J. McGlade, T. Nicolaides, T. Tihan, J. Phillips, J. Majewski, A. Montpetit, G. Bourque, G. D. Bader, A. T. Reddy, G. Y. Gillespie, M. Warmuth-Metz, S. Rutkowski, U. Tabori, M. Lupien, M. Brudno, U. Schuller, T. Pietsch, A. R. Judkins, C. E. Hawkins, E. Bouffet, S. K. Kim, P. B. Dirks, M. D. Taylor, A. Erdreich-Epstein, C. H. Arrowsmith, D. D. De Carvalho, J. T. Rutka, N. Jabado and A. Huang (2016). "Integrated (epi)-Genomic Analyses Identify Subgroup-Specific Therapeutic Targets in CNS Rhabdoid Tumors." Cancer Cell **30**(6): 891-908.

Torchia, J., D. Picard, L. Lafay-Cousin, C. E. Hawkins, S. K. Kim, L. Letourneau, Y. S. Ra, K. C. Ho, T. S. Chan, P. Sin-Chan, C. P. Dunham, S. Yip, H. K. Ng, J. Q. Lu, S. Albrecht, J. Pimentel, J. A. Chan, G. R. Somers, M. Zielenska, C. C. Faria, L. Roque, B. Baskin, D. Birks, N. Foreman, D. Strother, A. Klekner, M. Garami, P. Hauser, T. Hortobagyi, L. Bognar, B. Wilson, J. Hukin, A. S. Carret, T. E. Van Meter, H. Nakamura, H. Toledano, I. Fried, D. Fults, T. Wataya, C. Fryer, D. D. Eisenstat, K. Scheineman, D. Johnston, J. Michaud, S. Zelcer, R. Hammond, D. A. Ramsay, A. J. Fleming, R. R. Lulla, J. R. Fangusaro, N. Sirachainan, N. Larbcharoensub, S. Hongeng, M. A. Barakzai, A. Montpetit, D. Stephens, R. G. Grundy, U. Schuller, T. Nicolaides, T. Tihan, J. Phillips, M. D. Taylor, J. T. Rutka, P. Dirks, G. D. Bader, M. Warmuth-Metz, S. Rutkowski, T. Pietsch, A. R. Judkins, N. Jabado, E. Bouffet and A. Huang (2015). "Molecular subgroups of atypical teratoid rhabdoid tumours in children: an integrated genomic and clinicopathological analysis." Lancet Oncol **16**(5): 569-582.

Trichas, G., J. Begbie and S. Srinivas (2008). "Use of the viral 2A peptide for bicistronic expression in transgenic mice." BMC Biol **6**: 40.

Tsurusaki, Y., N. Okamoto, H. Ohashi, T. Kosho, Y. Imai, Y. Hibi-Ko, T. Kaname, K. Naritomi, H. Kawame, K. Wakui, Y. Fukushima, T. Homma, M. Kato, Y. Hiraki, T. Yamagata, S. Yano, S. Mizuno, S. Sakazume, T. Ishii, T. Nagai, M. Shiina, K. Ogata, T. Ohta, N. Niikawa, S. Miyatake, I. Okada, T. Mizuguchi, H. Doi, H. Saitsu, N. Miyake and N. Matsumoto (2012). "Mutations affecting components of the SWI/SNF complex cause Coffin-Siris syndrome." Nat Genet **44**(4): 376-378.

Tsurusaki, Y., N. Okamoto, H. Ohashi, S. Mizuno, N. Matsumoto, Y. Makita, M. Fukuda, B. Isidor, J. Perrier, S. Aggarwal, A. B. Dalal, A. Al-Kindy, J. Liebelt, D. Mowat, M. Nakashima, H. Saitsu, N. Miyake and N. Matsumoto (2014). "Coffin-Siris syndrome is a SWI/SNF complex disorder." Clin Genet **85**(6): 548-554.

Valencia, A. M., C. K. Collings, H. T. Dao, R. St Pierre, Y. C. Cheng, J. Huang, Z. Y. Sun, H. S. Seo, N. Mashtalir, D. E. Comstock, O. Bolonduro, N. E. Vangos, Z. C. Yeoh, M. K. Dornon, C. Hermawan, L. Barrett, S. Dhe-Paganon, C. J. Woolf, T. W. Muir and C. Kadoch (2019). "Recurrent SMARCB1 Mutations Reveal a Nucleosome Acidic Patch Interaction Site That Potentiates mSWI/SNF Complex Chromatin Remodeling." Cell **179**(6): 1342-1356 e1323.

Versteege, I., S. Medjkane, D. Rouillard and O. Delattre (2002). "A key role of the hSNF5/INI1 tumour suppressor in the control of the G1-S transition of the cell cycle." Oncogene **21**(42): 6403-6412.

Versteege, I., N. Sevenet, J. Lange, M. F. Rousseau-Merck, P. Ambros, R. Handgretinger, A. Aurias and O. Delattre (1998). "Truncating mutations of hSNF5/INI1 in aggressive paediatric cancer." Nature **394**(6689): 203-206.

Vitte, J., F. Gao, G. Coppola, A. R. Judkins and M. Giovannini (2017). "Timing of Smarcb1 and Nf2 inactivation determines schwannoma versus rhabdoid tumor development." Nat Commun **8**(1): 300.

Vladoiu, M. C., I. El-Hamamy, L. K. Donovan, H. Farooq, B. L. Holgado, Y. Sundaravadanam, V. Ramaswamy, L. D. Hendrikse, S. Kumar, S. C. Mack, J. J. Y. Lee, V. Fong, K. Juraschka, D. Przelicki, A. Michealraj, P. Skowron, B. Luu, H. Suzuki, A. S. Morrissy, F. M. G. Cavalli, L. Garzia, C. Daniels, X. Wu, M. A. Qazi, S. K. Singh, J. A. Chan, M. A. Marra, D. Malkin, P. Dirks, L. Heisler, T. Pugh, K. Ng, F. Notta, E. M. Thompson, C. L. Kleinman, A. L. Joyner, N. Jabado, L. Stein and M. D. Taylor (2019). "Childhood cerebellar tumours mirror conserved fetal transcriptional programs." Nature **572**(7767): 67-73.

Wang, W., J. Cote, Y. Xue, S. Zhou, P. A. Khavari, S. R. Biggar, C. Muchardt, G. V. Kalpana, S. P. Goff, M. Yaniv, J. L. Workman and G. R. Crabtree (1996). "Purification and biochemical heterogeneity of the mammalian SWI-SNF complex." EMBO J **15**(19): 5370-5382.

Wang, W., Y. Xue, S. Zhou, A. Kuo, B. R. Cairns and G. R. Crabtree (1996). "Diversity and specialization of mammalian SWI/SNF complexes." Genes Dev **10**(17): 2117-2130.

Wang, X., J. R. Haswell and C. W. Roberts (2014). "Molecular pathways: SWI/SNF (BAF) complexes are frequently mutated in cancer--mechanisms and potential therapeutic insights." Clin Cancer Res **20**(1): 21-27.

Wang, X., S. Wang, E. C. Troisi, T. P. Howard, J. R. Haswell, B. K. Wolf, W. H. Hawk, P. Ramos, E. M. Oberlick, E. P. Tzvetkov, F. Vazquez, W. C. Hahn, P. J. Park and C. W. M. Roberts (2019). "BRD9 defines a SWI/SNF sub-complex and constitutes a specific vulnerability in malignant rhabdoid tumors." Nat Commun **10**(1): 1881.

Wei, D., D. Goldfarb, S. Song, C. Cannon, F. Yan, D. Sakellariou-Thompson, M. Emanuele, M. B. Major, B. E. Weissman and Y. Kuwahara (2014). "SNF5/INI1 deficiency redefines chromatin remodeling complex composition during tumor development." Mol Cancer Res **12**(11): 1574-1585.

Wieczorek, D., N. Bogershausen, F. Beleggia, S. Steiner-Haldenstatt, E. Pohl, Y. Li, E. Milz, M. Martin, H. Thiele, J. Altmuller, Y. Alanay, H. Kayserili, L. Klein-Hitpass, S. Bohringer, A. Wollstein, B. Albrecht, K. Boduroglu, A. Caliebe, K. Chrzanowska, O. Cogulu, F. Cristofoli, J. C. Czeschik, K. Devriendt, M. T. Dotti, N. Elcioglu, B. Gener, T. O. Goecke, M. Krajewska-Walasek, E. Guillen-Navarro, J. Hayek, G. Houge, E. Kilic, P. O. Simsek-Kiper, V. Lopez-Gonzalez, A. Kuechler, S. Lyonnet, F. Mari, A. Marozza, M. Mathieu Dramard, B. Mikat, G. Morin, F. Morice-Picard, F. Ozkinay, A. Rauch, A. Renieri, S. Tinschert, G. E. Utine, C. Vilain, R. Vivarelli, C. Zweier, P. Nurnberg, S. Rahmann, J. Vermeesch, H. J. Ludecke, M. Zeschnigk and B. Wollnik (2013). "A comprehensive molecular study on Coffin-Siris and Nicolaides-Baraitser syndromes identifies a broad molecular and clinical spectrum converging on altered chromatin remodeling." Hum Mol Genet **22**(25): 5121-5135.

Wiedenheft, B., S. H. Sternberg and J. A. Doudna (2012). "RNA-guided genetic silencing systems in bacteria and archaea." Nature **482**(7385): 331-338.

Wilson, B. G. and C. W. Roberts (2011). "SWI/SNF nucleosome remodellers and cancer." Nat Rev Cancer **11**(7): 481-492.

Wilson, B. G., X. Wang, X. Shen, E. S. McKenna, M. E. Lemieux, Y. J. Cho, E. C. Koellhoffer, S. L. Pomeroy, S. H. Orkin and C. W. Roberts (2010). "Epigenetic antagonism between polycomb and SWI/SNF complexes during oncogenic transformation." Cancer Cell **18**(4): 316-328.

Wong, D. J., H. Liu, T. W. Ridky, D. Cassarino, E. Segal and H. Y. Chang (2008). "Module map of stem cell genes guides creation of epithelial cancer stem cells." Cell Stem Cell **2**(4): 333-344.

Wu, J. I., J. Lessard and G. R. Crabtree (2009). "Understanding the words of chromatin regulation." Cell **136**(2): 200-206.

Xu, X., D. Gao, P. Wang, J. Chen, J. Ruan, J. Xu and X. Xia (2018). "Efficient homology-directed gene editing by CRISPR/Cas9 in human stem and primary cells using tube electroporation." Sci Rep **8**(1): 11649.

Xue, Y., J. C. Canman, C. S. Lee, Z. Nie, D. Yang, G. T. Moreno, M. K. Young, E. D. Salmon and W. Wang (2000). "The human SWI/SNF-B chromatin-remodeling complex is related to yeast rsc and localizes at kinetochores of mitotic chromosomes." Proc Natl Acad Sci U S A **97**(24): 13015-13020.

Yen, J., L. Yin and J. Cheng (2014). "Enhanced Non-Viral Gene Delivery to Human Embryonic Stem Cells via Small Molecule-Mediated Transient Alteration of Cell Structure." J Mater Chem B **2**(46): 8098-8105.

Yu, C., Y. Liu, T. Ma, K. Liu, S. Xu, Y. Zhang, H. Liu, M. La Russa, M. Xie, S. Ding and L. S. Qi (2015). "Small molecules enhance CRISPR genome editing in pluripotent stem cells." Cell Stem Cell **16**(2): 142-147.

Yu, X., X. Liang, H. Xie, S. Kumar, N. Ravinder, J. Potter, X. de Mollerat du Jeu and J. D. Chesnut (2016). "Improved delivery of Cas9 protein/gRNA complexes using lipofectamine CRISPRMAX." Biotechnol Lett **38**(6): 919-929.

Zhang, J. H., P. Adikaram, M. Pandey, A. Genis and W. F. Simonds (2016). "Optimization of genome editing through CRISPR-Cas9 engineering." Bioengineered **7**(3): 166-174.

Zhang, J. P., X. L. Li, G. H. Li, W. Chen, C. Arakaki, G. D. Botimer, D. Baylink, L. Zhang, W. Wen, Y. W. Fu, J. Xu, N. Chun, W. Yuan, T. Cheng and X. B. Zhang (2017). "Efficient precise knockin with a double cut HDR donor after CRISPR/Cas9-mediated double-stranded DNA cleavage." Genome Biol **18**(1): 35.

Zhang, J. Z., V. Termglinchan, N. Y. Shao, I. Itzhaki, C. Liu, N. Ma, L. Tian, V. Y. Wang, A. C. Y. Chang, H. Guo, T. Kitani, H. Wu, C. K. Lam, K. Kodo, N. Sayed, H. M. Blau and J. C. Wu (2019). "A Human iPSC Double-Reporter System Enables Purification of Cardiac Lineage Subpopulations with Distinct Function and Drug Response Profiles." Cell Stem Cell.

Zhang, X., B. Li, W. Li, L. Ma, D. Zheng, L. Li, W. Yang, M. Chu, W. Chen, R. B. Mailman, J. Zhu, G. Fan, T. K. Archer and Y. Wang (2014). "Transcriptional repression by the BRG1-SWI/SNF complex affects the pluripotency of human embryonic stem cells." Stem Cell Reports **3**(3): 460-474.

Zhang, Y., X. Ge, F. Yang, L. Zhang, J. Zheng, X. Tan, Z. B. Jin, J. Qu and F. Gu (2014). "Comparison of non-canonical PAMs for CRISPR/Cas9-mediated DNA cleavage in human cells." Sci Rep **4**: 5405.

Zheng, T., Y. Hou, P. Zhang, Z. Zhang, Y. Xu, L. Zhang, L. Niu, Y. Yang, D. Liang, F. Yi, W. Peng, W. Feng, Y. Yang, J. Chen, Y. Y. Zhu, L. H. Zhang and Q. Du (2017). "Profiling single-guide RNA specificity reveals a mismatch sensitive core sequence." Sci Rep **7**: 40638.

7. Appendix

7.1. Materials

7.1.1. List of oligonucleotides

Table 46 contains all oligonucleotides and the respective annealing temperatures used for cloning or RT-qPCR. The primer numbers refer to the numbers the primers were given in the primer database of the Stem Cell and Developmental Biology group at the Technical University of Darmstadt.

Table 46: List of oligonucleotides used for cloning or RT-qPCR analyses in this thesis. $T_{Annealing}$ indicated the temperature used in the annealing step of PCR. Temperatures linked by "+" indicate the use of a 2-cycle PCR, "or" indicates if more than one annealing temperature can be used for PCR. The numbers refer to the identification numbers the primers were given in the primer database of the Stem Cell and Developmental Biology group at the Technical University of Darmstadt.

#	NAME	SEQUENCE 5'→3'	$T_{ANNEALING}$
299	CSS us BssSaI Fwd	tttttCACGAGGTACCCCTGGCCCTGTG	56° C
300	gRNA C3- FWD	CACCGATCATTGCGGCGGCAGAGGC	-
301	gRNA C3- REV	AAACGCCTCTGCCGCCGCAATGATC	-
302	gRNA C3+ FWD	CACCGTGGCGCTGAGCAAGACCTTC	-
303	gRNA C3+ REV	AAACGAAGGTCTTGCTCAGCGCCAC	-
305	sgRNA_D1+_Fwr	CACCGACGGAGCATCTCAGAAGATT	-
306	sgRNA_D1+_Rev	AAACAATCTTCTGAGATGCTCCGTC	-
307	sgRNA_D1/2-_Fwr	CACCGTTACCAGGCCGGGGCCGTGT	-
308	sgRNA_D1/2-_Rev	AAACACACGGCCCCGGCCTGGTAAC	-
309	sgRNA_D2+_Fwr	CACCGCCATCAGCACACGGCTCCCA	-
310	sgRNA_D2+_Rev	AAACTGGGAGCCGTGTGCTGATGGC	-
311	sgRNA_D3+_Fwr	CACCGTAACCAGCCCATCAGCACA	-
312	sgRNA_D3+_Rev	AAACTGTGCTGATGGGCTGGTTAC	-
313	sgRNA_D3-_Fwr	CACCGGCAAGACGCCTCATCCGCC	-
314	sgRNA_D3-_Rev	AAACGGCGGATGAGGCGTCTTGCC	-
315	Upstream-hArm_Fwr *	tttttTATAAGAGCCTAGGGAGAGCCAAGT	59° C
316	Upstream_hArm_Rev **	tttttTGTACACCAGGCCGGGGCCGTGTT	56° C
317	Downstream-hArm_Fwr *	tttttCCTCGAGCCAGCCCATCAGCACACG	60° C
318	Downstream-hArm_Rev	CATGTGAATTCTTCATTGCCGAGGTTCCTAC	60° C
666	Multiplex CRISPR Step2 Fwr	GCCTTTTGCTGGCCTTTTGCTC	61° C
667	Multiplex CRISPR step2 Rev	CGGGCCATTTACCGTAAGTTATGTAACG	61° C
668	mTagBFP AvrII Fwr	ttttTCCTAGGATGAGCGAGCTGATTAAGGAGA	56 + 72° C
669	mTagBFP ClaI Rev	ttttTATCGATTTAATTAAGCTTGTGCCCCAGT	59 or 56 + 72° C
743	FWD_T2A opti HDR Acc65I AvrII	GTACCGGAAGCGGAGAGGGCAGAGGAAGTCT GCTGACATGCGGTGACGTGGAGGAGAATCCT GGAC	-
744	REV_T2A opti HDR Acc65I AvrII	CTAGGTCCAGGATTCTCCTCCACGTCACCGCA TGTCAGCAGACTTCCTCTGCCCTCTCCGCTTC CG	-

745	FWD_T2A opti pX330A BbvCIAvrII	TGAGGGAAGCGGAGAGGGCAGAGGAAGTCT GCTGACATGCGGTGACGTGGAGGAGAATCCT GGAC	-
746	REV_T2A opti pX330A BbvCIAvrII	CTAGGTCCAGGATTCTCCTCCACGTCACCGCA TGTCAGCAGACTTCCTCTGCCCTCTCCGCTTC CC	-
787	DsRed-AvrII-fwd	TATTCCTAGGATGGCCTCCTCCGAGG	54° C
801	dsRedExpress ClaI REV	ttttttATCGATCTAGAGCGGCCGCTTCAG	54 or 50 + 60° C
887	HL PAM mut rev (Ihry, Worringer et al.)	TATTGTCGACTTACCAGGCCGGGGCCGTGTT CGCAAGACGCCTCATCCGCCTGTAAGA	59° C
888	HR PAM mut fwd (EcoRI)	TATTGAATTCCAGCCCATCAGCACACGTCTCC CACGTAGCATCTCAGAAGATTGGTCCGCC	59° C
889	HR rev (XbaI)	TATTTCTAGATTCATTGCCGAGGTTCCTACC	59° C
890	IRES SalI fwd	TATTGTCGACTAACCCCTCTCCCTCC	50 or 58 + 60° C
891	IRES NcoI rev	TATTCCATGGTTGTGGCCATATTATCATCG	58° C
892	GFPZeoR-loxP NcoI fwd	TATTCCATGGTGAGCAAGGGC	52° C
893	GFPZeoR-loxP HindIII rev	TATTAAGCTTATAACTTCGTATAATGTATGC	52° C
928	HL_PsiI_Fwd	tttttTATAAGAGCCTAGGGAGAGCCAAGTGGA GGTGCCC	65° C
929	HL_CSS_us_BssSaI_Rev	tttttTCTCGTGTTCCTGTCCTGGTCGCGGATCT TCTCCATC	65° C
978	PspXI-loxP-ClaI FWD	TCGAGGATAACTTCGTATAGCATACATTATAC GAAGTTATAT	-
979	PspXI-loxP-ClaI REV	CGATATAACTTCGTATAATGTATGCTATACGA AGTTATCC	-
980	ClaI GFP::ZeoR FWD	tttttATCGATATGGTGAGCAAGGGC	50 + 57° C
981	GFP::ZeoR NcoI REV	tttttCCATGGTTCAGTCCGCTCCTC	50 + 57° C
982	NcoI-GSGT2A-EcoRI FWD	CATGGGGAAGCGGAGAGGGCAGAGGAAGTCT GCTGACATGCGGTGACGTGGAGGAGAATCCT GGACCTG	-
983	NcoI-GSGT2A-EcoRI REV	AATTCAGGTCCAGGATTCTCCTCCACGTCACC GCATGTCAGCAGACTTCCTCTGCCCTCTCCGC TTCCC	-
984	E1 HDR HL fwd_new	TAAGAGAGGCAGGGTCTCCCTTTGTTGCCCA GGCTGCAG	71.5° C
985	PspXI E1 HDR HL rev	tttttCCTCGAGGTGCGGCGGCAGAGGCGGTCG GCC	71.5° C
987	EcoRI E1 HDR HR fwd	tttttGAATTCATGATGATGATGGCGCTGAGCAA GACCTTCGGTCAGAAGC	66° C
988	PciI E1 HDR HR rev	tttttACATGTCTCATCCATGGGACTCAGTGTGA CCATCTTGAGGC	66° C
1034	hTBP-fw1	CTTGTGCTCACCCACCAAC	54-58° C
1035	hTBP-rev2	CTGCTCTGACTTTAGCACCTG	54-58° C
1062	ClaI mCardinal FWD	tttttATCGATATGGTGAGCAAGGGCGAGG	54 + 61° C
1063	mCardinal NcoI REV	ttttCCATGGttcCTTGTACAGCTCGTCC	54 + 61° C
1064	mCardinal ClaI REV	tttttATCGATttaCTTGTACAGCTCGTCCATGCC	58 + 60° C
1104	ClaI mKate2 fwd	tttttATCGATATGGTGAGCGAGCTGATTAAGG	57 + 59° C
1105	NcoI mKate2 rev	ttttCCATGGTCTGTGCCCCAGTTTGCTAG	57 + 59° C
1106	NcoI mKate2 fwd	ttttCCATGGATGGTGAGCGAGCTGATTAAGG	57 + 61° C

1107	ClaI mKate2 rev	tttttATCGATTCATCTGTGCCCCAGTTTGCTAG	57 + 61° C
1123	Hes1_fw_e3	TGTGAAGCACCTCCGGAAC	60° C
1124	Hes1_rev_e4	TCACCTCGTTCATGCACTC	54 or 60° C
1137	NcoI mKate2 fwd_corr	ttttCCATGGTGAGCGAGCTGATTAAGG	60° C
1139	hHES1 fwd_4 (Weng et al, e2/3)	TGAAGAAAGATAGCTCGCGGC	54° C
1205	Hes5 fwd_2	GCCCCAAAGAGAAAAACCGAC	58° C
1206	Hes5 rev_2	GACGAAGGCTTTGCTGTGCT	58° C
1207	TagBFP2 ClaI fwd	ttttATCGATATGGTGTCTAAGGGCGAAGAG	59° C
1208	TagBFP2 NcoI rev	tttCCATGGATTAAGCTTGTGCCCCA	54 + 60° C
1268	mHes5 fwd	GAGAAAAACCGACTGCGGAAGCC	60° C
1269	mHes5 rev	GGCGAAGGCTTTGCTGTGTTTC	60° C
1285	IRES PspXI fwd	ttttttACtcgagCCCCTCTCCCTCC	50 + 61° C
1306	Nes fwd_3	GAACAGAGATTGGAAGGCCGC	60° C
1307	Nes rev_3	CTTCTCCTGCTCCAGGGCTTC	60° C
1308	mKate2 XbaI rev	ttttttttCTAGATCATCTGTGCCCCAGTTTGCTAG	50 + 61° C
1309	ATRT 1148delC SalI rev	ttttGTCGACTTACCAGGCCGGGCCGTG	59° C
1314	E1 c.93GC HR rev	CCCGGGCTACgTCGGAGCCGATC	59° C
1315	E1 c.93GC HR fwd	GATCGGCTCCGAcGTAGCCCGGG	59° C
1381	E1 HR *c.20_43delins T* rev new	CTGGAACTTCACaTCAGCGCCATCATCATCATG	59° C
1435	GSG-P2A Acc65I AvrII fwd	GTACCGGAAGCGGAGCTACTAACTTCAGCCTGCTGAAGCAGGCTGGAGACGTGGAGGAGAACCCTGGAC	-
1436	GSG-P2A Acc66I AvrII rev	CTAGGTCCAGGGTTCTCCTCCACGTCTCCAGCCTGCTTCAGCAGGCTGAAGTTAGTAGCTCCGCTTCCG	-
1437	PuroR ClaI fwd	ttttATCGATATGACCGAGTACAAGCCCACGGTGCGCC	66° C
1438	PuroR Acc65I rev	tttttGGTACCGGCACCGGGCTTGCGGG	66° C
1439	TagBFP2 AvrII fwd	tttCCTAGGATGGTGTCTAAGGGCGAAG	54 + 60° C
1440	BSD EcoRI fwd	ttttGAATTCATGGCCAAGCCTTTGTC	54 + 56° C
1441	BSD EcoRI rev	ttttGAATTCTAGACCCGGGATAACTTC	54 + 56° C
1479	p53 NheI fwd	tttgctagcATGACTGCCATGGAGGAGTC	50 + 60° C
1480	p53DD rev	GGCAGCGCTCTCTTGAGGCTGATATCCG	50 + 60° C
1481	p53DD fwd	CGGATATCAGCCTCAAGAGAGCGCTGCC	50 + 60° C
1482	p53 NotI rev	tttGCGGCCGCGTGAAGTCATAAGACAGCAAG	50 + 60° C

7.1.2. List of restriction endonucleases

Table 47 contains the NEB restrictions endonucleases used for cloning in this thesis, including their concentration, optimal reaction buffer, reaction temperature, and if applicable inactivation conditions.

Table 47: Restriction Endonucleases used for cloning in this thesis. Conc., U/mL abbreviates the concentration of the enzyme in Units per millilitre; Temp. abbreviates the required incubation temperature for efficient restriction endonuclease cleavage.

Enzyme	Recognition sequence	Conc., U/mL	Reaction buffer	Temp.	Inactivation conditions
Acc65I	5'...GGTACC...3' 3'...CCATGG...5'	10.000	NEB 3.1	37° C	20 minutes at 65° C
AgeI-HF	5'...ACCGGT...3' 3'...TGGCCA...5'	20.000	CutSmart	37° C	20 minutes at 65° C
AvrII	5'...CCTAGG...3' 3'...GGATCC...5'	5.000	CutSmart	37° C	-
BamHI-HF	5'...GGATCC...3' 3'...CCTAGG...5'	20.000	CutSmart	37° C	-
BbsI-HF	5'...GAAGAC(N)$_2$...3' 3'...CTTCTG(N)$_6$...5'	20.000	CutSmart	37° C	20 minutes at 65° C
BbvCI	5'...CCTCAGC...3' 3'...GGAGTCG...5'	2.000	CutSmart	37° C	-
BsaI-HF	5'...GGTCTC(N)$_1$...3' 3'...CCAGAG(N)$_5$...5'	20.000	CutSmart	37° C	20 minutes at 65° C
BsrGI-HF	5'...TGTACA...3' 3'...ACATGT...5'	20.000	CutSmart	37° C	20 minutes at 80° C
BssSαI	5'...CACGAG...3' 3'...GTGCTC...5'	10.000	CutSmart	37° C	-
BstBI	5'...TTCGAA...3' 3'...AAGCTT...5'	20.000	CutSmart	65° C	-
ClaI	5'...ATCGAT...3' 3'...TAGCTA...5'	10.000	CutSmart	37° C	20 minutes at 65° C
EcoRI-HF	5'...GAATTC...3' 3'...CTTGGA...5'	20.000	CutSmart	37° C	20 minutes at 65° C
EcoRV-HF	5'...GATATC...3' 3'...CTATAG...5'	20.000	CutSmart	37° C	20 minutes at 65° C
HindIII-HF	5'...AAGCTT...3' 3'...TTCGAA...5'	20.000	CutSmart	37° C	20 minutes at 80° C
NcoI-HF	5'...CCATGG...3' 3'...GGTACC...5'	20.000	CutSmart	37° C	20 minutes at 80° C
NdeI	5'...CATATG...3' 3'...GTATAC...5'	20.000	CutSmart	37° C	20 minutes at 65° C
NheI-HF	5'...GCTAGC...3' 3'...CGATCG...5'	20.000	CutSmart	37° C	20 minutes at 80° C
NotI-HF	5'...GCGGCCGC...3' 3'...CGCCGGCG...5'	20.000	CutSmart	37° C	20 minutes at 65° C
PacI	5'...TTAATTAA...3' 3'...AATTAATT...5'	10.000	CutSmart	37° C	20 minutes at 65° C
PciI	5'...ACATGT...3' 3'...TGTACA...5'	10.000	NEB 3.1	37° C	20 minutes at 80° C
PsiI-v2	5'...TTATAA...3' 3'...AATATT...5'	10.000	CutSmart	37° C	20 minutes at 65° C
PspXI	5'...VCTCGACB...3' 3'...BGAGCTCV...5'	5.000	CutSmart	37° C	-
SalI-HF	5'...GTCGAC...3' 3'...CAGCTG...5'	20.000	CutSmart	37° C	20 minutes at 65° C
SmaI	5'...CCCGGG...3' 3'...GGGCCC...5'	20.000	CutSmart	25° C	20 minutes at 65° C
XbaI	5'...TCTAGA...3' 3'...AGATCT...5'	20.000	CutSmart	37° C	20 minutes at 65° C
XhoI	5'...CTCGAG...3' 3'...GAGCTC...5'	20.000	CutSmart	37° C	20 minutes at 65° C

7.1.3. Guide RNA positioning within the genomic sequence of *SMARCB1*

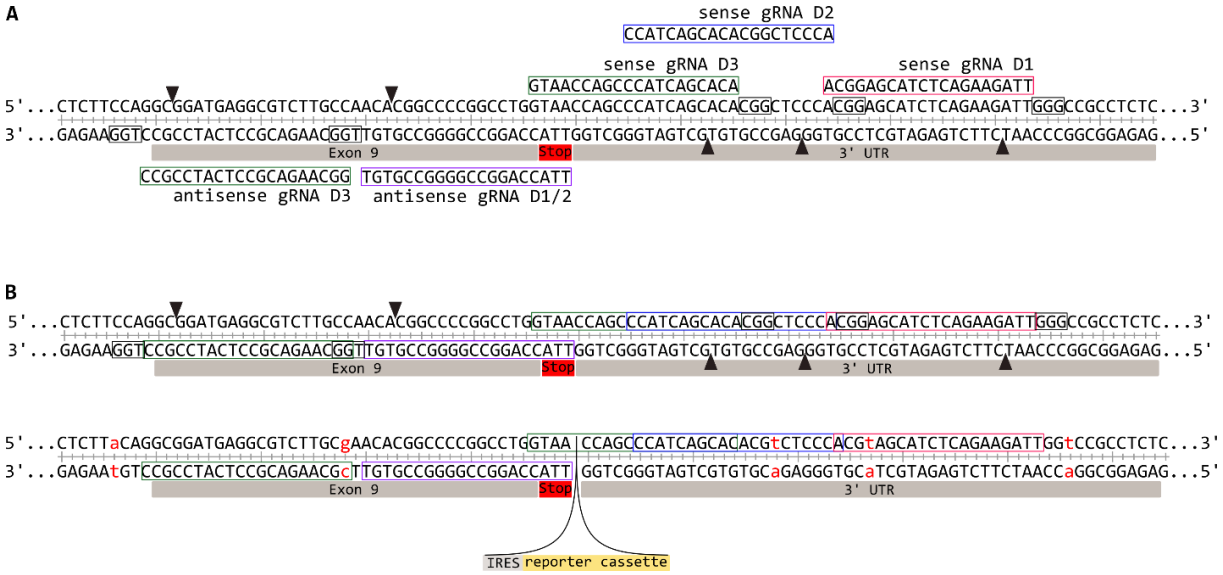

Figure 31: Schematic overview of the positioning of the gRNA pairs selected to target the sequences adjacent to the stop codon of the *SMARCB1* gene. **(A)** gRNA and complementary genomic sequences as well as the corresponding protospacer adjacent motifs (PAM, black boxes), and Cas9 cleavage site (black arrow heads) are depicted on the genomic sequence of exon 9 and the 3' UTR of the *SMARCB1* gene. **(B)** Indication of the gRNA sequences in the genomic sequence of *SMARCB1* and the silent point mutations of the PAM sites included in the HDR construct and inserted following CRISPR/Cas9-mediated genome engineering of the *SMARCB1* gene (red letters).

Figure 32: Schematic overview of the positioning of the gRNA pair selected to target the sequences adjacent to the start codon of the *SMARCB1* gene. **(A)** gRNA and complementary genomic sequences as well as the corresponding protospacer adjacent motifs (PAM, black boxes), and Cas9 cleavage site (black arrow heads) are depicted on the genomic sequence of the 5' UTR and exon 1 of the *SMARCB1* gene. **(B)** Indication of the gRNA sequences in the genomic sequence of *SMARCB1* and the silent point mutations of the PAM sites included in the HDR construct and inserted following CRISPR/Cas9-mediated genome engineering of the *SMARCB1* gene (red letters)

7.1.4. Graphical overview of all constructs generated for the CRISPR/Cas9-mediated genome engineering of the human *SMARCB1* locus

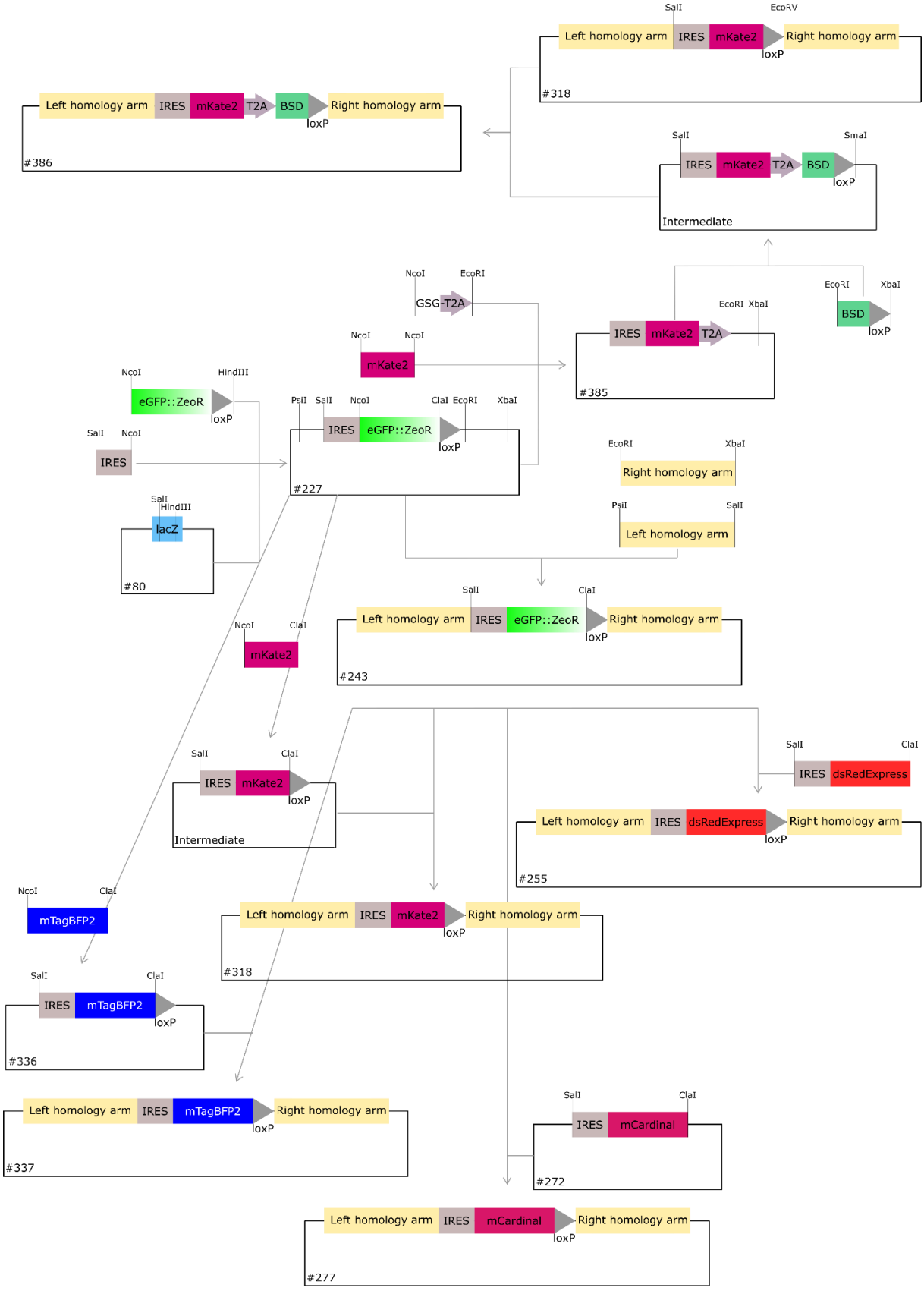

Figure 33: Genealogy of HDR constructs cloned to insert an IRES-fluorescent reporter cassette downstream of exon 9 of the *SMARCB1* gene. The first intermediate plasmid #227 was generated by combining PCR amplified IRES2 sequence (from plasmid #128 using primers #890 and #891) and eGFP::ZeoR-loxP cassette (from plasmid #83 using primers #892 and #893) via SalI, NcoI, and HindIII restriction endonuclease recognition sites in plasmid #80. The sequences homologous to the genomic DNA sequences up- and downstream of the Stop codon of the *SMARCB1* gene were amplified from gDNA of hiPSC#33 using primers #315 and #887 (left homology arm), #888 and #889 (right homology arm). Cloning via PsiI and SalI (left homology arm) or EcoRI and XbaI (right homology arm) generated the *SMARCB1* e9 HDR construct #243. Plasmid #243 served as the starting point to exchange the reporter cassette for different fluorophores. An IRES-dsRedExpress2 cassette was amplified from plasmid #128 (primers #890 and #801) and cloned into #243 via SalI and ClaI restriction endonuclease recognition sites resulting in plasmid #254. The IRES-mCardinal cassette was amplified from plasmid #272 (primers #890 and #1064) and cloned into #243 via SalI and ClaI. The exchange of eGFP::ZeoR for mKate2 was achieved by PCR amplifying the mKate2 sequence from plasmid #311 (primers #1106 and #1107), and cloning it into plasmid #227 to obtain an intermediate. The IRES-mKate2 cassette was then cut from the intermediate via SalI and ClaI and cloned into #243 to generate plasmid #318. Addition of a blasticidin resistance cassette (BSD) was accomplished by first cloning mKate2 (PCR amplification, primers #1105 and #110) and a downstream T2A sequence (oligonucleotides #982 and #983) via NcoI and EcoRI into plasmid #227 resulting in plasmid #385. Secondly, the BSD-loxP cassette was amplified from plasmid #355 (primers #1440 and #1441) and cloned into intermediate #385 via EcoRI and XbaI. Finally, the complete selectable reporter cassette of IRES-mKate2-T2A-BSD-loxP was cloned into plasmid #318 via SalI and EcoRV/SmaI. The left homology arm covers the sequence of the NCBI reference genome NG_009303.1 positions 50,538 to 52,218. The right homology arm covers the sequence of NCBI reference genome NG_009303.1 positions 52,219 to 53,787, directly adjacent.

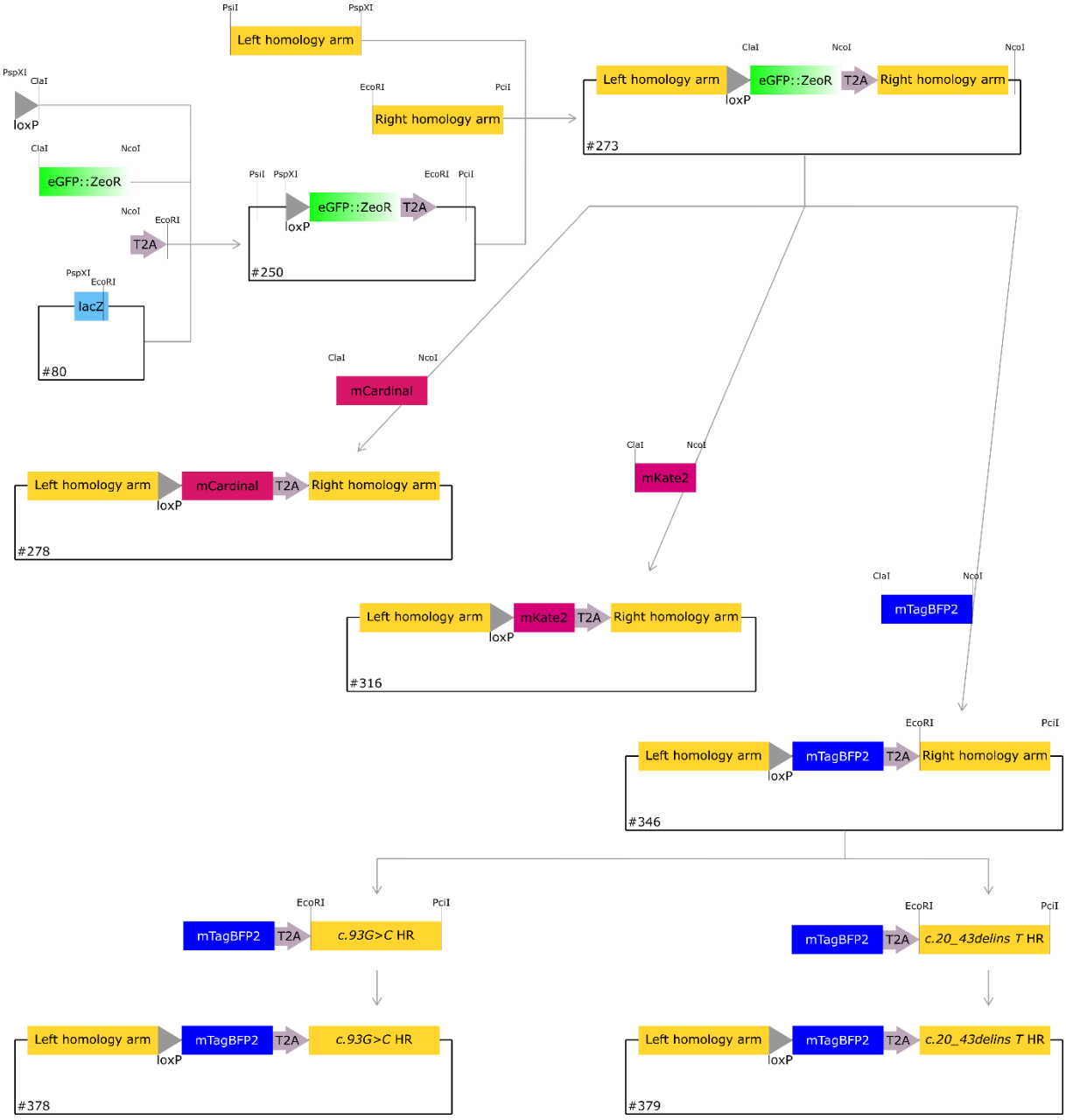

Figure 34: Genealogy of the cloning of *SMARCB1* e1 HDR constructs with different fluorescence reporter cassettes with and without the AT/RT-associated mutations *c.20_43delins T* or *c93G>C* in exon 1 of the *SMARCB1* gene. For the generation of the first intermediate #250, a loxP site (oligonucleotides #978 and #979), the PCR amplified eGFP::ZeoR cassette (from #243, primers #980 and #981), and a T2A sequence (oligonucleotides #982 and #983) were cloned into plasmid #80 step by step. The right homology arm containing sequences homologous to the DNA sequences downstream of the start codon of *SMARCB1* was PCR amplified from gRNA of hiPSC#33 (primers #987 and #988) and cloned into #250 via EcoRI and PciI restriction endonuclease digestion. Due to cloning issues, the left homology arm, homologous to the genomic sequences upstream of the start codon of *SMARCB1*, was PCR amplified from hiPSC#33 gDNA (primers #984 and #985) and cloned into #80 via TA cloning. The left homology arm was then transferred to the intermediate already containing the HR via PsiI and PspXI resulting in plasmid #273. The eGFP::ZeoR reporter cassette was subsequently exchanged for mCardinal (from plasmid #129, primers #1062 and #1063), mKate2 (from plasmid #311, primers #1104 and #1105), or mTagBFP2 (from plasmid #338, primers #1207 and #1208) via ClaI and NcoI restriction endonuclease digestion resulting in plasmids #278, #316, and #346 respectively. The mutated homology arms were PCR amplified from plasmid #346. For *c.93G>C* HR, the overlap extension method was applied (section 2.1.14) using primers #1207 (A), #1314 (B), #1315 (C), and #988 (D). The final PCR product was cloned into plasmid #346 via EcoRI and PciI. The *c.20_43delins T* mutation in exon 1 of *SMARCB1* was introduced via PCR from plasmid #346 using the primers #1207 and #1381. The PCR product was cloned into plasmid #346 via EcoRI and PciI. The left homology arm covers the sequence of the NCBI reference genome NG_009303.1 positions 3,737 to 5,207. The right homology arm covers the sequence of NCBI reference genome NG_009303.1 positions 5,208 to 6,848, directly adjacent.

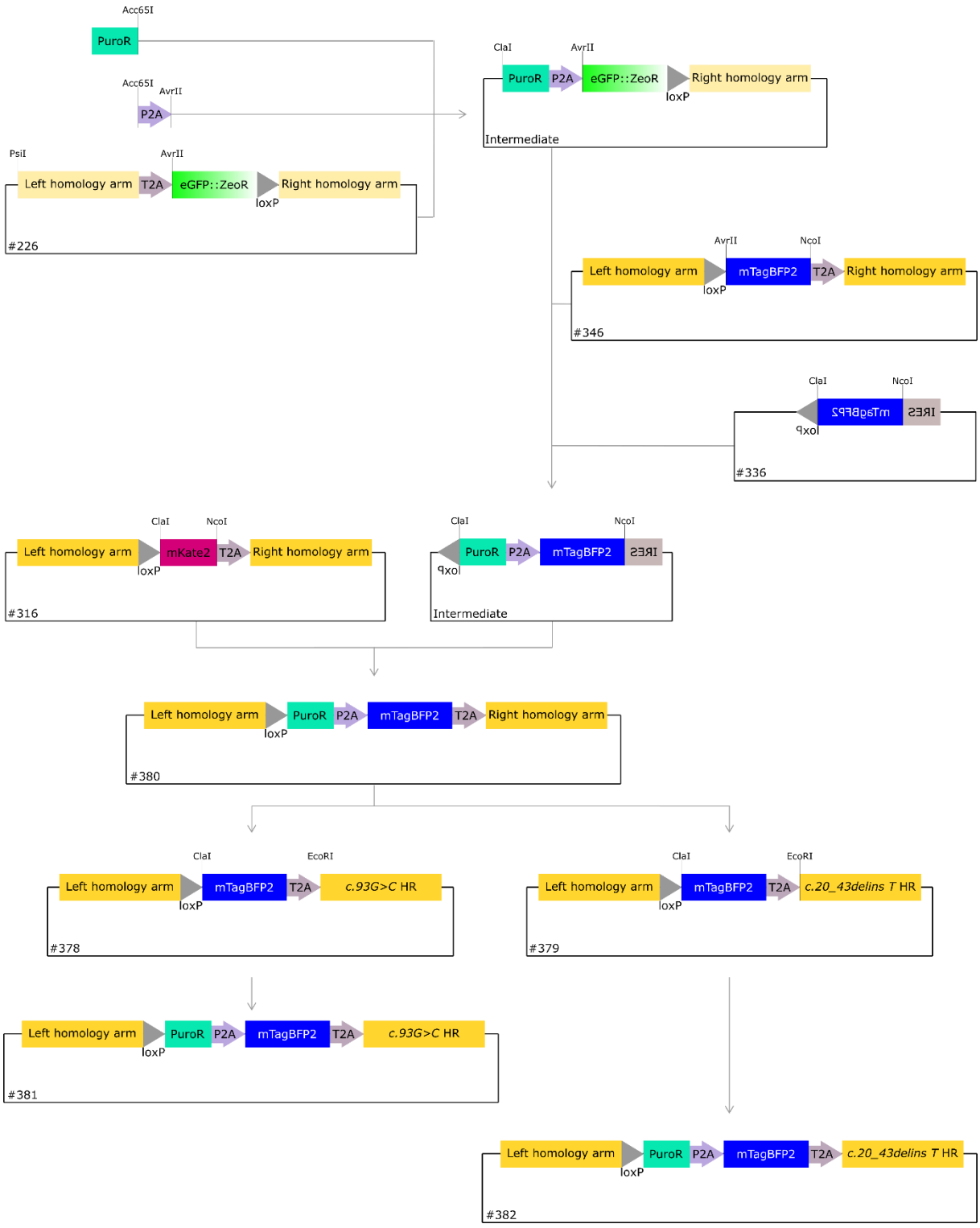

Figure 35: Schematic overview of the cloning of the *SMARCB1* e1 HDR constructs carrying the Puromycin resistance (PuroR)-mTagBFP2 selectable reporter cassette with or without the AT/RT-associated germline mutations *c.20_43delins T*, or *c.93G>C* in exon 1 of the *SMARCB1* gene starting from plasmids #226 and #346. An intermediate was generated by insertion of PCR amplified PuroR gene (from plasmid #263, primers #1437, #1438) and a P2A sequence (oligonucleotides #1435, #1436) via PsiI, Acc65, and AvrII. Completion of the selectable reporter cassette was achieved by PCR amplification of mTagBFP2 (from plasmid #346, primers #1439, #1208) and AvrII/NcoI restriction endonuclease recognition sites. The complete PuroR-P2A-mTagBFP2 cassette was transferred to plasmid #346 via ClaI and NcoI restriction endonuclease digestion resulting in *SMARCB1* e1 HDR #380. ClaI EcoRI restriction endonuclease digestion was used to transfer the whole reporter cassette and generate the HDR constructs containing the mutated HRs *c.20_43delins T* (from #378 from #378) and *c.93G>C* (from #379 from #379). The left homology arm covers the sequence of the NCBI reference genome NG_009303.1 positions 3,737 to 5,207.

The right homology arm covers the sequence of NCBI reference genome NG_009303.1 positions 5,208 to 6,848, directly adjacent.

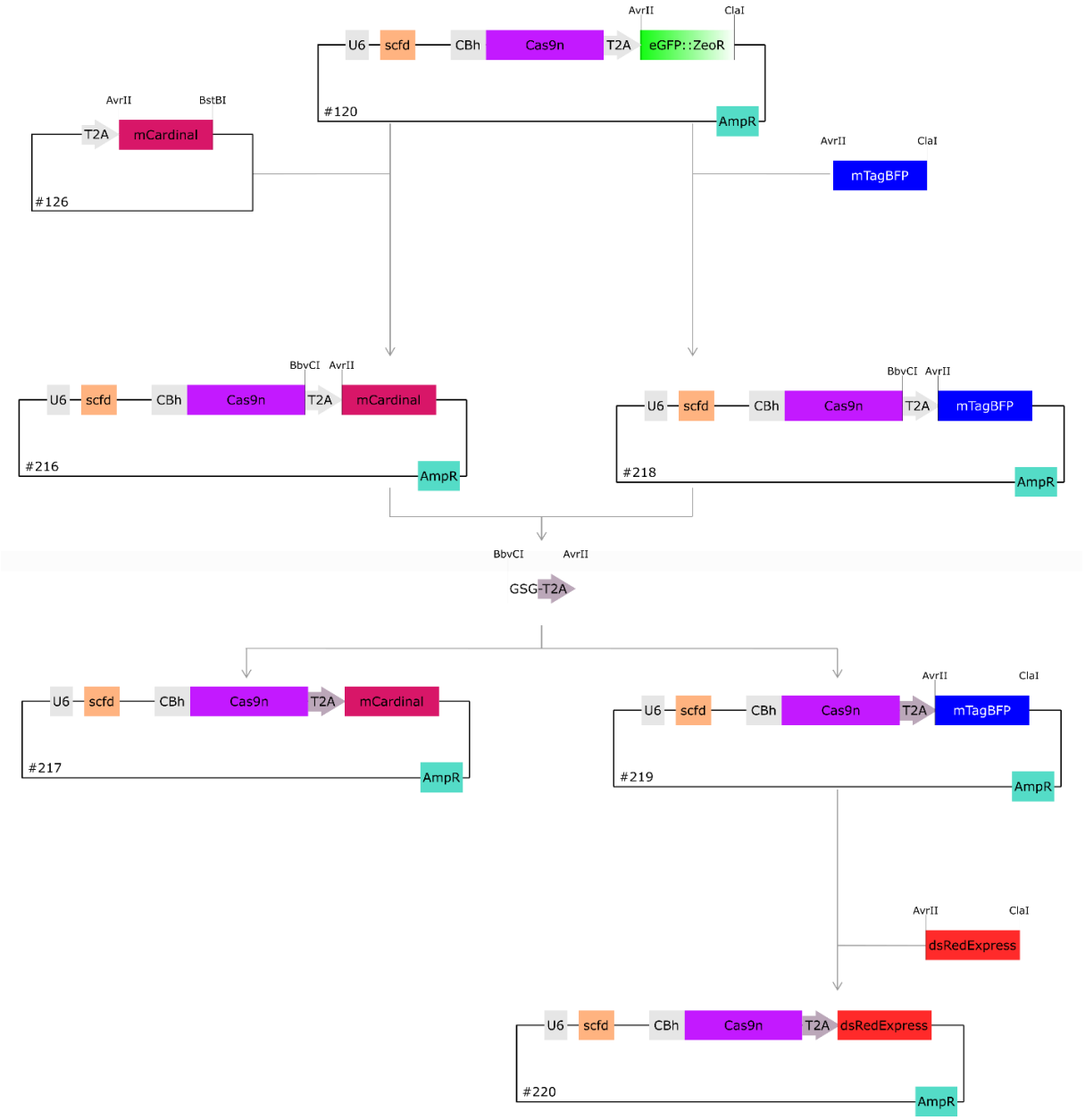

Figure 36: Schematic overview of the cloning of the gRNA and Cas9 multiplex plasmids which facilitate the co-expression of Cas9 and different fluorophores as reporters. The original eGFP::ZeoR reporter cassette on plasmid #120 was exchanged for mCardinal from plasmid #126 via AvrII and ClaI/BstBI cloning (plasmid #216). mTagBFP was amplified from plasmid #215 (primers #668 and #669) and cloned into plasmid #120 via AvrII and ClaI overhangs resulting in gRNA and Cas9 plasmid #218. Enhancement of the self-cleavage of the T2A peptide linking the Cas9 and fluorophore open reading frame was achieved by exchange of the original T2A sequence for one with a 5' GSG linker (oligonucleotides #745 and #746) via BbvCI and AvrII restriction endonuclease sites. The resulting gRNA and Cas9 plasmids encoding either mCardinal (plasmid #217) or mTagBFP (plasmid #219) were used for the finalization with gRNA sequences targeting the tumour suppressor gene *SMARCB1*. To complete the set of reporters to choose from, mTagBFP was exchanged for dsRedExpress (PCR amplification from plasmid #128 with oligonucleotides #787 and #801) yielding plasmid #220.

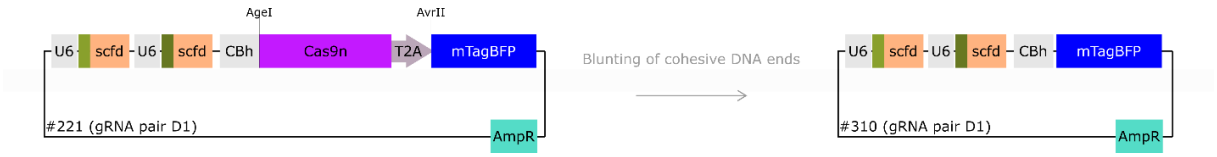

Figure 37: Schematic overview of the deletion of the Cas9n open reading frame from gRNA and Cas9n plasmid #221 via AgeI and AvrII restriction endonuclease digestion, followed by blunting of the cohesive DNA ends, and blunt-end ligation. Finally yielding the gRNA pair D1 plasmid #310.

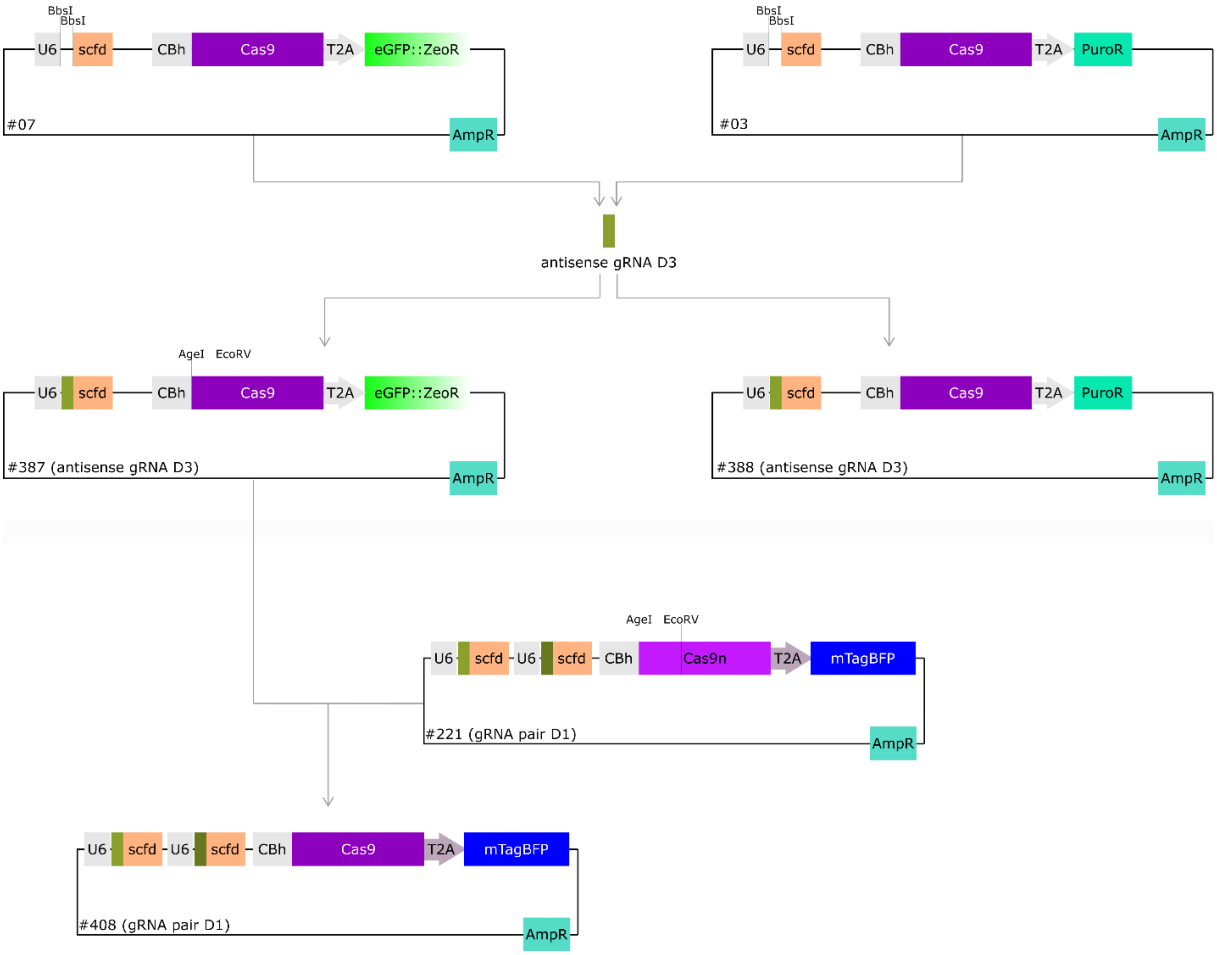

Figure 38: Schematic overview of the cloning steps to generate the gRNA and Cas9 nuclease plasmids #387, #388, and #408. Golden Gate cloning using BbsI was utilised to insert the antisense gRNA of pair D3 targeting the region directly upstream of the stop codon of the *SMARCB1* gene into Cas9 nuclease plasmids #07 (eGFP::ZeoR reporter) and #03 (PuroR reporter) yielding plasmids #387 (eGFP::ZeoR reporter) and #388 (PuroR reporter) respectively. Via AgeI and EcoRV digestion, the sequence of Cas9n containing the RuvC domain inactivating mutation D10A (base 26 A to C transversion) in Cas9n plasmid #221 was exchanged for the wildtype sequence obtained from plasmid #387.

7.1.5. Graphical overview of the cloning of the original lentiviral Hes5-IRES-mKate2 plasmid for overexpression of *Hes5*

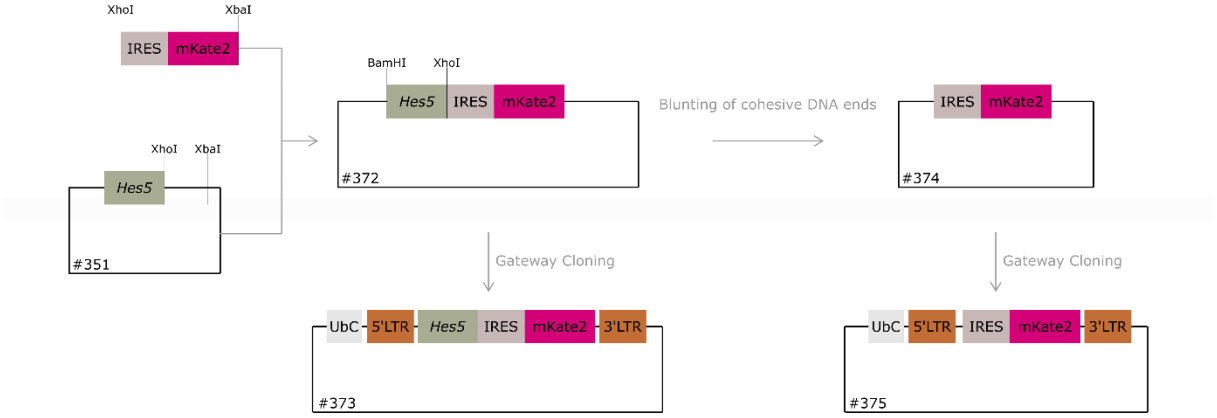

Figure 39: Schematic overview of the cloning steps leading to the original set of lentiviral *Hes5*-IRES-mKate2 plasmids for overexpression of *Hes5*. The sequence of *Hes5* was amplified from embryonic mouse cDNA and cloned into pENTR (plasmid #174) to generate the plasmid #351. PCR amplification of the IRES-mKate2 cassette (from plasmid #318, oligonucleotides #1285 and #1308) and cloning into plasmid #351 via XhoI/PspXI and XbaI restriction endonuclease recognition sites resulted in the pENTR plasmid #372. Removal of the *Hes5* sequence was achieved by BamHI and XhoI cleavage followed by end blunting and ligation (plasmid #374). The LR reaction of the gateway cloning then transferred the gene cassette to be expressed into pLenti6-UbC (plasmid #160), generating the lentiviral *Hes5* plasmid #373 and its corresponding control plasmid #375. Abbreviations: UbC = human ubiquitin C promoter, LTR = long terminal repeat

7.1.6. Information of plasmids generated or used in this thesis

In Table 48 relevant information is given to all plasmids generated or used in this work. For the sequences (SnapGene and FASTA format) please refer to the electronic storage device attached to the printed version of this thesis.

Table 48: Summary and short description of all plasmids generated or used in this thesis.

#	PLASMID NAME	DESCRIPTION
1	338pMTE-Oz	Transposable backbone vector
3	pSpCas9(Sekeres, Riggs et al.)-2A-Puro (PX459) V2.0	Basic Cas9/gRNA expression vector, Puromycine resistance cassette T2A-linked
7	V3 (PX459-Cas9(BB)-2A-EGFPZeo) V55L T2A Glu-Asp	Basic Cas9/gRNA expression vector, eGFP::ZeoR cassette T2A-linked
80	pBluescript II SK (+)	Bluescript backbone, multiple cloning site in lacZ gene
83	pBS_PuroR_EGFP+ZeoR	Basis vector for cloning of plasmid #226
110	pCl-VSVG	Lentiviral VSV-G envelope gene to facilitate generation of lentiviral particles
111	psPAX2	Lentiviral packaging plasmid
120	pX330A_D10A-eGFPZeo-1x2	Basic Cas9n/gRNA pair expression vector, eGFP::ZeoR cassette T2A-linked
128	pCMMP-IRES-dsRedExpress	source of dsRedExpress2 sequence
131	pX330A_D10A-1x2	Basic Cas9n/gRNA pair expression vector from CRISPR/Cas9 Assembly System Kit #1000000055, Addgene
160	pLenti6 UbC	empty lentiviral backbone vector for Gateway Cloning
174	pENTR4	empty donor backbone vector for Gateway Cloning
215	EpiC BFP-Cs2l GFP	source of mTagBFP sequence, kind gift of Rolf Marschalek, Frankfurt am Main
216	pX330A_D10A-mCardinal-1x2	Basic Cas9n/gRNA pair expression vector, mCardinal reporter T2A-linked
217	pX330A_D10A-mCardinal-1x2 GSG-T2A	Basic Cas9n/gRNA pair expression vector, mCardinal reporter T2A-linked, optimised T2A sequence with Gly-Ser-Gly linker
218	pX330A_D10A-BFP-1x2	Basic Cas9n/gRNA pair expression vector, mTagBFP reporter T2- linked
219	pX330A_D10A-BFP-1x2 GSG-T2A	Basic Cas9n/gRNA pair expression vector, mTagBFP reporter T2A-linked, optimised T2A sequence with Gly-Ser-Gly linker
220	pX330A_D10A-dsRed-1x2 GSG-T2A	Basic Cas9n/gRNA pair expression vector, dsRedExpress reporter T2A-linked, optimised T2A sequence with Gly-Ser-Gly linker
221	pX330A_D10A-mTagBFP gRNA pair D1 (SMARCB1 Cas9n gRNA E9 pair D1)	Cas9n/gRNA pair D1 expression vector targeting exon 9 of the coding region of the human *SMARCB1* gene, mTagBFP reporter T2A-linked
222	pX330A_D10A-mTagBFP gRNA pair D2 (SMARCB1 Cas9n gRNA E9 pair D2)	Cas9n/gRNA pair D2 expression vector targeting exon 9 of the coding region of the human *SMARCB1* gene, MTagBFP reporter T2A-linked

223	pX330A_D10A-mTagBFP gRNA pair D3 (SMARCB1 Cas9n gRNA E9 pair D3)	Cas9n/gRNA pair D3 expression vector targeting exon 9 of the coding region of the human *SMARCB1* gene, MTagBFP reporter T2A-linked
225	pX330A_D10A-dsRedExpress gRNA pair C3 (SMARCB1 Cas9n gRNA E1 pair C3)	Cas9n/gRNA pair C3 expression vector targeting exon 1 of the coding region of the human *SMARCB1* gene, dsRedExpress reporter T2A-linked
226	pBS_HL-T2A-eGFPZeoR-loxP-HR (SMARCB1 HDR E9 T2A-eGFPZeoR-loxP)	HDR construct for Cas9-mediated genome engineering upon cleavage in exon 9 of the human *SMARCB1* gene
227	pBS_IRES-eGFPZeoR-loxP	Basic vector for the cloning of HDR constructs with eGFP::ZeoR reporter insert
243	pBS_HL-IRES-eGFPZeoR-loxP-HR (SMARCB1 HDR E9 IRES-eGFPZeoR-loxP	HDR construct for Cas9-mediated genome engineering upon cleavage in exon 9 of the human *SMARCB1* gene
253	pBS-HL-IRES-eGFPZeoR-loxP-HR CSS (SMARCB1 HDR E9 CSS c.1091-1093delAGA)	HDR construct for Cas9-mediated genome engineering upon cleavage in exon 9 of the human *SMARCB1* gene introducing the CSS-associated mutation c.1091-1093delAGA in exon 8 of the human *SMARCB1* gene
254	pBS_HL-IRES-dsRedExpress-HR (SMARCB1 HDR E9 IRES-dsRedExpress)	HDR construct for Cas9-mediated genome engineering upon cleavage in exon 9 of the human *SMARCB1* gene
255	pBS_HL-IRES-dsRedExpress-loxP-HR (SMARCB1 HDR E9 IRES-dsRedExpress-loxP)	HDR construct for Cas9-mediated genome engineering upon cleavage in exon 9 of the human *SMARCB1* gene
256	pX330A_D10A-mTagBFP gRNA pair C3 (SMARCB1 Cas9n gRNA E1 pair C3)	Cas9n/gRNA pair C3 expression vector targeting exon 1 of the coding region of the human *SMARCB1* gene, MTagBFP reporter T2A-linked
257	pMD2.G	VSV-G envelope plasmid
258	pS-IcKVenus-Cre-WRPE	Lentiviral plasmid for expression of the Venus*Cre* fusion gene under control of the human SFFV promoter
272	pBS_HL-IRES-mCardinal-HR (SMARCB1 HDR E9 IRES-mCardinal)	HDR construct for Cas9-mediated genome engineering upon cleavage in exon 9 of the human *SMARCB1* gene
273	pBS_E1HL-loxP-GFPZeoR–T2A-E1HR (SMARCB1 HDR E1 loxP-mCardinal-T2A)	HDR construct for Cas9-mediated genome engineering upon cleavage in exon 1 of the human *SMARCB1* gene
277	pBS_HL-IRES-mCardinal-loxP-HR (SMARCB1 HDR E9 IRES-mCardinal-loxP)	HDR construct for Cas9-mediated genome engineering upon cleavage in exon 9 of the human *SMARCB1* gene
278	pBS_E1HL-loxP-mCardinal–T2A-E1HR (SMARCB1 HDR E1 loxP-mCardinal-T2A)	HDR construct for Cas9-mediated genome engineering upon cleavage in exon 1 of the human *SMARCB1* gene

279	pBS_E1HL-mCardinal–T2A-E1HR (SMARCB1 HDR E1 mCardinal-T2A)	HDR construct for Cas9-mediated genome engineering upon cleavage in exon 1 of the human *SMARCB1* gene
282	pBS_HL-IRES-mCardinal-loxP-HR CSS (SMARCB1 HDR E9 CSS IRES-mCardinal-loxP)	HDR construct for Cas9-mediated genome engineering upon cleavage in exon 9 of the human *SMARCB1* gene
309	pX330A-mTagBFP gRNA C3 SMARCB1 E1	gRNA pair C3 plasmid, gRNA sequences targeting exon 1 of the human *SMARCB1* gene, mTagBFP reporter T2A-linked
310	pX330A-mTagBFP SMARCB1 E9 gRNA pair D1	gRNA pair D1 plasmid, gRNA sequences targeting exon 9 of the human *SMARCB1* gene, mTagBFP reporter T2A-linked
311	pmKate-Hyg-N1	source of mKate2 sequence, only mKate2 sequenced, kind gift of Johannes Fels, UKE Münster
316	pBS_E1HL-loxP-mKate2-T2A-E1HR (SMARCB1 HDR E1 loxP-mKate-T2A)	HDR construct for Cas9-mediated genome engineering upon cleavage in exon 1 of the human *SMARCB1* gene
317	pBS_E1HL-mKate2-T2A-E1HR (SMARCB1 HDR E1 mKate-T2A)	HDR construct for Cas9-mediated genome engineering upon cleavage in exon 1 of the human *SMARCB1* gene
318	pBS_HL-IRES-mKate2-loxP-HR (SMARCB1 E9 HDR IRES-mKate2-loxP)	HDR construct for Cas9-mediated genome engineering upon cleavage in exon 9 of the human *SMARCB1* gene
319	pBS_HL-IRES-mKate2-HR (SMARCB1 E9 HDR IRES-mKate2)	HDR construct for Cas9-mediated genome engineering upon cleavage in exon 9 of the human *SMARCB1* gene
339	pX330A_D10A-mCardinal gRNA pair D1 (SMARCB1 Cas9n gRNA E9 pair D1)	Cas9n/gRNA pair D1 expression vector targeting exon 9 of the coding region of the human *SMARCB1* gene, mCardinal reporter T2A-linked
340	pS_IcK-Venus	Lentiviral expression vector of Venus reporter under control of the human SFFV promoter
346	pBS_E1HL-loxP-mTagBFP2-T2A-E1HR (SMARCB1 HDR E1 loxP-mTagBFP2-T2A)	HDR construct for Cas9-mediated genome engineering upon cleavage in exon 1 of the human *SMARCB1* gene
355	EMX2 HDR T2A TagBFP2 Blasticidin	source of the blasticidin resistance gene (BSD) sequence
363	pBS-HL c.1148delC-IRES-eGFPZeoR-loxP-HR (ATRT E9 HDR c.1148delC)	HDR construct for Cas9-mediated genome engineering upon cleavage in exon 9 of the human *SMARCB1* gene introducing the AT/RT-associated point-mutation c.1148delC
372	pENTR4_mHes5-IRES-mKate2	Donor vector with Hes5-IRES-mKate2 cassette for Gateway Cloning
373	pLenti-UbC-mHes5-IRES-mKate2	Lentiviral expression vector of the Hes5-IRES-mKate2 cassette under control of the human UbC promoter
374	pENTR4_IRES-mKate2	Donor vector with IRES-mKate2 cassette for Gateway Cloning

375	pLenti-UbC-IRES-mKate2	Lentiviral expression vector of the IRES-mKate2 cassette under control of the human UbC promoter
376	pMAX-GFP	plasmid for GFP overexpression, positive control for transfection and electroporation, source: Lonza Nucleofector 4D kit
378	pBS_E1HL-loxP-mTagBFP2-T2A-E1HR c.93G>C (SMARCB1 AT/RT HDR E1 c.93G>C loxP-mTagBFP2-T2A)	HDR construct for Cas9-mediated genome engineering upon cleavage in exon 1 of the human *SMARCB1* gene introducing the AT/RT-associated splice-site mutation c.93G>C
379	pBS_E1HL-loxP-mTagBFP2-T2A-E1HR *c.20_43delins T* (SMARCB1 AT/RT HDR E1 *c.20_43delins T* loxP-mTagBFP2-T2A)	HDR construct for Cas9-mediated genome engineering upon cleavage in exon 9 of the human *SMARCB1* gene introducing the AT/RT-associated indel *c.20_43delins T*
380	SMARCB1 E1 HDR loxP-PuroR-P2A-mTagBFP2-T2A	HDR construct for Cas9-mediated genome engineering upon cleavage in exon 1 of the human *SMARCB1* gene, **final version**
381	SMARCB1 E1 HDR loxP-PuroR-P2A-mTagBFP2-T2A c.93G>C	HDR construct for Cas9-mediated genome engineering upon cleavage in exon 1 of the human *SMARCB1* gene introducing the AT/RT-associated splice-site mutation c.93G>C, **final version**
382	SMARCB1 E1 HDR loxP-PuroR-P2A-mTagBFP2-T2A *c.20_43delins T*	HDR construct for Cas9-mediated genome engineering upon cleavage in exon 9 of the human *SMARCB1* gene introducing the AT/RT-associated indel *c.20_43delins T*, **final version**
383	pBS_PuroR-P2A-eGFPZeoR-SMARCB1 E9HR	Cloning intermediate for the final version of the SMARCB1 E1 HDR vectors
384	pBS_PuroR-P2A-mTagBFP2	PuroR-P2A-mTagBFP cassette in pBluescript
385	pBS_IRES-mKate2-T2A	IRES-mKate2-T2A cassette in pBluescript
386	SMARCB1 HDR E9 IRES-mKate2-T2A-BSD-loxP	HDR construct for Cas9-mediated genome engineering upon cleavage in exon 9 of the human *SMARCB1* gene, **final version**
387	pX549 Cas9 GFPZeoR gRNA SMARCB1 E9 D3 antisense	Cas9/gRNA D3 antisense expression vector targeting exon 9 of the human *SMARCB1* gene, eGFP::ZeoR cassette T2A-linked
388	pX549 Cas9 PuroR gRNA SMARCB1 E9 D3 antisense	Cas9/gRNA D3 antisense expression vector targeting exon 9 of the human *SMARCB1* gene, PuroR cassette T2A-linked
406	pS_IcK Hes5-IRES-mKate2	Lentiviral expression vector of the Hes5-IRES-mKate2 cassette under the control of the human SFFV promoter
407	pS_IcK IRES-mKate2	Lentiviral expression vector of the IRES-mKate2 cassette under the control of the human SFFV promoter
408	pX330A Cas9 SMARCB1 E9 gRNA pair D1	Cas9/gRNA pair D1 expression vector targeting exon 9 of the human *SMARCB1* gene, mTagBFP reporter T2A-linked

415	pMTE-p53DD	Transposable expression vector of the dominant negative form of murine p53DD under the control of the human Ef1α promoter
422	pBS_CSS HL-IRES-mKate2-T2A-BSD-loxP-HR (SMARCB1 E9 HDR CSS mKate2)	HDR construct for Cas9-mediated genome engineering upon cleavage in exon 9 of the human *SMARCB1* gene, introducing the CSS-associated mutation c.10911093delAGA in exon 8 of the *SMARCB1* gene, **final version**
438	pCD-NL-BH	Lentiviral packaging plasmid

7.2. Publications

Filatova, A., Rey, L.K., **Lechler, M.B.** *et al.* Mutations in *SMARCB1* and in other Coffin–Siris syndrome genes lead to various brain midline defects. *Nat Commun* **10,** 2966 (2019) doi:10.1038/s41467-019-10849-y

7.3. Scholarship

Graduate College 1657 Radiation Biology of the German Research Foundation (Deutsche Forschungsgemeinschaft, DFG), April 2017 to May 2020.

7.4. Contributions of others

Elias Sellner cloned of pBS_T2A-eGFP::ZeoR-loxP (plasmid #83), and made a first draft of the design of gRNA sequences targeting the genomic region of the *SMARCB1* gene's stop codon before I started the project.

Simon Rosowski generated the plasmids *SMARCB1* CSS e9 HDR IRES-eGFP::ZeoR (plasmid #253) under my direct supervision.

Debashmita Mukherjee helped in the cloning of the murine *Hes5* overexpression and control constructs (plasmids #406, 407) under my direct supervision.

Ulrike Hoppe removed the *Cre* recombinase gene sequence from plasmid #258 to generate the Venus encoding control plasmid #340 by instructions of Ulrike Nuber.

7.5. Curriculum vitae

Wurde aus Datenschutzgründen entfernt

IV. Acknowledgements

First and foremost, I want to express my gratitude to Prof. Dr. Ulrike A. Nuber for the chance to be part of the amazing team of the Stem Cell and Developmental Biology group of the Technical University of Darmstadt and for nurturing my scientific and personal development.

I also want to thank the principal investigators involved in the GrK1657 who invested a lot of their precious time to attend the retreats and gave valued input on my research.

V. Assertion – Ehrenwörtliche Erklärung

Ich erkläre hiermit ehrenwörtlich, dass ich die vorliegende Arbeit entsprechend den Regeln guter wissenschaftlicher Praxis selbstständig und ohne unzulässige Hilfe Dritter angefertigt habe.

Sämtliche aus fremden Quellen direkt oder indirekt übernommenen Gedanken sowie sämtliche von Anderen direkt oder indirekt übernommenen Daten, Techniken und Materialien sind als solche kenntlich gemacht. Die Arbeit wurde bisher bei keiner anderen Hochschule zu Prüfungszwecken eingereicht.

Darmstadt, den

_____

Marion Brigitte Lechler